SYNTHESIS OF SMALL ORGANIC PHOTOLUMINISCENT MATERIALS AND THEIR APPLICATIONS IN SUPRAMOLECULAR CHEMISTRY

A THESIS SUBMITTED IN PARTIAL FULFILLMENT for THE DEGREE of

DOCTOR OF PHILOSOPHY

IN THE SCHOOL OF CHEMICAL SCIENCES
GOA UNIVERSITY

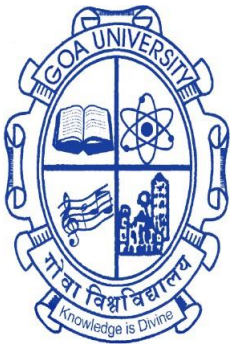

By

MR. VISHAL GOPALRAO MORE
GOA UNIVERSITY
TALEIGAO
GOA

NOVEMBER 2022

DECLARATION

I, Mr. Vishal Gopalrao Morehereby declare that this thesis represents work which has been carried out by me and that it has not been submitted, either in part or full, to any other University or Institution for the award of any research degree.

Place: Taleigao Plateau
Date: 29-11-2022

Mr. Vishal G. More
Research Scholar
School of Chemical Sciences
Goa University, Goa

CERTIFICATE

I hereby certify that the above Declaration of the candidate, Mr. Vishal Gopalrao More is true and the work was carried out under my supervision.

Prof. Sheshanath V. Bhosale
Research Guide
School of Chemical sciences
Goa University, Goa

ACKNOWLEDGEMENT

Life is a journey of moments and experiences we gain in this endless and unbound time of universe. The PhD work, the thesis and the moments spent during this time form an important part of my life which would not have been possible without the support, supervision and unrestricted help provided by many people. I owe a BIG thanks to all of them.

I would like to express my sincere gratefulness to my thesis supervisor ***Prof. Sheshnath V. Bhosale****. His patience, enthusiasm, co-operation and suggestions made me present this research work in the existing form. His brilliant, skillful supervision enriched this study higher than my expectations. I could not remain any more without giving heartfelt thanks to him for his painstaking supervision throughout the study period. This research work would not be possible without his stimulation, inspiration and cooperation. Special thanks to my subject experts* ***Prof. Vishnu. S. Nadkarni*** *and* ***Dr. Subhasish Roy, y****our encouraging words and thoughtful, detailed feedback have been very important to me.*

I take this opportunity to thank all my teachers and faculty members of School of Chemical Sciences ***Prof. V. M. S. V. Verenkar****,* ***Prof. R. N. Shirsat****, and* ***Prof. S. G. Tilve*** *for their encouragement and support. I would also like to thank* ***Dr. Pranay Morajkar, Dr. Vinod Mandrekar, Dr. Mahesh Majik****,* ***Dr. Sandesh Bugde****,* ***Dr. Rupesh Patre****,* ***Dr. Rupesh Kunkalkar****,* ***Dr. Rohan Kunkalekar, Mr. Vishnu Chari*** *for their timely motivation, help and constant support. A special thanks goes out to* ***Dr. Sidhanath Bhosale*** *(CSIR-IICT, Hyderabad) his knowledge and ingenuity is something I will always keep aspiring to carryout high level research. I wish to thank my collaborators Prof.* ***Subhajit Bandyopadhyay*** *(IISER, Kolkatta) for cis-tran isomerization study.*

I owe my gratitude towards my group members ***Mr. Ratan Jadhav, Mr. Dinesh Nadimetla, Mr. Kerba More, Miss Geeta Zalmi, Mr. Harshad Mirgane, Mr. Vilas Gaude*** *and* ***Miss. Pooja Shreechippa*** *for their constant help and advice. Also, I am thankful to other seniors from School of Chemical Sciences, Goa University* ***Dr. Rahul Kelkar****:* ***Dr. Amrja Naik, Dr. Akshay Salkar,*** *,* ***Dr. Prajyoti****,* ***Dr. Pratik Asogekar****,* ***Dr. Celia****,* ***Dr. Vishal****,* ***Dr. Jayakanthan****,* ***Dr. Santoshkumar, Dr. Shashank Mhaldar****,* ***Dr. Ketan Mandrekar****,* ***Dr. Neha Parsekar****,* ***Dr. Sudesh****,* ***Dr. Johnross****,* ***Ms. Lima Rodrigues, Dr. Sudarshana****,* ***Dr. Abhijeet Ms. Apurva, Mr.Nitesh, Mrs. Gautami, Mr. Chetan*** *and* ***Mr. Pritesh Mr. Pravin , Mr. Abhishek, Mr. Rohtash, Mr. Mahindra,*** *for their help to strike a balance with life outside the dark depths of the lab. As such, I cannot stress enough about the importance of the support and constant motivation of my friends and colleagues. I also take this*

*opportunity to give big thanks to **Dr. Y. D. Mane**, who always constantly inspire me during my master degree as well as compitative exams such as NET and GATE.*

I also thank to my friends, Prof. Jyotiba Pawar, Dr. Madhukar Pratapure, Dr. Bapurao Rupnawar, Mr. Ajit Sagre, Mr. Sandeep Suryavanshi, Mr. Shivaji Ban, Dr. Manojkumar Kalshetty and Dr. Ambaji Pawar for their kind support during the Ph.D.

*I sincerely thank the **non-teaching staff** of the School of Chemical Sciences, Goa University, the librarian and other staff in the library of Goa University for being kind and helpful. Special gratitude goes out to **Goa University** for fellowship for providing the funding for the work.*

*Finally, I thank my parents for their patience and encouragements my father **Mr. Gopalrao More**, my mother **Miss. Saroja G. More** and my brother **Mr. Amol G. More** for all the bounties and the blessings they bestowed upon me and for granting me the strength and patience to complete my research.*

Mr. Vishal G. More

Dedicated this thesis to *my father Mr. Gopalrao More, my mother Miss. Saroja G. More*

Contents

List of Abbreviation

NDIs	-	Naphthalenediimides
TPE	-	Tetraphenylethylene
TAPPs	-	Tetraarylpyrrolo [3,2-b] pyrroles
OLEDs	-	Organic light-emitting diodes
NDA	-	1,4,5,8-naphthalenetetracarboxylic acid dianhydride
cNDIs	-	Core substituted Naphthalenediimides
dsDNA	-	Double-stranded deoxyribonucleic acid
ssDNA	-	Single-stranded deoxyribonucleic acid
DBU	-	1,8-diazabicyclo[5.4.0]undec-7-ene
THF	-	Tetrahydrofuran
TFA	-	Trifluoroacetic acid
TEA	-	Triethylamine
MeCN	-	Methyl cyanide
Py-cNDI	-	Pyridyl-monoannulated Core substituted Naphthalenediimides
CNTs	-	Carbon nanotubes
SWCNTs	-	Single-walled Carbon nanotubes
MWCNTs	-	Multi-walled Carbon nanotubes
AIE	-	Aggregation-induced emission
AIEgens	-	Aggregation-induced emission luminogens
OFETs	-	Organic field-effect transistor
BODIPY	-	Boron-Dipyrromethene
DSSCs	-	Dye-sensitized solar cells
DDQ	-	2,3-Dichloro-5,6-dicyano-1,4-benzoquinone
PTSA	-	p-toluene sulfonic acid
AcOH	-	Acetic acid
TfOH	-	Trifluoromethanesulfonic acid
TsOH	-	Tosylic acid
DMF	-	Dimethylformamide
DMSO	-	Dimethyl sulfoxide
DCM	-	Dicholoromethane
$Pd(PPh_3)_4$	-	Palladium-tetrakis(triphenylphosphine)

DABCO	-	1,4-diazabicyclo[2.2. 2]octane
STM-BJ	-	Scanning tunnelling microscopy-break junction
PhosPP	-	Phosphindolpyrrolo[3,2-b]pyrrole
BPhosPP	-	Bisphosphindol-pyrrolo[3,2-b]pyrrole
SEAr	-	Aromatic Electrophilic Substitution
DHPPs	-	1,4 dihydropyrrolo[3,2-b]pyrroles
DPP	-	Diketopyrrolopyrrole
ACQ	-	Aggregation-caused quenching
HOMO	-	Highest occupied molecular orbital
LUMO	-	Lowest unoccupied molecular orbital
BHJ-OSCs	-	Bulk heterojunction organic solar cells
ICT	-	Intramolecular charge transfer
MOF	-	Metal–organic frameworks
TFAA	-	Trifluoroacetic acid anhydride
IR	-	Infrared
NMR	-	Nuclear magnetic resonance
PL	-	Photoluminescence
UV-Vis	-	UV-Visible
ESI-MS	-	Electron spray ionization mass spectroscopy
CV	-	Cyclic voltammetry
PET	-	Photo-induced electron transfer
FRET	-	Fluorescence resonance energy transfer
DFPDA	-	2,2-difluoropropanediamide
μM	-	Micrometer
TBA	-	Tetrabutylammonium salt
TD-DFT	-	Time-dependent density functional theory
ΔE_{act}	-	Activation energy
DLS	-	Dynamic light scattering
SEM	-	Scanning electron microscopy
DMTPS	-	1,1- dimethyl-2,3,4,5-tetraphenylsilole
HPS	-	Hexaphenylsilole
TPBD	-	Tetraphenyl-1,4-butadiene

List of Schemes

List of Tables

List of Figures

Chapter 1

Chapter 2

Chapter 4

Chapter 5

Abstract

From last decade we have seen that number of organic molecules which are photoactive in nature and because of structural features these photoactive molecule having wide number of applications in sensor, self-assembly, host–guest chemistry, ion channels, solar cells and OLEDs. Among these organic photoluminiscent materials, molecules such as tetraarylpyrrolo [3,2-b] pyrroles (TAPPs), naphthalenediimide-benzothiazole-based chemodosimeter, azobenzene-based tetraphenylethylene (TPE) exhibited potential applications.

Therefore, this thesis presents some novel organic photoluminiscent materials such as AIEgens: tetraarylpyrrolo [3,2-b] pyrroles (TAPPs) with detailed literature survey of new AIE-active TAPP class of molecules and derivatives through various synthetic routes and present their emerging applications. We also discuss some new methods for synthesis of tetraester-substituted tetraaryl-1, 4-dihydropyrrolo [3, 2-b] pyrrole (TAPP) with possible mechanism. Here we present new 'off-on' system based on core-substituted naphthalene diimide with dimethylamine for reversible acid-base sensor in which optical changes in acid-base condition can be visualised by naked eye by changing blue to reddish and reverse the color. Further we focus on naphthalenediimide-Benzothiazole-based chemodosimeter for selective and sensitive chromogenic for cyanide ion which plays key role in many chemical, medicinal and biological processes. Also we highlight on photoswitchable azobenzene based tetraphenylethylene (TPE) with photoresponsive properties and thermally induced reversal from the cis to the thermodynamically stable trans state applied as molecular glue for carbon nanotubes reversibly controls electronic mobility with light.

All these synthesized molecules are characterized and studied by ^{1}H NMR, ^{13}C NMR, ESI mass, elemental analysis, FT-IR, UV-Vis spectroscopy, Fluorescence emission spectroscopy, DFT calculations, Job's plot analysis, SEM & TEM imaging techniques. Furthermore, the potential application of synthesized organic photoluminiscent materials have been investigated by performing cyclic voltammetry, DLS study. The remarkable results obtained from all the above investigation has been concisely summarized in this synopsis.

Thesis objectives

The main objectives of the thesis are as follows:

- To Design and synthesize new class of AIEgens: tetraarylpyrrolo [3,2-b] pyrroles (TAPPs) as novel organic photoluminiscent material
- To Design and synthesize novel organic photoluminiscent materials based on core-substituted naphthalene diimide.
- To design and synthesize naphthalenediimide-benzothiazole-based chemodosimeter for selective and sensitive chromogenic for cyanide Ion.
- To Design and synthesize photoswitchable azobenzene-based tetraphenylethylene (TPE) molecular glue for carbon nanotubes reversibly controls electronic mobility with light.
- To design new methods for synthesis of tetraester-substituted tetraaryl-1, 4-dihydropyrrolo [3, 2-b] pyrrole (TAPP) as organic photoluminiscent material.

Thesis organization and results:

This thesis entitled "Synthesis of Small Organic Photoluminiscent Materials and Their Applications in Supramolecular Chemistry" is divided into six chapters as follows:

A brief highlight of each chapter is as presented below:

Chapter 1: Introduction and Literature Survey on New Class of AIEgens: Tetraarylpyrrolo [3,2-b]pyrroles (TAPPs) as Novel oOrganic Photoluminiscent Material

This chapter highlighted on introduction and a detailed literature survey of new AIE-active TAPP class of molecules and derivatives through several synthetic routes and present their emerging applications. [1]

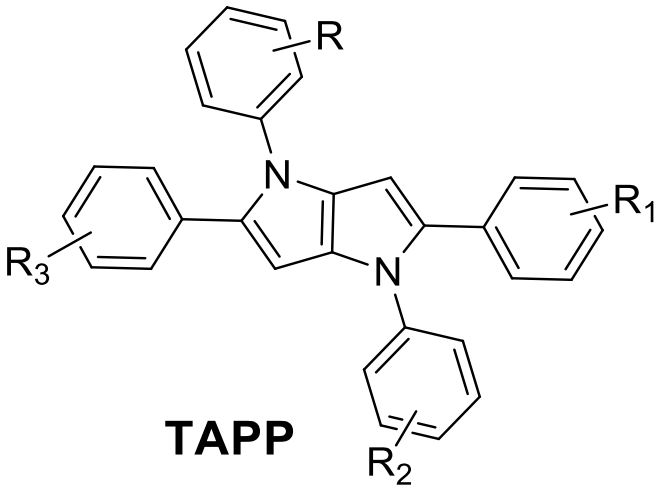

Figure 1: General structure of TAPP

Also we elaborated synthetic versatility of the TAPP core that can be leveraged to control the absorbance, emission, and physical properties of the analogues, allowing for fine-tuning of properties for each application. [2-4]

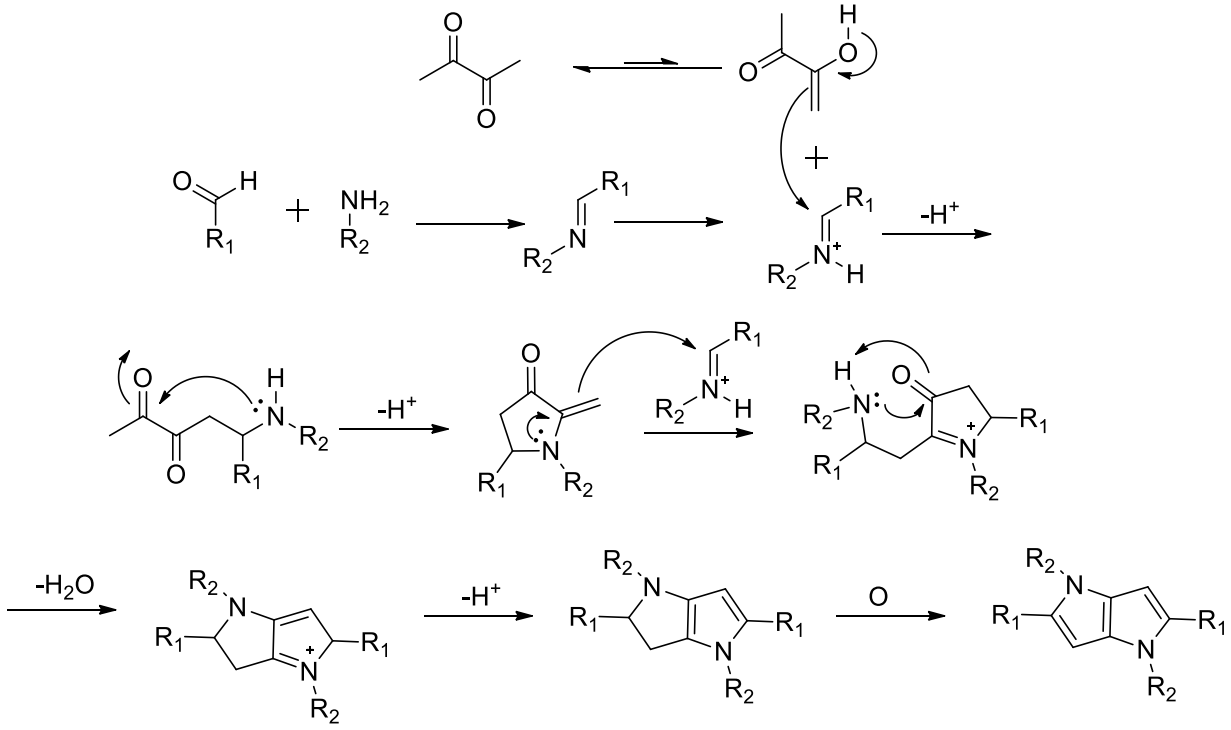

Figure 2: Plausible mechanism for the synthesis of TAPPs

This chapter also summarized the discovery of TAPP, the development of synthetic methods, the reaction mechanism, the reactivity of TAPP, the π-expansion of TAPP, and their photophysical properties. Development of this new AIE-active TAPP core will give excellent applications in the field of sensor, self-assembly, host– guest chemistry, ion channels, solar cells, and medicinal chemistry in future prospective. Also, simplicity and scalable synthesis of TAPP and its derivate will also have great potential to functionalization at the periphery of four benzene rings and use them for various applications successfully.

On the other hand, tetraphenyl ethylene (TPE)[3] and naphthalene diimides (NDIs)[5] also have been shown to be good photoluminiscent materials. Thus, in this thesis I have given briefly use of NDI and TPE derivatives for sensing and cis-trans isomerization of azo system to use as a glue for multiwall carbon nanotubes. Furthermore, I have also developed synthesis of TAPP using molecule iodine as a catalyst to improve the yield of tetraester-TAPP derivative.

Chapter 2: A new 'Off-On' System Based on Core-substituted Naphthalenediimide with Dimethylamine for Reversible Acid-Base Sensor

In this chapter we described design and synthesis of new Off-On system based on core-substituted naphthalene diimide with dimethylamine produces (4,9-bis(dimethylamino)-2,7-dioctylbenzo[lmn] [3,8]phenanthroline-1,3,6,8(2H,7H)-tetraone) coded as: DDPT **1.** [5, 6]

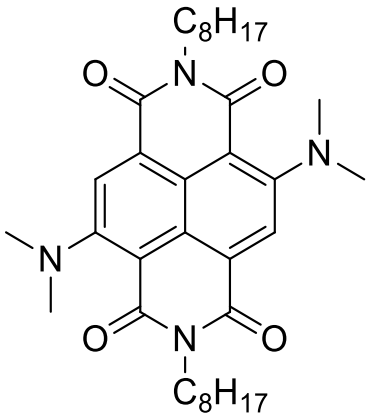

DDPT 1

Figure 3: Structure of DDPT **1**

In synthesis of DDPT **1** simple aromatic nucleophilic substitution was carried out by using Br_2-NDI with dimethylamine at 110 ^oC. Synthesized DDPT was fully characterized by ^1H NMR, ^{13}C NMR, ESI mass and elemental analysis techniques.[7, 8]

In application part DDPT **1** further used for acid-base sensing which shows 'switch-on' emission upon protonation of dimethylamine core of NDI with trifluoroacetic acid acid (TFA), the absorption band which appears in solution at 600 nm which blue-shifted to 545 nm. Remarkably fluorescence of DDPT **1** is weak in solution with quantum yield □ = 0.09, upon addition of TFA fluorescence enhanced to □ = 0.78. This suggests that protonation of N atom of dimethyl restricts the photoinduced electron transfer (PET) leading to the increase in fluorescence. All these changes get reversed to original state by addition of base triethylamine (TEA). The binding constant and stoichiometry of the compound was calculated to be 2.1×10^{-3} M^{-1}.

All such optical changes in Acid-Base condition can be visualised by naked eye by changing blue to reddish and reverse the color, respectively.

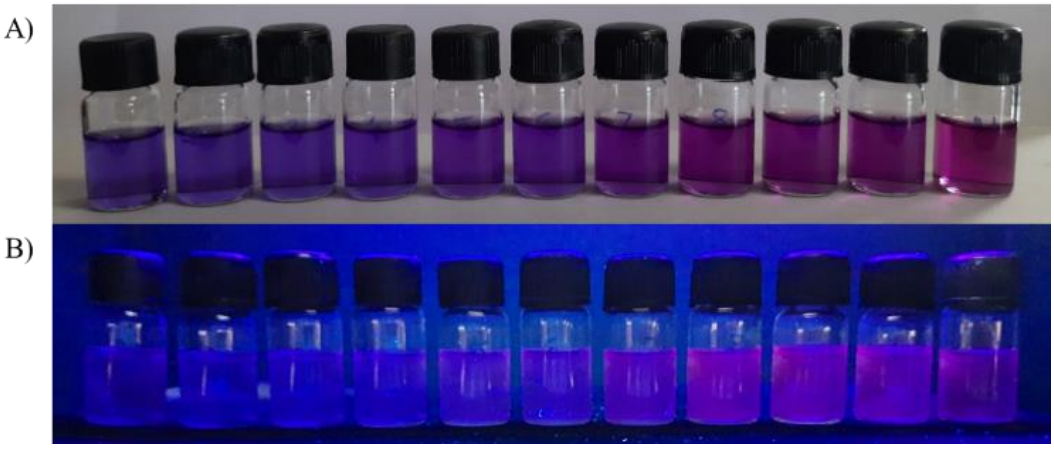

Figure 4: Sensing performance of the probe DDPT **1** (90μM) in THF with the addition of trifluoroacetic acid (0.2 to 2 equiv) A) under visible light B) under UV light illumination at 365nm.

Further, DDPT **1** used for strip-test sensing in which color changes from blue to reddish when expose to TFA vapours and reverse in the presence of triethyleamine vapours which clearly indicates that the synthesized probe is highly selective to H^+ ion in the solution. By studying optical properties such as UV-Vis absorption and fluorescence spectroscopy of probe DDPT **1,** we hope it may useful in future to replace litmus paper.

Chapter 3: Naphthalenediimide-Benzothiazole-Based Chemodosimeter for Selective and Sensitive Chromogenic for Cyanide Ion

This chapter deals with design and synthesis of new receptor based on naphthalene diimide-benzothiazole **(NDI-1)** chemosensor selectively for CN- ion.[9]

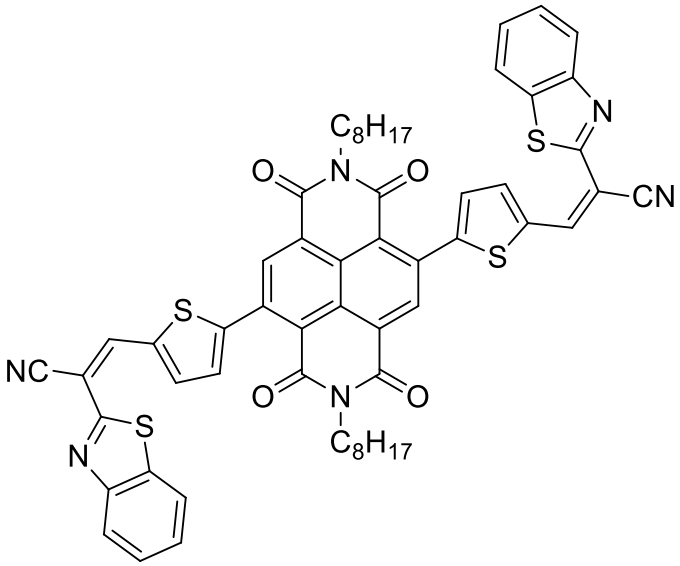

Figure 5: Structure of chromophore **NDI-1**.

Synthesized **NDI-1** after nucleophilic addition of cyanide ion Showed color change which can be observed by naked eye. Sensing of CN^- ion is studied by UV-Vis spectroscopy measurements in chloroform solution. As **NDI-1** displayed high sensitivity and selectivity

towards CN^- ions shows change in color from red to green, which was clearly visible to the naked eyes. Whereas, the addition of other anions i.e. F^-, Cl^-, I^-, Br^-, HSO_4^-, $H_2PO_4^-$, OAc^-, ClO_4^- and HCO_3^- resulted into no visible color change of the sensor **NDI-1**. The detecting mechanism of CN^- ion with **NDI-1** was demonstrated by ^1H NMR, DFT calculations, Job's plot analysis and cyclic voltammetry.[10-12]

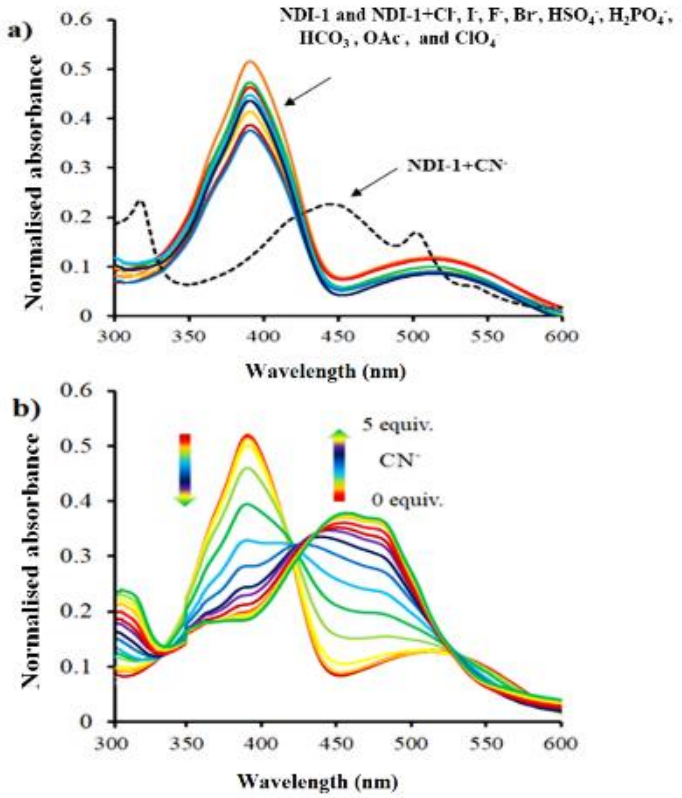

Figure 6: UV-Vis absorption spectra of NDI^{-1} (1.8×10^{-4} M) (a) in presence of 5 equiv. different anions and (b) titrated with CN^- ion.

Moreover, designed **NDI-1** exhibited very low limit of detection 85 nM, which reveals that **NDI-1** could be a good sensor for CN^- ions and can be used for practical applications effectively.

Chapter 4: Photoswitchable molecular glue for Carbon Nanotubes Reversibly Controls Electronic Mobility with Light

In this chapter we discussed photoswitchable azobenzene based tetraphenylethylene (TPE) system because of their photoresponsive properties and thermally induced reversal from the cis to the thermodynamically stable trans state that can play an important role in molecular devices.[13, 14]

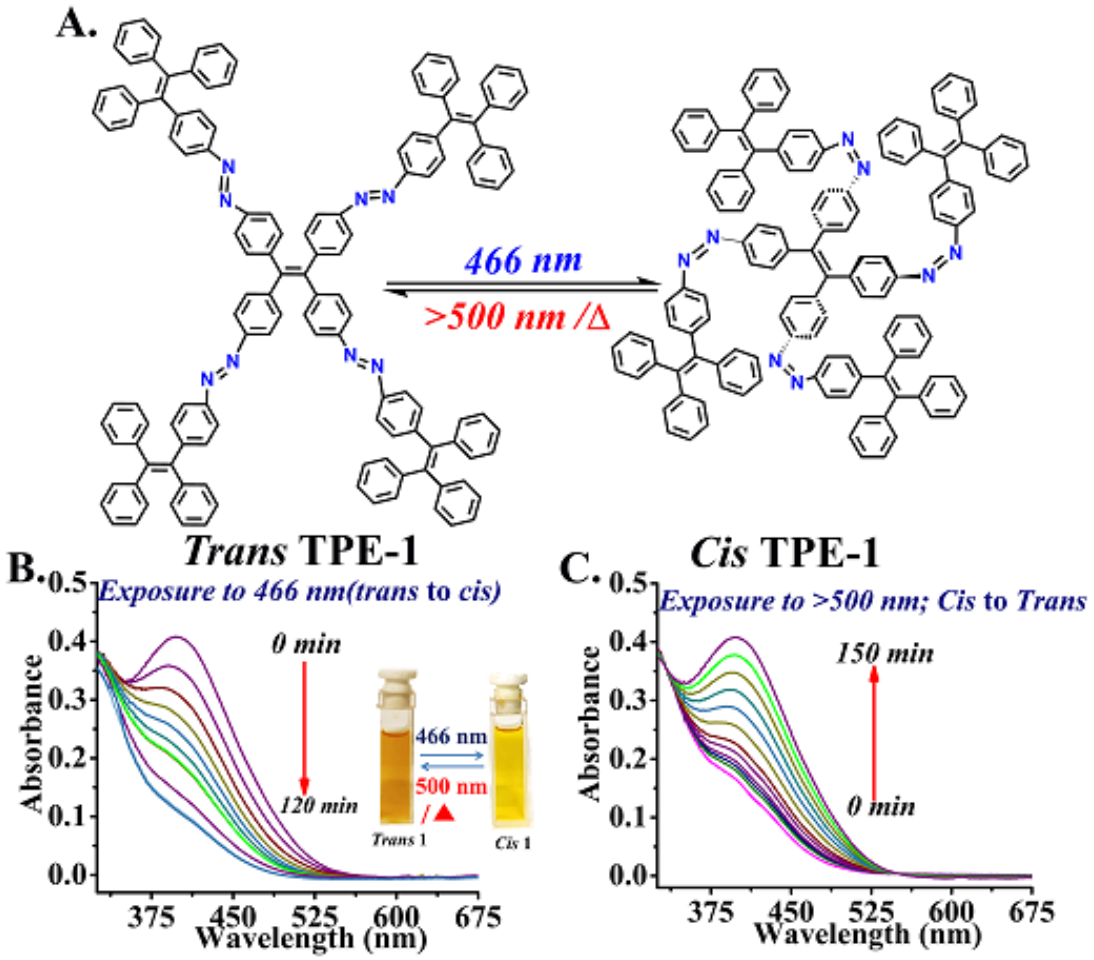

Figure 7: Photoisomerization of TPE-1 (6 µM) in THF solvent (A). Schematic representation of the photoisomerized TPE-1 in THF solvent at 273 K temperature (B). trans-1 to cis-1 conversion upon irradiation with 466 nm at 273 K temperature; in the inset

visual colour changes (c). cis-1 to trans-1 conversion upon irradia-tion with >500 nm at 273 K temperature or heat >333 K.

The designed system was capable of aggregation-induced emission (AIE) behavior, can act as molecular glue that can non-covalently functionalize multiwalled carbon nanotubes (MWCNT). This novel photoswitchable compound with five TPE units that undergoes reversible trans-cis isomerization under UV and visible light respectively. Out of cis-trans isomer, the trans-form showed a clear AIE behaviour in aqueous THF mixtures whereas the cis form did not also the trans form efficiently binds to multiple MWCNTs and thus acts as a molecular glue for the CNT.[15]

All these interactions were studied by UV-vis, fluorescence, Raman, FT-IR and ^{13}C NMR spectroscopy in addition to the PXRD studies.[16]

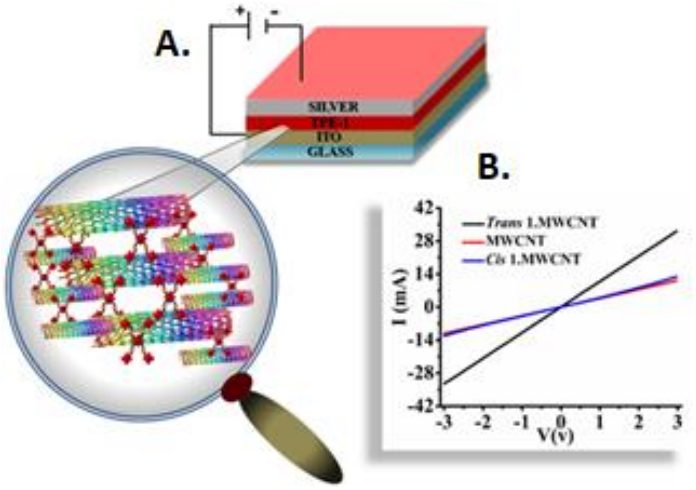

Figure 8: (A) Schematic representation of the interaction between [***trans*-1.MWCNT**]; (B) I Vs V plot of the **TPE-1** dropped over MWCNT where black is for the [***trans*-1.MWCNT**], blue is [***cis*-1.MWCNT**] and red is only MWCNT.

From this study we can conclude that, cis and trans isomerization of the molecular glue proves efficient example of controlling the conductance of CNTs with a photoswitchable molecular glue and has excellent potential applications in electronic devices such as solar cells and OLEDs.

Chapter 5: Iodine Catalysed New Method for Synthesis of Tetraester-Substituted Tetraaryl-1,4-Dihydropyrrolo [3, 2-b]pyrrole

This chapter deals with the synthesis of Tetraester-substituted tetraaryl-1, 4-dihydropyrrolo [3,2-b] pyrroles (TAPP) using molecular iodine as catalyst.[17, 18]

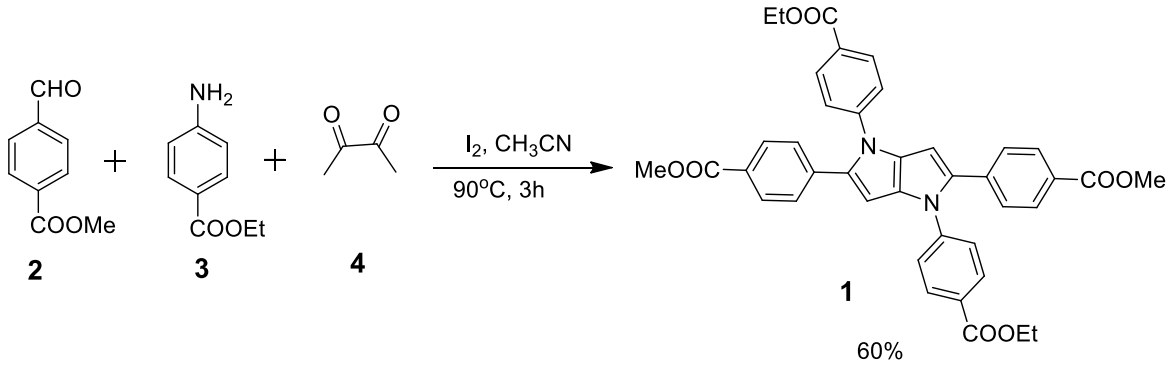

Figure 9: Synthesis of tetraester-substituted tetraaryl-1, 4-dihydropyrrolo [3, 2-b] pyrroles.

As TAPP molecules have been widely used for different applications like sensing, solar cells, cellular imaging etc, by taking into consideration, we developed new method for the synthesis of (TAPP 1) by cyclocondensation of aromatic amine, aromatic aldehyde and 2,3-butanedione in presence of iodine-catalyst. Also we explained the detailed mechanism of synthesis of TAPP.[19]

Chapter 6: Conclusion

This chapter concludes all thesis work, as our focus on novel organic photoluminiscent materials firstly detailed literature survey was done for well understanding. So accordingly we have designed and synthesized probe DDPT **1** with substituted dimethylamine at the core

of NDI showed reversible for 4 cycles with the frequent addition of acid and base to the synthesized NDI system. With simple route of synthesis of DDPT **1** it may useful to control of pH in various biological and physiological processes occurring in the system.

In another work we synthesized naphthalene diimide-benzothiazole (NDI-1) conjugate for nucleophilic addition of cyanide ion. This molecule detects selectively cyanide ion which can be further demonstrated by using other ions such as F^-, Cl^-, I^-, Br^-, HSO_4^-, $H_2PO_4^-$, OAc^-, ClO_4^- and HCO_3^-. The sensing of cyanide ion with very low limit of detection (85 nM) is studied by UV-Vis, emission, ^{1}H-NMR, cyclic voltammetry and further can be demonstrated by naked eyes and it is suggested that the NDI-1 could be a good sensor for practical applications successfully. Also we developed novel photoswitchable compound based on five in aqueous THF mixtures whereas the cis form has more of a twisted shape and did not displayed a clear AIE behaviour. The trans form efficiently binds to multiple MWCNTs and thus acts as a molecular glue for the CNT whereas the cis form, weakly interacts with the MWCNT samples. These interactions were studied by various methods like UV-vis, fluorescence, Raman, FT-IR and ^{13}C NMR spectroscopy in addition to the PXRD studies. DLS study performed to study aggregates of the nanotubes in the presence of the trans-form and were observed under SEM and TEM imaging. Results obtained from this study indicates that the cis and the trans isomerization of the molecular glue proves a fine example of controlling the conductance of CNTs with a photoswitchable molecular glue. We have also studied iodine catalyzed reaction increases the reaction yield of tetra-ester TAPP. We synthesized TAPP 1 by iodine-catalysed cyclocondensation of aromatic amine, aromatic aldehyde and 2,3-butanedione at 90^o C for 3h in acetonitrile solvent. Notable yield for tetra-ester-TAPP analogue obtained was up to 60%.

Overall, the outcome of the thesis led to the design and synthesis of novel organic

photoluminiscent materials based on TAPP, DDPT **1**, naphthalene diimide-benzothiazole (NDI-1), photoswitchable azobenzene based tetraphenylethylene (TPE) system exhibits a great potential for its applications in sensor, self-assembly, host–guest chemistry, ion channels, solar cells and OLEDs.

TPE units that undergoes reversible trans-cis isomerization under UV and visible light respectively. The trans form of TPE-1 is almost planar and displayed a clear AIE behavior.

Chapter 1: Introduction and Literature Survey

1.1 General Introduction:

As per thesis title synthesis of small organic photoluminiscent materials and their applications in supramolecular chemistry we studied related literature in detail. There are numerous photoluminiscent materials reported and studies in past decades perylene, terrylene, quaterrylenes, naphthalenediimides (NDIs), tetraphenylethylene (TPE), diarylethenes, tetraarylpyrrolo [3,2-b] pyrroles (TAPPs), spiropyrans, oxazines, stilbenes and azobenzenes with potential applications in the sensor, self-assembly, host–guest chemistry, ion channels, solar cells and OLEDs. But out of these materials specifically naphthalenediimide (NDIs), tetraphenylethylene (TPE) and tetraarylpyrrolo [3,2-b] pyrroles (TAPPs) exhibited superior properties therefore we focus on these materials.

The main objectives of the thesis are as follows:

- To Design and synthesize new class of AIEgens: tetraarylpyrrolo [3,2-b] pyrroles (TAPPs) as novel organic photoluminiscent material
- To Design and synthesize novel organic photoluminiscent materials based on core-substituted naphthalene diimide.
- To design and synthesize naphthalenediimide-benzothiazole-based chemodosimeter for selective and sensitive chromogenic for cyanide Ion.
- To Design and synthesize photoswitchable azobenzene-based tetraphenylethylene (TPE) molecular glue for carbon nanotubes reversibly controls electronic mobility with light.
- To design new methods for synthesis of tetraester-substituted tetraaryl-1, 4-dihydropyrrolo [3, 2-b] pyrrole (TAPP) as organic photoluminiscent material.

1.2 Novel organic photoluminiscent materials based on core-substituted naphthalene diimide.Naphthalene diimide (cNDIs)

As we know that naphthalene diimides (NDI)[1],[2] are well known for their good charge carrier mobility, high electron affinity, outstanding thermal and oxidative stability. Because of such features naphthalene diimide (NDI) (**2**) exhibited potential applications in the field of photovoltaic devices, organic electronics applications, sensors and organic light-emitting diodes (OLEDs).[3,4] These NDI derivatives are mainly synthesized from 1,4,5,8-naphthalenetetracarboxylic acid dianhydride (NDA) (**1**) (Figure 1.1), which is the chief precursor and also it can be freely functionalized, through the anhydride position, with either arylamino or alkylamino groups.[5,6]

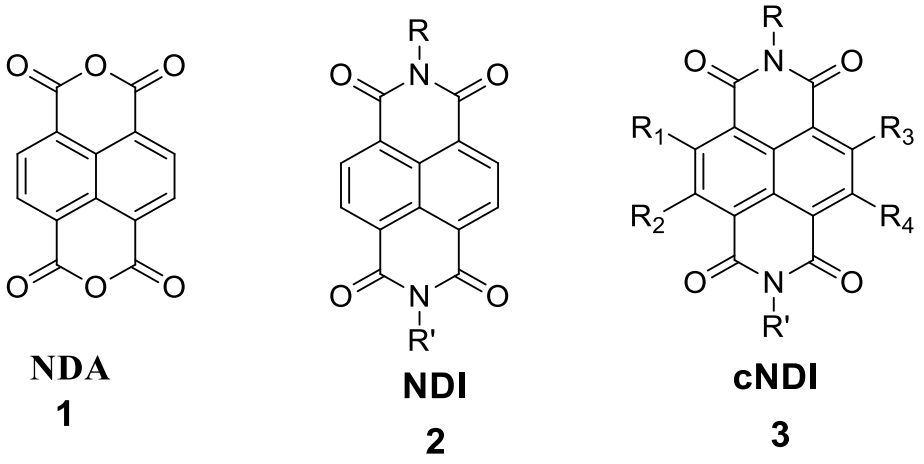

Figure 1.1: Structures of NDA, NDI and cNDI

We carried out literature survey to study the details of synthesis, properties, and applications of NDIs and also our research group previously worked on it. It was found that NDIs are planar, neutral, redox-active, chemically robust, electron-deficient class of aromatic compound with high melting point and efficiently applied in a different field as discussed above.[7] NDIs are the furthermost versatile and attractive class of aromatic molecules used in the design of various electronic conducting functional materials.[8] However, when we carried out functionalization through core-substitution to the core (**3**) produces NDI

analogues shows different absorption and fluorescence properties.[9]

cNDIs exhibited high fluorescence quantum yields (~0.9) in generally all common organic solvents. When NDI molecule is functionalized through the imide nitrogen atoms with *N*,*N*′-dioctyl-substitution, it resulted in the formation of colorless solids, which in CH_2Cl_2 solvent absorb in the UV region and also has a weak mirror image emission with a 7 nm Stokes shift exactly. But in toluene as solvent, it showed excimer-like emissions, indicated that ground-state aggregates are formed freely.[10] Also it was observed that NDI derivatives with two annulated electron-withdrawing imide groups acts as a planar aromatic scaffold and are simply and reversibly reducible. Additionally, the electron withdrawing groups present at the imide position leads to the strong polarization of the π-systems, and it founds low π-electron density makes them capable of electron acceptors. From literature we found that imide-functionalized NDIs have displayed potential applications in supramolecular self-assembled architectures,[11,12] artificial photosynthesis,[13,14] and in donor-acceptor systems.[15,16]

1.2.1 NDI as Molecular Sensors:

Researchers interestingly combined their research efforts in the all chemical, physical, analytical, biological, and medical sciences for the better understanding of interaction at the atomic-level, also how elements, ions, and molecules interact with each other used to sense significant species such as amino acids, heavy metals, ions, explosives etc. in natural systems.[17] Molecular recognition takes place by noncovalent bonding interactions such as hydrogen-bonding, metal coordination, π−π interactions, host−guest interactions.[18] Generally chemical sensors can be classified into two types: biosensors or chemosensors. We are focusing on chemosensors which are use synthetically designed receptor units to

produce selective recognition/sensors particularly. In last decade, interestingly fluorescent chemosensors have been reported widely as compared to non-fluorescent dyes, because of excellent features like real-time visualization, rapid response time and high sensitivity. Significantly, chemosensors shows observable changes both in UV−visible absorption and fluorescence at a specific wavelength, also color changes that can be seen with the naked eye.[19]

As discussed above NDIs are very much capable of intercalation because of their planar aromatic structure. Therefore, by using these properties, Takenaka *et al*. studied DNA sensing in detail, in this study NDIs, bearing two redox-active ferrocenyl moieties, (Figure 1.2) were used specifically to sense and discriminate between double-stranded DNA (dsDNA) and single stranded DNA (ssDNA) by electrochemical methods. In the observation it was found that the dsDNA/NDI complex is thermodynamically and kinetically more stable than the complex ssDNA/NDI because of the NDIs capacity to intercalate with the former dsDNA.[20]

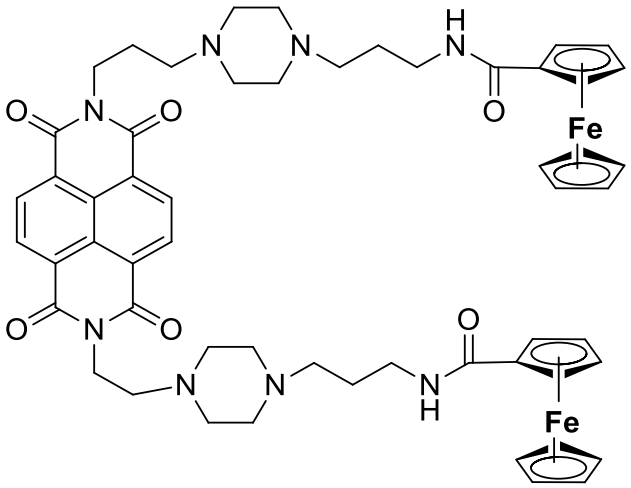

4

Figure 1.2: Naphthalene diimide derivative **4**

From this initial study, considerable research has been carried out in which NDI used

as a host component for sensing of ions such as anions, cations, and amines.

1.2.2 NDI as anion Sensors:

Recently considerable research has been carried out to study the anion−π interaction among electron-deficient arenes mainly NDI-based systems and anions in both of the chemical[21] and biological systems.[22] In this direction Haldar group designed and synthesized two NDI moieties connected to L-phenylalanine **(5)** (Figure 1.3) and L-tyrosine through an imide linkage to form donor-acceptor derivatives and successfully used for self-assembly and fluoride-sensing via H-bonding and π-π stacking.

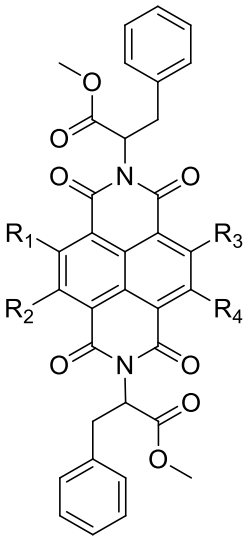

5

Figure 1.3: Structure of NDI moieties connected to L-phenylalanine **5**

In aqueous media, synthesized NDIs used as turn-on fluorescence by fluoride sensing through single-electron-transfer reaction specifically.[23]

As we know NDIs due to its small size, soluble in a wide-range of solvents, very easy to functionalize and they have tunable fluorescent properties mainly helps them to makes desirable sensors. In 2009 our group designed and synthesized novel, fluorescent and neutral core-substituted NDI chromophores appended with *N*,*N*′-bissulfonamide-quinoxalines (**6**) (Figure 1.4) acts as selective colorimetric sensors for fluoride (F^-) ions at micromolar

concentration efficiently.[24] Notably, the designed sensor was shown to be highly selective for fluoride ion with Ka ~ 1.2 ± 0.5×10^6 M^{-1} over other anions such as $H_2PO_4^-$, AcO^-, Cl^-, Br^-, I^-, and HSO_4^- in DMSO solvent. In the observation it was found that on addition of fluoride ions to the NDI in DMSO solvent, a significant bathochromic shift of 100 nm and such sensing of fluoride ions can be observed by naked eye selectively over the other ions.[25]

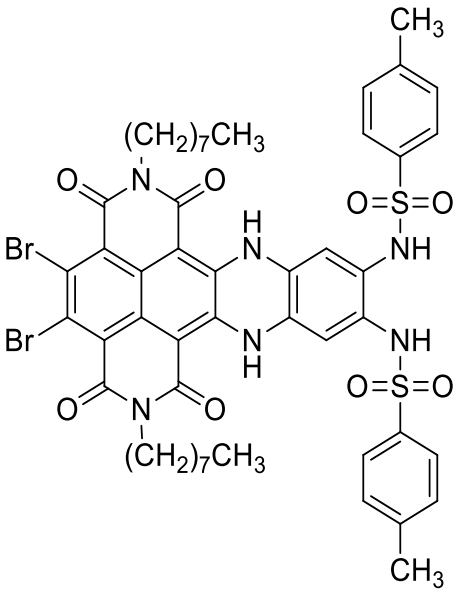

6

Figure 1.4: Structure of NDI chromophores appended with *N*,*N*′-bissulfonamide-quinoxalines **6**

1.2.3 NDI as Cation Sensors:

Recently considerable research has been carried out in which NDIs moieties were used for sensing of different cations. In 2012 Mukhopadhyay *et al*. studied and demonstrated the development of a persistent radical cation in an NDI moiety (**7**) with Cu^{2+}/ Fe^{3+} metal ions, and further immediate generation of the NDI radical ion with reducing anion in THF solvent, in the presence of the CN^- anion particularly. In the observation color changes from deep-blue to brown-red within 10 minutes and UV-Vis absorption spectroscopy were used to characterize such formation of cation and anion. (Figure 1.5).[26]

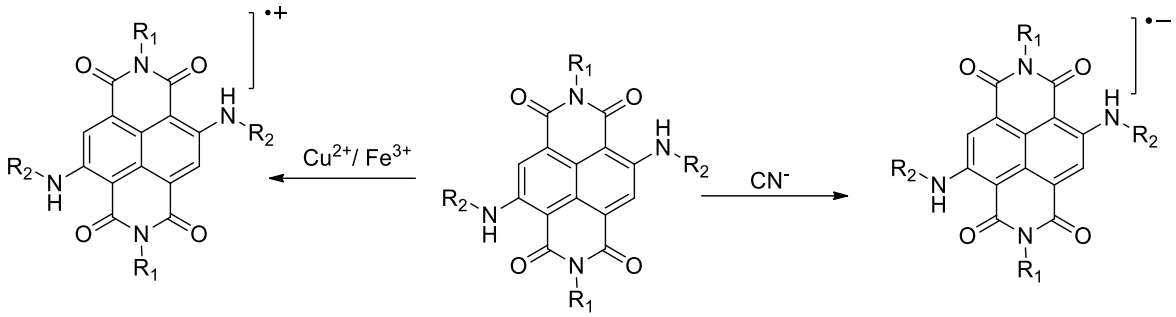

7

Figure 1.5: Structures of NDI moieties (**7**) with Cu^{2+}/ Fe^{3+} metal ions and CN^- to form radical cation and radical anion respectively

Similarly in 2016, Bhosale group designed and synthesized receptor based on NDI (**8**) applied for selective detection of Cu^{2+} and Fe^{3+} ions as compared to other metal ions such as Pb^{2+}, Zn^{2+}, Ba^{2+}, Mg^{2+}, Mn^{2+}, Ni^{2+}, Co^{2+}, and Cr^{3+} were studied in detail.[27] The developed NDI based receptor (Figure 1.6) is found to be active both optically and calorimetrically. In conclusion, due to simple nature and cost-effectiveness this receptor would be an excellent colorimetric sensing platform to determine trace amounts of Cu^{2+} and Fe^{3+} ions selectively.

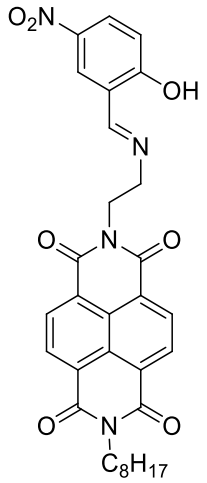

8

Figure 1.6: Structure of NDI based receptor **8**

1.2.4 NDI as pH Sensors

From the reported literature it was also found that core substituted NDIs possesses strong photoluminescence moreover it was also observed that when substituents on NDI changes it affects absorbance and fluorescence of the NDI undergo favorable photophysical changes necessary to act as excellent sensor.

In another study by Li group reported a new pH-controlled fluorescence switch based on molecule pentacyclic-core-substituted NDI. For the synthesis of targeted switch, NDI allowed to react with 1,8-diazabicyclo[5.4.0]undec-7-ene (DBU) in the presence of CuI in THF/toluene solvent at 70 °C to give green colored product. Synthesized NDI-DBU (**9**) acts as a wonderful pH sensor (Figure 1.7), it was confirmed from its absorption and emission spectra which shows dramatic changes (turn-on fluorescence) upon addition of trifluoroacetic acid (TFA) in MeCN solution, and on further addition of triethylamine (TEA) it reversed to original (turn-off fluorescence). Also up to seven cycles, compound shows reversible performance without losing any activity.[28]

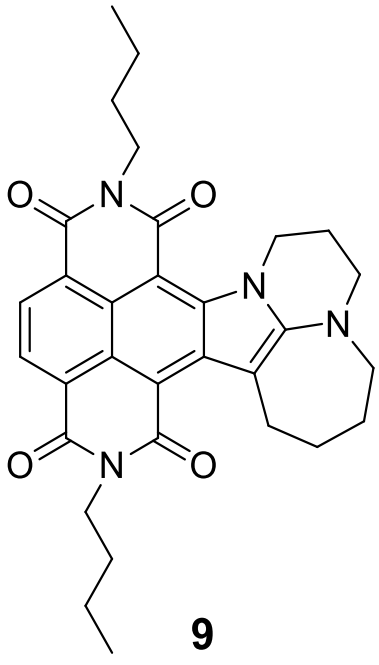

9

Figure 1.7: Structure of NDI-DBU pH sensor **9**

With same concept in 2011 Cox *et al*. designed and synthesized cNDI substituted piperidine on both sides of the NDI (**10**) displayed a reversible switch on−off response through both color and emission by alternative addition of trifluoroacetic acid (TFA) and triethylamine (TEA) in chloroform solution.[29] In 2012 again Cox *et al*. synthesized cNDI functionalized with piperidine at only one side (**11**) exhibited similar response. (Figure 1.8).[30]

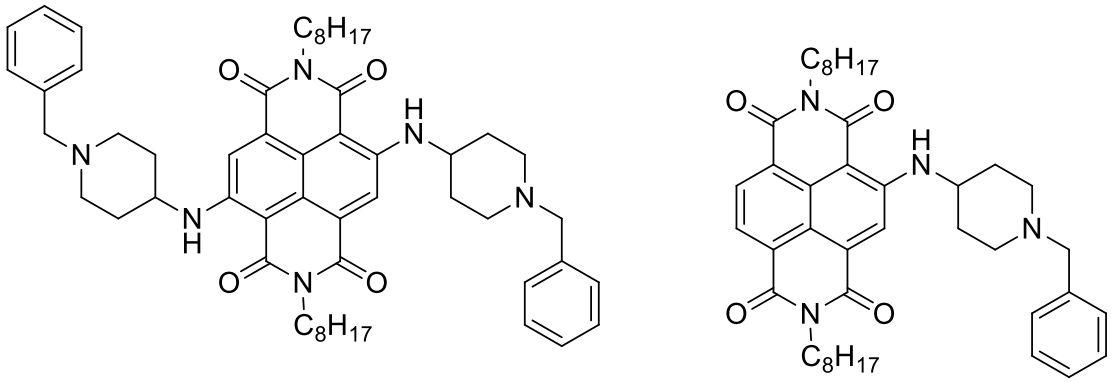

10 **11**

Figure 1.8: Structure of cNDI substituted piperidine as pH sensors **10** & **11**

With similar approach, our research group in 2013 reported pyridyl-monoannulated cNDI (**12**) motif and studied for its dual applications such as a reversible probe for acid/base sensing and Py-cNDI (**12**) self-assembled into a different nanostructures, moreover the morphology of these nanostructures is dependent on the pH and the solvent polarity mainly (Figure 1.9).[31]

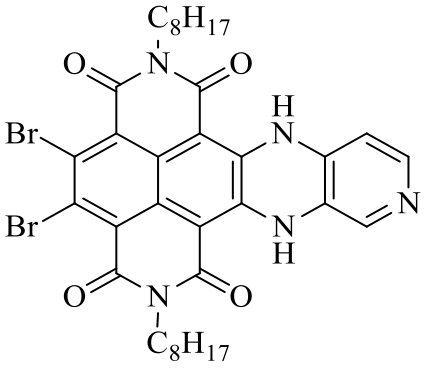

12

Figure 1.9: Structure of pyridyl-monoannulated cNDI as pH sensors **12**

In the above discussion we explore the developments of NDIs and cNDIs in the field of molecular sensing, anionic and cationic sensing, pH sensors and artificial photosynthesis, i.e. energy and electron transduction systems by using the covalent and supramolecular self-assembly approach.

1.3 Tetraphenylethylene (TPE) based Photoswitchable molecules

There is considerable interest in the area of nanotechnology in which carbon nanotube (CNT) are efficiently used as promising scaffolds.[32,33] Mainly CNTs are of two types, can be either (1) single-walled (SWCNT),[34] or (2) multi-walled (MWCNTs),[35] Both nanotubes having similar properties like high thermal and electrical conductivity because of which successfully applied in different fields.

Interestingly, in this area controlled reversible photoswitching of conductivity by using an external stimulus at the molecular level remains as challenging task. Till now from reported work, tetraphenylethylene (TPE) unit with four phenyl groups, a well-known system for its Aggregation-induced emission (AIE) properties applied as a building block for receptors of carbon-based frameworks successfully [36, 37]

Aggregation-induced emission (AIE) is another important photophysical phenomenon associated with chromophore aggregation at the molecular level.[38] Generally in the AIE process, due to aggregate formation non-emissive luminogens are induced to emit.[39] The term “luminophores” is used for emissive chromophores as molecular species and term “luminogens” is used for non-emissive as molecules but emissive under proper conditions such as aggregates. Particularly luminogens showing AIE features are termed as AIEgens.

In 2019 our group studied and reported for the issue discussed above, our group designed and synthesized photoswitchable TPE based supramolecular host (13) which can

control C_{60} binding and release on demand and also can encapsulate C_{60} in the Z-form with a noticeably different visual colour change. Different spectroscopic methods and mass spectrometry were used to characterize the Z-1 bound C_{60}. In the visible light (>490nm), it was observed that the host switches to the E-form at that time C_{60} is disassembled from the host due to structural complementarity with the guest is destroyed (Figure 1.10).[37]

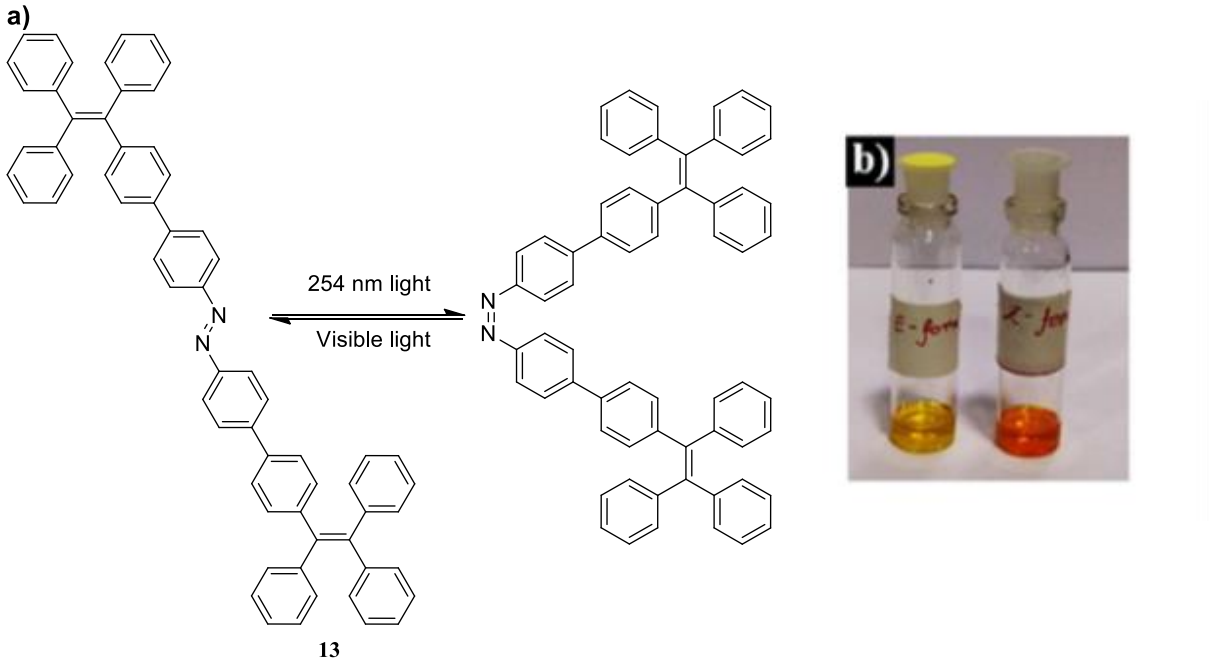

Figure 1.10: Photoswitchable TPE based supramolecular host: (a) chemical illustration of E-Z isomerization of the molecule 13. (b) Naked eye visualisation of E-Z isomers.

In another study of TPE which still retain the AIE property, though there is displacement of one phenyl ring or two phenyl rings. An analogue of TPE, namely, compound 14, was therefore constructed.[40] shows typical AIE behaviours displaying considerable emission enhancement in its THF/water mixtures with fw > 60 vol %. Similar analogues of TPE such as compound 15, 16 and 17 are reported and as per characteristics of AIE, all these analogues are non-emissive in the solution state but highly emissive in the aggregate or solid state[41] (Figure 1.11).[42], [43]

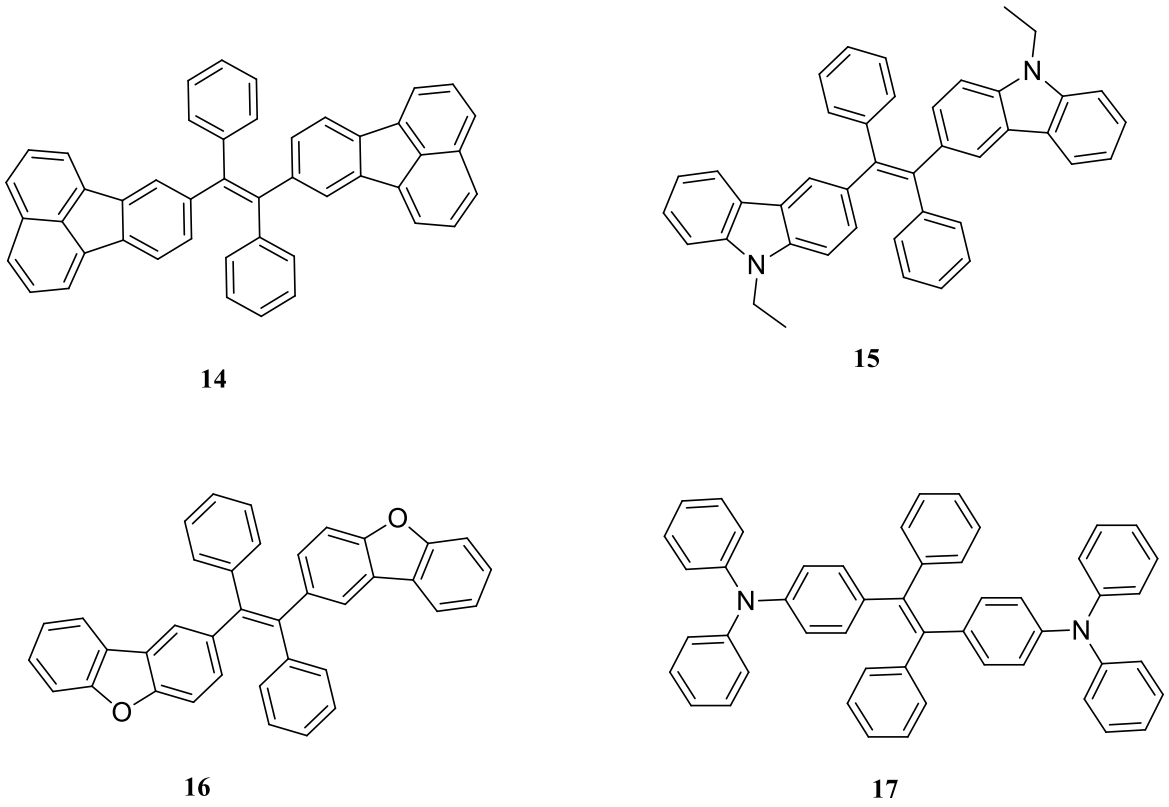

14 **15** **16** **17**

Figure 1.11: Structures of analogues of TPE **14, 15, 16** and **17**.

1.4 New Class of AIEgen based on Tetraarylpyrrolo [3,2-b] pyrroles (TAPP) as Novel Organic Photoluminiscent Material

1.4.1 Introduction of Tetraarylpyrrolo [3,2-b] pyrroles (TAPP)

In the recent years, there is considerable interest in the study of interaction of light with luminogens because of its variety of applications in the field of photochemical processes, sensing and other developing technologies. The term luminescence refers to a process in which a molecule upon excitation, emits light generally and may be affected by the aggregation of the molecule, mainly depending on the interaction which may either induce the emission or quench.[44] Currently in the reported work, based on luminophore molecules that emit in the aggregated state was found to be stimulating applications such as organic

field-effect transistors (OFETs) and organic light-emitting diodes (OLEDs).[45] Among these luminophore molecules, Tetraphenylethylene (TPE) (**18**) is one of the best examples of aggregation-induced emission luminogens (AIEgens) because in the aggregated or solid state, it form highly luminescent materials (Figure 1.12). Tetraphenylethylene (TPE) looks like propeller-shaped molecule that generally self-assemble, results into the aggregation-induced emissive (AIE) effect with emission of light till the solvent environment permits the self-assembly to occur in the system.[46] All such processes observed because of restricted intramolecular rotation shown by TPE molecule. Also these molecules exhibit dynamic rotation in solution, whereas rotation is restricted in the aggregated state, which results into the emission phenomenon.[36,46] Some examples of common AIEgens that are reported to show AIE activity in the solid states and aggregated state are shown in figure 1.12 list.[47, 48] In the literature work, though there are number of AIEgens capable for supramolecular self-assembly in several applications but they show several drawbacks, like tedious synthetic methods leading to poor yield and also because of expensive reagents used in synthetic methods. Therefore, it is very much essential to search new AIEgens that can be easily synthesized by using low-cost reagents generally in one- or two-step processes.

In recent times, tetraarylpyrrolo[3,2-b]pyrroles (TAPPs) have been reported to be suitable AIEgens (Figure 1.13) with simple synthetic protocol and can be synthesized in a single step easily from low-cost starting materials. Remarkably, isolation of products can be done by simple filtration and no need for column chromatography techniques and other purification methods and can also be easily functionalized to suit targeted applications effectively.[45] TAPP has a unique favorable combination of both photophysical and electronic properties mainly useful in solar cells optoelectronics and organic photovoltaics.[49]

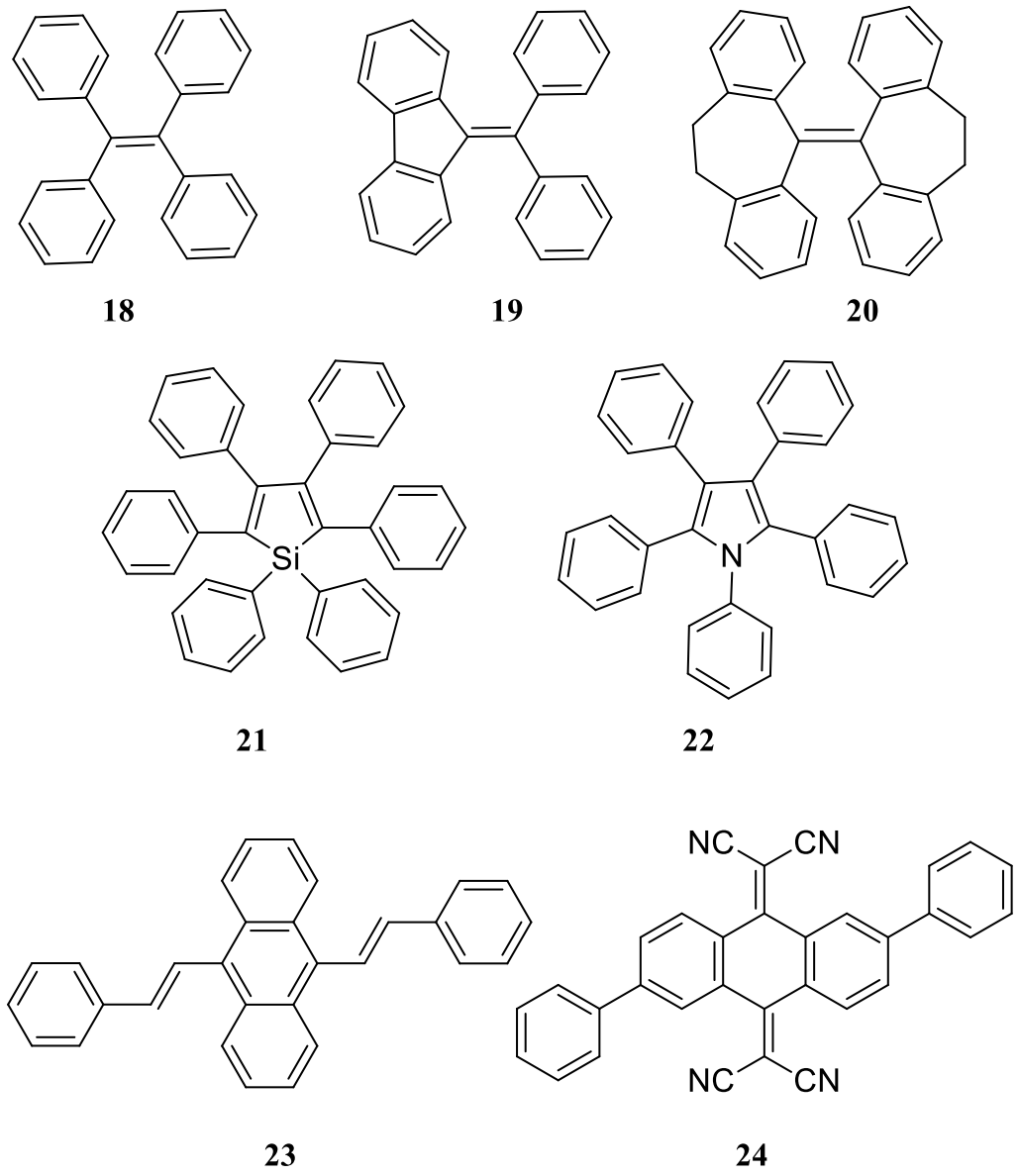

Figure 1.12: Various substituted AIEgens.

It is very important to know the proper functionalization in organic compounds, with basic understanding of structure–function relationships and also their linear and nonlinear optical properties necessary for OLEDs, OFETs and organic photovoltaics applications successfully.[50],[51]

In this chapter, we introduce the new AIE-active TAPP class of molecules and derivatives through different synthetic routes and present their emergent applications. The

progress of new fluorescent dyes has successfully proved to be an important field of organic chemistry, and the need for dyes with a broad range of spectral and physicochemical properties is growing day by day. As we know that classic fluorescent chemical classes such as coumarins,[52] fluorescein,[53] and BODIPY[54] reported but in addition to these, a larger range of molecule classes are needed for effective applications.[55] In the area concern new dyes for specialized applications including single-photon fluorescence imaging,[45] two-photon absorption, and two-photon fluorescence microscopy are still required.[56] It was found that, TAPP derivatives are the least studied family of 10 π electron heterocycles called di-heteropentalenes. The similar thieno[3,2-b]-thiophene and thieno[3,2-b]pyrrole cores are well known and have been thoroughly studied and utilized in diverse fields of research. Actually their electronic structures make them interesting from both theoretical and synthetic perspectives, with applications as polymers for OLEDs, and photovoltaics,[57] in optoelectronics, as well as organic dyes in dye-sensitized solar cells.[58]

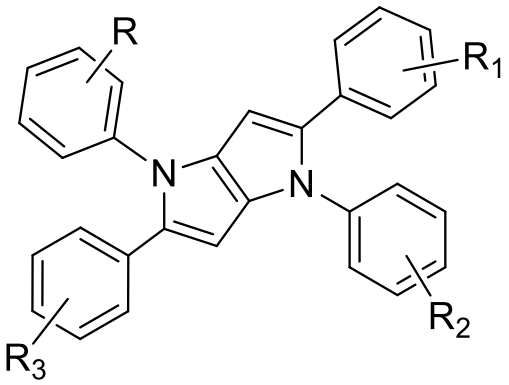

Figure 1.13: General structure of TAPP

Interestingly in addition to their applications in material science, thieno[3,2-b]thiophenes and thieno[3,2-b]pyrroles have also found use in biology and medicine.[38] The

1,4-dihydropyrrolo[3,2-b]pyrrole scaffold was discovered in 1972 by Hemetsberger and Knittel.[59] Only a few methods for the synthesis of these cores were known until 2013, all requiring multiple-step synthesis in low overall yields. Mukai and coworkers obtained a derivative of TAPP from the reaction between 1,4-bis(trimethylsilyl)benzene and methyl azido formate followed by subsequent oxidation by DDQ.[60] In spite of many advantages such as the simple one-pot synthesis, inexpensive starting materials and very easy isolation methods, it results to low-to-average overall yields. Actually more efficient synthetic methods are thus still needed, despite dramatic progress in the recent years.

1.4.2 The Accidental Discovery of TAPP

The start of research work on TAPP and its derivatives was quite incidental. Krzeszewski *et al*.[49] reported the accidental discovery of TAPP in a condensation reaction between 4-cyanobenzaldehyde (**25**), p-toluidine (**26**), and butane-2,3-dione (**27**) resulted into fluorescent yellow crystalline product that is TAPP (1,2,4,5-tetraarylpyrrolo[3,2-b]pyrrole (**29**) (Figure 1.14) as a main product, whereas the expected imidazole (**28**) product was only observed in a 2% yield. The exciting properties of product **29** led to further studies on better synthetic routes.

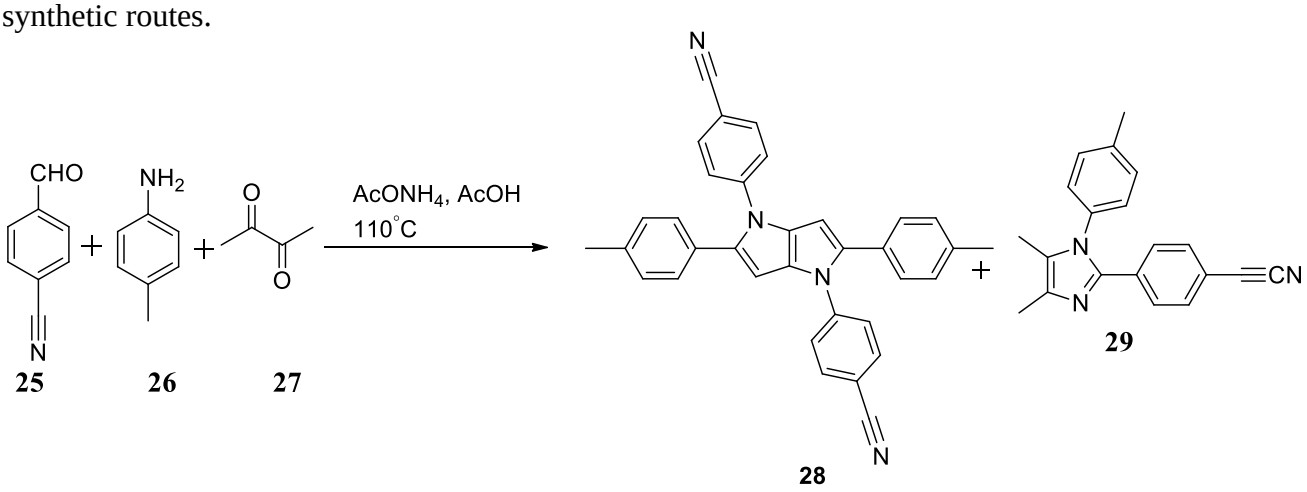

Figure 1.14: Accidental discovery of the multicomponent reaction leading to TAPP: tetraarylpyrrolo[3,2-b]pyrrole (**29**).[49]

1.4.3 Synthesis of TAPP

In the reported work, the procedure for the viable synthesis of TAPP derivatives is a one-pot reaction, where the product can be isolated by a simple filtration easily. A multicomponent reaction mixture of an aromatic aldehyde, an aromatic amine, and butane-2,3-dione in the presence of a suitable acid catalyst leads to TAPP, whereas aliphatic amines and ketones do not react. There are a range of aromatic aldehydes and aromatic amines commercially available for the synthesis of new derivatives of TAPP.[49] From 1,4-dihydropyrrolo[3,2-b]pyrroles, known since 1972, TAPP was prepared for the first time in a one-pot synthesis in 2013.[45] There is tremendous scope to increase the yield of TAPP, which is quite low. In the literature studies, it was suggested that using a catalytic amount of strong acid increases the reaction yield, and with p-toluene sulfonic acid (PTSA), the yield was improved up to 49%.[61]

In another report, Gryko group developed 2,5-bis(azulenyl)pyrrolo[3,2-b]pyrroles bearing two azulene moieties at positions 2 and 5 (**30, 31**) (Figure 1.15).[62] The important step in this synthesis is the three-step transformation of pyridine scaffolds into azulene via sequential N-arylation, followed by ring-opening and reaction with cyclopentadiene. The synthesized molecules found to show excellent optical properties such as bathochromically shifted absorption. As azulene can stabilize a charge-separated structure, the photophysical properties of these TAPP derivatives are very interesting.

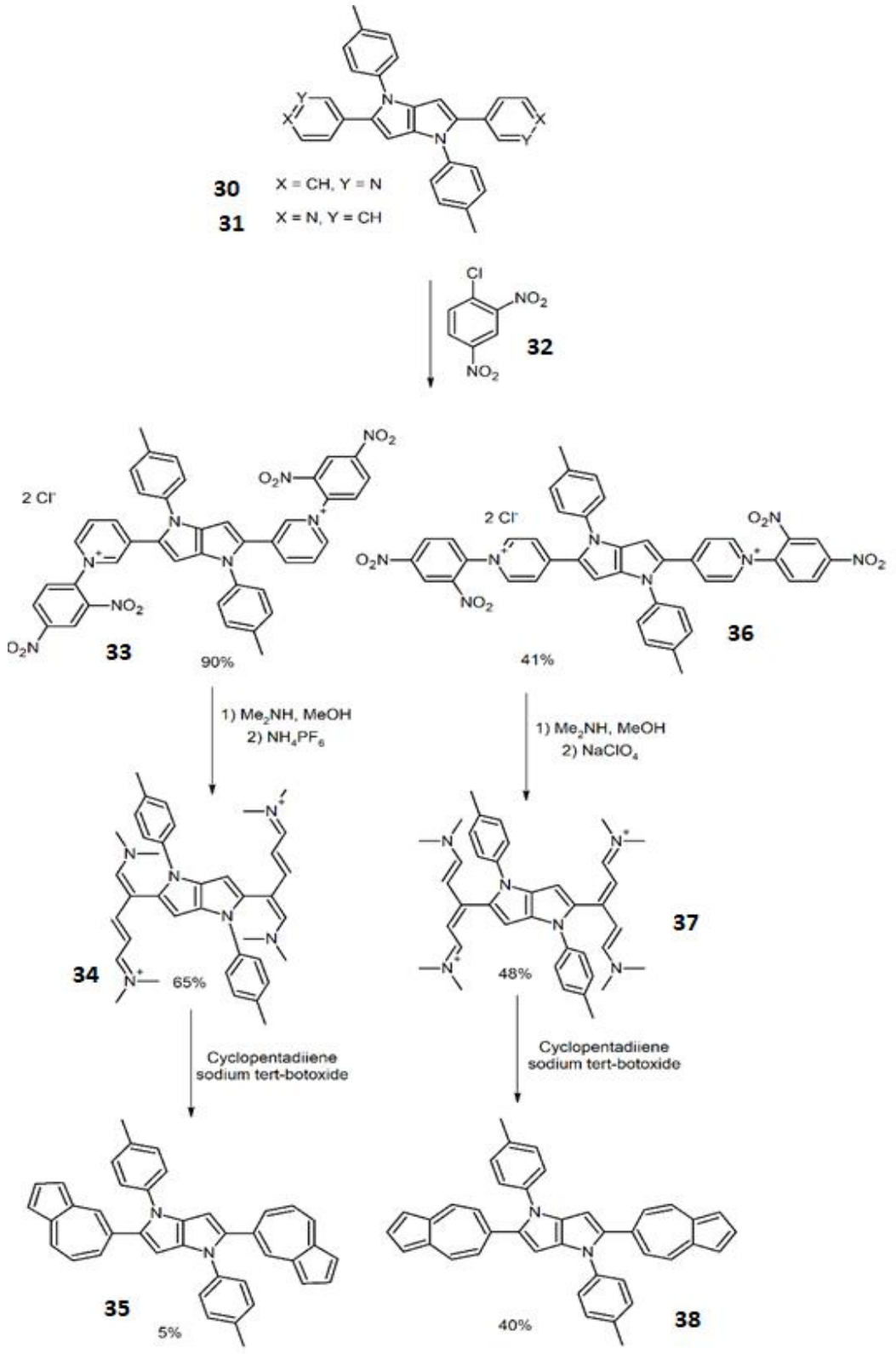

Figure 1.15: The synthetic transformation of heterocycles (**30, 31**) into bis-azulenyl TAPPs (**35, 38**).[62]

This group further reported the synthesis of a heteroatom-doped buckybowl (**39**), containing two fused nitrogen-doped pentagonal rings (pyrrolopyrrole core), and also studied their optoelectronic and physicochemical properties in detail (see Figure 1.16).[63]

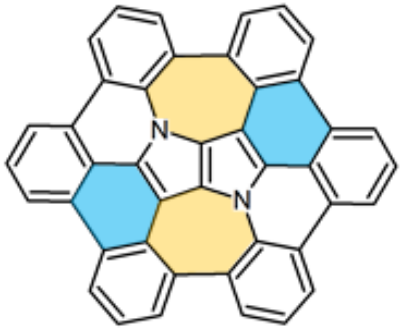

39

Figure 1.16: Fully conjugated nitrogenembedded buckybowl. [63]

Hemetsberger and Knittel group in 1972, synthesized first compound bearing the 1,4-dihydropyrrolo [3,2-b]pyrrole (**42**) core in a two-step reaction (see Figure 1.17). The reaction of 2-formyl-methylpyrrole (**40**) with ethyl azidoacetate followed by thermal cyclization led to pyrrolo [3,2-b]pyrrole.[64]

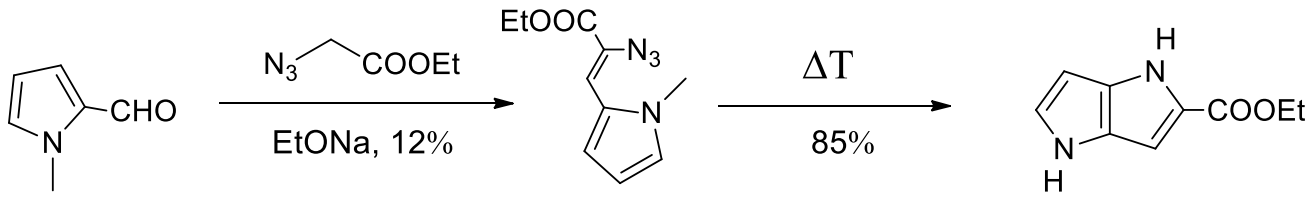

40 **41** **42**

Figure 1.17: The Hemetsberger approach toward 1,4 dihydropyrrolo[3,2-b]pyrroles (**42**). [64]

Afterwards Aratani and coworkers synthesized a larger aromatic core, leading to the 1,4-dihydropyrrolo[3,2-b]pyrrole (**47**) skeleton (see Figure 1.18).[65]

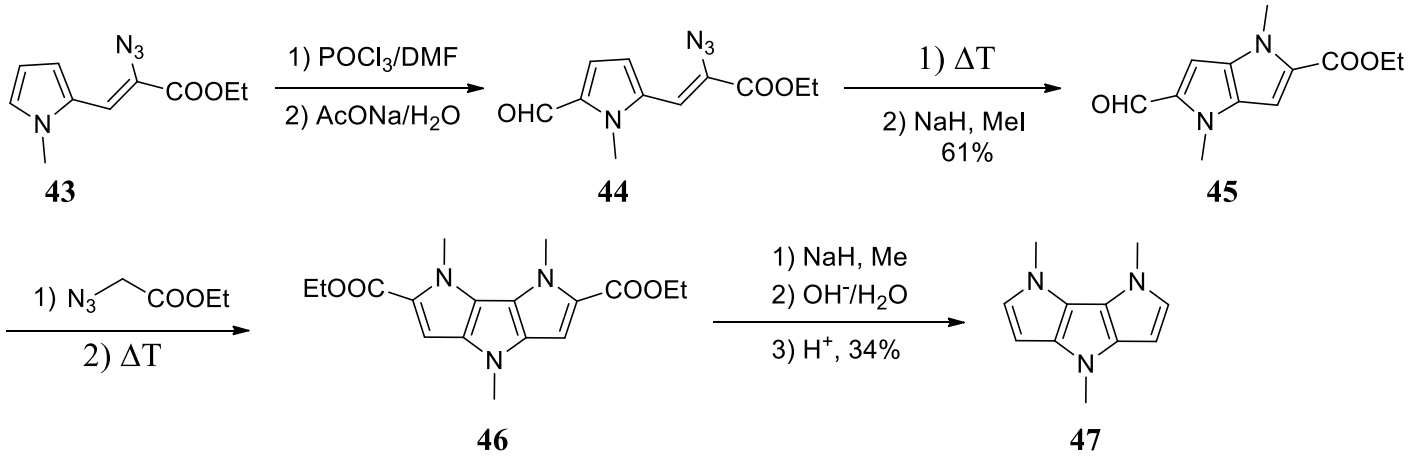

Figure 1.18: The synthesis of dipyrrolo[3,2-b:2′,3′-d]pyrrole (**47**).[65]

One more important derivative is 1,4-dihydropyrrolo[3,2-b]pyrrole, where the commercially significant Maillard reaction was used to produce 1,4-dihydropyrrolo[3,2-b]pyrrole derivatives, commonly known as melanoids,[66,67] which are natural, brown polymers (see Figure 1.19).[68,69]

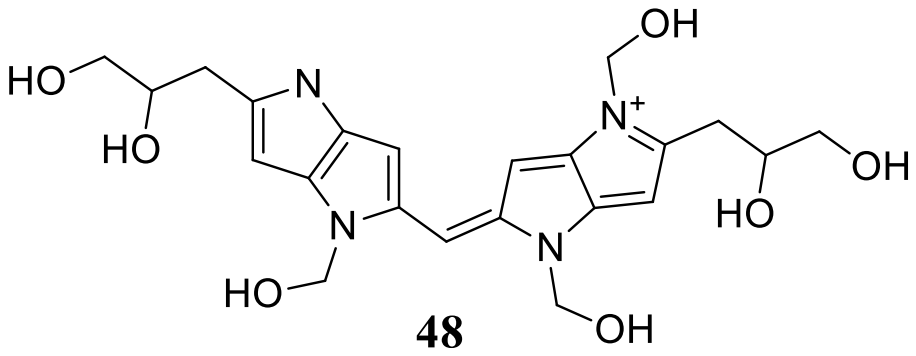

Figure 1.19: Maillard reaction product[66-69]

Moreover, Gryko group design and synthesized remarkable ladder-type electron-rich heterohexacene structure in a two-step reaction. Dihydropyrrolo[3,2-b]pyrroles bearing two 2-nitrophenyl (**49**) units were transformed into final products such as diindolo[2,3-b:2′,3′-

f]pyrrolo[3,2-b]pyrroles (**51**), representing the longest ladder-type heteroacenes, through double Cadogan reactions. These compounds were found to be stable in the presence of oxygen and chlorinated solvent, and in nonchlorinated solvents, they were found to be photostable. These compounds show a violet-blue fluorescence in solution and very interesting optical and electrochemical properties due to their electron-rich centres (see Figure 1.20).[70]

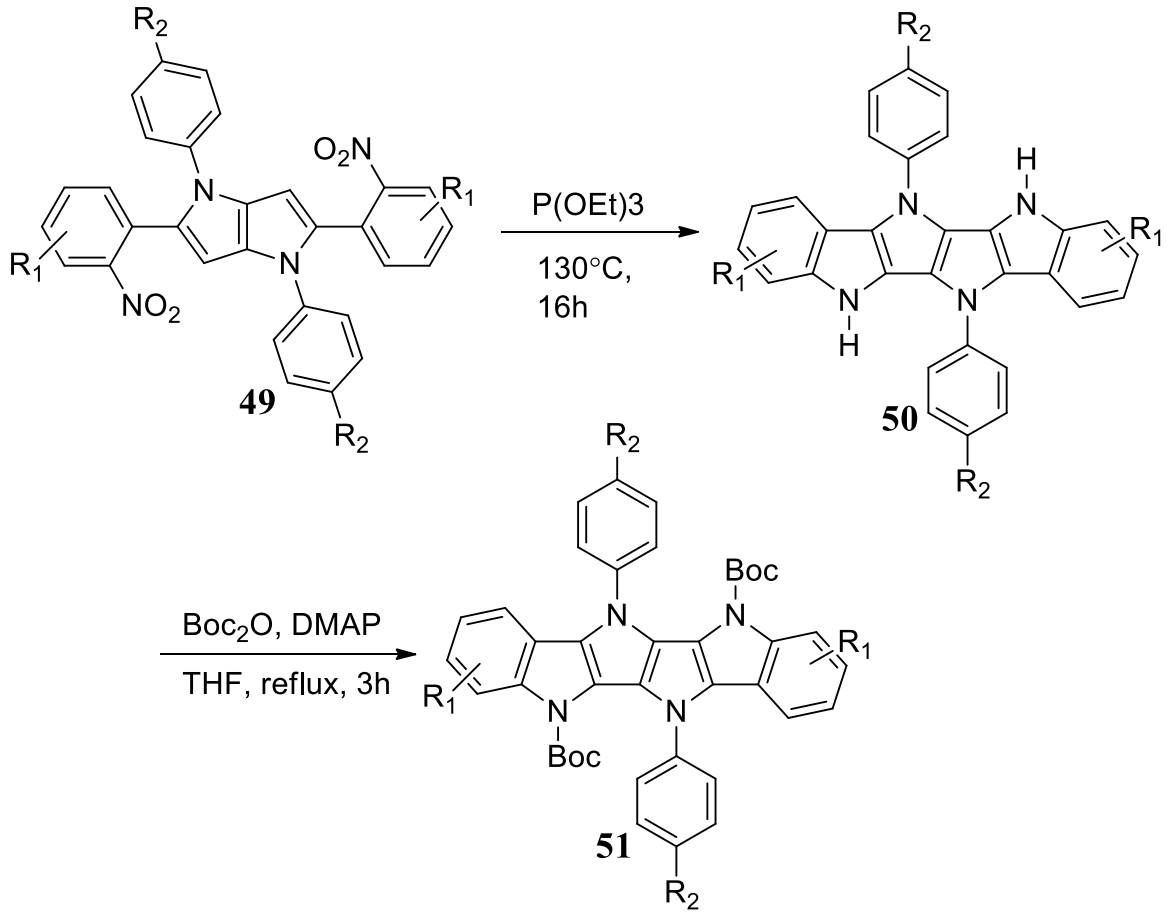

Figure 1.20: Two-step synthesis of heterohexacene (**51**).[70]

Additionally, Gryko group also established an efficient one-pot synthesis method of tetra-, penta-, and hexasubstituted derivatives of TAPP using various solvents, acids, and reaction temperatures, where they observed that PTSA is the best catalyst (see Table 1.1).

Table 1.1 Optimization of reaction conditions for synthesis of TAPP.[61]

Entry	Solvent	Catalyst	Temp, °C	% Yield
1	AcOH		90	35
2	TfOH		150	Tar
3	TsOH		150	Tar
4	TFA		80	0
5	AcOH	TFA	90	46
6	AcOH	H2SO4	90	36
7	AcOH	AlCl3	90	43
8	AcOH	TfOH	90	39
9	AcOH	TsOH	90	49
10	AcOH	TsOH	90	49
11	AcOH	TsOH	90	tar

Particularly, this method was very effective for sterically hindered aldehydes and substrates possessing strong electron-withdrawing groups such as CN and SF_5.[61] This group also developed a method for the synthesis of pyrrolo[3,2-b]pyrroles containing hexaphenyl benzene moieties at the 2 and 5 positions, or the 1 and 4 positions and observed that the reaction of formyl-hexaphenylbenzene (**52**) with 3,5-bis(tert-butyl)aniline (**53**) and biacetyl

(**54**) did not lead to the formation of the corresponding product (**55**) (see Figure 1.21). However, the reaction of amino-hexaphenylbenzene (**56**) with 2-methoxybenzaldehyde (**57**) and biacetyl (**54**) afforded the corresponding pyrrolo[3,2-b]pyrrole (**58**) in low yield (see Figure 1.21).[71] Pyrrolopyrole (**58**) exhibited strong violet emission and a large Stokes shift of approximately 5300 cm−1, suggesting that there is a large difference in the geometry of the ground and excited states of the molecule.[71]

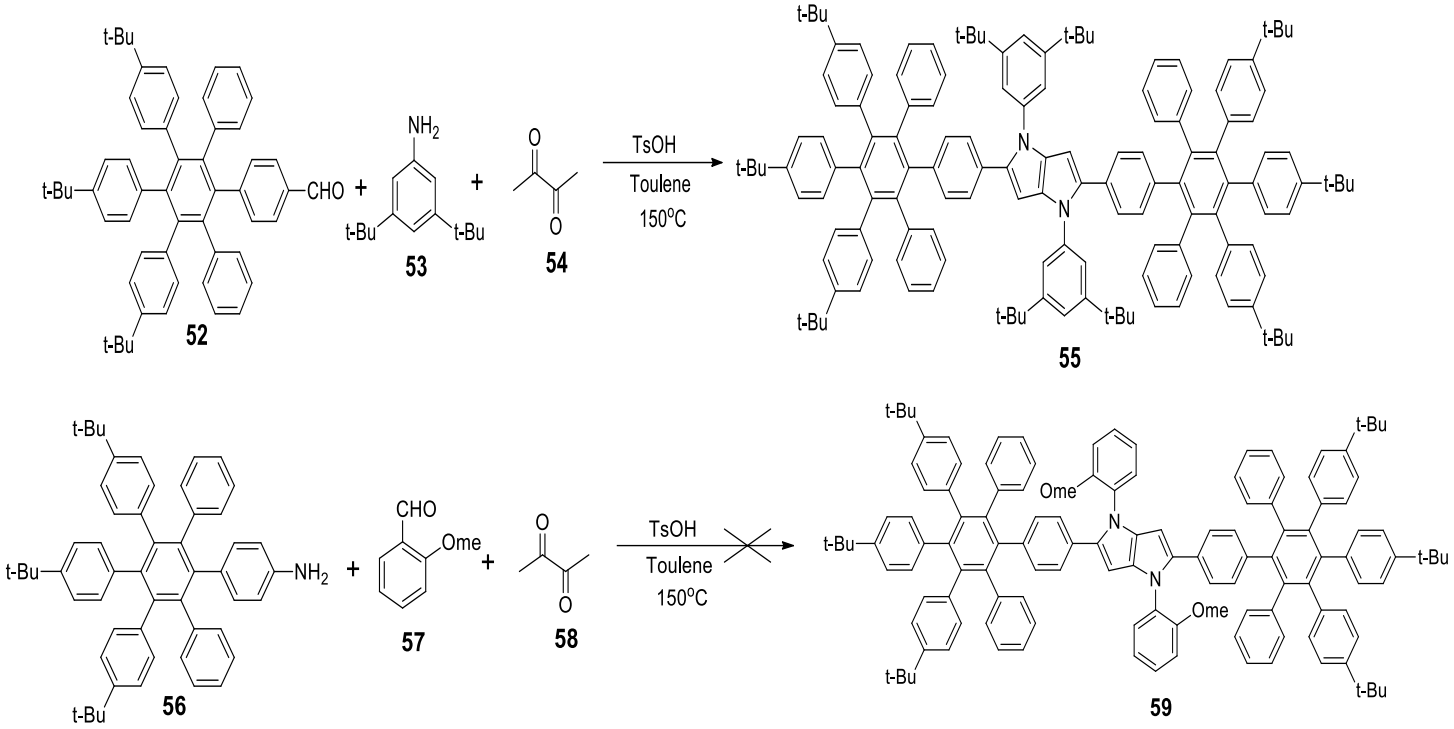

Figure 1.21: (a) Attempted multicomponent reaction leading to 2,5-bis(hexaphenyl)pyrrolo[3,2-b] pyrrole and (b) the synthesis of 2,5-bis(hexaphenyl)pyrrolo[3,2-b]pyrrole.[71]

1.4.4 Possible Mechanism of TAPP Synthesis

It has been postulated a plausible mechanism for the synthesis of TAPP derivatives. The intermediate tetrahydropyrrolo[3,2-b]pyrrole is oxidized by the excess of Schiff base present in the reaction mixture (Figure 1.22). Initially, enol formation of butan-2,3-dione takes

place, followed by iminium ion formation from the aromatic aldehyde, and the aromatic amine in the presence of acid occurs in the second step, and then the enol form of butane-2-3-dione attacks the highly unstable iminium ion. In the third step, intramolecular cyclization occurs to form an unstable N-substituted five-membered ring, which further reacts with the iminium ion followed by intramolecular cyclization and aerobic oxidation to give TAPP as a stable product. It is important to note that in the second step, acid plays an important role, and the choice of an acid affects the yield of the final product. From this study we can conclude, there is still scope to develop a higher yield protocol by changing the acid used in the reaction.

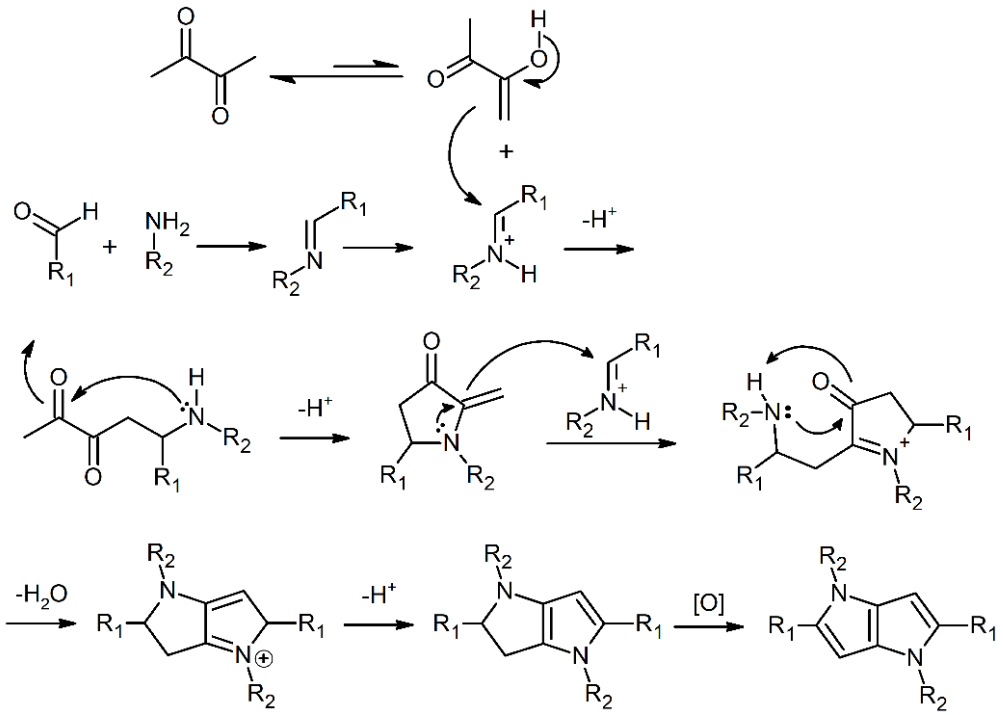

Figure 1.22: Plausible mechanism for the synthesis of TAPPs.[49]

It is notable that there are primary aromatic amines and aromatic aldehydes, such as those shown in Figure 1.23, which do not produce TAPP, and this suggests that the mechanism is favourable for aromatic amines and aldehydes for R_1 and R_2 in the mechanism proposed above[49]

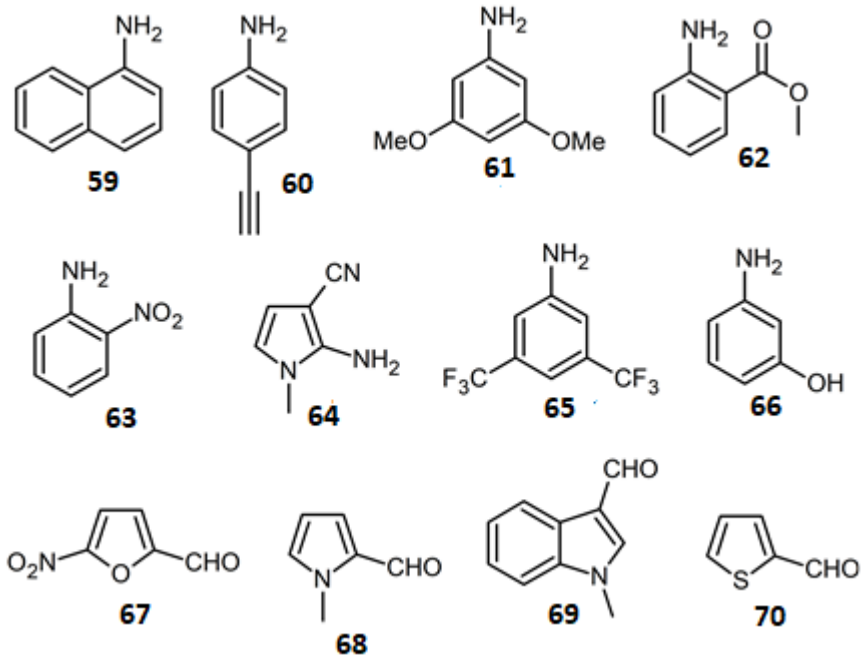

Figure 1.23: Substrate amines and aldehydes that do not produce TAPP derivatives.[49]

1.4.5 Reactivity of TAPP

By studying the TAPP structure, it possesses two electron-rich positions (positions 3 and 6), which are active sites for electrophilic aromatic substitution reactions including nitration, bromination, iodination, formylation, and cyanation with the chlorosulfonyl isocyanate/DMF system (see Figure 1.24).[65] Figure 1.23 displays how these active positions can be used to functionalize the core and change the electronic properties of the TAPP structure, allowing further elaboration of the TAPP core structure, as shown in selected examples in subsequent sections below.

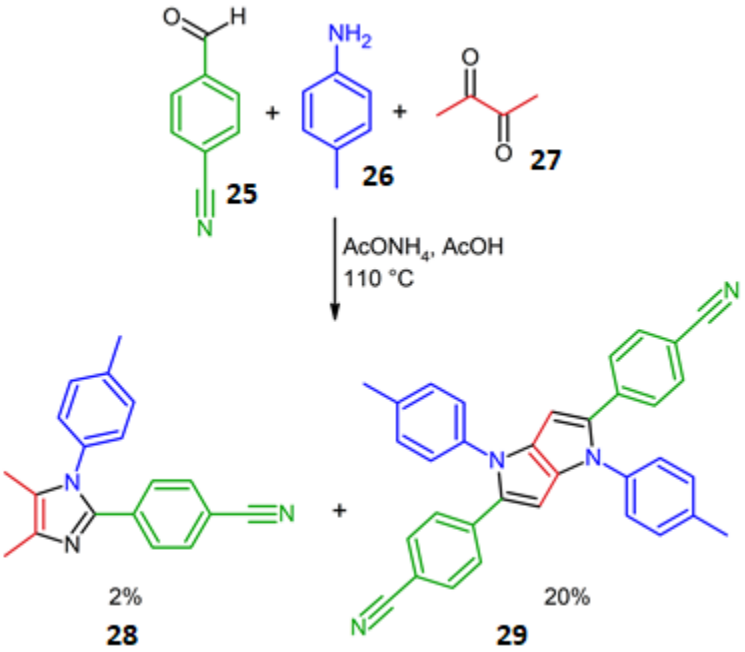

Figure 1.24: Electrophilic aromatic substitutions of TAPP.[49]

1.4.6 π-Expansion of TAPP

Particularly, 1,4-Dihydropyrrolo[3,2-b]pyrrole can be extended by using the Sonogashira coupling reaction[72] and direct arylation. The nitro group-functionalized TAPP (**75**) is very beneficial for the expansion of the π-system, as the reaction between nitro-substituted pyrrolo[3,2-b]pyrroles and triethyl phosphite results into the formation of products with extended π-systems containing four adjacent fused pyrrole rings.[49] Reduction of the nitro groups followed by reaction with t-butyl nitrate, dichlorophenylborane, and aldehydes leads to the formation of dicinnolinopyrrolo-[3,2-b]pyrroles (**77**),[70] pyrrolo[3,2- b]pyrrole-based BN heteroacenes (**78**),[73] and diquinolinopyrrolo[3,2-b]-pyrroles (**79**), respectively[74] (Figure 1.25).

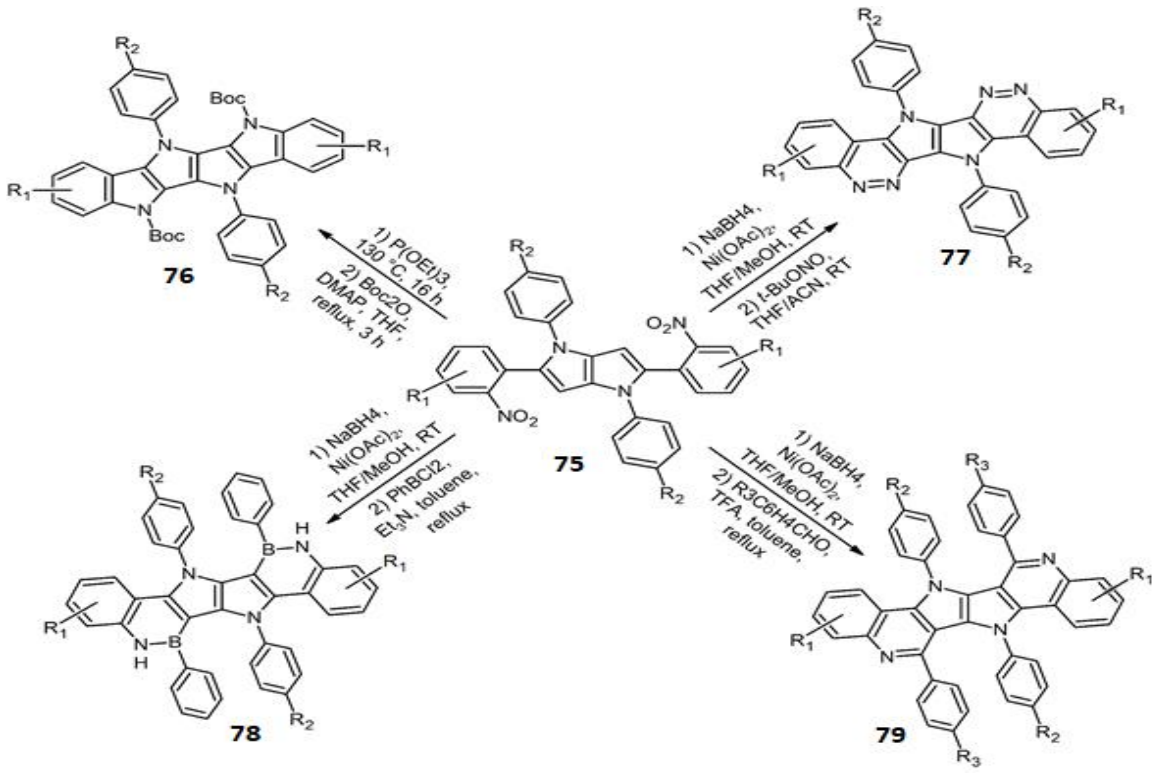

Figure 1.25: Various π-expanded aza analogues of TAPP.[49]

In recent times, the Dong and Tang groups[75] studied and reported the AIE behavior of the TAPP core substituted with electron-withdrawing moieties at the 1 and 4 positions.[76],[77] Janiga et al. described a synthesis of acceptor–donor–acceptor (A–D–A) TAPP derivatives linked via a triple bond and extended π-conjugation by using Sonogashira coupling reactions (see Table 1.2).[72]

Table 1.2 Optimization of the Sonogashira reaction leading to compound 4. [72]

Reaction conditions	% Yield
$Pd(PPh_3)_4$, CuI, Et_3N THF, 70 °C, 16 h	24
$Pd(PhCN)_2Cl_2$, $P(t\text{-}Bu)_3$, CuI, $HN(i\text{-}Pr)_2$, dioxane, rt, 16 h	0
Pd_2dba_3, $AsPh_3$, Et_3N, toluene, rt/80 °C, 24 h	20
Cs_2CO_3, CuI, DABCO, dioxane, 135 °C, 16 h	0
$Pd_2(dba)_3$, $P(t\text{-}Bu)_3$, Et_3N, THF, rt, 16 h	9
Cs_2CO_3, CuI, phenanthroline, dioxane, 135 °C, 16 h	10

In this study by using several reaction conditions, they found that only the silane version of the Sonogashira coupling reaction is an efficient method for the synthesis of desired products. Product (**80**) in figure 1.26 shows a strong absorption in the violet-blue region and also shows an intense blue-green fluorescence.

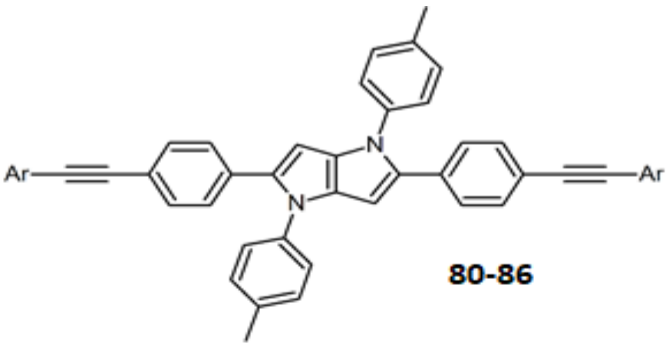

80-86

	Aryl halide	Yield (%)
80	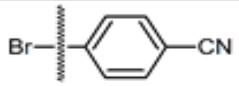	56
81	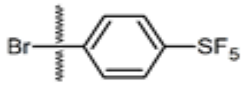	21
82	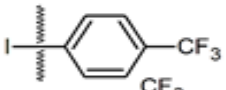	15
83	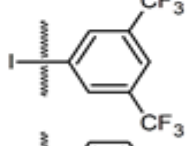	33
84	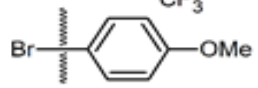	0
85	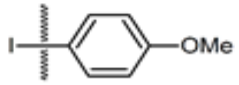	30
86	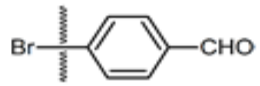	Traces

s

Figure 1.26: Results of the one-pot silane Sonogashira coupling reaction to give π-expanded TAPP molecules with quadrupolar, emission-tuneable 1,4-dihydropyrrolo[3,2-b]pyrroles[72]

In another study the Gryko group synthesized Z-shaped 1,4-dihydropyrrolo[3,2-b]-pyrroles having sterically hindered substituents via sila-Sonogashira reactions (see Figure 1.27).[78] In this reaction, due to presence of $InCl_3$ alkynes undergo rapid double annulation to give hexacyclic π-expanded indolo[3,2-b]indole products. Formed Z-shaped dyes show high fluorescence in solution and undergo radiative relaxation in high fluorescence quantum yield. As we know that, TAPPs possess two electron-rich free positions at positions 3 and 6, which offer an ideal site for a number of transformations that

increase the π-conjugation of the system, allowing the synthesis of organic π-conjugated materials by linking a chromophore with an aromatic unit.[49] In previous work it has been shown that steric hindrance plays a crucial role in the synthesis of TAPP.[48] Polycyclic aromatic and heterocyclic hydrocarbons having π-expanded structures have potential applications in OLEDs,[79],[80] OFETs,[81],[82] and dye-sensitized solar cells.[83]

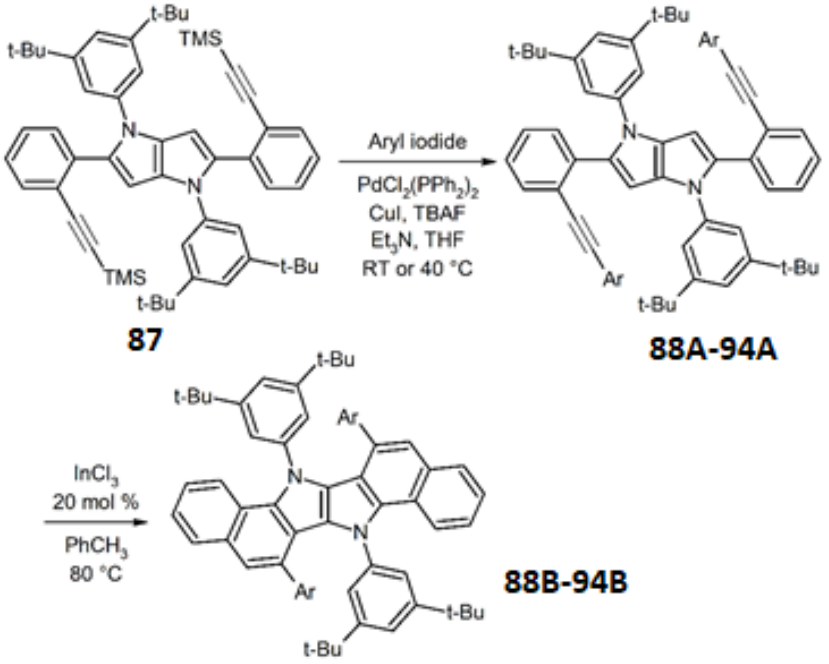

	Aryl	Yield (%) of A	Yield (%) of B
88	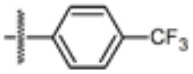	77	87
89	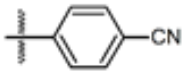	83	80
90	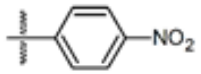	75	99
91	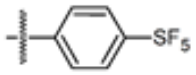	87	83
92	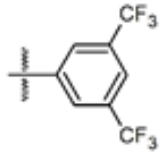	77	82
93	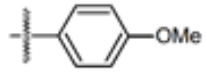	71	75
94	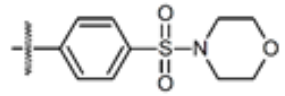	87	86

Figure 1.27: Synthesis of Z-shaped dyes and π-expanded indoloindoles[78]

1.4.7 π-Expanded 1,4-dihydropyrrolo[3,2-b]pyrrole

So far π-conjugated molecules are concern we know its importance in OLEDs, OFETs, and organic solar cells, expanding the π-conjugation of the TAPP molecule has been a primary

research objective of all researchers working in this field.[65] Out of these π-extended molecules, indolo[3,2-b]indole has been the most widely studied and investigated, comprising the pyrrolo[3,2-b]pyrrole skeleton (see Figure 1.28). There are few distinct methods reported for the synthesis of indolo[3,2-b]indole, also known as dibenzopyrrolo[3,2-b]pyrrole (**96**), have been proposed. Indolo[3,2-b]indole is a starting skeleton unsubstituted at the N-position of TAPP, and the favourable combination of optical properties and electron-rich character makes dibenzopyrrolo[3,2- b]pyrroles very beneficial in present technology.

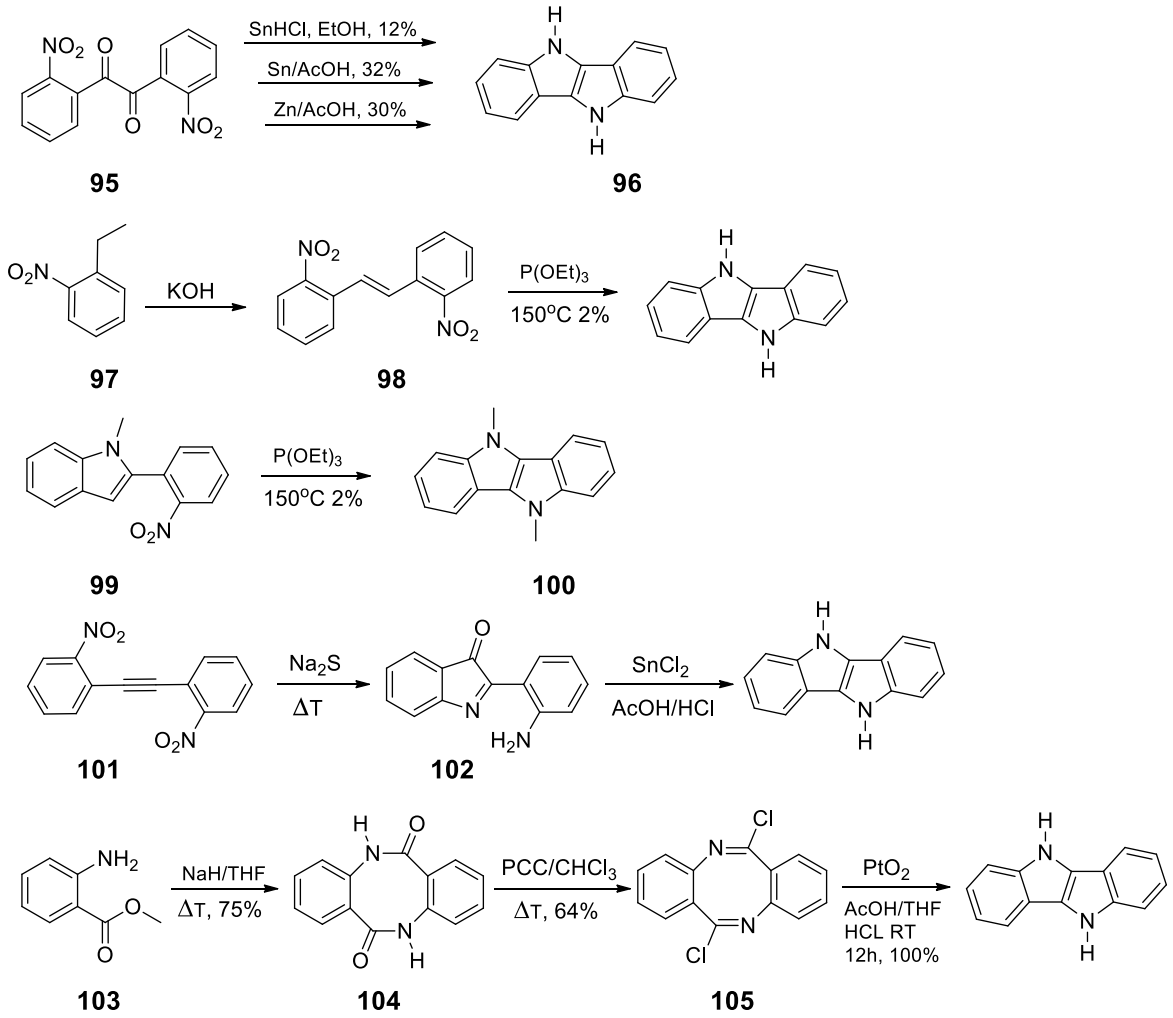

Figure 1.28: The historical routes, the Cadogan reaction, Ruggli's reaction, and Liu–Cooper route to indolo[3,2-b]indole through.[65]

In another study, Janiga *et al*. demonstrated the synthesis of diindolo[2,3-b:2′,3′-f]pyrrolo[3,2-b]pyrroles (**106**) comprising four pyrrole rings by a double Cadogan reaction for the first time successfully (see Figure 1.29)[65]

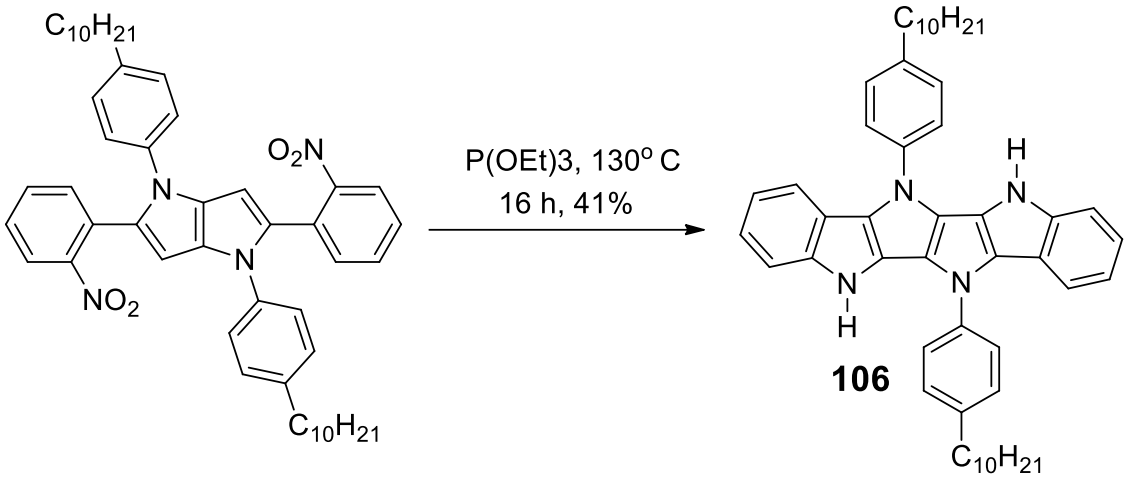

Figure 1.29: Synthesis of diindolo[2,3-b:2′,3′-f]pyrrolo [3,2-b]pyrroles.[65]

From the early studies it was assumed that, TAPP derivatives have A–D–A charge transfer characteristics and have thus been used in applications requiring this configuration effectively. Another research group Basak and coworkers presented 4-nitrophenyl and 3-nitrophenyl substituents at the 2 and 5 positions of TAPP and studied their performance in organic-resistive memory (ORM) devices, noting a significant difference in the behavior of the two molecules. The 2,5-bis(4-nitrophenyl)-TAPP derivative shows characteristics of a 'write-once– read-many' type of memory device, whereas 2,5-bis(3-nitrophenyl)-TAPP behaved like a 'write– read–erase–read' FLASH memory device.[84] Insertion of electron-donating substituents on TAPP permits strong electronic coupling between the electron-rich core and the substituents. Leung and coworkers studied and exposed a technique for the detection of $CHCl_3$ using a 2,5-bis(triphenylamine)-substituted (highly electron-donating) pyrrolo[3,2-b]pyrrole (TAPP), which forms coloured species upon reaction with $CHCl_3$,

permitting the quick detection of $CHCl_3$ with the naked eye easily.[85] Dong and coworkers studied and reported a altered method for chloroform detection; they observed a change in the emission of a thin film of 1,2,4,5- tetraphenylpyrrolo[3,2-b]pyrrole in the presence of chloroform and light.[86] It was found that introduction of more complex substituents on the nitrogen positions of TAPP generates three different polymorphic forms, which differ in emission maxima, and can be interconverted by exposure to chloroform vapour.[77] Langa and coworkers in other study inserted strong electron-withdrawing groups at positions 2 and 5 of TAPP but observed that the efficiency of these molecules in solar cells was limited because of low charge mobility.[87] Gryko *et al*. discovered that the multicomponent reactions of aldehydes, primary amines, and 2,3-butanedione yield TAPPs, and chemists have expanded the π-system of TAPP by taking advantage of these two free electron-rich positions on the TAPP core.[88] It is observed that, TAPP is often a symmetrical molecule, but unsymmetrical TAPP derivatives can be prepared by using two different benzaldehyde reagents.[89] An unsymmetrical product was observed in good yield with sterically hindered, crowded ortho-substituted benzaldehydes. In another study Mukai and coworkers reported the fast decomposition of TAPP parent molecules under ambient conditions due to the electron-rich nature of TAPP.[90] Because of four benzene rings, the decomposition of TAPP is prevented, and the first oxidation potential is reduced by electron-donating substituents, so that for some structures, oxygen decomposition is very fast in the presence of light, especially in solution. The synthesis of new ladder-type heterocenes is an area of research interest in material chemistry, which has led to heteroatoms being incorporated into heterocenes such as B,[91,92] N,[93,94] O,[95,96] Si,[97,98] P,[99, 100] and S,[101, 102] which were found to have applications in electro-optical fields. The central heteroatom was found to have the greatest effect on the photophysical and electrochemical properties of TAPP. Gryko group synthesized a family of TAPP molecules using different aromatic aldehydes, aromatic

amines, and diacetyls and studied their optical properties, observing that the fluorescence quantum yield decreased with increased polarity. The molecules showed emission in toluene and cyclohexane, but there was a sharp decrease in emission in solvents such as methanol, which may be due to hydrogen bonding in protic solvents. The Mathey group prepared phosphindole-fused ladder-type heteroacenes with a central TAPP core and observed that the newly synthesized molecules have high thermal stability, good luminescence efficiency, and tuneable conductivity. The conductivity measurements were undertaken by scanning tunnelling microscopy-break junction (STM-BJ) studies (see Figure 1.30).[103]

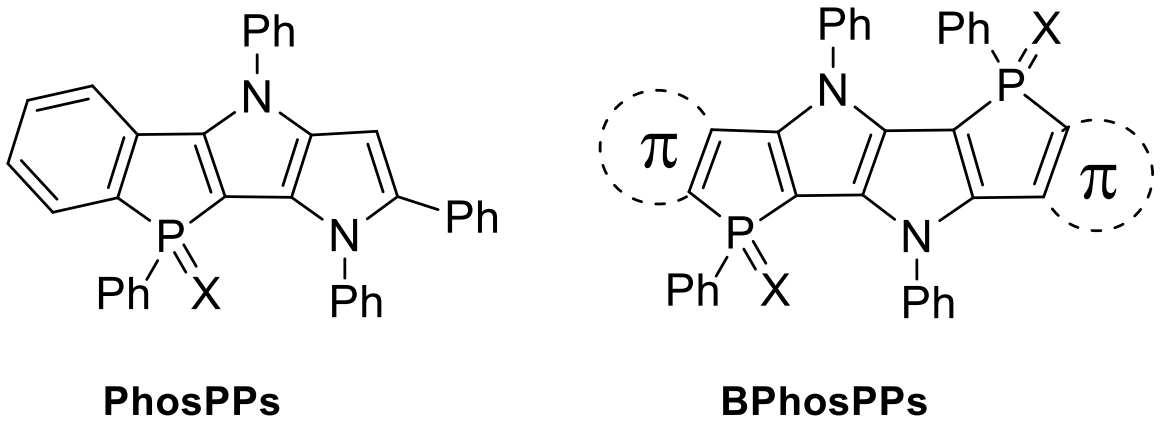

Figure 1.30: Fused phosphindolpyrrolo[3,2-b]pyrrole (PhosPP) and bisphosphindol-pyrrolo[3,2-b]pyrrole (BPhosPP) derivatives.[103]

To introduce a phosphorous atom into the TAPP core, a traditional dilithiobiaryl procedure was used by the François Mathey group, where the intramolecular noncatalyzed SEAr reaction of chlorophosphine provided the five-membered phosphole (**107, 108**) under mild conditions (see Figure 1.31). ^{31}P NMR spectra showed two peaks at δ = 75 ppm for diarylphosphine chloride and at $\delta = -32$ ppm for pyrrole-fused phosphines. These molecules showed interesting optical properties, with absorption at 393–440 nm in 4-(dicyanomethylene)-2-methyl-6-(4-(dimethylamino) styryl)-4H-pyran (DCM), which gradually increased to the long-wavelength region with an increase in π-conjugation. In

DCM, an intense photoluminescence emission was observed, with fluorescence quantum yields ranging from 28 to 87%.[103]

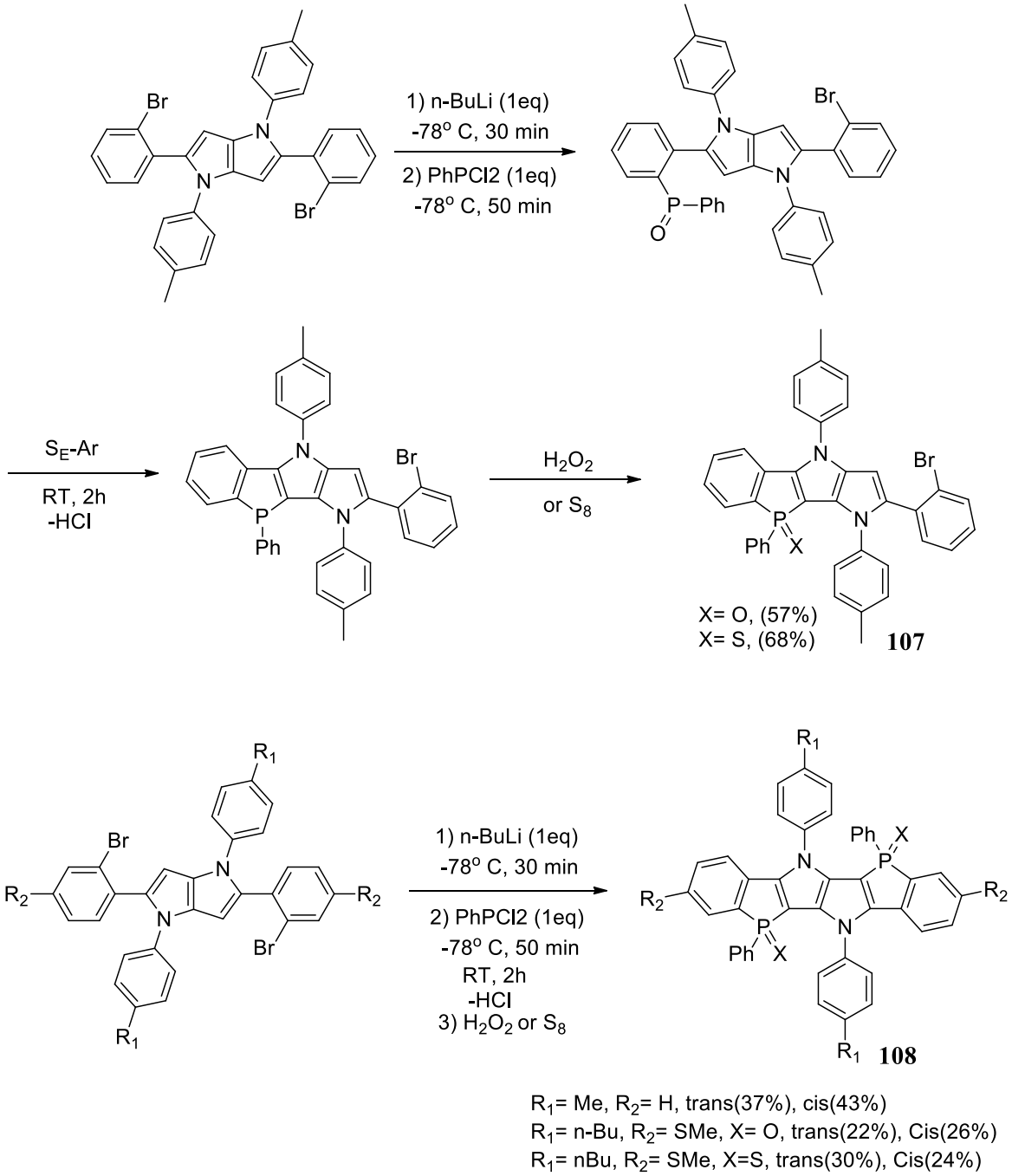

Figure 1.31: Synthesis of PhosPPs and BPhosPPs. [103]

The Gryko group studied and prepared nearly planar, χ-shaped π-expanded 1,4 dihydropyrrolo[3,2-b]pyrroles (DHPPs) from the central DHPP core via condensation of 2-

aryl or 2-heteroarylbenzaldehydes with aromatic amines and 2,3-butanedione, followed by double intramolecular oxidative aromatic coupling, and studied their photophysical properties. The overall yield of products formed in this two-step procedure ranged from 5 to 36%. The final products exhibited a strong blue fluorescence in solution (see Figure 1.32).[51]

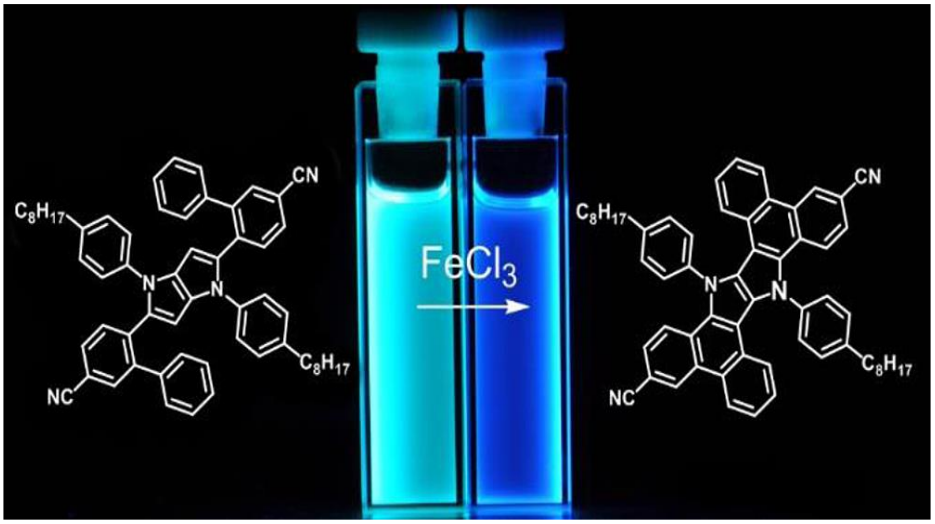

Figure 1.32: Intramolecular oxidative aromatic coupling. Source: Adapted with permission from Ref.[51] (Copyright 2015 American Chemical Society)

As positions 3 and 6 of DHPP are electron dense, they can be used to obtain π-expanded DHPP (**109**) derivatives in good yield. Krzeszewski and Gryko reported the intramolecular oxidative aromatic coupling of DHPP by using a classic one-electron oxidant, iron (III) chloride in nitromethane, which gave a π-expanded DHPP in a 75% yield, and their structure was confirmed by X-ray crystallography (see Figure 1.33).[51] Optical studies of TAPP derivatives and their π-expanded analogues show signature absorption bands between 350 and 400 nm and emission in the range from 439 to 524 nm corresponding to cyan and green light.

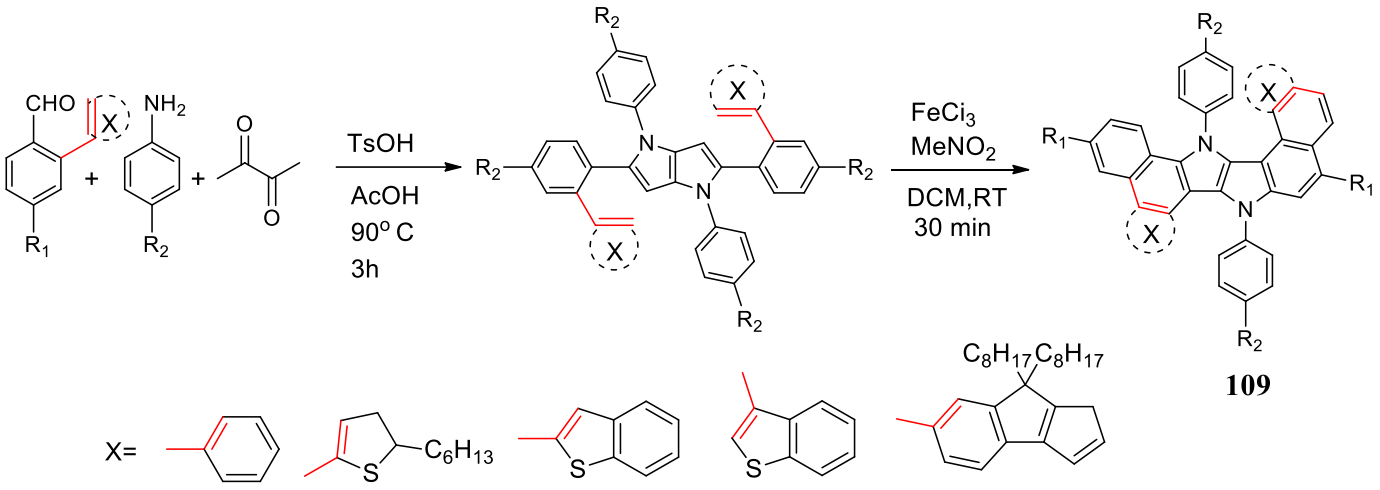

Figure 1.33: General method for the synthesis of π-expanded DHPP.[51] Substituents are responsible for the emission spectra of polycyclic compounds (see Figure 1.34).[73]

The extension of the π-system of TAPP derivatives results in a bathochromic shift in absorption bands to λmax = 372–421 nm.[51] Recently, the synthesis of ladder-type thiophene-based heterocycles has fascinated much attention due to their applications in n-type field-effect transistors,[104] nonlinear optical materials,[105] and mechanosensitive membrane probes.[106],[107] The Gryko group studied and reported the extension of the pyrrolopyrrole π-system by a three-step approach, which resulted in quinolone fused pyrrolopyrroles. The condensation of 2-aminophenyl-substituted pyrrolopyrroles with aromatic aldehydes led to the formation of hexacyclic ladder-type dyes (**110**), which fluoresced at 450–510 nm. The presence of pyridine-type and pyrrole-type nitrogen atoms with electron donating and electron-withdrawing substituents is responsible for the emission spectra of polycyclic compounds (see Figure 1.34).[73]

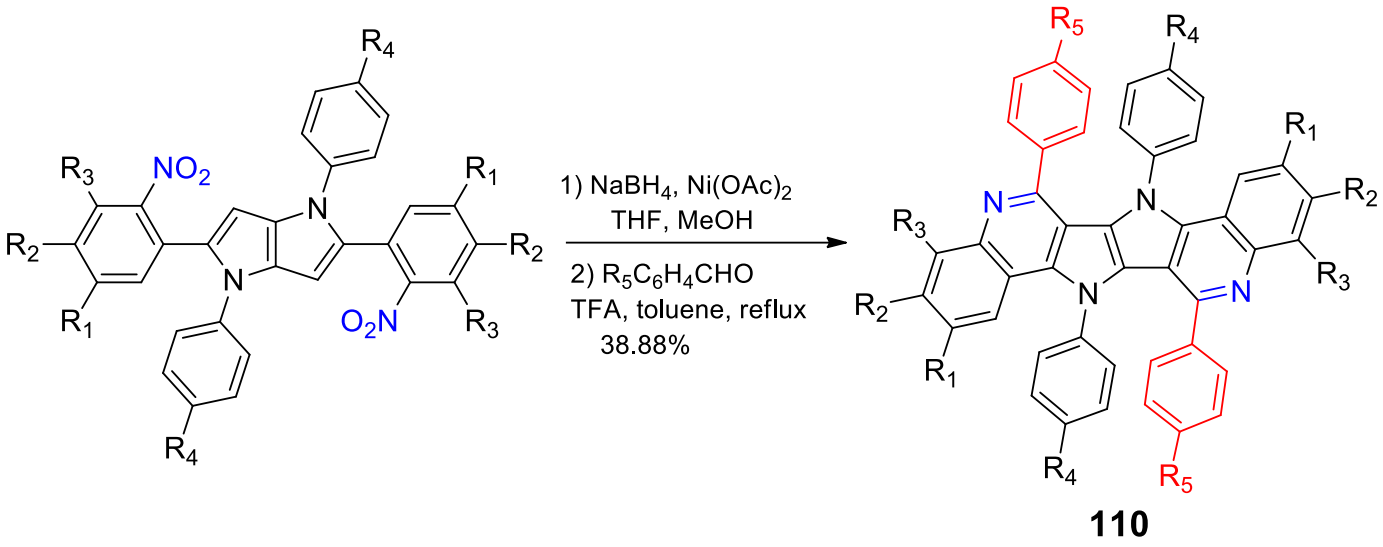

Figure 1.34: The crucial condensation of 2-aminophenyl-substituted pyrrolopyrroles in a facile three-step approach to synthesizing quinoline-fused pyrrolopyrroles (**110**).[73]

For another approach, the Gryko group also reported the formation of a six-membered ring over a seven-membered ring, which is energetically favored, by oxidative coupling of aryl substituents on the TAPP core (see **111-117** in Figure 1.35). The common oxidative coupling reaction of TAPP [94] and the table listing the various aryl aldehydes used to produce a family of core-substituted TAPPs are shown below. Formation of this product involved a twofold 1,2-aryl shift under oxidative aromatic coupling conditions through an arenium cation intermediate, and the radical mechanism gives a rearranged product, which is shown in (Figure 1.35). The six-membered ring formation is favored for compounds **111–117**a, b for π-exp PP, instead of the seven-membered ring formation for **111–117** a–g for TAPP.[94]

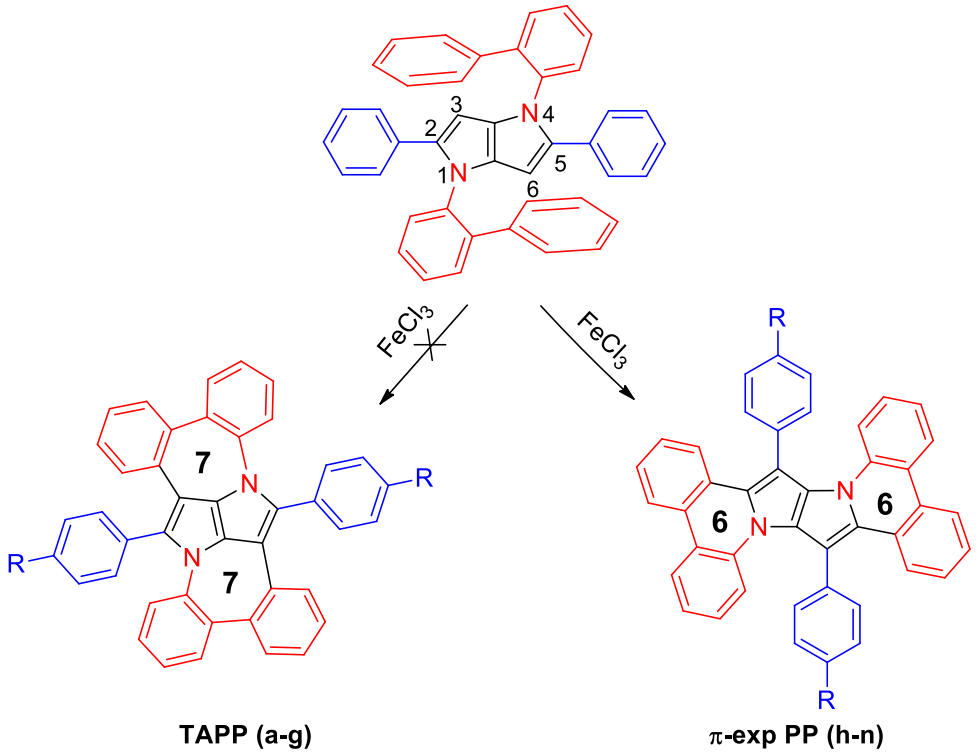

Comp. No.	R	TAPP	Yield (%)	π-exp PP	Yield (%)
111	Me	a	18	h	70
112	H	b	30	i	54
113	CN	c	14	j	60
114	NO_2	d	15	k	66
115	CF_3	e	19	l	33
116	Br	f	6	m	64
117	Ph	g	24	n	53

Figure 1.35: General oxidative coupling reaction of TAPP, and the lists of the π-extended pyrrolo[3,2- b]pyrroles with seven-membered ring expansion (**111-117**, a–g) and six-membered ring expansion (**111–117**, h–n) and their respective formation yields.[94]

Further, the Gryko group synthesized TAPP hybrid dyes possessing TPE moieties (as TPE is an AIE-active molecule), which showed a weak emission in solution, but an increase in the fluorescence quantum yield in the solid state was observed. The molecules exhibiting AIE are of interest for application in OLEDs, field-effect transistors, and as fluorescent probe (Figure 1.36). The authors used TPE-amine (AIEgen) for the synthesis of TAPP, which greatly enhanced its photophysical properties by controlling the dynamic molecular rotors, as these dyes are strongly emissive in both solution and solid state.[93] In this report, the Gryko group used a TPE-amine and a TPE-aldehyde for the synthesis of TAPP and studied their optical properties, observing that the absorption band of both compounds is bathochromically shifted in the solid state due to aggregation of TPE. Dynamic intramolecular rotation persists in solution, which weakens emission, but a strong enhancement of emission quantum yield occurs in the solid state.[93]

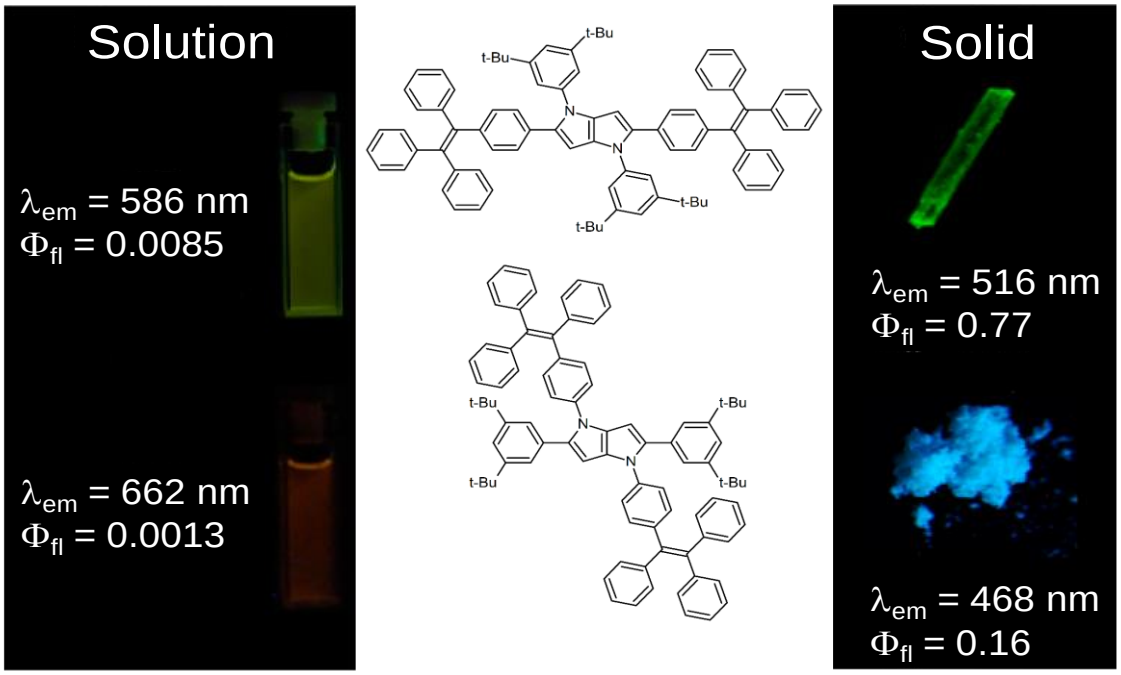

Figure 1.36: The weak emission in solution and an ~100-fold increase in the fluorescence quantum yield in the solid state of two regioisomers of TPE-substituted pyrrolo[3,2-b]pyrrole.[93] Source: Adapted with permission from Ref.[93] (Copyright 2015 American Chemical Society).

Sterically hindered aromatic amines and aromatic aldehydes have been used to synthesize TAPP derivatives, and it was observed that the presence of steric hindrance causes the intramolecular oxidative aromatic coupling of TAPPs to proceed via a different reaction pathway (see Figure 1.37). This suggests that large substituents present at positions adjacent to the site of oxidative aromatic coupling can completely alter the expected reaction pathway, leading to the formation of tuneable π-systems with strongly enhanced fluorescence.[48] The absorption and emission of these dyes shifted bathochromically due to changes in the π-system when compared to the parent TAPP or their π-expanded analogues.

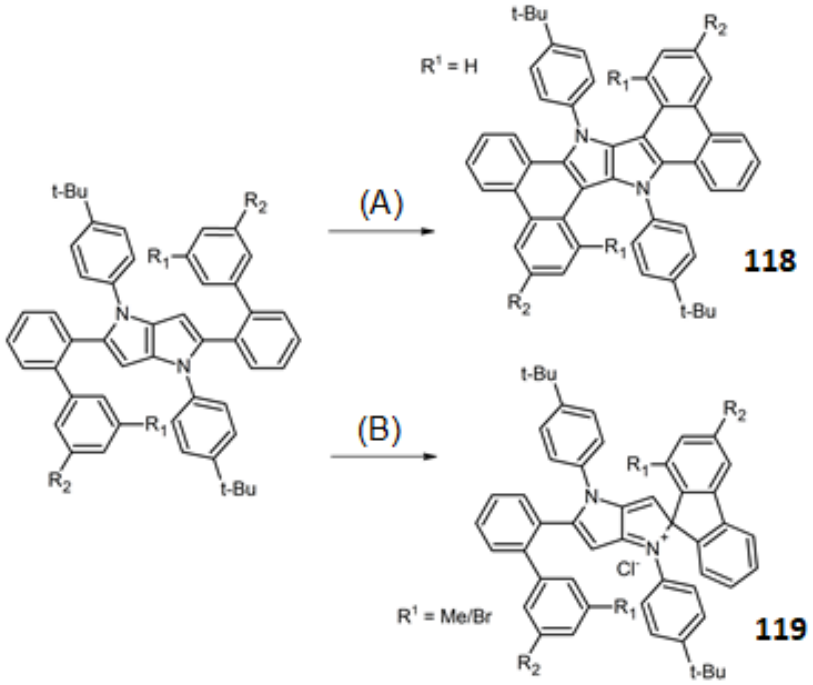

Figure 1.37: General method for the synthesis of π-expanded compounds at (a) toluenesulfonic acid (TsOH) and acetic acid (AcOH), 90 °C, three hours; (b) $FeCl_3$, $MeNO_2$, and DCM at room temperature for 30-minutes conditions.[48]

Dong and coworkers synthesized 13 aryl-substituted pyrrolo[3,2-b]pyrrole derivatives and studied the effect of substituents on the AIE phenomenon of these molecules

(Figure 1.38). They observed that among these compounds: DPP-1CN, DPP-1MF, DPP-1MF-2Me, and DPP-1MF-2IP, with electron-withdrawing groups on the phenyl groups at the 1,4-positions, and electron-donating groups on the phenyl groups at the 2,5-positions of pyrrolo[3,2-b]pyrrole core, the AIE effect was observed, whereas the other structures demonstrated aggregation-caused quenching (ACQ) phenomenon.[108]

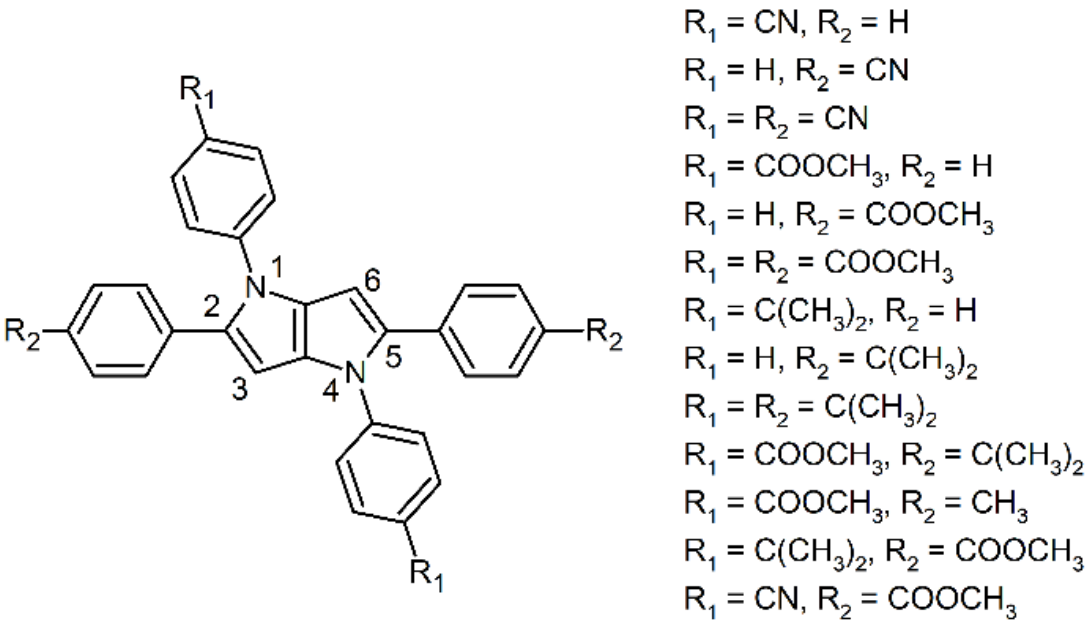

Figure 1.38: The synthesis and structures of the 13 aryl-substituted pyrrolo[3,2- b]pyrrole-based derivatives.[108]

1.4.8 Photophysical optical properties of TAPP

Absorption and photoluminescence spectra demonstrated that TAPP derivatives displaying the AIE phenomenon have a weak absorption band with a large Stokes shift.[108] The Vauthey group introduced an A–D–A TAPP molecule, where a cyanophenyl substituent acts as the acceptor and the electron-rich TAPP core acts as the donor, as shown in Figure 1.39.[109] The Langa group synthesized a series of three small molecules with the A–D–A configuration

containing a TAPP central core.[87] During the characterization of these molecules, it was observed that the molecules possess high thermal stability, with acceptable highest occupied molecular orbital–lowest unoccupied molecular orbital (HOMO–LUMO) energy levels to act as electron donors in bulk heterojunction organic solar cells (BHJ-OSCs). Quantum chemical calculations revealed that the pyrrole–pyrrole moiety retained the electron density of the HOMO, and the electron density of the LUMO is delocalized on the phenyl group. Small donor molecules and semiconducting polymers have been widely used in organic solar cells, achieving efficiencies above 10%. These new derivatives of TAPP show interesting optical properties, such as strong fluorescence in the blue region, moderate-to-large Stokes shifts, and fluorescence quantum yields up to 88%, making them suitable for many optoelectronic applications. Typically, the ultraviolet (UV)–vis absorption spectra of the films showed a bathochromic shift, along with broadening of the maximum absorption bands compared to the spectra in solution due to higher order of the molecules in the solid state (Figure 1.39).

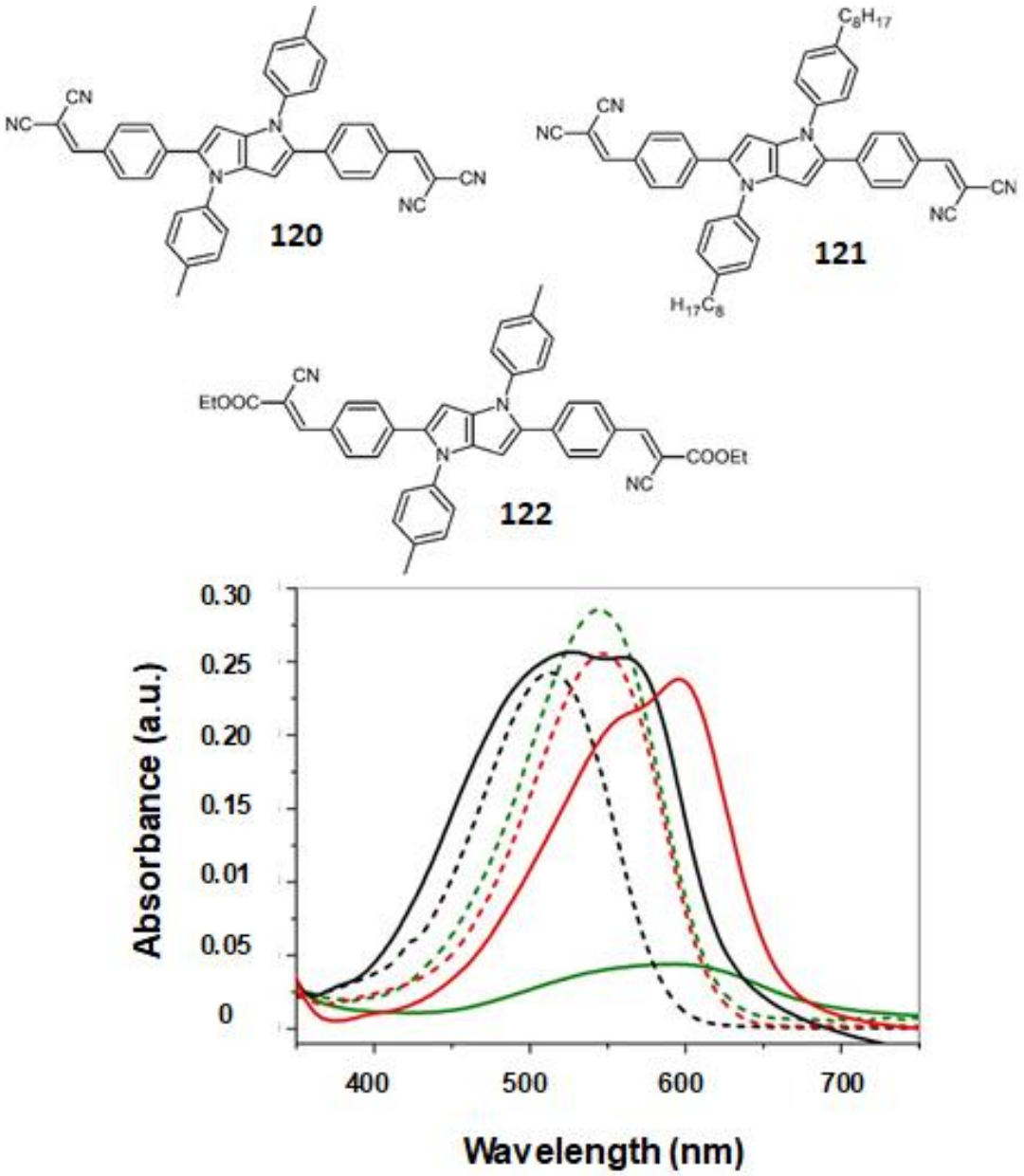

Figure 1.39: UV/vis absorption spectra of derivatives **120** (green), **121** (red), and **123** (black) in dichloromethane solution (3 × 10−6M at 25 °C) (dashed lines) and as a film (solid lines). Source: Adapted with permission from Ref.[87] (Copyright 2019 Wiley-VCH).

Gryko group presented a combined experimental and theoretical study of the two-photon absorption properties of electron-rich quadrupolar molecules based on the TAPP core and studied their optical properties (Figure 1.40).[110] They observed that quadrupolar TAPP molecules containing two 4-nitrophenyl substituents at positions 2 and 5 exhibited a

very strong solvatofluorochromic effect, with a fluorescence quantum yield of 0.96 in cyclohexane, whereas fluorescence was absent in dimethyl sulfoxide (DMSO). The TAPP derivatives consisted of a central electron-donor framework and terminal electron acceptor groups, and by changing the solvent from nonpolar to polar, the optical properties of these TAPP dyes may be influenced by stabilization of the intramolecular charge transfer (ICT) state. The optical properties of TAPP molecules such as (**123, 124**) were studied, and it was observed that both of these molecules exhibit totally different optical properties (Figure 1.40). [110] The two-photon absorption spectra show a bathochromic shift, which may be due to the two strongly electron-withdrawing nitrophenyl substituents. The presence of a strong electron donor with a very strong electron acceptor group such as the nitro group makes it possible to break the symmetry of the excited state. The presence of such groups is very useful in materials for two-photon fluorescence microscopy, two-photon excited polymerization, and optical-limiting processes. Hawes and coworkers reported the first crystalline coordination polymer containing the TAPP fluorophore. They prepared three new TAPP molecules containing nitrile, carboxylate, and mixed imidazole carboxylate groups, which showed strong fluorescence in solution, and used these molecules as a ligand in metal–organic frameworks to develop MOF-based fluorescent sensor devices. Here, ligands (**125-127**) contained nitrile, carboxylate, and mixed imidazolecarboxylate donor functionalities, respectively.[111] Ligand (**125**) was soluble in a variety of solvents and did not show concentration-dependent absorption or emission behaviour, but the ligands of both (**126, 127**) did show concentration dependence absorption and emission (Figure 1.40). It is well known that for the formation of robust and highly porous framework materials, rigid linear and square planar ligand molecules are desirable. Furthermore, the incorporation of luminescent materials into the ligand core is one of the most useful aspects of this ligand system. The above-mentioned TAPP derivatives avoid strong π–π interactions in the solid

state, which is a key concept for designing fluorescent porous materials.

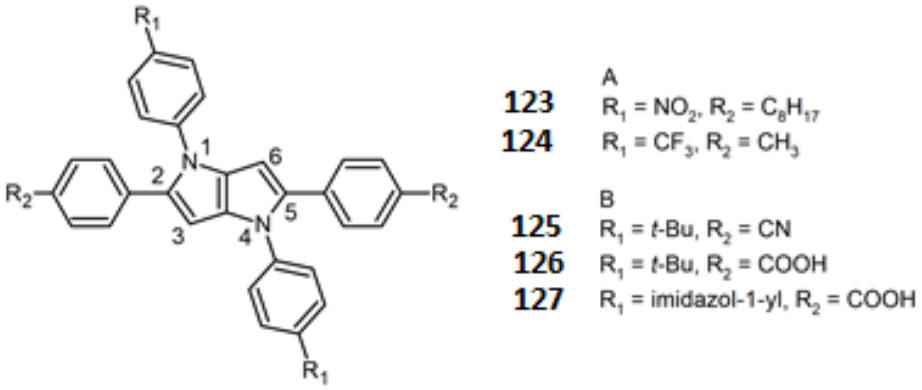

Figure 1.40: Chemical structure of pyrrolopyrrole derivatives.[110,111]

Janiga *et al*. synthesized nonfused 1,4-dihydropyrrole [3,2-b]pyrroles in a domino reaction between an aldehyde, a primary amine, and a diketone, with the six bonds forming in this process giving rise to tetrasubstituted pyrrole[3,2-b]pyrroles. The reaction is a simple, one-pot synthesis, and there is no need for chromatography, with product purification by simple filtration or recrystallization. During the course of the reaction, various functional groups were tolerated, though if all the substituents are electron rich, then the resulting TAPP derivative is very unstable. However, the derivatives isolated displayed very interesting optical properties. The 1,4-dihydropyrrole[3,2-b]pyrrole core was identified by virtual screening as a potent inhibitor of human microsomal prostaglandin synthase[112], [113]

Various methods for the synthesis of 1,4-dihydropyrrolo[3,2-b]pyrroles have been reported by researchers, as well as their π-expanded analogues. For example, indolo[3,2-b]indoles have attracted attention as they are highly fluorescent with interesting optical, electrochemical, and physicochemical properties. These molecules and π-expanded analogues are among the most electron-rich aromatic heterocycles and possess strong violet, blue, or green fluorescence in solution as well as in the solid state.

The Tieke group described the synthesis of polymers (**131, 132, 136 and 137**) containing the 1,3,4,6-tetraarylated pyrrolo[3,2-b]pyrrole-2,5-dione unit main chain and studied their photophysical properties, observing that all the polymers exhibited broad absorption bands with weak fluorescence (see Figure 1.41).[114] These polymers exhibited deep and broad absorption in the visible region and may be useful as dyes and colorants. These are also useful as photovoltaic polymers to increase light absorption in the visible region (see Figure 1.41).

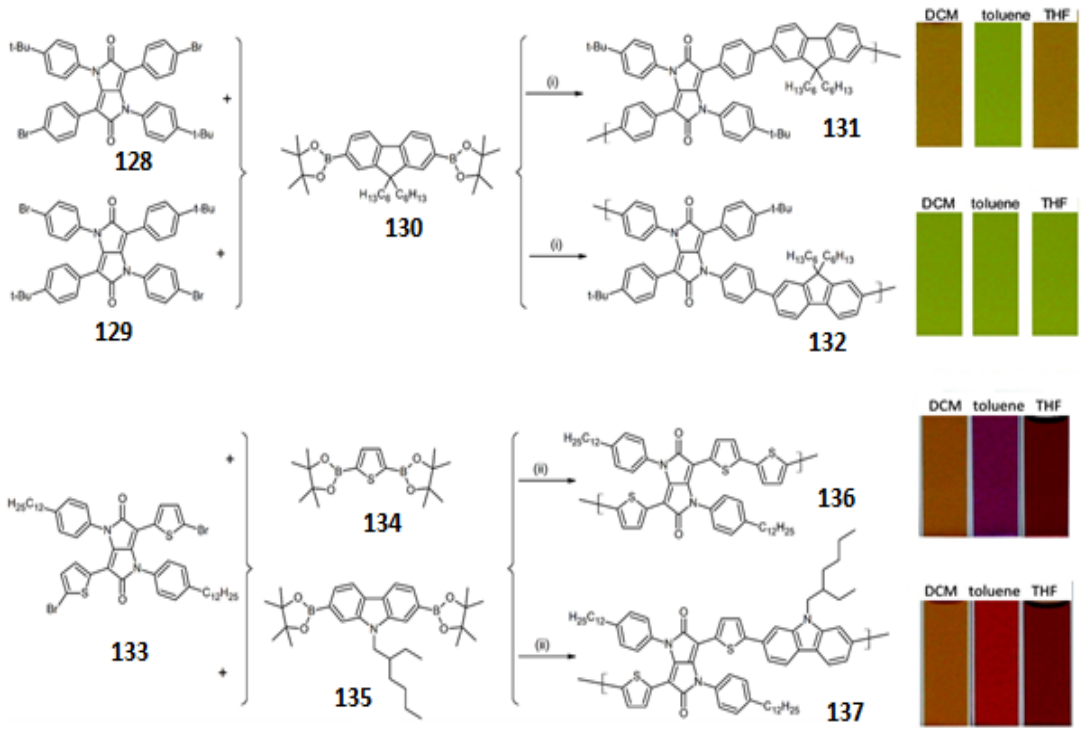

Figure 1.41: Synthesis of polymers (**131, 132, 136 and 137**). Reagents and conditions: (i) $Pd(PPh_3)_4$, K_2CO_3, toluene/dioxane/water, reflux, 24 hours; (ii) $Pd(PPh_3)_4$, K_2CO_3, toluene/water, reflux, 24 hours. Colors of (**131**) (a), (**132**) (b), (**136**) (c), and (**137**) (d) in various solvents. Source: Adapted with permission from Ref.[114] (Copyright 2012 American Chemical Society).

Polymer	M_W [Da]	PD	λ_{max} [nm]	λ_{em} [nm]	Stokes shift	Φ_F [%]	Extinct Coeff ε (λ) [L mol^{-1} cm^{-1}]
131	7600	1.3	328, 409[a]	625	216	0.7	30947 (409 nm)[a]
132	3400	1.4	331, 360[a]	611	251	0.4	27609 (360 nm)[a]
136	21000	5.6	489[b]	631, 720	231	0.5	21322 (489 nm)[b]
137	6500	1.6	345, 435[b]	643	208	0.3	19960 (345 nm)[b] 10400 (435 nm)[b]

[a] In chloroform. [b] In dichloromethane.

Ahn and coworkers synthesized the water-soluble quadrupolar pyrrolo[3,2-b]pyrrole (**138–140**), a A–D–A system, and studied its photophysical properties.[115] These dyes showed excellent emission properties, with solid-state luminescence. These dyes were used for fluorescence imaging of cells by confocal and two-photon microscopies (see Figure 1.42). The para analogue of these dyes was shown to stain cells in one- and two-photon excitation conditions, indicating that these dyes may have applications as bioimaging agents.

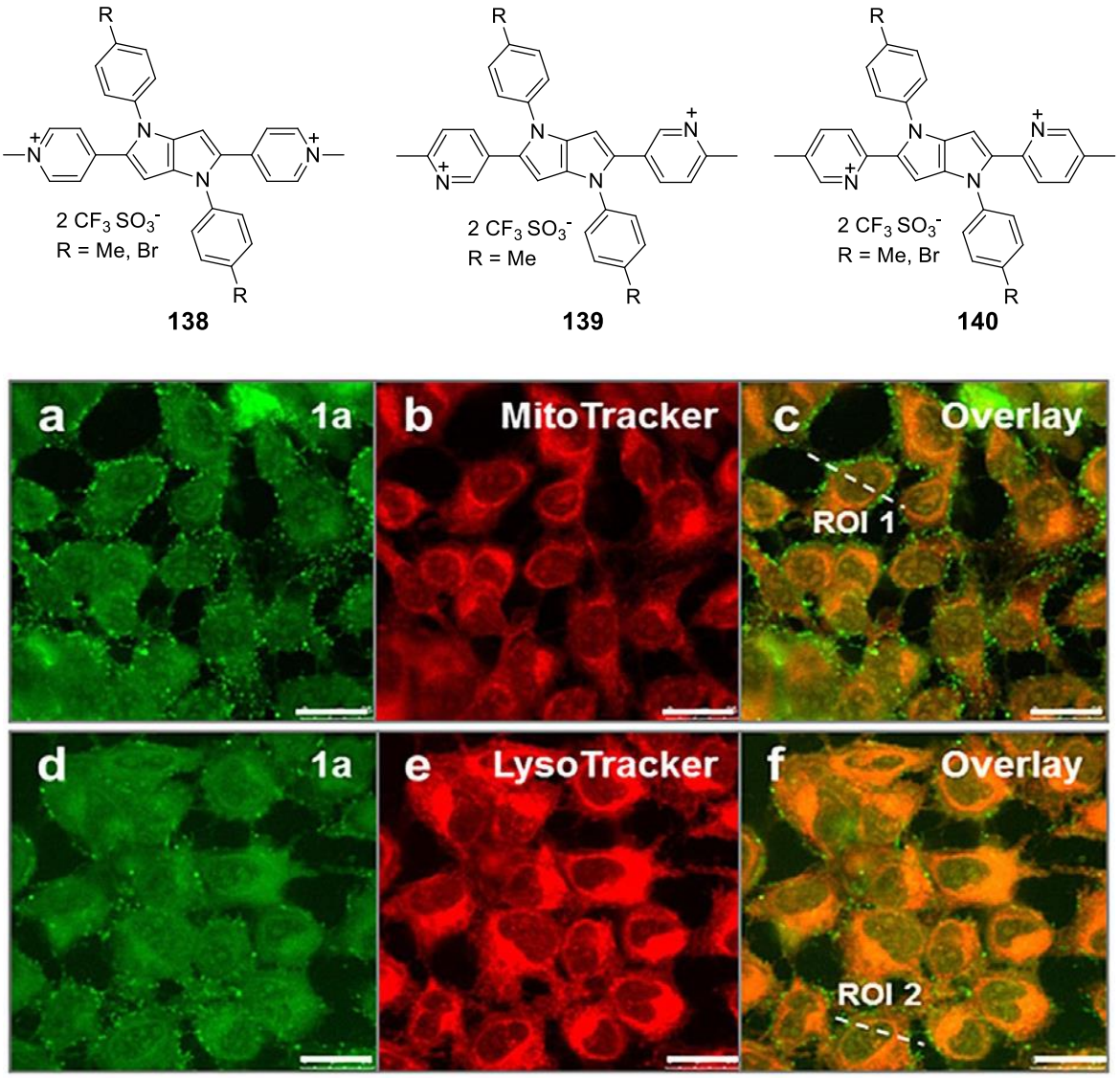

Figure 1.42: Water-soluble pyrrolo[3,2-b]pyrrole dyes (**138-140**) and cellular imaging by confocal fluorescence microscopy. Source: Adapted with permission from Ref.[115] (Copyright 2017 John Wiley and Sons)

They also synthesized structurally unique π-expanded pyrrolo[3,2-b]pyrrole in three steps, which demonstrated a low-energy absorption band in the visible region.[116] After hydrolysis under basic conditions, the resulting bis-carboxylic acid underwent a ring-closure reaction in the presence of trifluoroacetic acid anhydride (TFAA),[117] giving the highly polarized expected product pyrrolo[3,2-b]pyrrole-dione (**141**) (see Figure 1.43). The photophysical studies of this molecule showed a weak, broad absorption band[116]

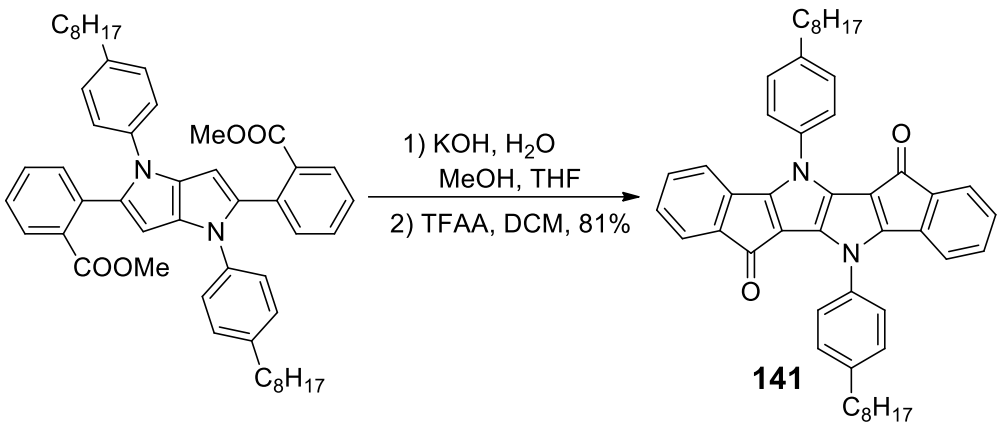

Figure 1.43: The synthesis of pyrrolo[3,2-b]pyrrole-dione (**141**).[116]

The Li group synthesized a TAPP molecule incorporated into an organic dye as a novel electron donor, which could be useful to enhance the light-harvesting ability and in photovoltaic and photocatalytic systems by suppressing electron recombination.[118] The Tieke group prepared new πconjugated polymers containing 1,3,4,6-tetraarylpyrrolo[3,2-b]pyrrole-2,5-dione (isoDPP) units by electrochemical polymerization of monomer units (**142-144** by anodic oxidation [see Figure 1.44]).[119] The synthesized polymers (**145–147**) precipitated as stable molecules, insoluble in organic solvents, and showed broad absorption spectra. These molecules demonstrated negligible fluorescence. These molecules have unusual optical and electrochemical properties, and their deep colour and low band gap make them promising materials for electrochromic displays. Polymer (**145**) exhibits two absorption maxima at 431 and 629 nm, whereas polymer (**146**) shows two absorption bands at 336 and 526 nm with a shoulder at about 704 nm, and polymer (**147**) shows two absorption maxima at 336 and 566 nm and a shoulder at 677 nm. The optical properties of the polymers are greatly influenced by the size and the position of the alkyl groups in the thiophene rings.

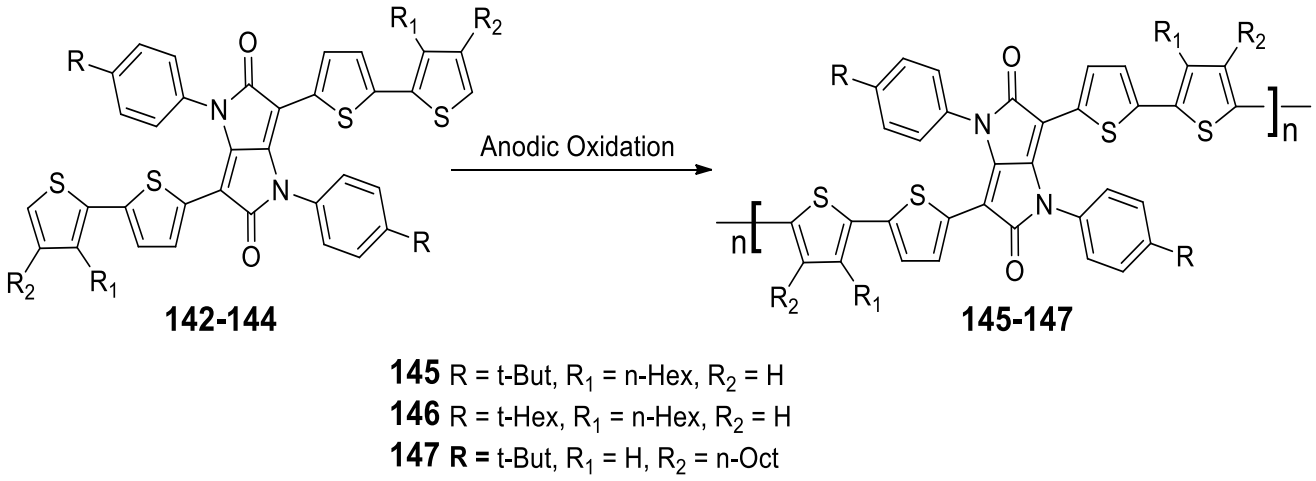

Figure 1.44: Electrochemical preparation of isoDPP-based polymers (**145–147**)[119]

Yang and coworkers synthesized new π-conjugated donor–acceptor (D–A) polymers containing the tetraaryl-diketopyrrolo[3,2-b]-pyrrole (isoDPP) core (**151, 152**) (see Figure 1.45).[120] These polymers were prepared by the palladium-catalysed Stile coupling reaction. Optical measurements indicated that these polymers had a low fluorescence quantum yield. Thermogravimetric analysis showed that the polymers have a high thermal stability and a high glass-transition temperature. These polymers are stable to UV and visible light in solution and exhibited broad absorption peaks at 523 and 620 nm. These polymers have a small band gap, which makes them useful in optoelectronics applications such as solar cells.

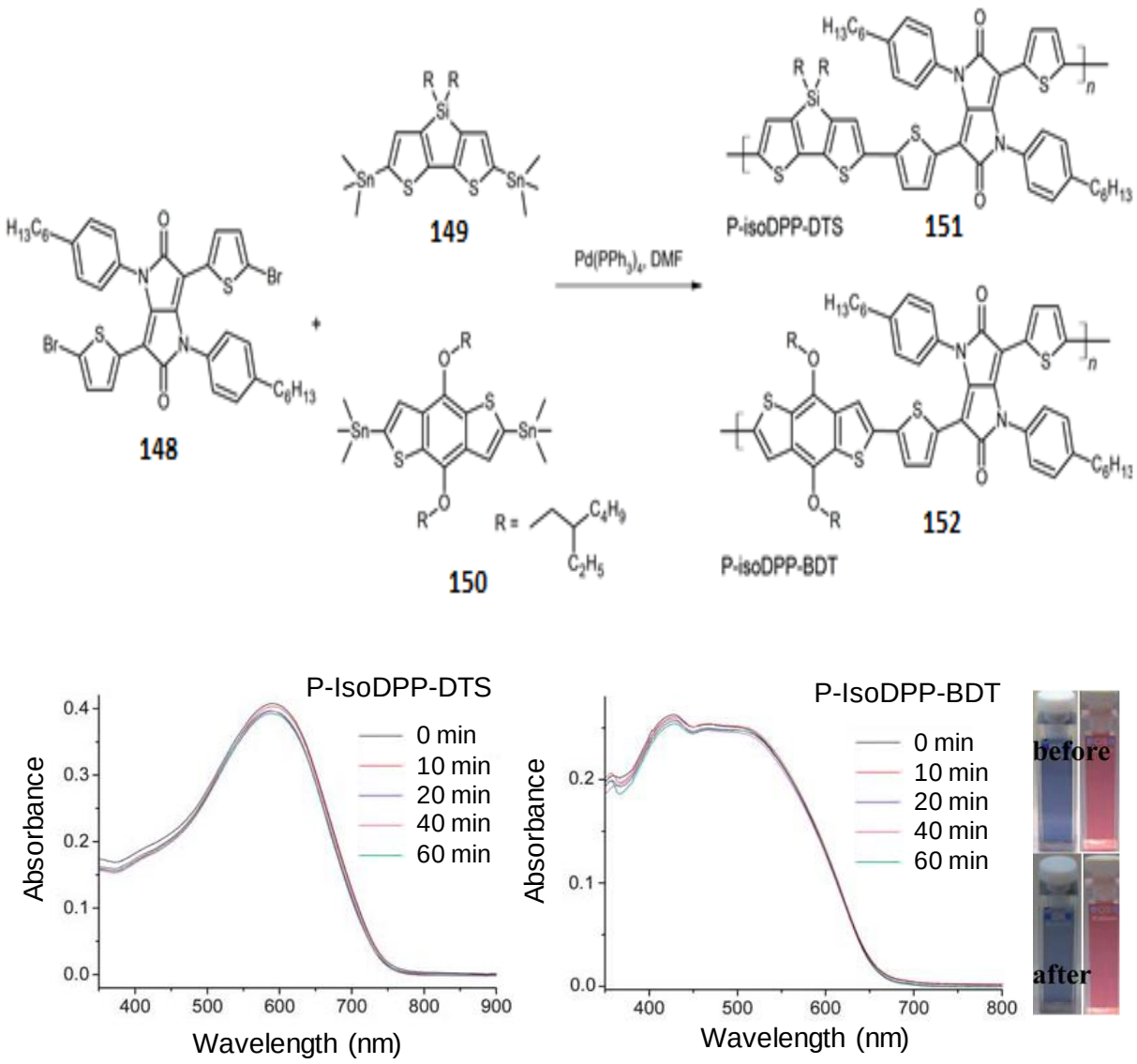

Figure 1.45: Synthesis and UV/vis absorption spectra of polymers P-IsoDPP-DTS and P-IsoDPP-BDT (**151, 152**). Source: Adapted with permission from Ref.[120] (Copyright 2010 of Royal Society of Chemistry).

TAPP derivatives show strong solvatofluorochromism, a broad absorption band between 400 and 300 nm and a blue fluorescence with a quantum yield of ~60%. As π conjugation is increased, changes in the photophysical properties of TAPP are observed. The synthesis of large π-conjugated systems has attracted much attention by researchers because of applications in field-effect transistors, organic photovoltaics, and OLEDs. TAPP

derivatives show absorption bands typically between 360 and 390 nm. The Gryko group observed a significant red-shift for compounds bearing strong electron-withdrawing groups such as CN and NO_2,[94] along with further photophysical properties of a broad range of TAPP derivatives. p-Nitrophenyl-substituted pyrrolo[3,2-b]pyrrole 4d emits at 544 nm (green) due to the pyrrolo[3,2-b]pyrroles possessing 4-nitrophenyl substituents at positions 2 and 5, leading to strong fluorescence in nonpolar solvents, which shows that the fluorescence quantum yield (Φ_{fl}) strongly depends on the nature of the peripheral substituents (Table 1.3).

Extension of π conjugation in all these compounds leads to a bathochromic shift of both absorption and emission compared to that of the parent TAPP core. A moderate fluorescence yield for all the compounds was observed, whereas the nitro-substituted derivative does not exhibit any measurable fluorescence. The photophysical properties of all the compounds are reported in Table 1.3.[94]

Table 1.3 Photophysical properties of (**153–166**) dyes measured in toluene.[94]

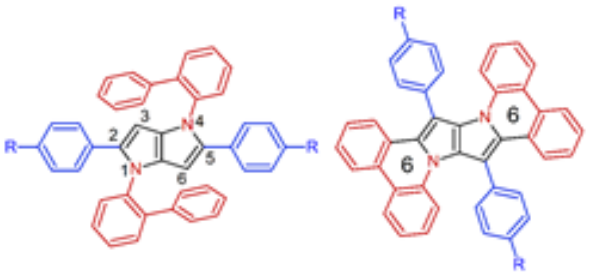

153, 160 R = Me
154, 161 R = H
155, 162 R = CN
156, 163 R = NO_2
157, 164 R = CF_3
158, 165 R = Br
159, 166 R = Ph

Comp. No.	**λ_{abs} [nm]**	**$\varepsilon_{max} \times 10^{-3}$**	**λ_{em} [nm]**	**ΔS_a [cm^{-1}]**	**Φ_{flb} [M^{-1} cm^{-1}]**
153	356	38	424	4500	0.17
154	357	34	406	3400	0.52
155	412	47	444	1700	0.85
156	470	42	544	2900	0.30
157	378	40	418	2500	0.97
158	368	44	416	3100	0.16
159	389	46	451	3500	0.75
160	412; 437	26; 18	455	900	0.33
161	411; 435	25; 18	455	1000	0.36
162	412; 435	22; 20	481	2200	0.18
163	386; 418	26; 20	-	-	-
164	409; 432	28; 23	450	900	0.32
165	410; 433	28; 22	450	900	0.25
166	413; 436	28; 21	456	1000	0.29

The structural variations of TAPP are thus quite well understood. At positions 2 and 5, the presence of electron-withdrawing substituents causes a bathochromic shift of the

absorption band, whereas at position 3, there is no such effect observed.[61] Absence of fluorescence was observed for nitro substituents, which may be due to the quenching effect of the nitro group. TAPP shows strong emission quantum yields above 60% in the solid state. The emission spectra of TAPP also depend on the type of substituents attached. λem shifts between 400 and 552 nm, whereas the presence of electron-withdrawing substituent on the aryl ring at 2 and 5 positions influences both the absorption and emission maxima causing a red-shift[110] due to electronic communication in the ground and the excited states (Figure 1.46).

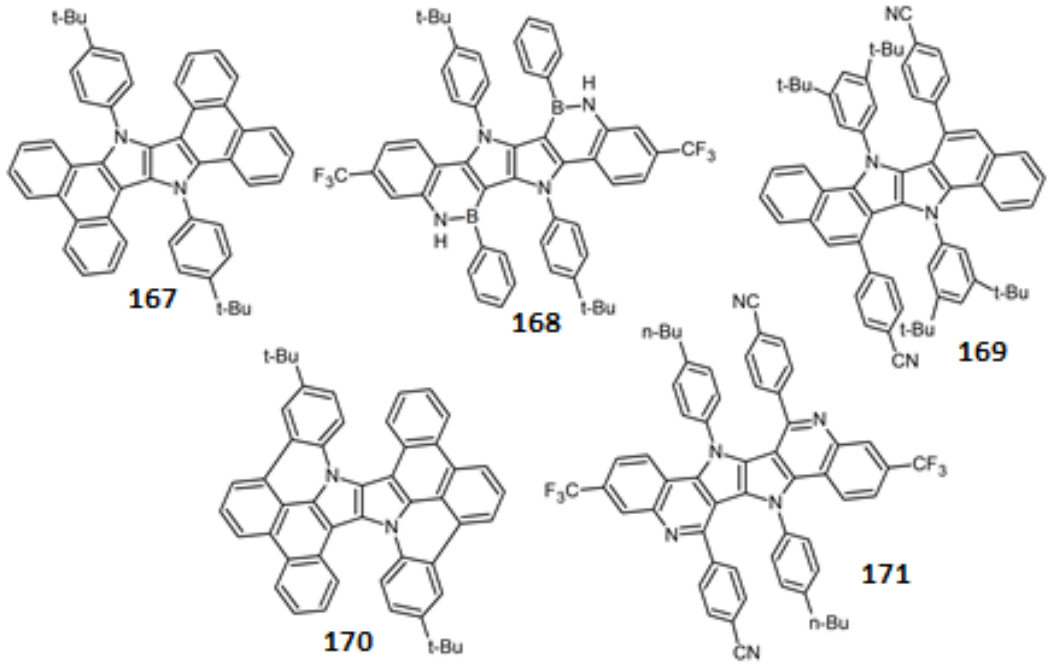

Figure 1.46: Optical properties of some selected π-expanded analogues of TAPP[49]

Comp. No.	λ_{abs} (nm)	λ_{em} (nm)	ε	Φ_{fl}	ΔS (cm^{-1})	Solvent
151	372	428	390000	45%	3500	DCM
152	402	413	190000	78%	660	Toluene

153	380	483	190000	34%	5600	Toluene
154	428	498	250000	18%	3300	DCM
155	318	499	68500	14%	11400	Toluene

1.5 Conclusion and Outlook

In this chapter, we have summarized, naphthalenediimide (NDIs), tetraphenylethylene (TPE), diarylethenes, tetraarylpyrrolo [3,2-b] pyrroles (TAPPs) as novel photoluminiscent materials used for wonderful applications. Given the electron-rich nature of the TAPP core, it is not surprising that most applications are found in areas where the interaction of light is paramount, such as optoelectronics, imaging, and solar cells. Given the enormous importance of organic molecules in OLEDS, organic solar cells and new generation solar cells that require organic materials in various cell configurations,[121] it is expected that TAPP derivatives will progress and find further use.[122],[123] We have demonstrated in this chapter how the synthetic versatility of the TAPP core can be leveraged to control the absorbance, emission, and physical properties of the analogues, allowing for fine-tuning of properties for each application. TAPP, as a new and unique AIE core, has long been plagued by inefficient and complex synthesis problems. Until 2013, Gryko and his group broke the TAPP synthesis bottleneck, and they discovered a one-pot method for transforming simple and readily available building blocks into an unsurpassed variety of TAPP. Since then, the synthesis and application of TAPP derivatives have been extensively studied. In this chapter, we have summarized the discovery of TAPP, the improvement of synthesis method, the reaction mechanism, the reactivity of TAPP, the π-expansion of TAPP, and their photophysical properties. The summary of TAPP research is timely and substantial in content. It will definitely expand people's understanding of this new AIE core. Thereafter, fundamental research efforts directed TAPP applications in the field of sensor, self-assembly, host– guest

chemistry, ion channels, solar cells, and medicinal chemistry need to be developed in future prospective given that simplicity and scalable synthesis of TAPP and its derivate will also have great potential to functionalization at the periphery of four benzene rings and use them for various applications. If synthetic protocols can be improved to allow further derivatives with closely controlled physical properties, a greater range of application will come on top of those described here, and we expect TAPP derivatives to play an important role in these fields of application in the near future.

1.6 References:

(1) Huang, C.; Barlow, S.; Marder, S. R. Perylene-3,4,9,10-Tetracarboxylic Acid Diimides: Synthesis, Physical Properties, and Use in Organic Electronics. *J. Org. Chem.* **2011**, *76* (8), 2386–2407. https://doi.org/10.1021/jo2001963.

(2) Bhosale, S. V.; Jani, C. H.; Langford, S. J. Chemistry of Naphthalene Diimides. *Chem. Soc. Rev.* **2008**, *37* (2), 331–342. https://doi.org/10.1039/B615857A.

(3) Würthner, F. Perylene Bisimide Dyes as Versatile Building Blocks for Functional Supramolecular Architectures. *Chem. Commun.* **2004**, No. 14, 1564–1579. https://doi.org/10.1039/B401630K.

(4) Zhan, X.; Facchetti, A.; Barlow, S.; Marks, T. J.; Ratner, M. A.; Wasielewski, M. R.; Marder, S. R. Rylene and Related Diimides for Organic Electronics. *Adv. Mater.* **2011**, *23* (2), 268–284. https://doi.org/10.1002/adma.201001402.

(5) Würthner, F.; Stolte, M. Naphthalene and Perylene Diimides for Organic Transistors. *Chem. Commun.* **2011**, *47* (18), 5109–5115. https://doi.org/10.1039/C1CC10321K.

(6) Jones, B. A.; Facchetti, A.; Wasielewski, M. R.; Marks, T. J. Tuning Orbital Energetics in Arylene Diimide Semiconductors. Materials Design for Ambient Stability of n-Type Charge Transport. *J. Am. Chem. Soc.* **2007**, *129* (49), 15259–15278.

https://doi.org/10.1021/ja075242e.

(7) Guha, S.; Goodson, F. S.; Corson, L. J.; Saha, S. Boundaries of Anion/Naphthalenediimide Interactions: From Anion−π Interactions to Anion-Induced Charge-Transfer and Electron-Transfer Phenomena. *J. Am. Chem. Soc.* **2012**, *134* (33), 13679–13691. https://doi.org/10.1021/ja303173n.

(8) Katz, null; Lovinger, null; Johnson, null; Kloc, null; Siegrist, null; Li, null; Lin, null; Dodabalapur, null. A Soluble and Air-Stable Organic Semiconductor with High Electron Mobility. *Nature* **2000**, *404* (6777), 478–481. https://doi.org/10.1038/35006603.

(9) Suraru, S.-L.; Würthner, F. Strategies for the Synthesis of Functional Naphthalene Diimides. *Angew. Chem. Int. Ed.* **2014**, *53* (29), 7428–7448. https://doi.org/10.1002/anie.201309746.

(10) Thalacker, C.; Röger, C.; Würthner, F. Synthesis and Optical and Redox Properties of Core-Substituted Naphthalene Diimide Dyes. *J. Org. Chem.* **2006**, *71* (21), 8098–8105. https://doi.org/10.1021/jo0612269.

(11) Völker, S. F.; Schmiedel, A.; Holzapfel, M.; Böhm, C.; Lambert, C. Charge Transfer Dynamics in Squaraine–Naphthalene Diimide Copolymers. *Phys. Chem. Chem. Phys.* **2013**, *15* (45), 19831–19844. https://doi.org/10.1039/C3CP53455C.

(12) Vignon, S. A.; Jarrosson, T.; Iijima, T.; Tseng, H.-R.; Sanders, J. K. M.; Stoddart, J. F. Switchable Neutral Bistable Rotaxanes. *J. Am. Chem. Soc.* **2004**, *126* (32), 9884–9885. https://doi.org/10.1021/ja048080k.

(13) Chaignon, F.; Buchet, F.; Blart, E.; Falkenström, M.; Hammarström, L.; Odobel, F. Photoinduced Electron Transfer in Ruthenium(II) Trisbipyridine Complexes Connected to a Naphthalenebisimide via an Oligo(Phenyleneethynylene) Spacer. *New J. Chem.* **2009**, *33* (2), 408–416. https://doi.org/10.1039/B810856K.

(14) Iengo, E.; Pantoş, G. D.; Sanders, J. K. M.; Orlandi, M.; Chiorboli, C.; Fracasso, S.;

Scandola, F. A Fully Self-Assembled Non-Symmetric Triad for Photoinduced Charge Separation. *Chem. Sci.* **2011**, *2* (4), 676–685. https://doi.org/10.1039/C0SC00520G.

(15) Jin, S.; Ding, X.; Feng, X.; Supur, M.; Furukawa, K.; Takahashi, S.; Addicoat, M.; El-Khouly, M. E.; Nakamura, T.; Irle, S.; Fukuzumi, S.; Nagai, A.; Jiang, D. Charge Dynamics in a Donor-Acceptor Covalent Organic Framework with Periodically Ordered Bicontinuous Heterojunctions. *Angew. Chem. Int. Ed Engl.* **2013**, *52* (7), 2017–2021. https://doi.org/10.1002/anie.201209513.

(16) Mitra, A.; Hubley, C. T.; Panda, D. K.; Clark, R. J.; Saha, S. Anion-Directed Assembly of a Non-Interpenetrated Square-Grid Metal–Organic Framework with Nanoscale Porosity. *Chem. Commun.* **2013**, *49* (59), 6629–6631. https://doi.org/10.1039/C3CC43178A.

(17) Pu, L. Fluorescence of Organic Molecules in Chiral Recognition. *Chem. Rev.* **2004**, *104* (3), 1687–1716. https://doi.org/10.1021/cr030052h.

(18) Lippert, A. R.; Van de Bittner, G. C.; Chang, C. J. Boronate Oxidation as a Bioorthogonal Reaction Approach for Studying the Chemistry of Hydrogen Peroxide in Living Systems. *Acc. Chem. Res.* **2011**, *44* (9), 793–804. https://doi.org/10.1021/ar200126t.

(19) Bobe, S. R.; Bhosale, R. S.; Goskulwad, S. P.; Puyad, A. L.; Bhosale, S. V.; Bhosale, S. V. A Highly Selective Colorimetric Cys Sensor Based on Core-Substituted Naphthalene Diimides. *RSC Adv.* **2015**, *5* (122), 100697–100701. https://doi.org/10.1039/C5RA17809F.

(20) Takenaka, S.; Yamashita, K.; Takagi, M.; Uto, Y.; Kondo, H. DNA Sensing on a DNA Probe-Modified Electrode Using Ferrocenylnaphthalene Diimide as the Electrochemically Active Ligand. *Anal. Chem.* **2000**, *72* (6), 1334–1341. https://doi.org/10.1021/ac991031j.

(21) Dawson, R. E.; Hennig, A.; Weimann, D. P.; Emery, D.; Ravikumar, V.; Montenegro, J.; Takeuchi, T.; Gabutti, S.; Mayor, M.; Mareda, J.; Schalley, C. A.; Matile, S. Experimental Evidence for the Functional Relevance of Anion-Pi Interactions. *Nat. Chem.* **2010**, *2* (7), 533–538. https://doi.org/10.1038/nchem.657.

(22) Estarellas, C.; Frontera, A.; Quiñonero, D.; Deyà, P. M. Relevant Anion-π Interactions in Biological Systems: The Case of Urate Oxidase. *Angew. Chem. Int. Ed Engl.* **2011**, *50* (2), 415–418. https://doi.org/10.1002/anie.201005635.

(23) Jana, P.; Maity, S. K.; Bera, S.; Ghorai, P. K.; Haldar, D. Hierarchical Self-Assembly of Naphthalene Bisimides to Fluorescent Microspheres and Fluoride Sensing. *CrystEngComm* **2013**, *15* (13), 2512–2518. https://doi.org/10.1039/C3CE26700H.

(24) Balakrishnan, K.; Datar, A.; Oitker, R.; Chen, H.; Zuo, J.; Zang, L. Nanobelt Self-Assembly from an Organic n-Type Semiconductor: Propoxyethyl-PTCDI. *J. Am. Chem. Soc.* **2005**, *127* (30), 10496–10497. https://doi.org/10.1021/ja052940v.

(25) Bhosale, S. V.; Bhosale, S. V.; Kalyankar, M. B.; Langford, S. J. A Core-Substituted Naphthalene Diimide Fluoride Sensor. *Org. Lett.* **2009**, *11* (23), 5418–5421. https://doi.org/10.1021/ol9022722.

(26) Ajayakumar, M. R.; Asthana, D.; Mukhopadhyay, P. Core-Modified Naphthalenediimides Generate Persistent Radical Anion and Cation: New Panchromatic NIR Probes. *Org. Lett.* **2012**, *14* (18), 4822–4825. https://doi.org/10.1021/ol302140x.

(27) Ghule, N. V.; Bhosale, R. S.; Puyad, A. L.; Bhosale, S. V.; Bhosale, S. V. Naphthalenediimide Amphiphile Based Colorimetric Probe for Recognition of Cu2+ and Fe^{3+} Ions. *Sens. Actuators B Chem.* **2016**, *C* (227), 17–23. https://doi.org/10.1016/j.snb.2015.12.041.

(28) Zhou, C.; Li, Y.; Zhao, Y.; Zhang, J.; Yang, W.; Li, Y. An Unusual Addition Reaction for Constructing a Novel PH-Controlled Fluorescence Switch. *Org. Lett.* **2011**, *13* (2),

292–295. https://doi.org/10.1021/ol102742f.

(29) Cox, R. P.; Higginbotham, H. F.; Graystone, B. A.; Sandanayake, S.; Langford, S. J.; Bell, T. D. M. A New Fluorescent H+ Sensor Based on Core-Substituted Naphthalene Diimide. *Chem. Phys. Lett.* **2012**, *521*, 59–63. https://doi.org/10.1016/j.cplett.2011.11.028.

(30) Higginbotham, H. F.; Cox, R. P.; Sandanayake, S.; Graystone, B. A.; Langford, S. J.; Bell, T. D. M. A Fluorescent "2 in 1" Proton Sensor and Polarity Probe Based on Core Substituted Naphthalene Diimide. *Chem. Commun.* **2013**, *49* (44), 5061–5063. https://doi.org/10.1039/C3CC41622D.

(31) Bhosale, S. V.; Adsul, M.; Shitre, G. V.; Bobe, S. R.; Bhosale, S. V.; Privér, S. H. A Pyridyl-Monoannulated Naphthalene Diimide Motif Self-Assembles into Tuneable Nanostructures by Means of Solvophobic Control. *Chem. – Eur. J.* **2013**, *19* (23), 7310–7313. https://doi.org/10.1002/chem.201300120.

(32) Bisoyi, H. K.; Li, Q. Light-Driven Liquid Crystalline Materials: From Photo-Induced Phase Transitions and Property Modulations to Applications. *Chem. Rev.* **2016**, *116* (24), 15089–15166. https://doi.org/10.1021/acs.chemrev.6b00415.

(33) Zheng, Z.; Li, Y.; Bisoyi, H. K.; Wang, L.; Bunning, T. J.; Li, Q. Three-Dimensional Control of the Helical Axis of a Chiral Nematic Liquid Crystal by Light. *Nature* **2016**, *531* (7594), 352–356. https://doi.org/10.1038/nature17141.

(34) *Springer Handbook of Nanomaterials*, 1st ed. 2013.; Vajtai, R., Ed.; Springer Handbooks; Springer Berlin Heidelberg : Imprint: Springer: Berlin, Heidelberg, 2013. https://doi.org/10.1007/978-3-642-20595-8.

(35) Crescenzo, A. D.; Ettorre, V.; Fontana, A. Non-Covalent and Reversible Functionalization of Carbon Nanotubes. *Beilstein J. Nanotechnol.* **2014**, *5* (1), 1675–1690. https://doi.org/10.3762/bjnano.5.178.

(36) Mei, J.; Leung, N. L. C.; Kwok, R. T. K.; Lam, J. W. Y.; Tang, B. Z. Aggregation-Induced Emission: Together We Shine, United We Soar! *Chem. Rev.* **2015**, *115* (21), 11718–11940. https://doi.org/10.1021/acs.chemrev.5b00263.

(37) Samanta, M.; Rananaware, A.; Nadimetla, D. N.; Rahaman, S. A.; Saha, M.; Jadhav, R. W.; Bhosale, S. V.; Bandyopadhyay, S. Light Triggered Encapsulation and Release of C60 with a Photoswitchable TPE-Based Supramolecular Tweezers. *Sci. Rep.* **2019**, *9* (1), 9670. https://doi.org/10.1038/s41598-019-46242-4.

(38) Luo, J.; Xie, Z.; Lam, J. W. Y.; Cheng, L.; Chen, H.; Qiu, C.; Kwok, H. S.; Zhan, X.; Liu, Y.; Zhu, D.; Tang, B. Z. Aggregation-Induced Emission of 1-Methyl-1,2,3,4,5-Pentaphenylsilole. *Chem. Commun.* **2001**, No. 18, 1740–1741. https://doi.org/10.1039/B105159H.

(39) Tang, B. Z.; Zhan, X.; Yu, G.; Lee, P. P. S.; Liu, Y.; Zhu, D. Efficient Blue Emission from Siloles. *J. Mater. Chem.* **2001**, *11* (12), 2974–2978. https://doi.org/10.1039/B102221K.

(40) Liu, Y.; Lv, Y.; Zhang, X.; Chen, S.; Lam, J. W. Y.; Lu, P.; Kwok, R. T. K.; Kwok, H. S.; Tao, X.; Tang, B. Z. From A Fluorescent Chromophore in Solution to An Efficient Emitter in the Solid State. *Chem. – Asian J.* **2012**, *7* (10), 2424–2428. https://doi.org/10.1002/asia.201200489.

(41) Liu, Y.; Ye, X.; Liu, G.; Lv, Y.; Zhang, X.; Chen, S.; Lam, J. W. Y.; Kwok, H. S.; Tao, X.; Tang, B. Z. Structural Features and Optical Properties of a Carbazole-Containing Ethene as a Highly Emissive Organic Solid. *J. Mater. Chem. C* **2014**, *2* (6), 1004–1009. https://doi.org/10.1039/C3TC32145B.

(42) Xie, N.; Liu, Y.; Hu, R.; Leung, N. L. C.; Arseneault, M.; Tang, B. Z. Synthesis, Aggregation-Induced Emission, and Electroluminescence of Dibenzothiophene- and Dibenzofuran-Containing Tetraarylethenes. *Isr. J. Chem.* **2014**, *54* (7), 958–966.

https://doi.org/10.1002/ijch.201400058.

(43) Liu, Y.; Chen, X.; Lv, Y.; Chen, S.; Lam, J. W. Y.; Mahtab, F.; Kwok, H. S.; Tao, X.; Tang, B. Z. Systemic Studies of Tetraphenylethene-Triphenylamine Oligomers and a Polymer: Achieving Both Efficient Solid-State Emissions and Hole-Transporting Capability. *Chem. Weinh. Bergstr. Ger.* **2012**, *18* (32), 9929–9938. https://doi.org/10.1002/chem.201201400.

(44) Debus, H. Ueber Die Einwirkung Des Ammoniaks Auf Glyoxal. *Justus Liebigs Ann. Chem.* **1858**, *107* (2), 199–208. https://doi.org/10.1002/jlac.18581070209.

(45) Janiga, A.; Glodkowska-Mrowka, E.; Stoklosa, T.; Gryko, D. T. Synthesis and Optical Properties of Tetraaryl-1,4-Dihydropyrrolo[3,2-b]Pyrroles. *Asian J. Org. Chem.* **2013**, *2* (5), 411–415. https://doi.org/10.1002/ajoc.201200201.

(46) Ding, D.; Li, K.; Liu, B.; Tang, B. Z. Bioprobes Based on AIE Fluorogens. *Acc. Chem. Res.* **2013**, *46* (11), 2441–2453. https://doi.org/10.1021/ar3003464.

(47) Krzeszewski, M.; Kodama, T.; Espinoza, E. M.; Vullev, V. I.; Kubo, T.; Gryko, D. T. Nonplanar Butterfly-Shaped π-Expanded Pyrrolopyrroles. *Chem. – Eur. J.* **2016**, *22* (46), 16478–16488. https://doi.org/10.1002/chem.201603282.

(48) Krzeszewski, M.; Świder, P.; Dobrzycki, Ł.; Cyrański, M. K.; Danikiewicz, W.; Gryko, D. T. The Role of Steric Hindrance in the Intramolecular Oxidative Aromatic Coupling of Pyrrolo[3,2-b]Pyrroles. *Chem. Commun.* **2016**, *52* (77), 11539–11542. https://doi.org/10.1039/C6CC05904J.

(49) Krzeszewski, M.; Gryko, D.; Gryko, D. T. The Tetraarylpyrrolo[3,2-b]Pyrroles—From Serendipitous Discovery to Promising Heterocyclic Optoelectronic Materials. *Acc. Chem. Res.* **2017**, *50* (9), 2334–2345. https://doi.org/10.1021/acs.accounts.7b00275.

(50) Orłowski, R.; Banasiewicz, M.; Clermont, G.; Castet, F.; Nazir, R.; Blanchard-Desce, M.; Gryko, D. T. Strong Solvent Dependence of Linear and Non-Linear Optical

Properties of Donor-Acceptor Type Pyrrolo[3,2-b]Pyrroles. *Phys. Chem. Chem. Phys. PCCP* **2015**, *17* (37), 23724–23731. https://doi.org/10.1039/c5cp03523f.

(51) Krzeszewski, M.; Gryko, D. T. χ-Shaped Bis(Areno)-1,4-Dihydropyrrolo[3,2-b]Pyrroles Generated by Oxidative Aromatic Coupling. *J. Org. Chem.* **2015**, *80* (5), 2893–2899. https://doi.org/10.1021/acs.joc.5b00052.

(52) Yuan, Z.; Xiao, Y.; Yang, Y.; Xiong, T. Soluble Ladder Conjugated Polymer Composed of Perylenediimides and Thieno[3,2-b]Thiophene (LCPT): A Highly Efficient Synthesis via Photocyclization with the Sunlight. *Macromolecules* **2011**, *44* (7), 1788–1791. https://doi.org/10.1021/ma1026252.

(53) Mishra, S. P.; Palai, A. K.; Kumar, A.; Srivastava, R.; Kamalasanan, M. N.; Patri, M. Highly Air-Stable Thieno[3,2-b]Thiophene-Thiophene-Thiazolo[5,4-d]Thiazole-Based Polymers for Light-Emitting Diodes. *Macromol. Chem. Phys.* **2010**, *211* (17), 1890–1899. https://doi.org/10.1002/macp.201000132.

(54) Che, Y.; Brooks, B. R.; Marshall, G. R. Protein Recognition Motifs: Design of Peptidomimetics of Helix Surfaces. *Biopolymers* **2007**, *86* (4), 288–297. https://doi.org/10.1002/bip.20744.

(55) *Introduction to Supramolecular Chemistry*; Kluwer Academic Publishers: Dordrecht, 2002. https://doi.org/10.1007/0-306-47587-1.

(56) Leu, W. C. W.; Hartley, C. S. A Push–Pull Macrocycle With Both Linearly Conjugated and Cross-Conjugated Bridges. *Org. Lett.* **2013**, *15* (14), 3762–3765. https://doi.org/10.1021/ol401697d.

(57) Pu, K.-Y.; Liu, B. Conjugated Polyelectrolytes as Light-Up Macromolecular Probes for Heparin Sensing. *Adv. Funct. Mater.* **2009**, *19* (2), 277–284. https://doi.org/10.1002/adfm.200800960.

(58) Guan, W.; Zhou, W.; Lu, C.; Tang, B. Z. Synthesis and Design of Aggregation-Induced

Emission Surfactants: Direct Observation of Micelle Transitions and Microemulsion Droplets. *Angew. Chem. Int. Ed.* **2015**, *54* (50), 15160–15164. https://doi.org/10.1002/anie.201507236.

(59) Koren, A. B.; Curtis, M. D.; Francis, A. H.; Kampf, J. W. Intermolecular Interactions in π-Stacked Conjugated Molecules. Synthesis, Structure, and Spectral Characterization of Alkyl Bithiazole Oligomers. *J. Am. Chem. Soc.* **2003**, *125* (17), 5040–5050. https://doi.org/10.1021/ja029216m.

(60) Mei, J.; Hong, Y.; Lam, J. W. Y.; Qin, A.; Tang, Y.; Tang, B. Z. Aggregation-Induced Emission: The Whole Is More Brilliant than the Parts. *Adv. Mater.* **2014**, *26* (31), 5429–5479. https://doi.org/10.1002/adma.201401356.

(61) Krzeszewski, M.; Thorsted, B.; Brewer, J.; Gryko, D. T. Tetraaryl-, Pentaaryl-, and Hexaaryl-1,4-Dihydropyrrolo[3,2-b]Pyrroles: Synthesis and Optical Properties. *J. Org. Chem.* **2014**, *79* (7), 3119–3128. https://doi.org/10.1021/jo5002643.

(62) Poronik, Y. M.; Mazur, L. M.; Samoć, M.; Jacquemin, D.; Gryko, D. T. 2,5-Bis(Azulenyl)Pyrrolo[3,2-b]Pyrroles – the Key Influence of the Linkage Position on the Linear and Nonlinear Optical Properties. *J. Mater. Chem. C* **2017**, *5* (10), 2620–2628. https://doi.org/10.1039/C7TC00276A.

(63) Mishra, S.; Krzeszewski, M.; Pignedoli, C. A.; Ruffieux, P.; Fasel, R.; Gryko, D. T. On-Surface Synthesis of a Nitrogen-Embedded Buckybowl with Inverse Stone–Thrower–Wales Topology. *Nat. Commun.* **2018**, *9* (1), 1714. https://doi.org/10.1038/s41467-018-04144-5.

(64) Hemetsberger, H.; Knittel, D. Synthese und Thermolyse von α-Azidoacrylestern. *Monatshefte Für Chem. Chem. Mon.* **1972**, *103* (1), 194–204. https://doi.org/10.1007/BF00912944.

(65) Janiga, A.; Gryko, D. T. 1,4-Dihydropyrrolo[3,2-b]Pyrrole and Its π-Expanded

Analogues. *Chem. Asian J.* **2014**, *9* (11), 3036–3045. https://doi.org/10.1002/asia.201402367.

(66) Hayase, F.; Usui, T.; Watanabe, H. Chemistry and Some Biological Effects of Model Melanoidins and Pigments as Maillard Intermediates. *Mol. Nutr. Food Res.* **2006**, *50* (12), 1171–1179. https://doi.org/10.1002/mnfr.200600078.

(67) Hayase, F.; Usui, T.; Ono, Y.; Shirahashi, Y.; Machida, T.; Ito, T.; Nishitani, N.; Shimohira, K.; Watanabe, H. Formation Mechanisms of Melanoidins and Fluorescent Pyridinium Compounds as Advanced Glycation End Products. *Ann. N. Y. Acad. Sci.* **2008**, *1126*, 53–58. https://doi.org/10.1196/annals.1433.009.

(68) Shirahashi, Y.; Watanabe, H.; Hayase, F. Identification of Red Pigments Formed in a D-Xylose-Glycine Reaction System. *Biosci. Biotechnol. Biochem.* **2009**, *73* (10), 2287–2292. https://doi.org/10.1271/bbb.90382.

(69) Ono, Y.; Watanabe, H.; Hayase, F. Identification of the Blue Pigment Formed in a D-Glucose-Glycine Reaction System. *Biosci. Biotechnol. Biochem.* **2010**, *74* (12), 2526–2528. https://doi.org/10.1271/bbb.100589.

(70) Janiga, A.; Krzeszewski, M.; Gryko, D. T. Diindolo[2,3-b:2′,3′-f]Pyrrolo[3,2-b]Pyrroles as Electron-Rich, Ladder-Type Fluorophores: Synthesis and Optical Properties. *Chem. – Asian J.* **2015**, *10* (1), 212–218. https://doi.org/10.1002/asia.201402925.

(71) Stężycki, R.; Reger, D.; Hoelzel, H.; Jux, N.; Gryko, D. T. Synthesis and Photophysical Properties of Hexaphenylbenzene–Pyrrolo[3,2-b]Pyrroles. *Synlett* **2018**, *29* (19), 2529–2534. https://doi.org/10.1055/s-0037-1610286.

(72) Janiga, A.; Bednarska, D.; Thorsted, B.; Brewer, J.; Gryko, D. T. Quadrupolar, Emission-Tunable π-Expanded 1,4-Dihydropyrrolo[3,2-b]Pyrroles – Synthesis and Optical Properties. *Org. Biomol. Chem.* **2014**, *12* (18), 2874–2881.

https://doi.org/10.1039/C4OB00143E.

(73) Tasior, M.; Chotkowski, M.; Gryko, D. T. Extension of Pyrrolopyrrole π-System: Approach to Constructing Hexacyclic Nitrogen-Containing Aromatic Systems. *Org. Lett.* **2015**, *17* (24), 6106–6109. https://doi.org/10.1021/acs.orglett.5b03129.

(74) Tasior, M.; Gryko, D. T. Synthesis and Properties of Ladder-Type BN-Heteroacenes and Diazabenzoindoles Built on a Pyrrolopyrrole Scaffold. *J. Org. Chem.* **2016**, *81* (15), 6580–6586. https://doi.org/10.1021/acs.joc.6b01209.

(75) Li, K.; Liu, Y.; Li, Y.; Feng, Q.; Hou, H.; Tang, B. Z. 2,5-Bis(4-Alkoxycarbonylphenyl)-1,4-Diaryl-1,4-Dihydropyrrolo[3,2-b]Pyrrole (AAPP) AIEgens: Tunable RIR and TICT Characteristics and Their Multifunctional Applications. *Chem. Sci.* **2017**, *8* (10), 7258–7267. https://doi.org/10.1039/C7SC03076B.

(76) Zhe, P.; Yingchun, J.; Zhi, W.; Bin, T.; Jianbing, S.; Yuping, D. Properties of Polymorphism and Acid Response of Pyrrolopyrrole-Based Derivative with Aggregation-Induced Emission Behavior. *Acta Chim. Sin.* **2016**, *74* (11), 942. https://doi.org/10.6023/A16080406.

(77) Ji, Y.; Peng, Z.; Tong, B.; Shi, J.; Zhi, J.; Dong, Y. Polymorphism-Dependent Aggregation-Induced Emission of Pyrrolopyrrole-Based Derivative and Its Multi-Stimuli Response Behaviors. *Dyes Pigments* **2017**, *139*, 664–671. https://doi.org/10.1016/j.dyepig.2016.12.061.

(78) Stężycki, R.; Grzybowski, M.; Clermont, G.; Blanchard-Desce, M.; Gryko, D. T. Z-Shaped Pyrrolo[3,2-b]Pyrroles and Their Transformation into π-Expanded Indolo[3,2-b]Indoles. *Chem. – Eur. J.* **2016**, *22* (15), 5198–5203. https://doi.org/10.1002/chem.201505052.

(79) Wang, X.; Zhang, F.; Liu, J.; Tang, R.; Fu, Y.; Wu, D.; Xu, Q.; Zhuang, X.; He, G.; Feng, X. Ladder-Type BN-Embedded Heteroacenes with Blue Emission. *Org. Lett.* **2013**,

15 (22), 5714–5717. https://doi.org/10.1021/ol402745r.

(80) Wang, C.; Nishida, J.; Bryce, M. R.; Yamashita, Y. Synthesis, Characterization, and OFET and OLED Properties of π-Extended Ladder-Type Heteroacenes Based on Indolodibenzothiophene. *Bull. Chem. Soc. Jpn.* **2012**, *85* (1), 136–143. https://doi.org/10.1246/bcsj.20110255.

(81) Back, J. Y.; Kim, Y.; An, T. K.; Kang, M. S.; Kwon, S.-K.; Park, C. E.; Kim, Y.-H. Synthesis and Electrical Properties of Novel Oligomer Semiconductors for Organic Field-Effect Transistors (OFETs): Asymmetrically End-Capped Acene-Heteroacene Conjugated Oligomers. *Dyes Pigments* **2015**, *112*, 220–226. https://doi.org/10.1016/j.dyepig.2014.07.008.

(82) Kim, Y.; Hong, J.; Oh, J. H.; Yang, C. Naphthalene Diimide Incorporated Thiophene-Free Copolymers with Acene and Heteroacene Units: Comparison of Geometric Features and Electron-Donating Strength of Co-Units. **2013**. https://doi.org/10.1021/CM401829X.

(83) Kim, J.; Jo, Y.; Choi, W.-Y.; Jun, Y.; Yang, C. Thiophene-Fused Coplanar Sensitizer for Dye-Sensitized Solar Cells. *Tetrahedron Lett.* **2011**, *52* (21), 2764–2766. https://doi.org/10.1016/j.tetlet.2011.03.091.

(84) Canjeevaram Balasubramanyam, R. K.; Kumar, R.; Ippolito, S. J.; Bhargava, S. K.; Periasamy, S. R.; Narayan, R.; Basak, P. Quadrupolar (A-π-D-π-A) Tetra-Aryl 1,4-Dihydropyrrolo[3,2-b]Pyrroles as Single Molecular Resistive Memory Devices: Substituent Triggered Amphoteric Redox Performance and Electrical Bistability. *J. Phys. Chem. C* **2016**, *120* (21), 11313–11323. https://doi.org/10.1021/acs.jpcc.5b11509.

(85) Wu, J.-Y.; Yu, C.-H.; Wen, J.-J.; Chang, C.-L.; Leung, M. Pyrrolo-[3,2-b]Pyrroles for Photochromic Analysis of Halocarbons. *Anal. Chem.* **2016**, *88* (2), 1195–1201. https://doi.org/10.1021/acs.analchem.5b03374.

(86) Peng, Z.; Feng, X.; Tong, B.; Chen, D.; Shi, J.; Zhi, J.; Dong, Y. The Selective Detection of Chloroform Using an Organic Molecule with Aggregation-Induced Emission Properties in the Solid State as a Fluorescent Sensor. *Sens. Actuators B Chem.* **2016**, *232*, 264–268. https://doi.org/10.1016/j.snb.2016.03.136.

(87) Domínguez, R.; Montcada, N. F.; de la Cruz, P.; Palomares, E.; Langa, F. Pyrrolo[3,2-b]Pyrrole as the Central Core of the Electron Donor for Solution-Processed Organic Solar Cells. *ChemPlusChem* **2017**, *82* (7), 1096–1104. https://doi.org/10.1002/cplu.201700158.

(88) Tasior, M.; Czichy, M.; Łapkowski, M.; Gryko, D. T. Dibenzothienopyrrolo[3,2-b]Pyrrole: The Missing Member of the Thienoacene Family. *Chem. – Asian J.* **2018**, *13* (4), 449–456. https://doi.org/10.1002/asia.201701639.

(89) Łukasiewicz, Ł. G.; Ryu, H. G.; Mikhaylov, A.; Azarias, C.; Banasiewicz, M.; Kozankiewicz, B.; Ahn, K. H.; Jacquemin, D.; Rebane, A.; Gryko, D. T. Symmetry Breaking in Pyrrolo[3,2-b]Pyrroles: Synthesis, Solvatofluorochromism and Two-Photon Absorption. *Chem. – Asian J.* **2017**, *12* (14), 1736–1748. https://doi.org/10.1002/asia.201700159.

(90) Kumagai, T.; Tanaka, S.; Mukai, T. Synthesis of 1,4-Dihydropyrrolo[3,2-b]Pyrrole. *Tetrahedron Lett.* **1984**, *25* (49), 5669–5672. https://doi.org/10.1016/S0040-4039(01)91408-X.

(91) Curiel, D.; Más-Montoya, M.; Usea, L.; Espinosa, A.; Orenes, R. A.; Molina, P. Indolocarbazole-Based Ligands for Ladder-Type Four-Coordinate Boron Complexes. *Org. Lett.* **2012**, *14* (13), 3360–3363. https://doi.org/10.1021/ol301339y.

(92) Iida, A.; Yamaguchi, S. Thiophene-Fused Ladder Boroles with High Antiaromaticity. *J. Am. Chem. Soc.* **2011**, *133* (18), 6952–6955. https://doi.org/10.1021/ja2019977.

(93) Sadowski, B.; Hassanein, K.; Ventura, B.; Gryko, D. T.

Tetraphenylethylenepyrrolo[3,2-b]Pyrrole Hybrids as Solid-State Emitters: The Role of Substitution Pattern. *Org. Lett.* **2018**, *20* (11), 3183–3186. https://doi.org/10.1021/acs.orglett.8b01011.

(94) Krzeszewski, M.; Sahara, K.; Poronik, Y. M.; Kubo, T.; Gryko, D. T. Unforeseen 1,2-Aryl Shift in Tetraarylpyrrolo[3,2-b]Pyrroles Triggered by Oxidative Aromatic Coupling. *Org. Lett.* **2018**, *20* (6), 1517–1520. https://doi.org/10.1021/acs.orglett.8b00223.

(95) Tsuji, H.; Nakamura, E. Design and Functions of Semiconducting Fused Polycyclic Furans for Optoelectronic Applications. *Acc. Chem. Res.* **2017**, *50* (2), 396–406. https://doi.org/10.1021/acs.accounts.6b00595.

(96) Cao, H.; Brettell-Adams, I. A.; Qu, F.; Rupar, P. A. Bridged Difurans: Stabilizing Furan with p-Block Elements. *Organometallics* **2017**, *36* (14), 2565–2572. https://doi.org/10.1021/acs.organomet.7b00135.

(97) Zhang, Z.; Zhu, X. Dithienosilole-Based Non-Fullerene Acceptors for Efficient Organic Photovoltaics. *J. Mater. Chem. A* **2018**, *6* (10), 4266–4270. https://doi.org/10.1039/C7TA10957A.

(98) Chan, J. C.-H.; Lam, W. H.; Yam, V. W.-W. A Highly Efficient Silole-Containing Dithienylethene with Excellent Thermal Stability and Fatigue Resistance: A Promising Candidate for Optical Memory Storage Materials. *J. Am. Chem. Soc.* **2014**, *136* (49), 16994–16997. https://doi.org/10.1021/ja5101855.

(99) Wang, C.; Taki, M.; Sato, Y.; Fukazawa, A.; Higashiyama, T.; Yamaguchi, S. Super-Photostable Phosphole-Based Dye for Multiple-Acquisition Stimulated Emission Depletion Imaging. *J. Am. Chem. Soc.* **2017**, *139* (30), 10374–10381. https://doi.org/10.1021/jacs.7b04418.

(100) Zhao, X.; Gan, Z.; Hu, C.; Duan, Z.; Mathey, F. Planar Polycyclic Oxaphosphoranes

Incorporating a Benzophosphole Unit. *Org. Lett.* **2017**, *19* (21), 5814–5817. https://doi.org/10.1021/acs.orglett.7b02769.

(101) Woodward, A. N.; Kolesar, J. M.; Hall, S. R.; Saleh, N.-A.; Jones, D. S.; Walter, M. G. Thiazolothiazole Fluorophores Exhibiting Strong Fluorescence and Viologen-Like Reversible Electrochromism. *J. Am. Chem. Soc.* **2017**, *139* (25), 8467–8473. https://doi.org/10.1021/jacs.7b01005.

(102) Cai, Z.; Lo, W.-Y.; Zheng, T.; Li, L.; Zhang, N.; Hu, Y.; Yu, L. Exceptional Single-Molecule Transport Properties of Ladder-Type Heteroacene Molecular Wires. *J. Am. Chem. Soc.* **2016**, *138* (33), 10630–10635. https://doi.org/10.1021/jacs.6b05983.

(103) Wu, D.; Zheng, J.; Xu, C.; Kang, D.; Hong, W.; Duan, Z.; Mathey, F. Phosphindole Fused Pyrrolo[3,2-b]Pyrroles: A New Single-Molecule Junction for Charge Transport. *Dalton Trans.* **2019**, *48* (19), 6347–6352. https://doi.org/10.1039/C9DT01299K.

(104) Tsutsumi, J.; Matsuoka, S.; Inoue, S.; Minemawari, H.; Yamada, T.; Hasegawa, T. N-Type Field-Effect Transistors Based on Layered Crystalline Donor–Acceptor Semiconductors with Dialkylated Benzothienobenzothiophenes as Electron Donors. *J. Mater. Chem. C* **2015**, *3* (9), 1976–1981. https://doi.org/10.1039/C4TC02481H.

(105) Zhang, A.; Xiao, H.; Cong, S.; Zhang, M.; Zhang, H.; Bo, S.; Wang, Q.; Zhen, Z.; Liu, X. A Systematic Study of the Structure–Property Relationship of a Series of Nonlinear Optical (NLO) Julolidinyl-Based Chromophores with a Thieno[3,2-b]Thiophene Moiety. *J. Mater. Chem. C* **2014**, *3* (2), 370–381. https://doi.org/10.1039/C4TC01896F.

(106) Dal Molin, M.; Verolet, Q.; Colom, A.; Letrun, R.; Derivery, E.; Gonzalez-Gaitan, M.; Vauthey, E.; Roux, A.; Sakai, N.; Matile, S. Fluorescent Flippers for Mechanosensitive Membrane Probes. *J. Am. Chem. Soc.* **2015**, *137* (2), 568–571. https://doi.org/10.1021/ja5107018.

(107) Inouchi, T.; Nakashima, T.; Kawai, T. Acid–Base-Responsive Intense Charge-

Transfer Emission in Donor–Acceptor-Conjugated Fluorophores. *Chem. – Asian J.* **2014**, *9* (9), 2542–2547. https://doi.org/10.1002/asia.201402463.

(108) Peng, Z.; Ji, Y.; Huang, Z.; Tong, B.; Shi, J.; Dong, Y. A Strategy for the Molecular Design of Aggregation-Induced Emission Units Further Modified by Substituents. *Mater. Chem. Front.* **2018**, *2* (6), 1175–1183. https://doi.org/10.1039/C8QM00096D.

(109) Dereka, B.; Rosspeintner, A.; Krzeszewski, M.; Gryko, D. T.; Vauthey, E. Symmetry-Breaking Charge Transfer and Hydrogen Bonding: Toward Asymmetrical Photochemistry. *Angew. Chem. Int. Ed.* **2016**, *55* (50), 15624–15628. https://doi.org/10.1002/anie.201608567.

(110) Friese, D. H.; Mikhaylov, A.; Krzeszewski, M.; Poronik, Y. M.; Rebane, A.; Ruud, K.; Gryko, D. T. Pyrrolo[3,2-b]Pyrroles—From Unprecedented Solvatofluorochromism to Two-Photon Absorption. *Chem. – Eur. J.* **2015**, *21* (50), 18364–18374. https://doi.org/10.1002/chem.201502762.

(111) Hawes, C. S.; Máille, G. M. Ó.; Byrne, K.; Schmitt, W.; Gunnlaugsson, T. Tetraarylpyrrolo[3,2-b]Pyrroles as Versatile and Responsive Fluorescent Linkers in Metal–Organic Frameworks. *Dalton Trans.* **2018**, *47* (30), 10080–10092. https://doi.org/10.1039/C8DT01784K.

(112) Waltenberger, B.; Wiechmann, K.; Bauer, J.; Markt, P.; Noha, S. M.; Wolber, G.; Rollinger, J. M.; Werz, O.; Schuster, D.; Stuppner, H. Pharmacophore Modeling and Virtual Screening for Novel Acidic Inhibitors of Microsomal Prostaglandin E2 Synthase-1 (MPGES-1). *J. Med. Chem.* **2011**, *54* (9), 3163–3174. https://doi.org/10.1021/jm101309g.

(113) Rörsch, F.; Wobst, I.; Zettl, H.; Schubert-Zsilavecz, M.; Grösch, S.; Geisslinger, G.; Schneider, G.; Proschak, E. Nonacidic Inhibitors of Human Microsomal Prostaglandin Synthase 1 (MPGES 1) Identified by a Multistep Virtual Screening Protocol. *J. Med.*

Chem. **2010**, *53* (2), 911–915. https://doi.org/10.1021/jm9012505.

(114) Welterlich, I.; Charov, O.; Tieke, B. Deeply Colored Polymers Containing 1,3,4,6-Tetraarylpyrrolo[3,2-b]Pyrrole-2,5-Dione (IsoDPP) Units in the Main Chain. *Macromolecules* **2012**, *45* (11), 4511–4519. https://doi.org/10.1021/ma300483u.

(115) Santra, M.; Jun, Y. W.; Bae, J.; Sarkar, S.; Choi, W.; Gryko, D. T.; Ahn, K. H. Water-Soluble Pyrrolo[3,2-b]Pyrroles: Synthesis, Luminescence and Two-Photon Cellular Imaging Properties. *Asian J. Org. Chem.* **2017**, *6* (3), 278–281. https://doi.org/10.1002/ajoc.201600613.

(116) Tasior, M.; Hassanein, K.; Mazur, L. M.; Sakellari, I.; Gray, D.; Farsari, M.; Samoć, M.; Santoro, F.; Ventura, B.; Gryko, D. T. The Role of Intramolecular Charge Transfer and Symmetry Breaking in the Photophysics of Pyrrolo[3,2-b]Pyrrole-Dione. *Phys. Chem. Chem. Phys.* **2018**, *20* (34), 22260–22271. https://doi.org/10.1039/C8CP03755H.

(117) Song, C.; Knight, D. W.; Whatton (neé Fagan), M. A. A New Method for the Acylation of Pyrroles. *Tetrahedron Lett.* **2004**, *45* (52), 9573–9576. https://doi.org/10.1016/j.tetlet.2004.10.133.

(118) Wang, J.; Chai, Z.; Liu, S.; Fang, M.; Chang, K.; Han, M.; Hong, L.; Han, H.; Li, Q.; Li, Z. Organic Dyes Based on Tetraaryl-1,4-Dihydropyrrolo-[3,2-b]Pyrroles for Photovoltaic and Photocatalysis Applications with the Suppressed Electron Recombination. *Chem. – Eur. J.* **2018**, *24* (68), 18032–18042. https://doi.org/10.1002/chem.201803688.

119) Welterlich, I.; Neudörfl, J.-M.; Tieke, B. Electrochemical Polymerization of 1,3,4,6-Tetraarylpyrrolo[3,2-b]Pyrrole-2,5-Dione (IsoDPP) Derivatives. *Polym. Chem.* **2015**, *6* (6), 1005–1013. https://doi.org/10.1039/C4PY01315H.

(120) Zhang, H.; Welterlich, I.; Neudörfl, J.-M.; Tieke, B.; Yang, C.; Chen, X.; Yang, W. Synthesis and Characterization of 1,3,4,6-Tetraarylpyrrolo[3,2-b]-Pyrrole-2,5-Dione

(IsoDPP)-Based Donor–Acceptor Polymers with Low Band Gap. *Polym. Chem.* **2013**, *4* (17), 4682–4689. https://doi.org/10.1039/C3PY00570D.

(121) Tasior, M.; Koszarna, B.; Young, D. C.; Bernard, B.; Jacquemin, D.; Gryko, D.; Gryko, D. T. Fe(III)-Catalyzed Synthesis of Pyrrolo[3,2-b]Pyrroles: Formation of New Dyes and Photophysical Studies. *Org. Chem. Front.* **2019**, *6* (16), 2939–2948. https://doi.org/10.1039/C9QO00675C.

(122) Purba, P. C.; Bhattacharyya, S.; Maity, M.; Mukhopadhyay, S.; Howlader, P.; Mukherjee, P. S. Linkage Induced Enhancement of Fluorescence in Metal–Carbene Bond Directed Metallacycles and Metallacages. *Chem. Commun.* **2019**, *55* (57), 8309–8312. https://doi.org/10.1039/C9CC04444B.

(123) Yano, Y.; Ono, T.; Hatanaka, S.; Gryko, D. T.; Hisaeda, Y. Salt–Cocrystal Continuum for Photofunction Modulation: Stimuli-Responsive Fluorescence Color-Tuning of Pyridine-Modified Intramolecular Charge-Transfer Dyes and Acid Complexes. *J. Mater. Chem. C* **2019**, *7* (29), 8847–8854. https://doi.org/10.1039/C9TC02524C.

Chapter 2: A new 'Off-On' System Based on Core-substituted Naphthalenediimide with Dimethylamine for Reversible Acid-Base Sensor

2.1 Introduction

As we know that in our daily life pH plays important role in many aspects such as chemical, environmental and biological processes. For this reason, accurate measurement of pH is of great importance in different fields of science and technology.[1] As per study the cell homeostasis regulation and many metabolic pathways are governed by pH not only limited to chemistry but also in biochemistry, cellular biology and drug delivery system.[2,3] Interestingly to understand pH changes, there are number of glass-pH-electrodes which are widely used as pH sensor that measures pH in wide range of pH range from acidic to neutral to basic media. Particularly the glass pH electrodes shows low detection limit, free from the interference, long term stability with excellent reproducibility.[4] Still, there are few drawbacks that limits the usage of this pH-glass electrode such as temperature dependent nature, complex design and fragility. In addition to these drawbacks, fabrication of the electrode is extra difficult task and invasive nature makes it difficult to use for further sensing application effectively. Nowadays optical pH sensing area has attracted attention of researchers and having a great demand as it is widely accepted method over various fabricated glass-pH electrodes.[5] In this regard, there are a number of fluorescent molecules have been developed which can be used for pH sensing application which are specifically based on absorption and fluorescence changes of the indicator. As per literature study the fluorescent based pH indicators display high sensitivity and therefore can be employed in different areas.[6] Actually there are various methods and devices available for measurement of pH but fluorescence microscopy becomes the most powerful tool for sensing application successfully. Basically the fluorescent materials follow two important charge transfer systems particularly the photoinduced electron transfer (PET)[7], intramolecular charge

transfer (ICT)[8] FRET Fluorescence resonance energy transfer[9]. All chemosensor which are representing the PET consists of fluorophore-spacer-receptor comprising of PET acceptor (denoted as fluorophore) and PET donor (an amine).[10] However, in actual practice the design, synthesis and application of the probe should be carried out by applying the simplest synthetic strategies. One additional important thing is proper cell permeability which is very necessary requirement that is able to detect pH weakly in acidic environment.[11]

Naphthalene diimides (NDIs) among the planar aromatic molecule, the has wide application in various field[10,12–15] due to easy synthesis, functionalisation to the both the anhydride position as well as substitutions at the core. Also NDIs exhibits very good optical properties and strong fluorescence.[12] In addition to this NDI shown to be excellent candidate in the field of supramolecular chemistry due to its planar nature. In literature various self-assembled structures have been produced due to their flexible π- π interactions with solvophobic control. Fascinatingly, the optical properties of the NDI can be altered by changing the core-substitution of NDIs such as nitrogen, sulphur and oxygen selectively.[16–18] Generally, it is observed that NDI based molecule shows non-fluorescent behaviour in aqueous medium especially water due aggregation caused quenching phenomenon which is the most common process observed in many fluorophores. NDI comprising of more π - acidity, and together with their redox behaviour have fascinated attention of many researchers in different fields such as sensing, semiconductor material, and self-assembly application successfully.[19] However due to easy functionalization to the NDIs core, it shows better solubility as compared with other organic molecules such as perylene, terrylene and quaterrylenes. By taking benefit several NDIs core substituted aromatic amines are synthesized for sensing applications.[20–25] Recently NDIs are especially more desirable in sensing application as they are small and can be simply functionalized with good solubility in different solvent exhibiting tunable fluorescence based on the core-substituents. In this

paper, we report a new cores-substituted NDI bearing dimethylamine at both 2- and 6-positions to produce 4,9-bis(dimethylamino)-2,7-dioctylbenzo [lmn][3,8]phenanthroline-1,3,6,8(2H,7H)-tetraone (Coded as: DDPT **1**; as shown in (Figure 2.1) by reacting dibromo-NDI with dimethylamine in the presence of *N,N'*-dimethylformamide (DMF) and triethylamine (TEA) at 110 ^{o}C for 48 hrs.

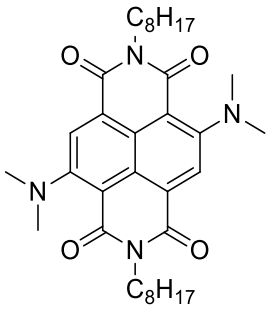

DDPT 1

Figure 2.1: Structure of DDPT **1**

The synthesised molecule characterised by means of ^{1}H NMR, ^{13}C NMR, ESI mass and elemental analysis. **DDPT 1** further used for acid-base sensing application and shows 'switch-on' emission upon addition of acid (TFA) and reversed to original state by addition of base (TEA), this phenomenon can be visualised by naked eye by changing blue to reddish and reverse the color, respectively. Furthermore, the DDPT 1 use for not only calorimetric sensing but also used optical spectroscopy by means of UV-Vis absorption and fluorescence spectroscopy and reversible by addition of TFA and TEA. **DDPT 1** can be used for strip-based sensing, which may in future useful to replace litmus paper, as **DDPT 1** strip can be reused number of time.

2.2 Results and Discussion

2.2.1 Sensing performance of probe 1

First of all, the sensing performance was studied for the DDPT 1 (9×10^{-5} M) in THF upon addition of TFA (0-2.0 equiv). The change in color under day light and UV-light (365 nm)

were as illustarted in (Figure 2.2). It is observed that under day light DDPT 1 in THF displays blue color which changes to purple then radish color while incremental addition of TFA (Fig. 2.2A). Under UV-light (365 nm), DDPT 1 produces blue fluorescence color, however, upon increamental additon from 0-2 equiv. of TFA. The color of the solution shows purple to red emission with increasing concentration of TFA. Thus the observed change in color indicated that the DDPT 1 can be utilized for naked-eye colorimetric and fluorescent sensor H^+ ion selectively.

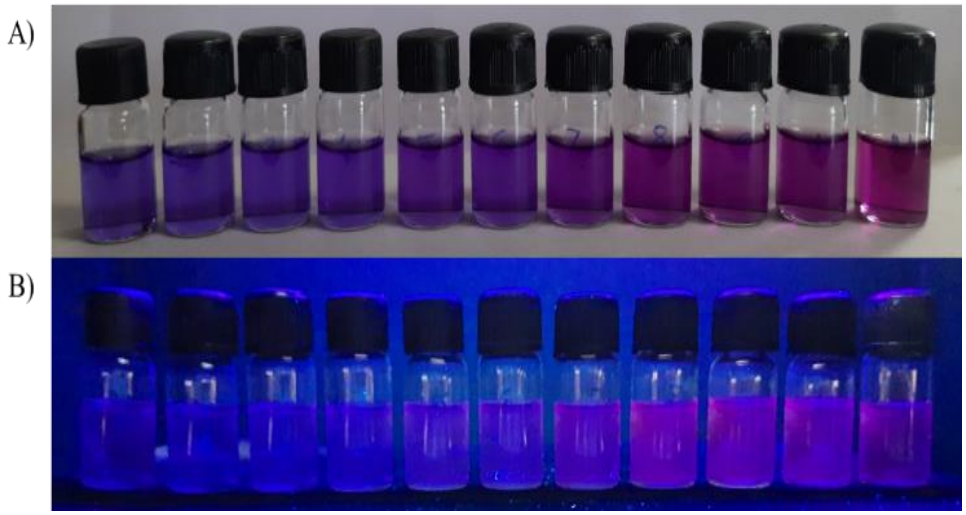

Figure 2.2: Sensing performance of the probe DDPT **1** (90 μM) in THF with the addition of trifluoroacetic acid (0.2 to 2 equiv) A) under visible light B) under UV lightillumination at 365nm.

2.2.2 UV-vis absorption study

In the UV-Vis absorption spectrum of DDPT 1 (9×10^{-5} M) was recorded in THF solvent, which typically produces characteristics absorption band between 350 to 400 nm that is corresponding to π- π^* transition of NDI core. However, the broad and strong absorption band appeared in longer wavelength band at 600 nm is due to n- π^* transition which is occurring because of electron donating nature of dimethylamine group to the core of the NDI (Fig. 2.3A). From these bands, it is clear that the transition is mainly through donation

of electron density in to NDI core from electron donating dimethyl groups present on both substituted sides of NDI core. Upon addition of TFA to the solution of probe the absorption band at 600nm is blue shift to 545 nm with appearance of broad band (Figure 2.3A). The change in absorption is due to photoinduced electron transfer from quaternary amine to the core of NDI. This prominent change in absorption change is due to protonation occurring at the tertiary amine on the NDI core to give the quaternary amine. However, the addition of TFA to the solution of NDI does not affect the absorption band appearing in the 350 to 400 nm. The UV-Vis changes in absorption ultimately suggest that the probe is highly selective towards H^+ ion. Further UV-Vis titration was performed for the probe as shown in (Figure 2.3B).

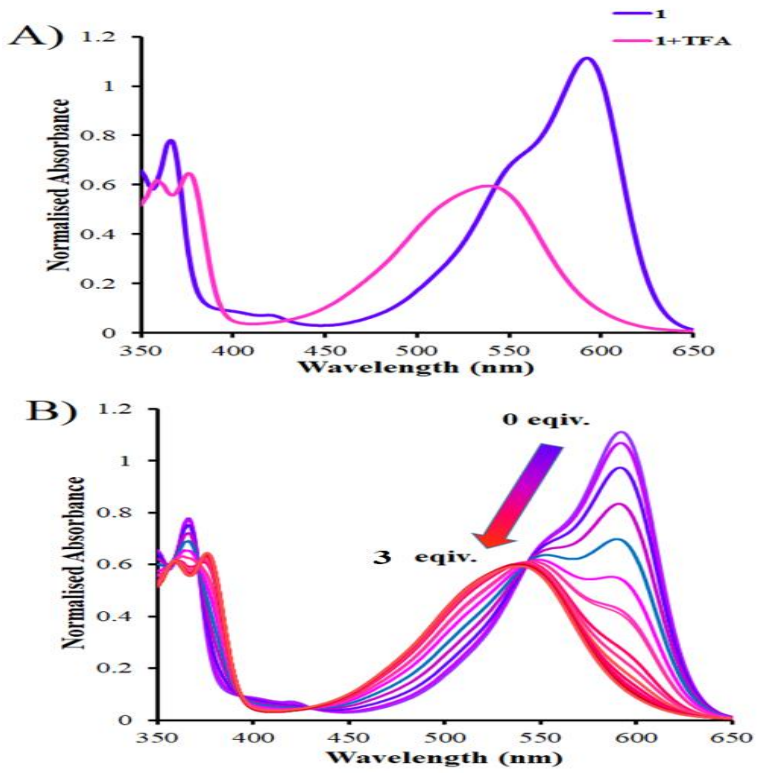

Figure 2.3: UV-Vis absorption spectra of **1** (90 μM) and DDPT **1**+TFA. B) Absorption spectra of DDPT **1** with incremental addition 0.2 equiv. of TFA started with 0 up to 3 equiv. in THF.

The absorption changes were recorded upon incremental addition of 0-2 equiv. TFA and it was observed that with increase in TFA in the solution of DDPT 1 there is shift in absorption with the frequent decrease in absorption band at 600 nm and blue shifted band to 545 nm with crossing at 565 nm.

2.2.3 Fluoresence emission study

Moreover the fluorescence emission study was performed for the DDPT 1 towards the senisng of H^+ ion in the solution. The emission spectra of DDPT 1 was studied in various solvents which were shown in (Figure 2.4)

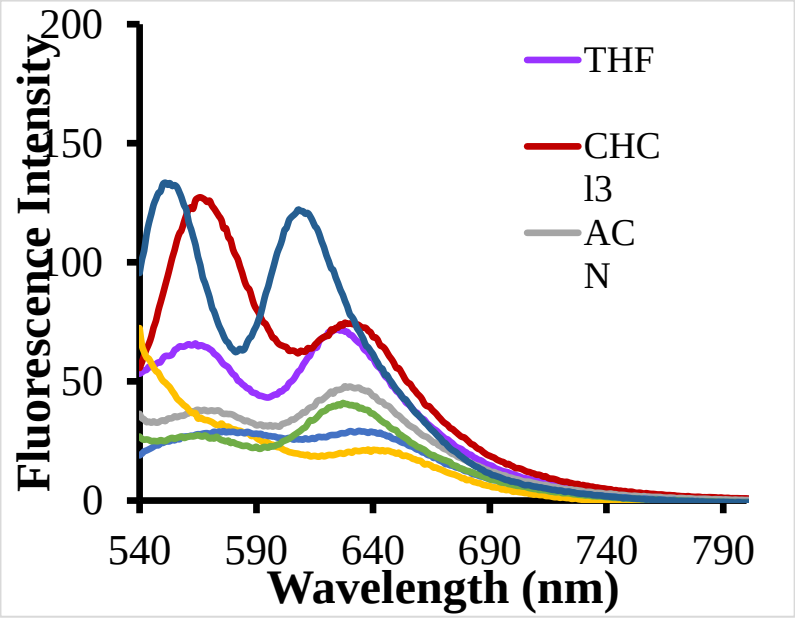

Figure 2.4: Emission spectra of DDPT **1** in various organic solvent.

Fluorescence results obtained are reperesnted in (Figure 2.5). It is observed that the DDPT 1 upon excitation at 520 nm showed emission band appears at 600 nm.The fluorescence color change was observed upon addition of TFA from blue to purple. Howerver, initally there was no significant change upon addition of TFA with weak emission intensity band but upon incremental addition from 0-3.0 equiv. fluorescence emission enhancement was

observed (Figure 2.5B), which is similar to color changes from blue to purple as shows in (Figure 2.2B) under 365 nm wavelength. Initially the fluorescence was very weak with quantum yield of the DDPT 1 in THF at room temperature was found to be ($\Phi = 0.09$), which is ehanced 9 times higher upon addition of 3 equiv. of TFA i.e. quantum yield was increased by upto $\Phi = 0.78$. The choice of 3 equiv. of TFA is to see the saturation point in fluorescence.

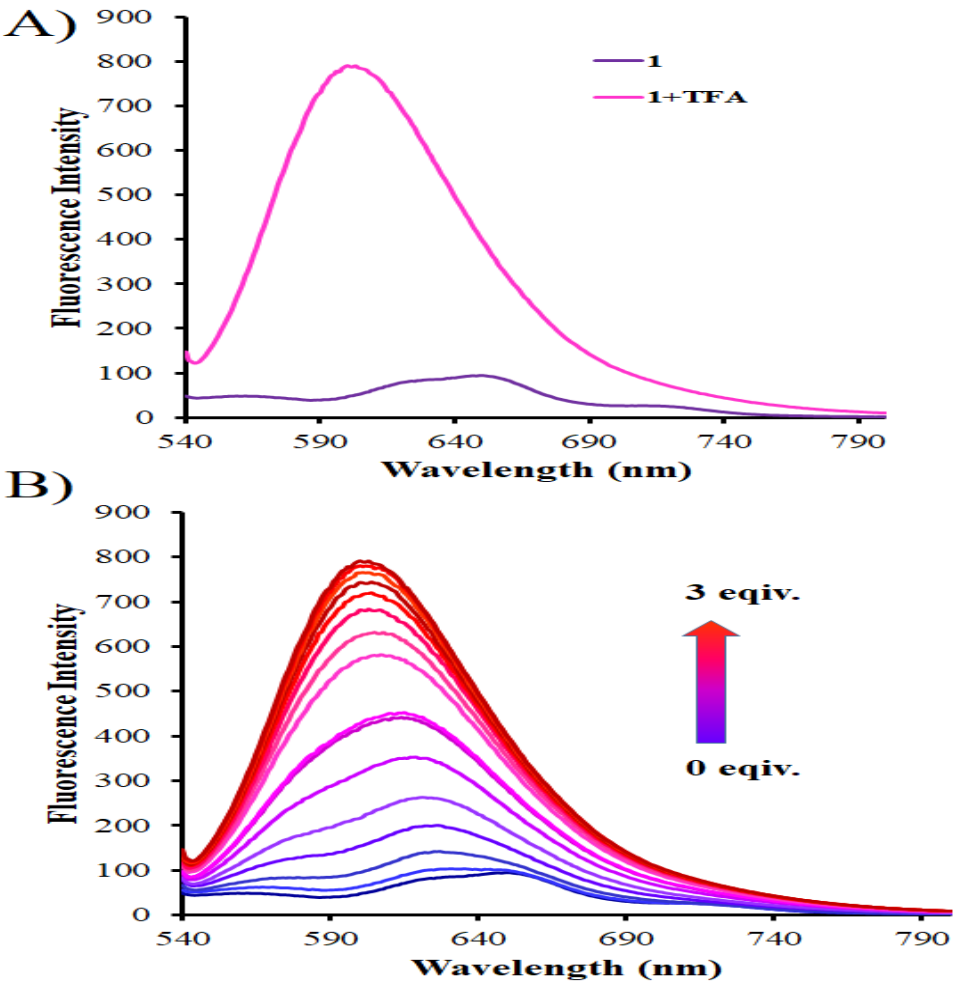

Figure 2.5: Emission spectra of DDPT **1** (90 µM) and 1+TFA. B) Emission spectra of DDPT **1** with incremental addition 0.2 equiv. of TFA started with 0 up to 3 equiv. (90 µM) in THF.

2.2.4 ^{1}H NMR titration with the addtion of TFA

The ^{1}H NMR titration was carried out in order to study effect on chemical shift upon protonation and deprotonation changes occuring in the molecule addition of TFA in solution of the DDPT **1**. It is observed in the ^{1}H NMR titration that upon addition of 2 equiv. of TFA there is appearance of new broad protons peaks (Fig. 2.6).

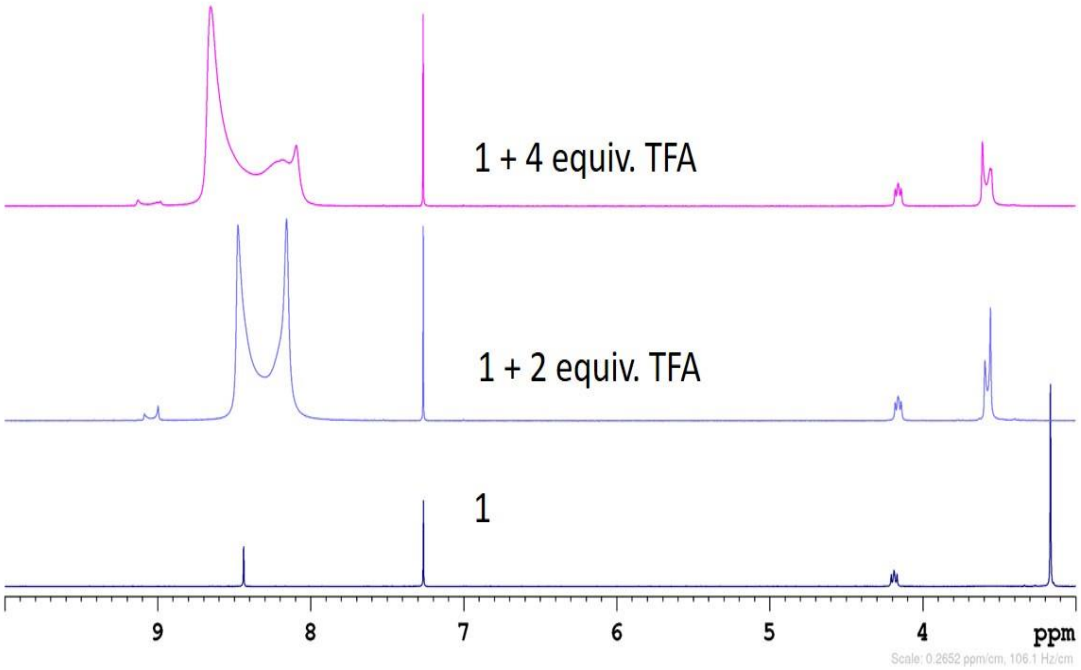

Figure 2.6: ^{1}H NMR titration of the probe 4,9-bis(dimethylamino)-2,7-dioctylbenzo[lmn][3,8]phenanthroline-1,3,6,8(2H,7H)-tetraone (DDPT **1**).

2.2.5 Binding constant

The binding constant of DDPT **1** was further determine by using the Benesi–Hildebrand plot. The binding constant for the H^{+} to receptor was found to be 2.1×10^{-3} M^{-1} (Figure 2.7A).

2.2.6 Limit of detection

The limit of detection can be calculated by (LOD = 3σ/S), where σ is the standard deviation of blank sample and S is the absolute value of the slope between absorption intensity and concentration of H^+ ion. The limit of detection for the probe DDPT **1** is 2.77 nM (Fig. 2.7B). This suggest that the probe DFPDA could be employed as a sensitive fluorescent probe for quantitative detection of H^+ ion.

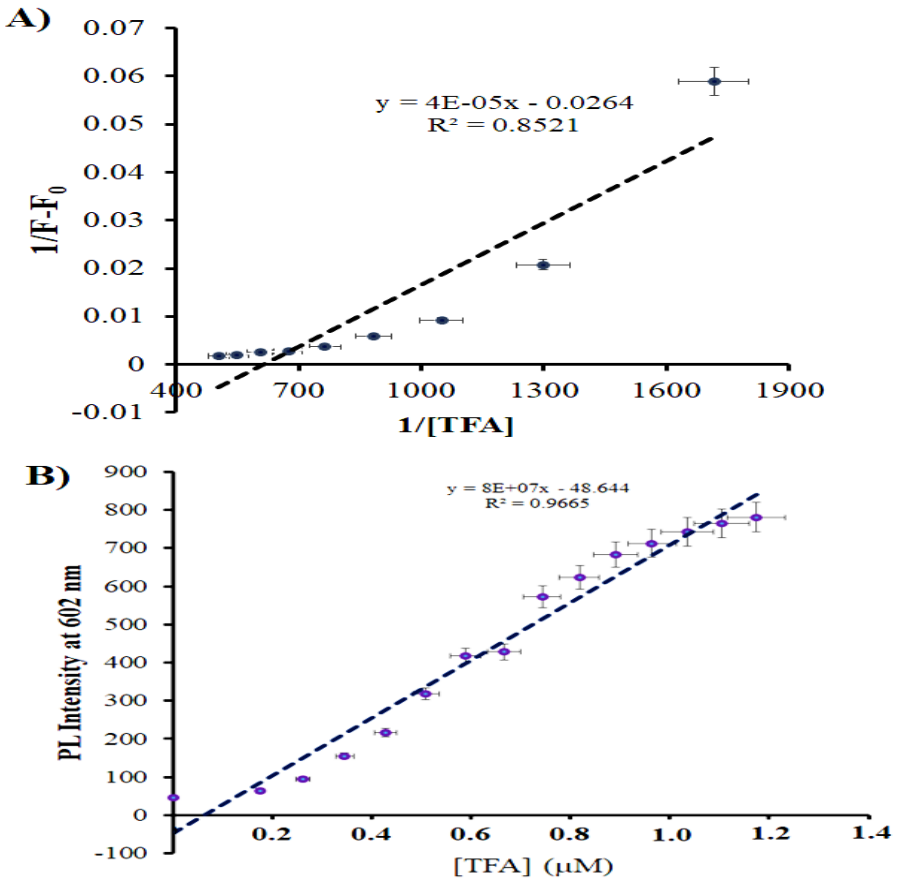

Figure 2.7: A) Benesi–Hildebrand plot, B) LOD plot, of the DDPT **1**.

The recent literature on pH sensor has been included in Table 2.1

Table 2.1: Comparison of pH sensing with recent literature

Sr.No	Compound	Sensing method	LOD	Test strip	Reversibility	References
1	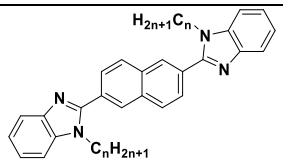	Fluorescence	-	No	Yes	[26]
2	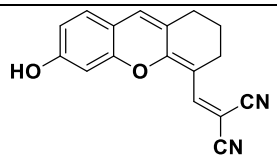	Fluorescence	-	No	Yes	[27]
3	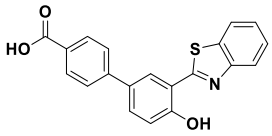	Ratiometric fluorescence	-	Yes	Yes	[28]
4	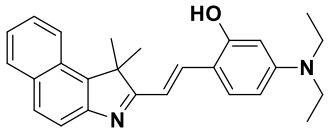	Fluorescence Turn ON	2.967μM	No	No	[29]
5	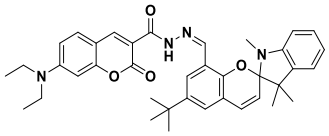	Colorimetric and fluorescence	-	No	Yes	[30]
6	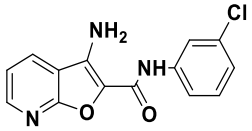	Fluorescence	-	No	No	[31]
7	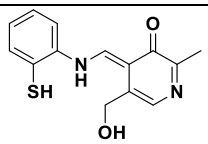	Fluorescence	-	No	No	[32]
8	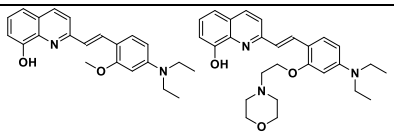	Fluorescent	-	No	No	[33]
9	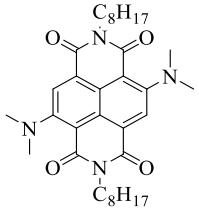	Naked eye colorimetric fluorescent “turn ON” receptor for pH sensing	2.77 nM	Yes	Yes	This work

2.2.7 Reversibility and reusability

The reversibility study was performed for the DDPT **1**, alternative addition of TFA and TEA. It was observed that upon addition of TFA the protonation occurs at the secondary amine while the reversible nature was well studied by addition of base triethylamine. Upon addition of 2 equiv. of triethylamine the DDPT **1** shows reversible nature to the original state. Initially the probe shows blue color but additon of TFA changes the color form blue to purple. However, on addition of base the color of the probe from purple which returns to the blue color of the initial solution of the probe. The absorption and fluorescence spectra was recorded at room temperature for the probe DDPT **1** as shows in (Figure 2.8)

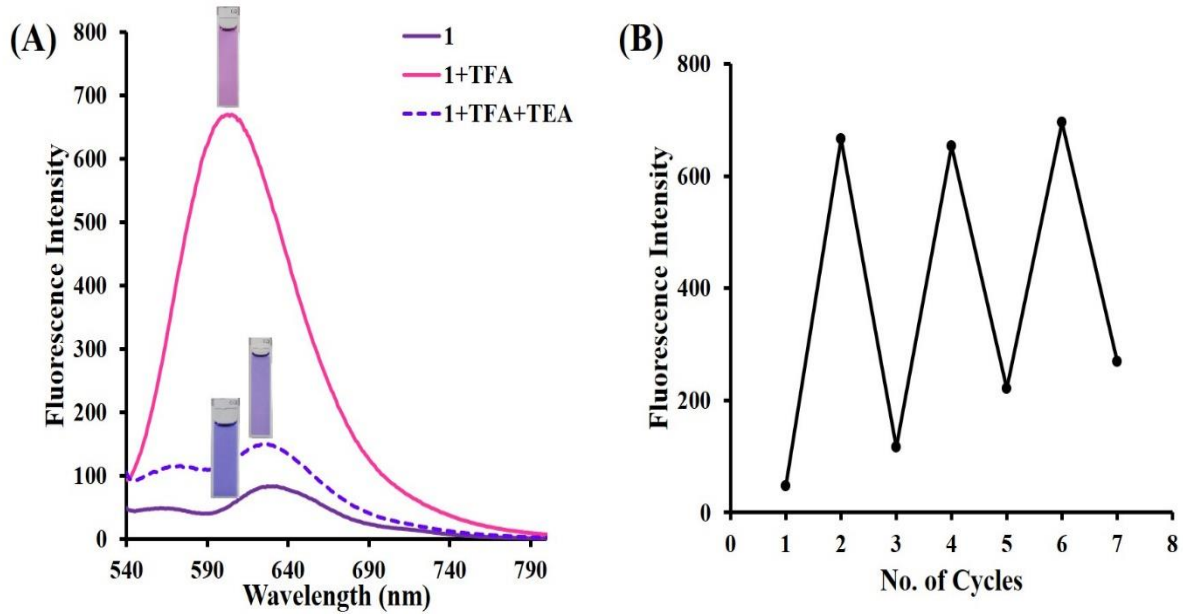

Figure 2.8: Reversibility study of the probe 4,9-bis(dimethylamino)-2,7-dioctylbenzo[lmn][3,8]phenanthroline-1,3,6,8(2H,7H)-tetraone DDPT (A) representing the fluorescence intensity changes occurring upon addition of TFA to the DDPT **1** (B) fluorescence intensity representing the number of reversible cycle for the DDPT **1**.

It is clearly observed that the addition of acid and base shows the reversible nature reproducing blue color and shows the absorption close to the blank (Figure 2.9).

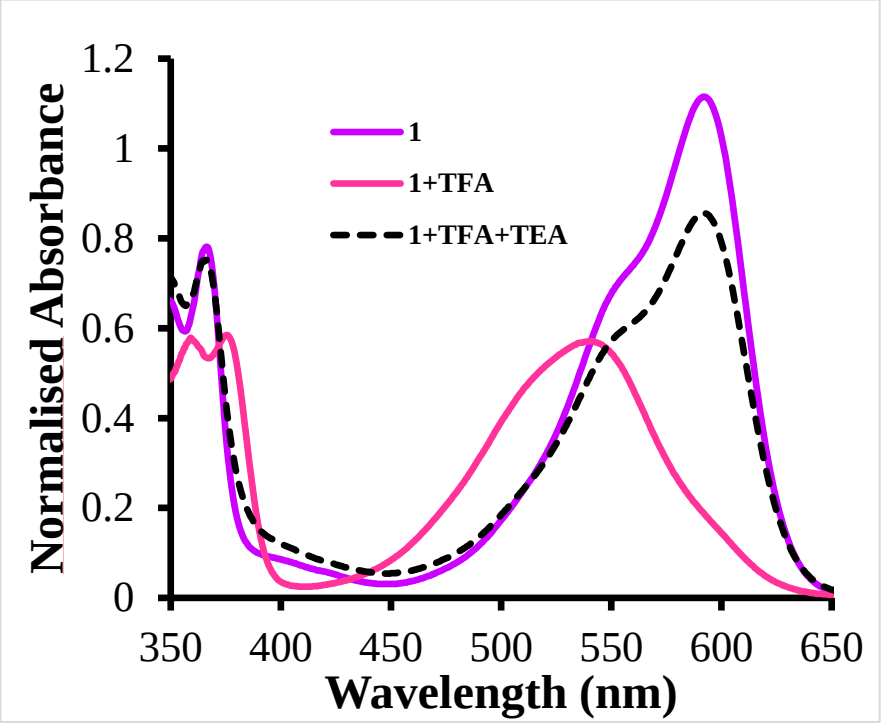

Figure 2.9: Reversibility study of the DDPT **1** the (purple color curve) represent DDPT **1** upon addition of acid i.e. TFA it gives (pink color curve) and its shown (black dotted curve) which shows reversibility while upon addition of base i.e. TEA.

2.2.8 Test strip for acid-base

Furthermore, we studied the strip-based sensing for DDPT **1** to show its practical applicability. The test strips were prepared by dissolving the DDPT **1** in THF solvent and simple loading the sample on the test strips prepared by using the Whatmann paper. The test strips were air dried and used for further sensing application. The prepared strips initially showed blue color in the visible light (Figure 2.10 A) Upon subjecting the test strip on TFA fumes blue color changes to light purple pink color further, in presence of base TEA again the color of the test strip changes to blue which indicates that the test strips show reversibility

and reusability and can be used for practical application in pH sensing, the test strip has been utilized up to 8 cycles. (Figure 2.11)

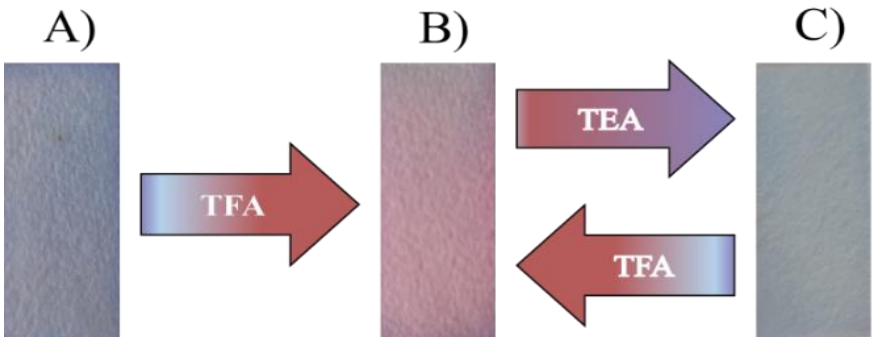

Figure 2.10: Test Strip sensing for DDPT **1** in THF solvent in presence of TFA and TEA. A) Test strip as blank. B) After exposed to TFA vapours. C) Further contact with TEA vapours.

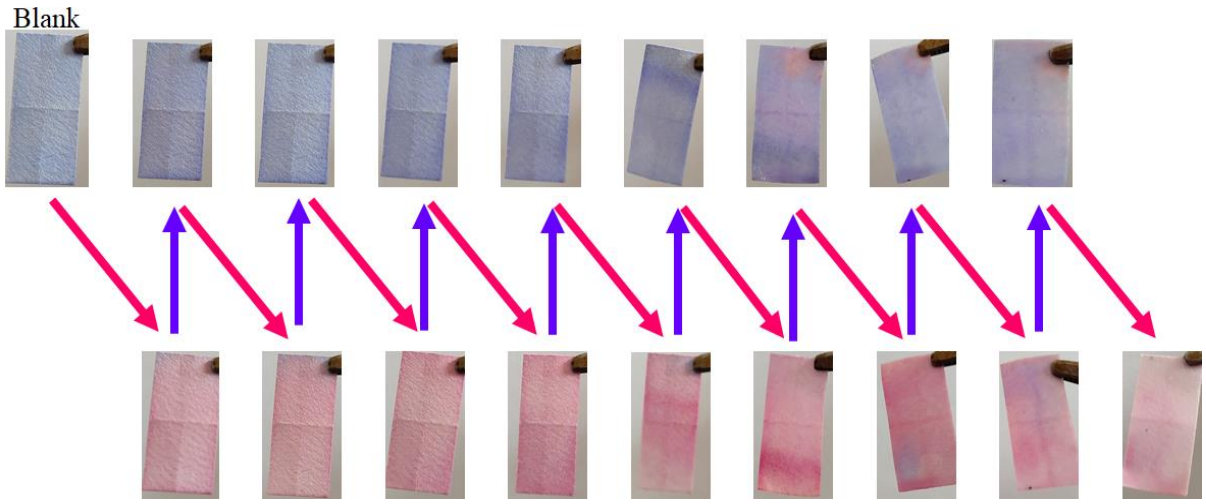

Figure 2.11: Reusability of test strip of DDPT **1** shows up to 8 cycles. (pink arrow and purple arrow indicates exposure to TFA and TEA fumes respectively)

2.3 Experimental details

2.3.1 Chemical and Reagents

Dibromo-NDI was prepared by following our earlier developed method.[7] Dimethylamine, trifluoroacetic acid and trimethylamine were purchased from Sigma-Aldrich. ^{1}H NMR spectra was recorded on Bruker spectrometer 400 MHz and ^{13}C NMR using 100 MHz. The $CDCl_3$ was used as a deuterated solvent for NMR with tetramethylsilane (TMS) was used as an internal standard. Mass spectrometry data was obtained by high resolution mass spectroscopy. IR spectra were recorded on a Perkin Elmer FT-IR 400 spectrometer. UV-Vis absorption spectra were recorded by UV-Vis-1800 Shimadzu spectrophotometer and fluorescence emission measured on RF-6000 (Shimadzu, Japan) spectrofluorophotometer.

2.3.2 Synthesis of DDPT 1

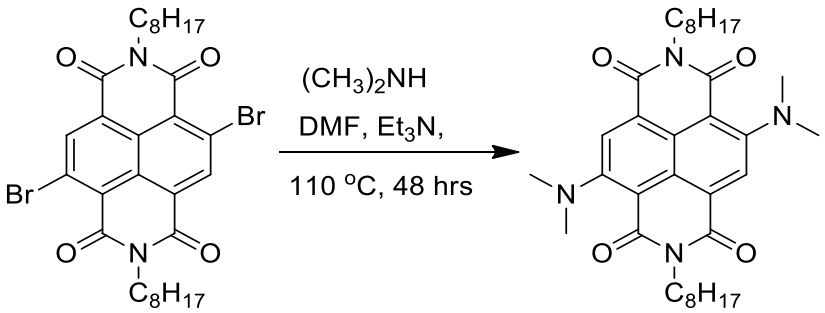

2 **1**

Scheme 2.1. Synthesis of DDPT **1.**

Synthesis of 4,9-bis(dimethylamino)-2,7-dioctylbenzo[lmn][3,8]phenanthroline-1,3,6,8(2H,7H)-tetraone (DDPT **1**). The DDPT **1** was synthesized by reacting 100 mg of **2** in 5 ml of dimethylamine, 5 ml of triethylamine and 5 ml of dimethylformamide under N_2 atmosphere by heating reaction mixture at 110 ^{o}C for 48 hrs. Upon completion of the reaction, mixture was extracted with ethyl acetate to give the desired product **1** as a violet

blue compound in 75% yield. ^{1}H NMR (400 MHz, $CDCl_3$) δ (ppm): 8.44 (1H, s), 4.19 (2H, *J* = 7.5 Hz, t), 3.17 (6H, s), 1.75-1.67 (2H, m), 1.41-1.24 (10H, m), 0.87 (3H, *J* = 6.8 Hz, t); ^{13}C NMR (100 MHz, CDCl3) δ (ppm): 163.5, 161.8, 151.6, 125.2, 123.6, 123.2, 107.2, 44.1, 40.9, 31.9, 29.3, 29.2, 28.3, 27.1, 22.6, 14.1. HRMS: Calcd. = 576.3676, found 576.3359; Elemental Analysis: Calcd. C, 70.80; H, 8.39; N, 9.71 and Found C, 70.68; H, 8.41; N, 9.78.

2.3.3 UV-Vis experiments

UV-Vis absorption spectra and titration

The stock solution of DDPT **1** (9×10^{-5} M) was prepared by dissolving it in THF. Then absorption spectra were recorded by placing of stock solution in the quartz cuvette with 1 cm path length. The change in absorption upon addition of TFA was recorded at room temperature. Furthermore, changes in absorption was monitored in titration experiments, firstly DDPT **1** was placed in cuvette and upon addition of 0-3.0 equiv. of TFA.

2.3.4 Fluorescence experiments

Fluorescence emission spectra of the DDPT 1

The stock solution (9×10^{-5} M) was prepared by dissolving the DDPT **1** in THF. The fluorescence spectra of the DDPT **1** was recorded by placing of stock solution in THF in the quartz cell. The fluorescence change upon addition of TFA was recorded at room temperature. And for titration experiment 0-3.0 equiv. TFA was added incrementally and the change in fluorescence spectra.

2.4 Conclusion

From this study we concluded that the probe 4,9-bis(dimethylamino)-2,7-dioctylbenzo[lmn][3,8] phenanthroline-1,3,6,8 (2H,7H)-tetraone (DDPT **1**) was synthesized

with substituted dimethylamine at the core of NDI with good yield. The molecule was successfully synthesized and further characterized showing the reversible response to trifluoroacetic acid which acts as proton source. The optical changes in the molecule exhibited the increase in fluorescence with the increase in proton source simultaneously. The reversible nature of the probe was further investigated by adding TEA as base acting as deprotonator. This clearly suggests that protonation of N atom of dimethyl restricts the PET transfer leading to the increase in fluorescence. The probe was reversible for 4 cycles with the frequent addition of acid and base to the synthesized NDI system. Further the probe was utilized for test strip sensing application which successfully indicates that the probe is highly selective to H^+ ion in the solution. In this way we believe that this simple route synthesis of DDPT **1** and use for reversible acid-base sensing may useful to control of pH in various biological and physiological processes occurring in the system successfully.

2.5 References

(1) Ghoneim, M. T.; Nguyen, A.; Dereje, N.; Huang, J.; Moore, G. C.; Murzynowski, P. J.; Dagdeviren, C. Recent Progress in Electrochemical PH-Sensing Materials and Configurations for Biomedical Applications. *Chem. Rev.* **2019**, *119* (8), 5248–5297. https://doi.org/10.1021/acs.chemrev.8b00655.

(2) Shrode, L. D.; Tapper, H.; Grinstein, S. Role of Intracellular PH in Proliferation, Transformation, and Apoptosis. *J. Bioenerg. Biomembr.* **1997**, *29* (4), 393–399. https://doi.org/10.1023/A:1022407116339.

(3) Di Costanzo, L.; Panunzi, B. Visual PH Sensors: From a Chemical Perspective to New Bioen-Gineered Materials. *Molecules* **2021**, *26* (10). https://doi.org/10.3390/molecules26102952.

(4) Ando, Y.; Iino, S.; Yamada, K.; Umezawa, K.; Iwasawa, N.; Citterio, D.; Suzuki, K. A

Ratiometric Fluorescent PH Glass Optode Based on a Boron-Dipyrromethene Derivative. *Sens. Actuators B Chem.* **2007**, *121* (1), 74–82. https://doi.org/10.1016/j.snb.2006.09.004.

(5) Yuqing, M.; Jianrong, C.; Keming, F. New Technology for the Detection of PH. *J. Biochem. Biophys. Methods* **2005**, *63* (1), 1–9. https://doi.org/10.1016/j.jbbm.2005.02.001.

(6) Guern, J.; Felle, H.; Mathieu, Y.; Kurkdjian, A. Regulation of Intracellular PH in Plant Cells. *Int. Rev. Cytol.* **1991**, *127* (C), 111–173. https://doi.org/10.1016/S0074-7696(08)60693-2.

(7) Bissell, R. A.; Prasanna de Silva, A.; Nimal Gunaratne, H. Q.; Mark Lynch, P. L.; Maguire, G. E. M.; McCoy, C. P.; Samankumara Sandanayake, K. R. A. Fluorescent PET (Photoinduced Electron Transfer) Sensors. **1993**, *168*, 223–264. https://doi.org/10.1007/3-540-56746-1_12.

(8) Wu, J.; Liu, W.; Ge, J.; Zhang, H.; Wang, P. New Sensing Mechanisms for Design of Fluorescent Chemosensors Emerging in Recent Years. *Chem. Soc. Rev.* **2011**, *40* (7), 3483–3495. https://doi.org/10.1039/c0cs00224k.

(9) Qiu, J.; Jiang, S.; Guo, H.; Yang, F. An AIE and FRET-Based BODIPY Sensor with Large Stoke Shift: Novel PH Probe Exhibiting Application in CO32− Detection and Living Cell Imaging. *Dyes Pigments* **2018**, *157*, 351–358. https://doi.org/10.1016/j.dyepig.2018.05.013.

(10) Lu, X.; Zhu, W.; Xie, Y.; Li, X.; Gao, Y.; Li, F.; Tian, H. Near-IR Core-Substituted Naphthalenediimide Fluorescent Chemosensors for Zinc Ions: Ligand Effects on PET and ICT Channels. *Chem. - Eur. J.* **2010**, *16* (28), 8355–8364. https://doi.org/10.1002/chem.201000461.

(11) Doria, F.; Folini, M.; Grande, V.; Cimino-Reale, G.; Zaffaroni, N.; Freccero, M.

Naphthalene Diimides as Red Fluorescent PH Sensors for Functional Cell Imaging. *Org. Biomol. Chem.* **2015**, *13* (2), 570–576. https://doi.org/10.1039/c4ob02054e.

(12) Kobaisi, M. Al; Bhosale, S. V.; Latham, K.; Raynor, A. M.; Bhosale, S. V. Functional Naphthalene Diimides: Synthesis, Properties, and Applications. *Chem. Rev.* **2016**, *116* (19), 11685–11796. https://doi.org/10.1021/acs.chemrev.6b00160.

(13) Maniam, S.; Higginbotham, H. F.; Bell, T. D. M.; Langford, S. J. Harnessing Brightness in Naphthalene Diimides. *Chem. - Eur. J.* **2019**, *25* (29), 7044–7057. https://doi.org/10.1002/chem.201806008.

(14) Sarkar, A.; Kölsch, J. C.; Berač, C. M.; Venugopal, A.; Sasmal, R.; Otter, R.; Besenius, P.; George, S. J. Impact of NDI-Core Substitution on the PH-Responsive Nature of Peptide-Tethered Luminescent Supramolecular Polymers. *ChemistryOpen* **2020**, *9* (3), 346–350. https://doi.org/10.1002/open.202000017.

(15) Qi, J.; Liu, D.; Liu, X.; Guan, S.; Shi, F.; Chang, H.; He, H.; Yang, G. Fluorescent PH Sensors for Broad-Range PH Measurement Based on a Single Fluorophore. *Anal. Chem.* **2015**, *87* (12), 5897–5904. https://doi.org/10.1021/acs.analchem.5b00053.

(16) Bell, T. D. M.; Bhosale, S. V.; Forsyth, C. M.; Hayne, D.; Ghiggino, K. P.; Hutchison, J. A.; Jani, C. H.; Langford, S. J.; Lee, M. A. P.; Woodward, C. P. Melt-Induced Fluorescent Signature in a Simple Naphthalenediimide. *Chem. Commun.* **2010**, *46* (27), 4881–4883. https://doi.org/10.1039/c0cc00865f.

(17) Li, Z. Z.; Niu, C. G.; Zeng, G. M.; Liu, Y. G.; Gao, P. F.; Huang, G. H.; Mao, Y. A. A Novel Fluorescence Ratiometric PH Sensor Based on Covalently Immobilized Piperazinyl-1,8-Napthalimide and Benzothioxanthene. *Sens. Actuators B Chem.* **2006**, *114* (1), 308–315. https://doi.org/10.1016/j.snb.2005.05.018.

(18) Zong, L.; Xie, Y.; Li, Q.; Li, Z. A New Red Fluorescent Probe for Hg2+ Based on Naphthalene Diimide and Its Application in Living Cells, Reversibility on Strip Papers.

Sens. Actuators B Chem. **2017**, *238*, 735–743. https://doi.org/10.1016/j.snb.2016.07.052.

(19) Buckland, D.; Bhosale, S. V.; Langford, S. J. A Chemodosimer Based on a Core-Substituted Naphthalene Diimide for Fluoride Ion Detection. *Tetrahedron Lett.* **2011**, *52* (16), 1990–1992. https://doi.org/10.1016/j.tetlet.2011.02.080.

(20) Bhosale, S. V.; Jani, C. H.; Langford, S. J. Chemistry of Naphthalene Diimides. *Chem. Soc. Rev.* **2008**, *37* (2), 331–342. https://doi.org/10.1039/b615857a.

(21) Basak, S.; Nandi, N.; Paul, S.; Banerjee, A. Luminescent Naphthalene Diimide-Based Peptide in Aqueous Medium and in Solid State: Rewritable Fluorescent Color Code. *ACS Omega* **2018**, *3* (2), 2174–2182. https://doi.org/10.1021/acsomega.7b01813.

(22) Bhosale, S. V.; Bhosale, S. V.; Kalyankar, M. B.; Langford, S. J. A Core-Substituted Naphthalene Diimide Fluoride Sensor. *Org. Lett.* **2009**, *11* (23), 5418–5421. https://doi.org/10.1021/ol9022722.

(23) Bhosale, S. V.; Kalyankar, M. B.; Bhosale, S. V.; Langford, S. J.; Reid, E. F.; Hogan, C. F. The Synthesis of Novel Core-Substituted Naphthalene Diimides via Suzuki Cross-Coupling and Their Properties. *New J. Chem.* **2009**, *33* (12), 2409–2413. https://doi.org/10.1039/b9nj00476a.

(24) Sharma, H.; Sidhu, J. S.; Hassen, W. M.; Singh, N.; Dubowski, J. J. Synthesis of a 3,4-Disubstituted 1,8-Naphthalimide-Based DNA Intercalator for Direct Imaging of Legionella Pneumophila. *ACS Omega* **2019**, *4* (3), 5829–5838. https://doi.org/10.1021/acsomega.8b03638.

(25) Singha, N.; Gupta, P.; Pramanik, B.; Ahmed, S.; Dasgupta, A.; Ukil, A.; Das, D. Hydrogelation of a Naphthalene Diimide Appended Peptide Amphiphile and Its Application in Cell Imaging and Intracellular PH Sensing. *Biomacromolecules* **2017**, *18* (11), 3630–3641. https://doi.org/10.1021/acs.biomac.7b01048.

SUPLLEMENTARY INFORMATION

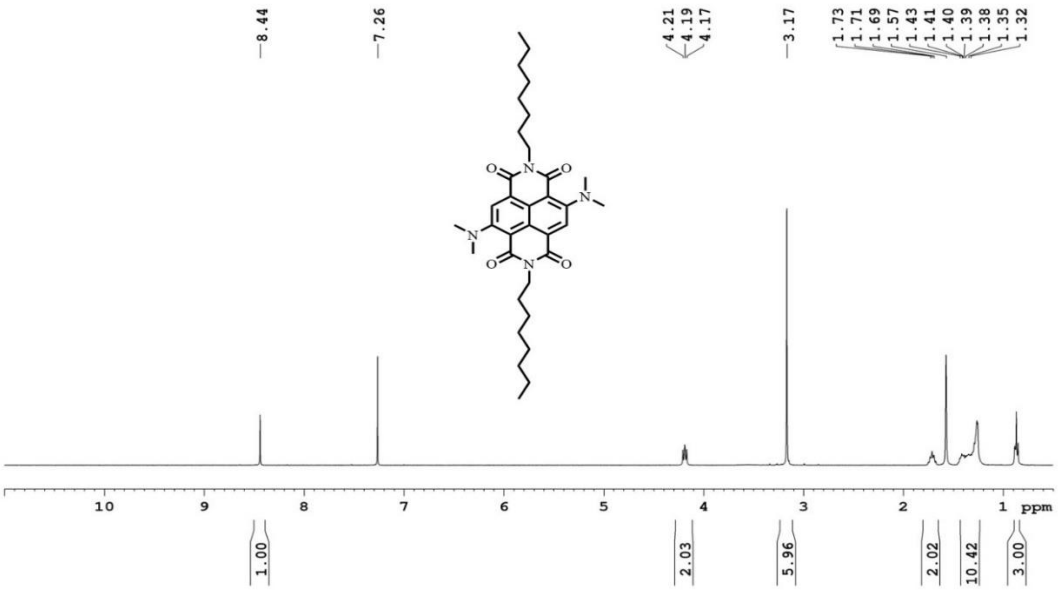

Figure 2.12: ^{1}H NMR spectra of the compound 4,9-bis(dimethylamino)-2,7-dioctylbenzo[lmn][3,8]phenanthroline-1,3,6,8(2H,7H)-tetraone **(**DDPT **1**).

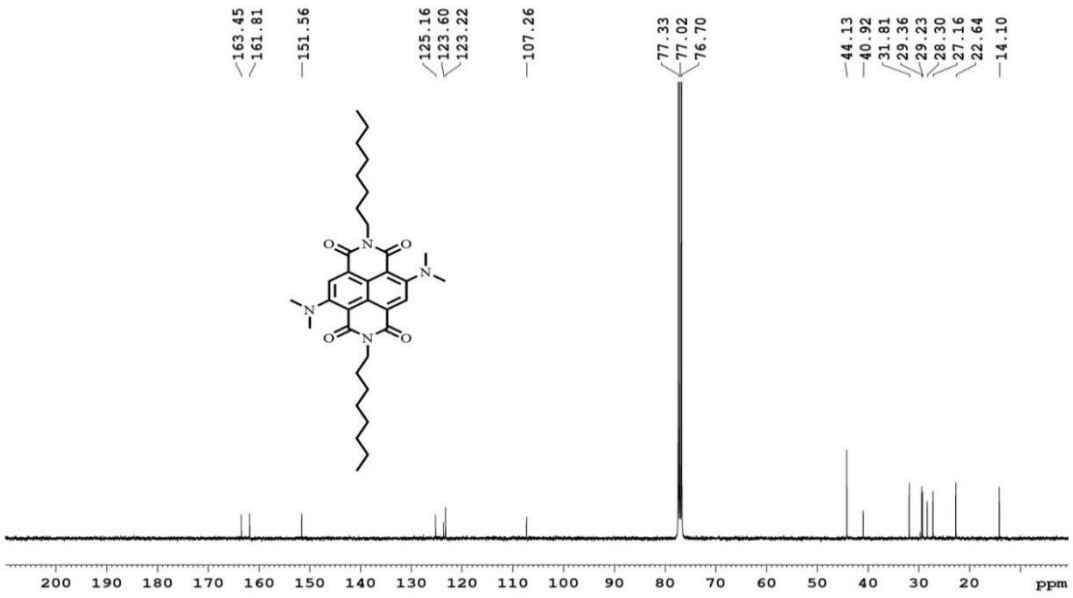

Figure 2.13: ^{13}C NMR spectra of the probe 4,9-bis(dimethylamino)-2,7-dioctylbenzo[lmn][3,8]phenanthroline-1,3,6,8(2H,7H)-tetraone (DDPT **1**).

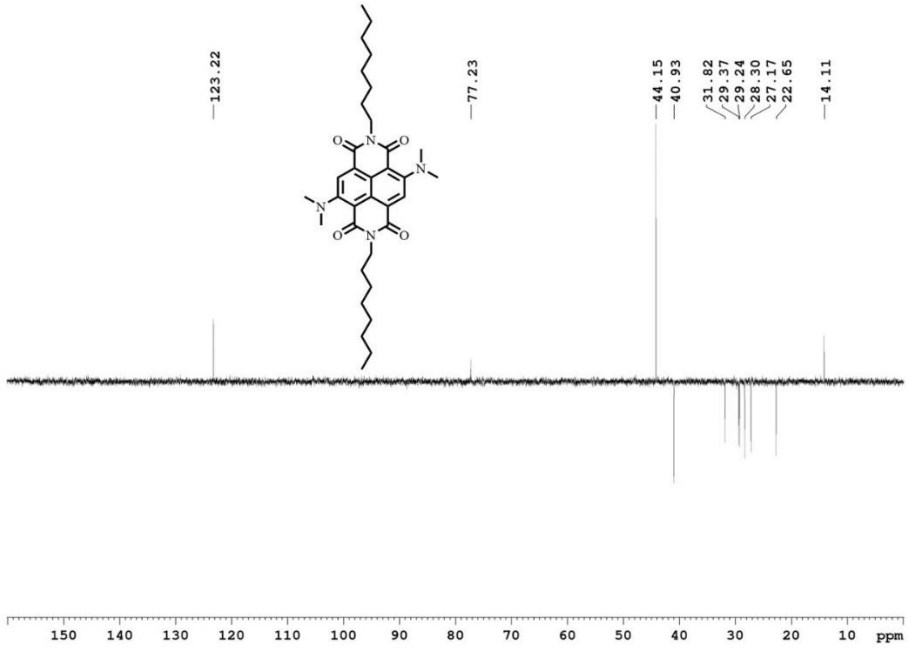

Figure 2.14: DEPT spectra of the probe 4,9-bis(dimethylamino)-2,7dioctylbenzo[lmn][3,8]phenanthroline-1,3,6,8(2H,7H)-tetraone (DDPT **1**).

Chapter 3: Naphthalenediimide-Benzothiazole-Based Chemodosimeter for Selective and Sensitive Chromogenic for Cyanide Ion

3.1 Introduction

From literature study we know that anion plays crucial role in many chemical, medicinal and biological processes.[1] Among these anions cyanide (CN^-) ion is more toxic in nature and harmful to environment and human health with serious effects.[2] When CN^- enters in human body, it binds to ferric form of metalloenzymes such as cytochrome-c causing histonic anoxia.[3] When cyanide ion concentrations in blood reaches a level of 23-26 μM lead to human life causalities on large proportion simultaneously.[4],[5] From the standards of World Health Organization (WHO) the determined permissible level of CN^- ions in drinking water required to be as low as 1.9 μM.[6] However, the CN^- ions utilization in the form of salts are greater in metallurgy, gold mining, electroplating and synthesis of new chemical entities as well as polymers such as acrylic plastics, nylon and nitriles.[7], [8] In addition to these activities, human being accumulated higher level of CN^- ions *via* utilization of certain foods and plants leads to serious effects to human health.[9],[10] Though monitoring of cyanide ion is carried out under strict control, an accidental liberation of CN^- ion into the environment happens sometimes.

From above reports, it is very necessary to design, synthesize and employ new materials to monitor CN^- ion in environmental and biological systems selectively. In this regard, several researcher designed and developed large number of sensitive and selective chemosensors[11], [12] for CN^- ion detection effectively.[13-19] Out of these developed materials colorimetric and fluorescence sensors are selective and low cost materials in real sense.[20-23] Till now all reported literature methods revealed that some chemosensors has been developed based on hydrogen-interactions, deprotonation approach, coordination with transition metal ions,

boron-cyanide interactions, and furthermore few other approaches i.e. displacement and supramolecular self-assembly also developed to detect cyanide ions.[24-27] But, few of them suffer from drawbacks like poor selectivity for CN^- ion detection in presence of interfering anions i.e. fluoride and acetate anions.[28] Furthermore, nucleophilicity of the CN^- ion has been employed for its nucleophilic addition reactions with different chromophores such as acyltriazine, acridinium, oxazine, pyrylium, squaraine,[9a] tetraphenylethylene, trifluoroacetophenone, trifluoroacetamide, carbazole, thiophene and naphthalene etc.[29-32] Still, some of these chemosensors show drawbacks i.e. complicated synthetic protocol, poor selectivity and a long reaction time for detection of cyanide ions.[33], [34] To overcome all these difficulties the development of simple and highly reactive chromophore towards CN^- ion still remains interesting challenge in sensing area.

Recently it is well known that core-substituted NDI derivatives exhibited tuneable colorimetric, UV-Vis and emission response.[35-38] Chemical and biosensors have been developed on the basis of core-substituted NDI and are one of the attractive chromophore in the recent times. Several research groups studied and investigated NDI based sensor towards cations, anions, pH and biosensor applications in detail.[39-44] As a part of our research interest in this field we designed an efficient sensor for selective and sensitive detection of CN^- ion. In this paper, we will report benzothiazole functionalized naphthalene diimide (NDI-1) based chemosensor, which could be efficiently detect CN- ion through nucleophilic addition reaction pathways.[13a] The design of the chromophore is illustrated in (Figure 1) with benzothiazole substituent at NDI core.[45] The chromophore showed excellent sensitivity and selectivity toward CN^- ion.

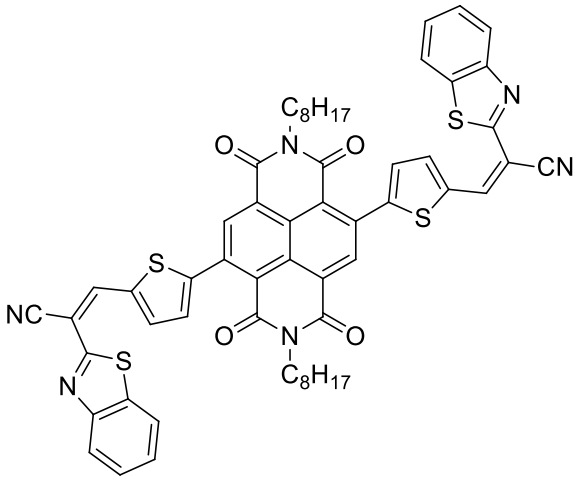

Figure 3.1:. Structure of chromophore NDI-1.

3.2 Colorimetric Properties

To examine the suitability of sensor NDI-1 to detect selective towards particular anion, initial investigation were performed in chloroform by addition of 5 equiv. different anions such as F^- , Cl^-, Br^-, I^-, HSO_4^-, $H_2PO_4^-$, OAc^-, ClO_4^- and HCO_3^- in the form of tetrabutylammonium (TBA) salt and CN^- (TEA salts). The color changes of the NDI-1 solution (1.8×10^{-4} M) were monitored under visible as well as UV light at 365 nm wavelength. The observed results are illustrated in (Figure 3.2). The color of the sensor NDI-1 exhibits red color under visible light. Interestingly, it is observed that CN- ion addition induced the change in color from red to green, which was clearly visible to the naked eyes (Figure 3.2a). Whereas, the addition of other anions i.e. F^- , Cl^-, Br^-, I^-, HSO_4^-, $H_2PO_4^-$, OAc^- , ClO_4^- and HCO_3^- resulted into no visible color change of the sensor NDI-1. Furthermore, to investigate the suitability of NDI-1 to detect CN^- ion, we studied colorimetric response under UV-light (365 nm). The color of NDI-1 solution in presence of CN- ion changes from dark red to brownish-yellow, in color (Figure 3.2b). Such changes were not detected with the addition of other anions such as F^- , Cl^-, Br^-, I^-, HSO_4^-, $H_2PO_4^-$, OAc^-, ClO_4^- and HCO_3^-. These clear color changes under visible and UV light indicate that sensor NDI-1 can be

utilized as a selective sensor for the detection of CN^- ion.

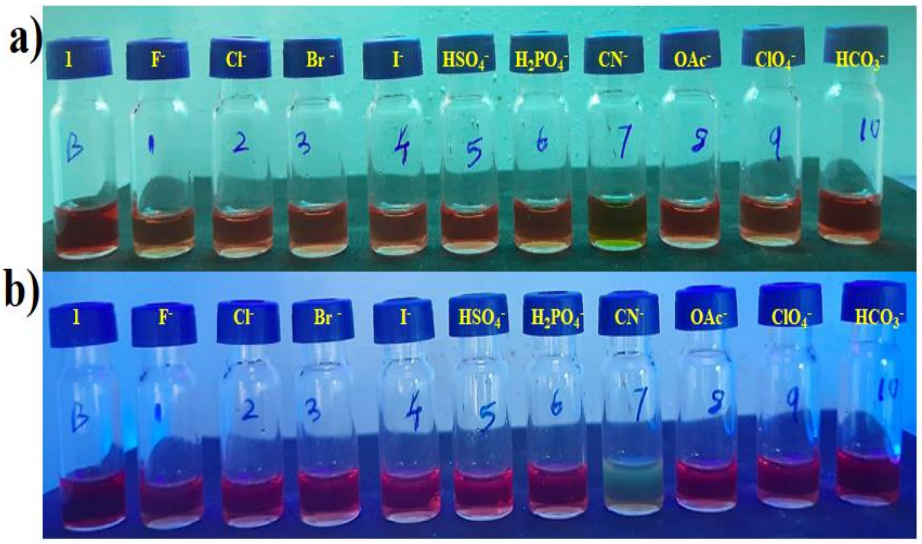

Figure 3.2: Naked-eye detection of CN^- ion in chloroform. Solutions of NDI-1 (1.8×10^{-4} M) in $CHCl_3$, NDI-1 without any anions upon addition of 5 equiv. of F^- , Cl^-, Br^-, I^-, HSO_4^-, $H_2PO_4^-$, OAc^-, ClO_4^- and HCO_3^- : (a) under visible light and (b) under UV light 365 nm.

Furthermore, the ability of NDI-1 to detect CN^- ion in $CHCl_3$ solvent system was then investigated by UV-Vis absorption spectra. The results are illustrated in (Figure 3.3) NDI-1 in $CHCl_3$ exhibit two absorption peaks, intense peak at 390 nm and broad at 525 nm. The changes in absorption peaks of NDI-1 was studied with the addition of various anions such as F^- , Cl^-, Br^-, I^-, HSO_4^-, $H_2PO_4^-$, OAc^-, ClO_4^- and HCO_3^-. As shown in (Figure 3a), the chemosensor NDI-1 exhibited only a distinct response to CN^- ion. The addition of other anions except CN^- has no obvious effect in UV-Vis spectra. Upon inclusion of CN^- ion to the NDI-1 solution resulted into changes into the absorption peaks. It was found that new peak appeared at 310 nm. Moreover, the peak at 390 nm was decreased and new peak appeared at 450 nm. The peak at 525 nm was disappeared and subsequently a new sharp peak was appeared at 510 nm. The new peak 450 nm may responsible for the color changes in solution (Figure 3.2). Furthermore, the UV-Vis peak at 525 nm was disappeared with appearance of new peak at 510 nm. As shown in (Figure 3.3b), NDI-1 was then titrated

against TBACN in $CHCl_3$. It was observed that two isosbestic points at 445 nm and 525 nm was observed. This indicates formation of entirely new product from that of NDI-1 with the addition of CN^- ions.

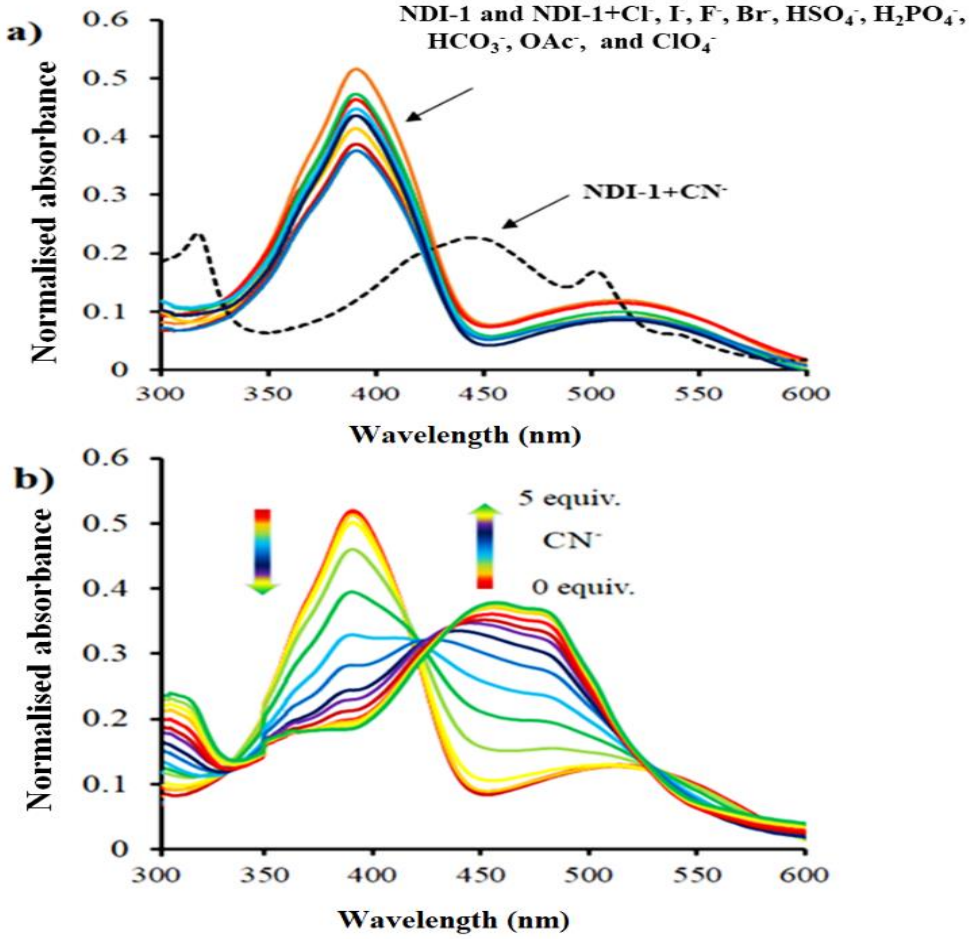

Figure 3.3: UV-Vis absorption spectra of NDI-1 (1.8×10^{-4} M) (a) in presence of 5 equiv. different anions and (b) titrated with CN^- ion.

Fluorescence study was investigated for the detection of CN^- with NDI-1 in $CHCl_3$. Firstly, the emission changes of sensor NDI-1 were examined upon inclusion of various anions i.e. such as F^-, Cl^-, Br^-, I^-, HSO_4^-, $H_2PO_4^-$, OAc^-, ClO_4^- and HCO_3^-. As illustrated in (Figure 3.4), free sensor NDI-1 exhibited emission peak at 430 nm ($\square_{\square\square}$ = 370 nm). In the presence CN^- ion, the emission peak is broadening with 10 nm shift with peak appeared at 420 nm and no significant change in fluorescence was detected for other anions. The sensor NDI-1

displayed a dramatic color change from red to brownish-yellow, by the naked eye under UV-light (365 nm) as shown in (Figure 3.2b). The emission titration experiments of sensor NDI-1 upon CN^- ion was also performed and the results are demonstrated in (Figure 3.4b). The titration of CN^- ion to the sensor NDI-1 showed changes in emission peak from sharp to broad peak.

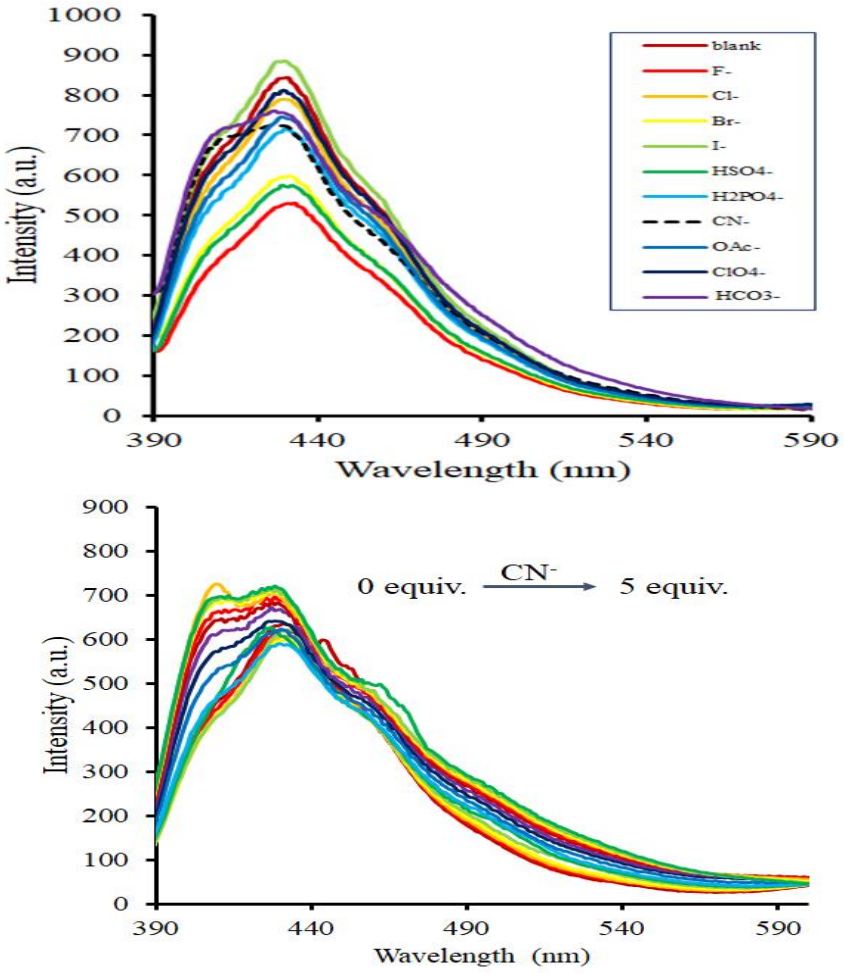

Figure 3.4: Fluorescence emission spectra of NDI-1 (1.8×10^{-4} M) (a) in presence of different anions 5 equiv. and (b) titrated with CN- ion 0 to 5 equiv.

The selective detection of CN^- ion by sensor NDI-1 in the presence of interfering anions was examined by UV-Vis spectroscopy and the results are illustrated in (Figure 3.5) The anion

interfering experiments of NDI-1 (1.8×10^{-4} M) was performed by employing various ions such as Cl^-, I^-, F^-, Br^-, HSO_4^-, $H_2PO_4^-$, HCO_3^-, OAc^-, and ClO_4^- (1×10^{-3} M). The bar with red gradient colour corresponds to the sensor NDI-1 and in presence of examined anions such as Cl^-, I^-, F^-, Br^-, HSO_4^-, $H_2PO_4^-$, HCO_3^-, OAc^-, and ClO_4^-. The greenish gradient bar is related to the sensor NDI-1 and NDI-1 with tested anions in presence of CN^- ion. The absorption intensity of NDI-1 at 395 nm significantly decreased with the addition of CN^- ion (0.9×10^{-3} M) in the presence of tested anions. These results indicate the tested ions has no impact on sensor NDI-1 for detection of CN^- ion. Hence, sensor NDI-1 is able to selectively detect CN^- ion via optical spectra as well as naked-eye colorimetric observation.

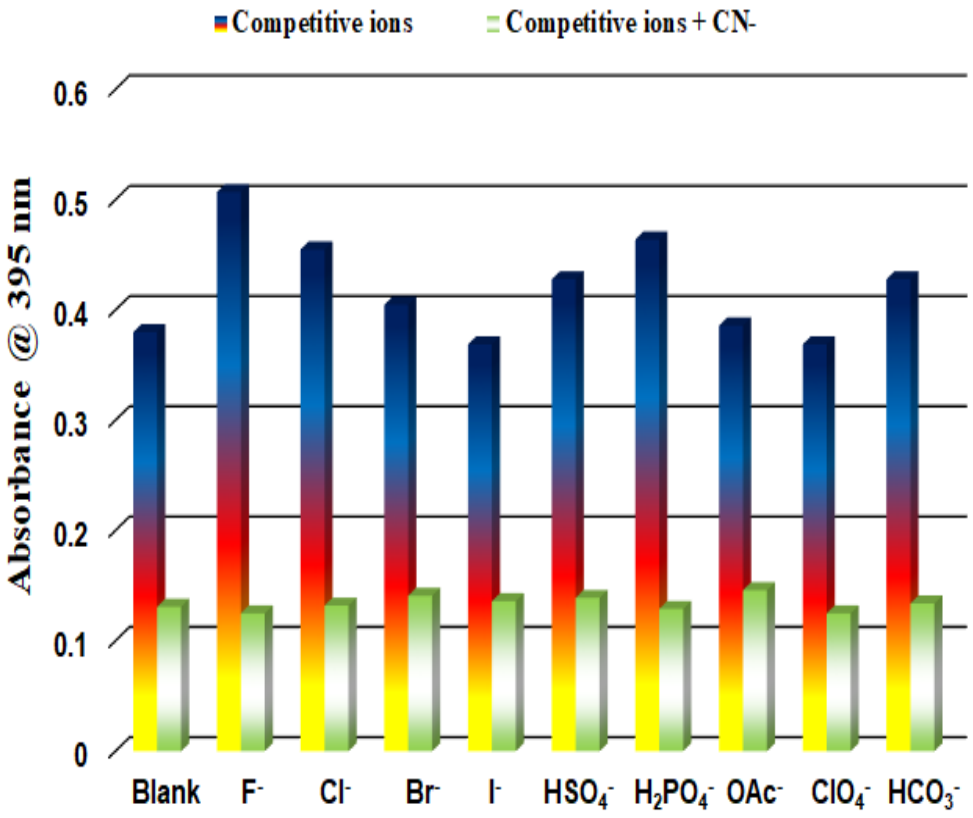

Figure 3.5: Comparison of UV-Vis absorption changes of NDI-1 (1.8×10^{-4} M) at 395 nm with the addition of different anions 5 equiv. and with CN- ion (0.9×10^{-3} M) in the presence of various anions (1×10^{-3} M).

3.3 Selective detection of CN^- ion

The naked eye, a colorimetric change is an optical response and emission changes observed, thus, confirm the binding of CN^- ion with the sensor NDI-1. Furthermore, to understand the bonding between sensor NDI-1 and CN^- ion, density functional theory (DFT) calculations were carried out. With the DFT calculations NDI-1 and the complex NDI-1+CN^- have been obtain by means of Gaussian 16 ab initio/DFT quantum chemical simulation package.[46] The geometry optimization of molecules NDI-1 and the complex NDI-1-CN^- with truncated alkyl chain have been carried out at B3LYP/6-31G* level, the solvent (chloroform) effect was included by means of polarizable continuum model (PCM) (Figure 3.6). The frequency calculations were carried out at the same level, in order to confirm the minima. The frontier molecular orbitals (FMO) are generated by using Avogadro[47], [48] and are given in (Figure 3.6). As illustrated in (Figure 3.6a), for the sensor NDI-1, the highest occupied molecular orbitals (HOMO) is delocalized on thiophene and benzothiazole ring systems, while the lowest unoccupied molecular orbital (LUMO) delocalized on the core of NDI and thiophene subunits.

As shown in (Figure 3.6b), after the binding with CN^- ion, the HOMO is localized on benzothiazole and cyanide subunits and LUMO located on NDI core and thiophene units. This indicates the reasonable change in electron density distribution in the sensor NDI-1 after the CN^- ion addition, this is attributed to inhibition of intramolecular charge transfer from donor BTH to acceptor NDI core moiety. Moreover, the energy gap of NDI-1 and the NDI-1-CN^- complex was found to be 2.245 eV and 1.335 eV, respectively. We presume that the difference in the energy level is due to the absence of π-conjugation in the complex NDI-1-CN^-. Furthermore, time-dependent density functional theory (TD-DFT) studies was performed using B3LYP/6-31G* level for excitations studies. TD-DFT results were

analysed by using Gauss-Sum 2.2.5 program[49] and shown in Table 1. TDDFT results clearly shows that ONE-NDI absorption at 671, 434 nm, and TWO-NDI-CN shows at 1220 nm, 589 nm with diminished intensity. Thus TD-DFT result provide rational explanation for the electronic states and optical properties of NDI-1 and NDI-1-CN^- complex.

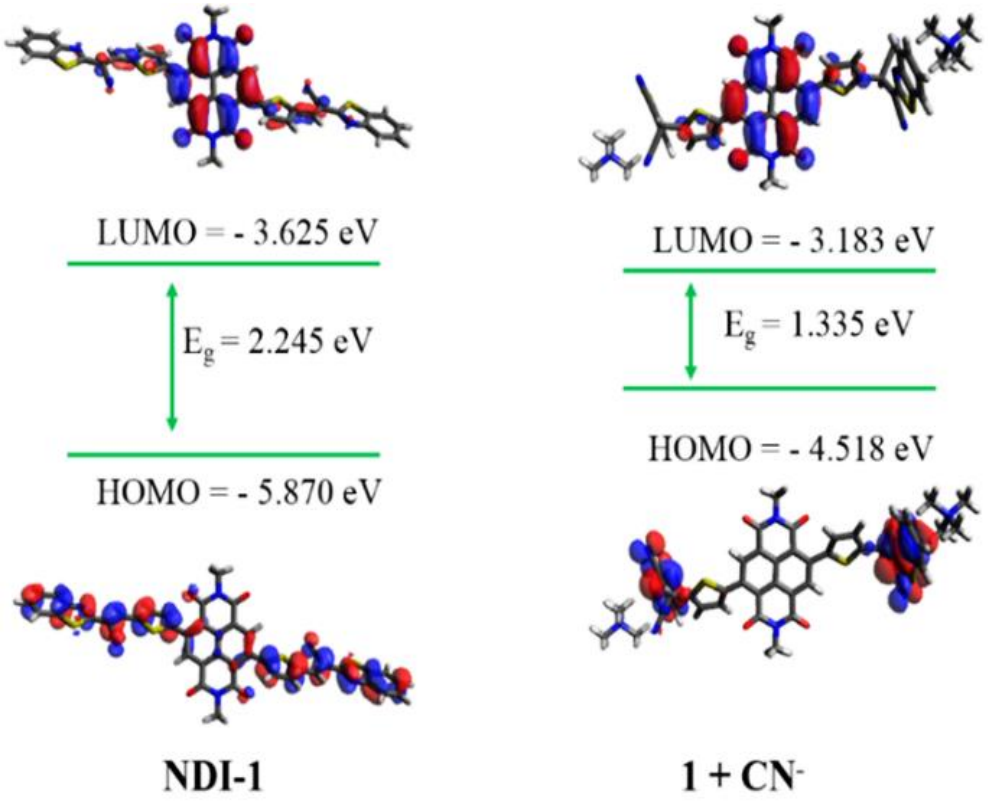

Figure 3.6: Molecular orbital diagram of NDI-1 and NDI-1-CN.

3.4 Cyclic voltammetry study

Cyclic voltammetry (CV) was engaged to evaluate the detection of CN^- ion. CV measurements are performed in 0.1. M (TBAPF6) in DCM and the results are demonstrated in (Figure 3.7) The cyclic voltammogram of NDI-1 in the absence of CN^- ion shows irreversible redox peaks with onset oxidation at 1.268 V and onset reduction at -0.662 V. Upon addition of CN^- ion to the NDI-1 sensor, the irreversible redox peaks exhibit onset oxidation and reduction at 0.79 V and -0.729 V. These onset oxidation and reduction values

were utilized to calculate highest occupied molecular orbitals (HOMO) and lowest unoccupied molecular orbitals (LUMO). The estimated HOMO energy levels of NDI-1 and NDI-1-CN^- complex are -5.968 eV and -5.49 eV and LUMO energy levels are -4.038 and 3.971 eV, respectively. The calculated energy level gap is about 1.93 eV (NDI-1) and 1.51 eV (NDI-1-CN^-). This indicated that binding of CN^- ion led to change in the electronic structure of NDI-1 resulting in a molecular architecture NDI-1-CN^- with less energy band gap. The trend in decreasing energy gap through CV experiments are similar with the DFT calculated results (Figure 3.6).

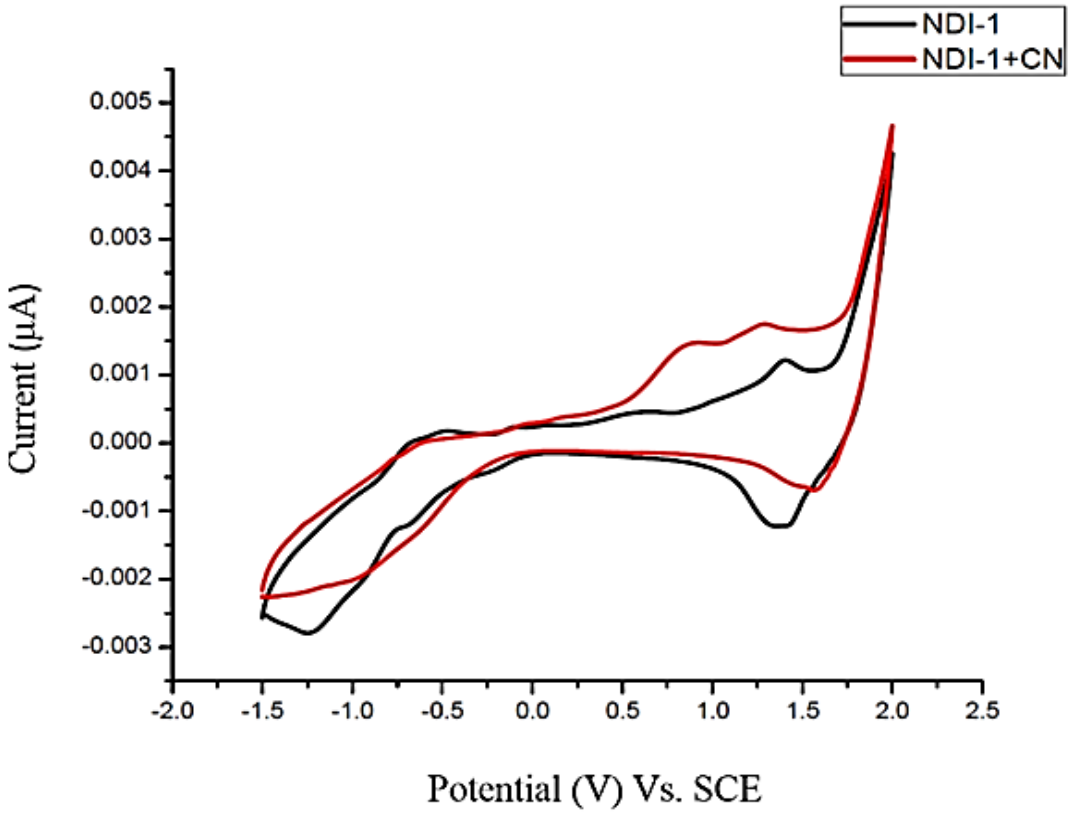

Figure 3.7: Cyclic voltammograms (CV) of NDI-1 (black line) and NDI-1-CN^- (Red line) in DCM (5×10^{-4} M) and 0.1 M TBAPF6.

Table 3.1. Cyclic voltammetry energy gap of NDI-1 and NDI-1-CN^-.

Molecules	NDI-1	NDI-1-CN^-
Eoxonset	1.268	0.79
Eredonset	-0.662	-0.729
HOMO (eV)	-5.968	-5.49
LUMO (eV)	-4.038	-3.971
Eelg (ev)	1.93	1.51

Thus, all the spectroscopic technique confirms the NDI-1-CN^- complex formation via nucleophilic addition reaction.[50] based on results the sensing mechanism of NDI-1 towards CN^- ion is depicted in (Figure 3.8).

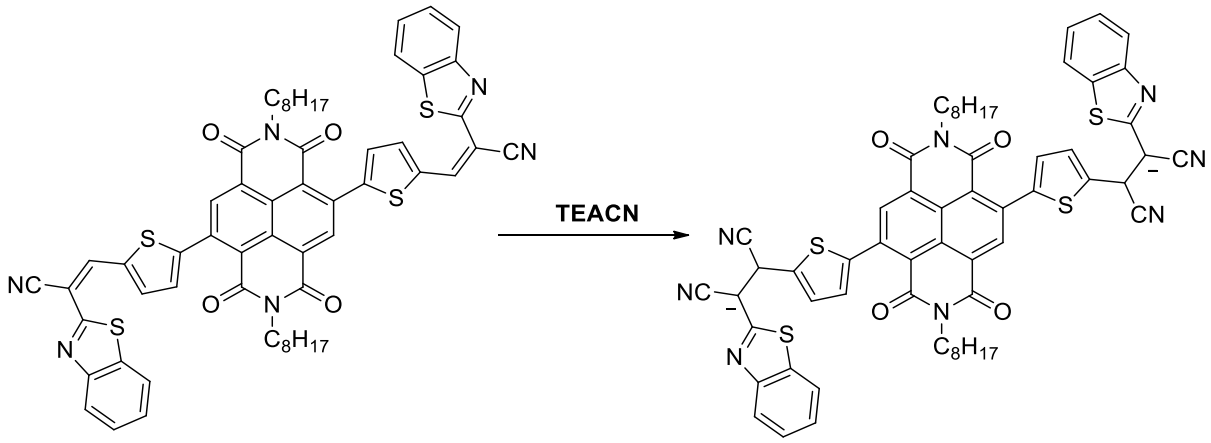

Figure 3.8: The possible sensing mechanism of sensor NDI-1 towards CN^- ion.

The determination of the stoichiometry by Job's plot from the absorption titration experiments of the NDI-1: CN^- complex formed by the probe 1 and CN^- ion. Job's plot result indicated stoichiometry of complex was 1:2. The Benesi-Hildebrand plot of NDI-1 with CN^- in $CHCl_3$ (Fig. 3.9b), the binding constant was 3.3×10^{-3} M for CN^- binding in probe NDI-1. The limit of detection was calculated by using formula 3σ/slope, where σ is the standard

deviation of blank probe samples and the slope is from the linear plot (Fig. 3.9d), the detection of limit was calculated from the titrations in the absorption spectra (Fig. 3.9c) and the detection limit of NDI-1 for CN^- was found 85 nM.

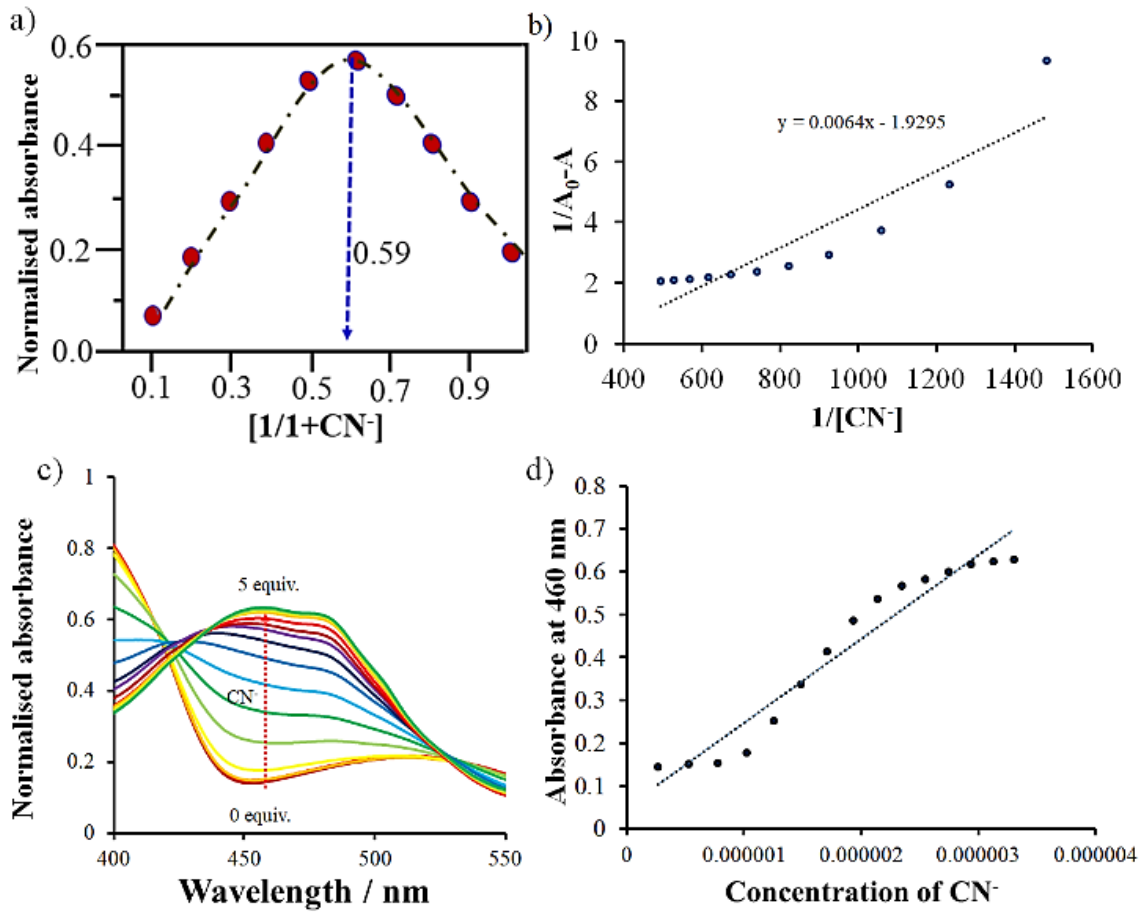

Figure 3.9: (a) Job's plot and (b) Benesi–Hildebrand plot of NDI-1 with CN^- ion in $CHCl_3$. c) Absorption spectra of NDI-1 titrated with CN^- ion in wavelength range 400-550 nm d) limit of detection plot calculated by absorption titration spectra of NDI-1 with CN^{-1} ion 3σ /slope

3.5 Experimental Section

3.5.1 Chemical and Reagents

The anions of tetrabutylammonium salts (Cl^-, I^-, F^-, Br^-, HSO_4^-, $H_2PO_4^-$, HCO_3^-, OAc^- and ClO_4^-) and tetraethylammonium cyanide (CN^-) salts were purchased from Sigma-Aldrich and TCI. UV-Vis absorption spectra were recorded by UV-Vis-1800 Shimadzu spectrophotometer and fluorescence emission measured on Agilent Cary Eclipse spectrofluorophotometer.

3.5.2 Synthesis of NDI-1

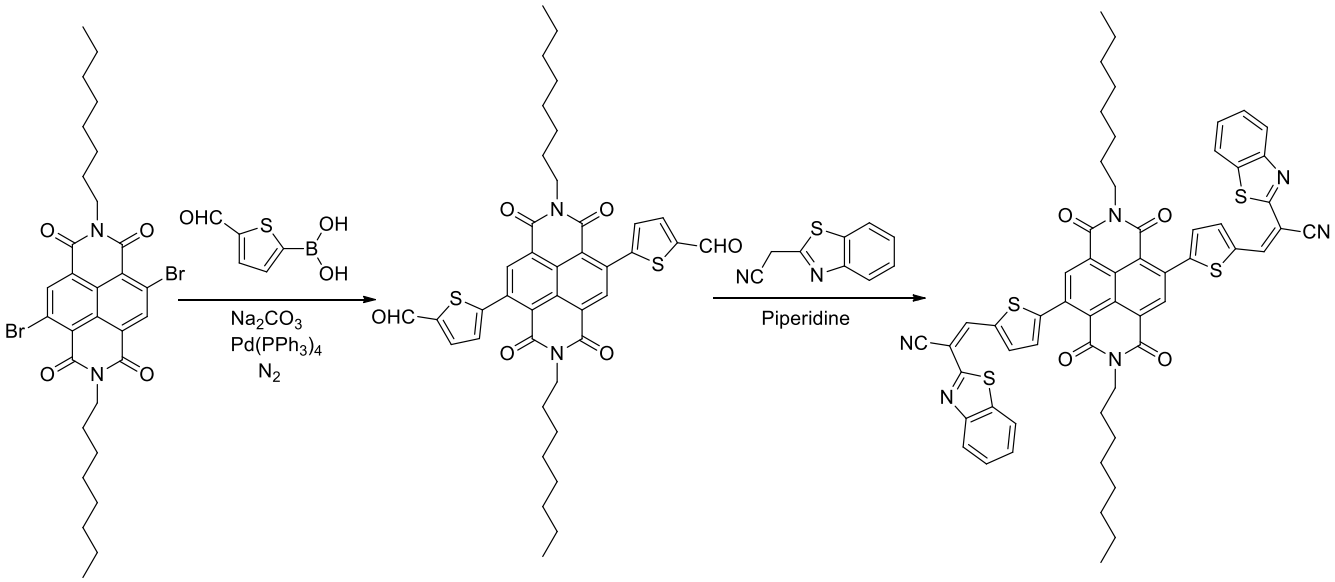

Synthesis of core substituted NDI-1

3.5.3 UV-Vis experiment

UV-*Vis absorption spectra of the* **NDI-1** *upon addition of different anions:* UV-Vis spectra were recorded in an 1800 Shimadzu spectrophotometer having 1 cm path length quartz cuvette. The stock solution of **NDI-1** ($1.8x10^{-4}$mol/L) was prepared in 10 ml of $CHCl_3$. The UV-Vis spectra of the **NDI-1** were recorded by placing 2 ml of stock solution in the quartz cell. The various anions of tetrabutylammonium salts of (Cl^-, I^-, F^-, Br^-, HSO_4^-, $H_2PO_4^-$,

HCO_3^-, OAc^- and ClO_4^-) and tetraethylammonium (CN^-) salt were dissolved in $CHCl_3$. The anions concentration 7.5×10^{-5} M were added and the absorption spectra were recorded at room temperature.

UV-Vis titration of the **NDI-1** *upon addition of* CN^- *anion:* The stock solution ($1.8x10^{-4}$mol/L) of the **NDI-1** was prepared in $CHCl_3$ solvent. The solution of tetraethyl ammonium cyanide (TEA CN^-) anion was prepared in $CHCl_3$. The stock solution was placed in a quartz cell and gradually addition of CN^- ion the corresponding absorbance spectra of the **NDI-1** was recorded at room temperature.

3.5.4 Fluorescence experiments

Fluorescence spectra of the **NDI-1** *upon addition of different anions:* The fluorescence emission spectra were recorded in an Agilent Cary Eclipse spectrofluorophotometer. Solution preparation is the same as mentioned in the UV-Vis study. Fluorescence spectra of the **NDI-1** were recorded by placing 2 ml of stock solution in a quartz cuvette and 370 nm excitation wavelength by adding different anions of tetrabutylammonium and tetraethylammonium salts.

Fluorescence titration of the **NDI-1** *upon addition of* CN^-*:* Fluorescence spectra of the **NDI-1** by progressively adding Cyanide ion in-stock solution placed in a quartz cuvette. Solutions preparation is a similar procedure as mentions in the UV-Vis study.

3.5.5 Naked-eye detection

The **NDI-1** dissolves in $CHCl_3$ and is added in a different vial. Then each vial was added different anions, the color change observed in cyanide containing vial. It is observed by naked-eye and as well as under the UV-lamp at 365 nm

3.5.6 Competitive experiments

To demonstrate the effect of cyanide anions over the series of other anions the competitive UV-Vis absorbance spectra recorded. This experiment was done by adding cyanide ion in

the solution of **NDI-1** and with the successive addition of other anions.

3.5.7 Cyclic voltammetry experiments

Cyclic voltammetry (CV) was performed in Dry DCM and 0.1. M ($TBAPF_6$) as an electrolyte of **NDI-1** and **NDI-1** with CN^- ion.

3.6 Conclusions

In summary, we have designed and synthesized naphthalene diimide-benzothiazole (NDI-1) conjugate and it is used for nucleophilic addition of cyanide ion. The detection of cyanide ion with NDI-1 can be demonstrated by means of UV-Vis, emission, ^{1}H-NMR, cyclic voltammetry and further can be demonstrated by naked eyes. The selectivity of cyanide can be further demonstrated using other ions such as F^- , Cl^-, Br^-, I^-, HSO_4^-, $H_2PO_4^-$, OAc^-, ClO_4^- and HCO_3^-. The high selective and sensitive towards cyanide ion with very low limit of detection (85 nM) was demonstrated, thus, suggested that the NDI-1 could be a good sensor for practical applications effectively.

3.7 References

(1) K. W. Kuling, Cyanide toxicity, Atlanta, GA: U.S. Department of Health and Human Services; **1991**.

(2) J. L. Gerberding, Toxicology profile for cyanide. Atlanta: U. S. Department of Health and Human Services, **2006**.

(3) Coughlan, M. P. Cyanide in Biology. B. Vennesland , E. E. Conn , C. J. Knowles , J. Westley , F. Wissing. *Q. Rev. Biol.* **1983**, *58* (1), 143–143. https://doi.org/10.1086/413208.

(4) Ishii, A.; Seno, H.; Watanabe-Suzuki, K.; Suzuki, O.; Kumazawa, T. Determination of

Cyanide in Whole Blood by Capillary Gas Chromatography with Cryogenic Oven Trapping. *Anal. Chem.* **1998**, *70* (22), 4873–4876. https://doi.org/10.1021/ac980498b.

(5) Moriya, F.; Hashimoto, Y. Potential for Error When Assessing Blood Cyanide Concentrations in Fire Victims. *J. Forensic Sci.* **2001**, *46* (6), 1421–1425.

(6) World Health Organization; Safety I. P. on C. *Guidelines for drinking-water quality. Vol. 2, Health criteria and other supporting information*; World Health Organization, 1996.

(7) Young, C.; Tidwell, L.; Anderson, C. G. *Cyanide: Social, Industrial, and Economic Aspects*; Minerals, Metals & Materials Society: Warrendale, Pa., 2001.

(8) Ellis, W. B. Books: Ullmann's Encyclopedia of Industrial Chemistry, 6th Edition. *J. Ind. Ecol.* **1999**, *3* (2–3), 192–195. https://doi.org/10.1162/jiec.1999.3.2-3.192.

(9) Government of Canada, C. F. I. A. *Natural toxins in fresh fruit and vegetables*. https://inspection.canada.ca/food-safety-for-consumers/fact-sheets/specific-products-and-risks/fruits-and-vegetables/natural-toxins/eng/1332276569292/1332276685336 (accessed 2022-10-24).

(10) Bolarinwa, I. F.; Orfila, C.; Morgan, M. R. A. Determination of Amygdalin in Apple Seeds, Fresh Apples and Processed Apple Juices. *Food Chem.* **2015**, *170*, 437–442. https://doi.org/10.1016/j.foodchem.2014.08.083.

(11) Men, G.; Han, W.; Chen, C.; Liang, C.; Jiang, S. A Cyanide-Sensing Detector in Aqueous Solution Based on Anion–π Interaction-Driven Electron Transfer. *Analyst* **2019**, *144* (7), 2226–2230. https://doi.org/10.1039/C9AN00135B.

(12) Sebastian, A.; Prasad, E. Cyanide Sensing in Water Using a Copper Metallogel through "Turn-on" Fluorescence. *Langmuir* **2020**, *36* (35), 10537–10547. https://doi.org/10.1021/acs.langmuir.0c01803.

(13) Badugu, R.; Lakowicz, J. R.; Geddes, C. D. Excitation and Emission Wavelength Ratiometric Cyanide-Sensitive Probes for Physiological Sensing. *Anal. Biochem.* **2004**,

327 (1), 82–90. https://doi.org/10.1016/j.ab.2003.12.026.

(14) Tomasulo, M.; Sortino, S.; White, A. J. P.; Raymo, F. M. Chromogenic Oxazines for Cyanide Detection. *J. Org. Chem.* **2006**, *71* (2), 744–753. https://doi.org/10.1021/jo052096r.

(15) Hudnall, T. W.; Gabbaï, F. P. Ammonium Boranes for the Selective Complexation of Cyanide or Fluoride Ions in Water. *J. Am. Chem. Soc.* **2007**, *129* (39), 11978–11986. https://doi.org/10.1021/ja073793z.

(16) Sessler, J. L.; Barkey, N. M.; Pantos, G. D.; Lynch, V. M. Acyclic Pyrrole-Based Anion Receptors: Design, Synthesis, and Anion-Binding Properties. *New J. Chem.* **2007**, *31* (5), 646–654. https://doi.org/10.1039/B615673H.

(17) Sun, C.; Gradzielski, M. Fluorescence Sensing of Cyanide Anions Based on Au-Modified Upconversion Nanoassemblies. *Analyst* **2021**, *146* (7), 2152–2159. https://doi.org/10.1039/D0AN01954B.

(18) Zelder, F. H. Specific Colorimetric Detection of Cyanide Triggered by a Conformational Switch in Vitamin B12. *Inorg. Chem.* **2008**, *47* (4), 1264–1266. https://doi.org/10.1021/ic702368b.

(19) Lou, X.; Zhang, L.; Qin, J.; Li, Z. An Alternative Approach to Develop a Highly Sensitive and Selective Chemosensor for the Colorimetric Sensing of Cyanide in Water. *Chem. Commun.* **2008**, No. 44, 5848–5850. https://doi.org/10.1039/B812746H.

(20) Zalmi, G. A.; Nadimetla, D. N.; Kotharkar, P.; Puyad, A. L.; Kowshik, M.; Bhosale, S. V. Aggregation-Induced Emission-Based Material for Selective and Sensitive Recognition of Cyanide Anions in Solution and Biological Assays. *ACS Omega* **2021**, *6* (26), 16704–16713. https://doi.org/10.1021/acsomega.0c06080.

(21) Nandhini, C.; Saravana Kumar, P.; Shanmugapriya, R.; Satheeshkumar, A.; Vennila, K. N.; Elango, K. P. A Multi-Site Probe for Selective Detection of Cyanide and Sulphite

Ions via Different Mechanisms with Concomitant Different Fluorescent Behaviors. *Results Chem.* **2022**, *4*, 100312. https://doi.org/10.1016/j.rechem.2022.100312.

(22) Nicoleti, C. R.; Nandi, L. G.; Machado, V. G. Chromogenic Chemodosimeter for Highly Selective Detection of Cyanide in Water and Blood Plasma Based on Si–O Cleavage in the Micellar System. *Anal. Chem.* **2015**, *87* (1), 362–366. https://doi.org/10.1021/ac504037v.

(23) Ullah, Z.; Sonawane, P. M.; Nguyen, T. S.; Garai, M.; Churchill, D. G.; Yavuz, C. T. Bisphenol–Based Cyanide Sensing: Selectivity, Reversibility, Facile Synthesis, Bilateral "OFF-ON" Fluorescence, C2v Structural and Conformational Analysis. *Spectrochim. Acta. A. Mol. Biomol. Spectrosc.* **2021**, *259*, 119881. https://doi.org/10.1016/j.saa.2021.119881.

(24) Sun, S.-S.; Lees, A. J. Anion Recognition through Hydrogen Bonding: A Simple, yet Highly Sensitive, Luminescent Metal-Complex Receptor. *Chem. Commun.* **2000**, No. 17, 1687–1688. https://doi.org/10.1039/B004541L.

(25) Lin, Q.; Liu, L.; Zheng, F.; Mao, P.-P.; Liu, J.; Zhang, Y.-M.; Yao, H.; Wei, T.-B. A Benzimidazole Functionalized NDI Derivative for Recyclable Fluorescent Detection of Cyanide in Water. *RSC Adv.* **2017**, *7* (61), 38458–38462. https://doi.org/10.1039/C7RA07247C.

(26) Balasaravanan, R.; Sadhasivam, V.; Sivaraman, G.; Siva, A. Triphenylamino α-Cyanovinyl- and Cyanoaryl-Based Fluorophores: Solvatochromism, Aggregation-Induced Emission and Electrochemical Properties. *Asian J. Org. Chem.* **2016**, *5* (3), 399–410. https://doi.org/10.1002/ajoc.201500488.

(27) Chung, Y.; Ahn, K. H. N-Acyl Triazenes as Tunable and Selective Chemodosimeters Toward Cyanide Ion. *J. Org. Chem.* **2006**, *71* (25), 9470–9474. https://doi.org/10.1021/jo061798t.

(28) Gimeno, N.; Li, X.; Durrant, J. R.; Vilar, R. Cyanide Sensing with Organic Dyes: Studies in Solution and on Nanostructured Al2O3 Surfaces. *Chem. – Eur. J.* **2008**, *14* (10), 3006–3012. https://doi.org/10.1002/chem.200700412.

(29) Hawthorne, M. F.; Hammond, G. S.; Graybill, B. M. The Nucleophilicity of the Cyanide Ion. *J. Am. Chem. Soc.* **1955**, *77* (2), 486–488. https://doi.org/10.1021/ja01607a083.

(30) García, F.; García, J. M.; García-Acosta, B.; Martínez-Máñez, R.; Sancenón, F.; Soto, J. Pyrylium-Containing Polymers as Sensory Materials for the Colorimetric Sensing of Cyanide in Water. *Chem. Commun.* **2005**, No. 22, 2790–2792. https://doi.org/10.1039/B502374B.

(31) Yang, Y.-K.; Tae, J. Acridinium Salt Based Fluorescent and Colorimetric Chemosensor for the Detection of Cyanide in Water. *Org. Lett.* **2006**, *8* (25), 5721–5723. https://doi.org/10.1021/ol062323r.

(32) Padghan, S. D.; Wang, C.-Y.; Liu, W.-C.; Sun, S.-S.; Liu, K.-M.; Chen, K.-Y. A Naphthalene-Based Colorimetric and Fluorometric Dual-Channel Chemodosimeter for Sensing Cyanide in a Wide PH Range. *Dyes Pigments* **2020**, *183*, 108724. https://doi.org/10.1016/j.dyepig.2020.108724.

(33) Zelder, F. H.; Männel-Croisé, C. Recent Advances in the Colorimetric Detection of Cyanide. *Chim. Int. J. Chem.* **2009**, *63* (1–2), 58–62. https://doi.org/10.2533/chimia.2009.58.

(34) Wang, F.; Wang, L.; Chen, X.; Yoon, J. Recent Progress in the Development of Fluorometric and Colorimetric Chemosensors for Detection of Cyanide Ions. *Chem. Soc. Rev.* **2014**, *43* (13), 4312–4324. https://doi.org/10.1039/C4CS00008K.

(35) Sakai, N.; Mareda, J.; Vauthey, E.; Matile, S. Core-Substituted Naphthalenediimides. *Chem. Commun.* **2010**, *46* (24), 4225–4237. https://doi.org/10.1039/C0CC00078G.

(36) Al Kobaisi, M.; Bhosale, S. V.; Latham, K.; Raynor, A. M.; Bhosale, S. V. Functional

Naphthalene Diimides: Synthesis, Properties, and Applications. *Chem. Rev.* **2016**, *116* (19), 11685–11796. https://doi.org/10.1021/acs.chemrev.6b00160.

(37) Röger, C.; Würthner, F. Core-Tetrasubstituted Naphthalene Diimides: Synthesis, Optical Properties, and Redox Characteristics. *J. Org. Chem.* **2007**, *72* (21), 8070–8075. https://doi.org/10.1021/jo7015357.

(38) Maniam, S.; Higginbotham, H. F.; Bell, T. D. M.; Langford, S. J. Harnessing Brightness in Naphthalene Diimides. *Chem. – Eur. J.* **2019**, *25* (29), 7044–7057. https://doi.org/10.1002/chem.201806008.

(39) Lu, X.; Zhu, W.; Xie, Y.; Li, X.; Gao, Y.; Li, F.; Tian, H. Near-IR Core-Substituted Naphthalenediimide Fluorescent Chemosensors for Zinc Ions: Ligand Effects on PET and ICT Channels. *Chem. – Eur. J.* **2010**, *16* (28), 8355–8364. https://doi.org/10.1002/chem.201000461.

(40) Cox, R. P.; Higginbotham, H. F.; Graystone, B. A.; Sandanayake, S.; Langford, S. J.; Bell, T. D. M. A New Fluorescent H+ Sensor Based on Core-Substituted Naphthalene Diimide. *Chem. Phys. Lett.* **2012**, *521*, 59–63. https://doi.org/10.1016/j.cplett.2011.11.028.

(41) Bhosale, S. V.; Bhosale, S. V.; Bhargava, S. K. Recent Progress of Core-Substituted Naphthalenediimides: Highlights from 2010. *Org. Biomol. Chem.* **2012**, *10* (32), 6455–6468. https://doi.org/10.1039/C2OB25798J.

(42) Guha, S.; Saha, S. Fluoride Ion Sensing by an Anion−π Interaction. *J. Am. Chem. Soc.* **2010**, *132* (50), 17674–17677. https://doi.org/10.1021/ja107382x.

(43) Doria, F.; Folini, M.; Grande, V.; Cimino-Reale, G.; Zaffaroni, N.; Freccero, M. Naphthalene Diimides as Red Fluorescent PH Sensors for Functional Cell Imaging. *Org. Biomol. Chem.* **2014**, *13* (2), 570–576. https://doi.org/10.1039/C4OB02054E.

(44) Hughes, W.; Rananaware, A.; La, D. D.; Jones, L. A.; Bhargava, S.; Bhosale, S. V.

Aza-Crown Ether-Core Substituted Naphthalene Diimide Fluorescence “Turn-on” Probe for Selective Detection of Ca2+. *Sens. Actuators B Chem.* **2017**, *244*, 854–860. https://doi.org/10.1016/j.snb.2017.01.044.

(45) Shaikh, D. B.; Ali Said, A.; Wang, Z.; Srinivasa Rao, P.; Bhosale, R. S.; Mak, A. M.; Zhao, K.; Zhou, Y.; Liu, W.; Gao, W.; Xie, J.; Bhosale, S. V.; Bhosale, S. V.; Zhang, Q. Influences of Structural Modification of Naphthalenediimides with Benzothiazole on Organic Field-Effect Transistor and Non-Fullerene Perovskite Solar Cell Characteristics. *ACS Appl. Mater. Interfaces* **2019**, *11* (47), 44487–44500. https://doi.org/10.1021/acsami.9b13894.

(46) *Citation | Gaussian.com*. https://gaussian.com/citation/ (accessed 2022-10-24).

(47) Team, T. A. *Avogadro - Free cross-platform molecular editor*. Avogadro. https://avogadro.cc/ (accessed 2022-10-24).

(48) Hanwell, M. D.; Curtis, D. E.; Lonie, D. C.; Vandermeersch, T.; Zurek, E.; Hutchison, G. R. Avogadro: An Advanced Semantic Chemical Editor, Visualization, and Analysis Platform. *J. Cheminformatics* **2012**, *4* (1), 17. https://doi.org/10.1186/1758-2946-4-17.

(49) O’Boyle, N. M.; Tenderholt, A. L.; Langner, K. M. Cclib: A Library for Package-Independent Computational Chemistry Algorithms. *J. Comput. Chem.* **2008**, *29* (5), 839–845. https://doi.org/10.1002/jcc.20823.

(50) Vidya, B.; Iniya, M.; Sivaraman, G.; Sumesh, R. V.; chellappa, D. Diverse Benzothiazole Based Chemodosimeters for the Detection of Cyanide in Aqueous Media and in HeLa Cells. *Sens. Actuators B Chem.* **2017**, *242*, 434–442. https://doi.org/10.1016/j.snb.2016.11.076.

Chapter 4: Photoswitchable molecular glue for Carbon Nanotubes Reversibly Controls Electronic Mobility with Light

4.1 Introduction:

As we know that in 1991 the discovery of carbon nanotube (CNT)[1] which have been recognized as promising scaffolds in nanotechnology and also have a great potential in various fields.[2-12] From the discovery, we know that CNTs can be either (1) single-walled (SWCNT),[13] usually having a diameter of 0.4–2 nm and lengths up to several cm or (2) multi-walled (MWCNTs), composed of multiple concentric cylinders of single-walled SWCNTs stacked on each other.[14] Both single-walled (SWCNT) and multi-walled (MWCNTs) have their own distinctive advantages and have been applied in various fields successfully.[15-28] From reported studies, MWCNTs have fascinated particular focus as they can be produced in bulky quantities and are also easier to purify. Hence, the cost of production for MWCNTs is considerably lower than the SWCNTs, which has been a main reason for their applications in many scientific research.[29-32] Commonly both CNTs possess similar properties in terms of their high thermal and electrical conductivity, which is necessary for its applications.[33-35] Current research has shown that the outer walls of CNTs can be modified with functional groups including carboxylic acids, hydroxides and amides, that can act as sites for covalent functionalization to improve overall usability of CNTs.[36] Recently this strategy has been used to design MWCNT-based hybrid materials with tailor-made properties including greater stability, dispersibility, and processibility.[37],[38] For this purpose the functionalization can be carried out either on the main skeleton and/or at the periphery of the CNTs with desirable structures.[39] Specifically when the functionalization of CNTs with photoswitchable molecules is carried out it offers an additional tunability of the material with light.[40-42] Such advancement of MWCNTs integrated with photoswitchable molecules leading to new dimensions in optoelectronic materials and other areas.[43],[44]

In recent trend, controlled reversible photoswitching of conductivity is of particular interest in molecular electronics [45] and several groups worked on it for exciting results.[46,47] Still, there is a challenging task to control the conductivity reversibly by using an external stimulus at the molecular level. The solution for this challenge is tetraphenylethylene (TPE) unit with four phenyl groups, a well-known system for its AIE properties, which serves as an outstanding candidate as a building block for receptors of carbon-based frameworks.[48,49]

From the literature studies amongst common photochromic molecules such as (diarylethenes,[50] spiropyrans,[51] oxazines[52], stilbenes[53] and azobenzenes), specifically azobenzenes responses to two main external stimuli, light and heat to reversibly switch between the isomers with dissimilar properties. Upon exposure to UV light, azobenzene switching from the thermodynamically favored *trans* isomer to the *cis* isomer.[54,55] Also the reverse reaction simultaneously occurs with visible light or heat, even at room temperature. Such type of transformation is mainly dependent on the structure of the azobenzene system and the local environment, such as the matrix or the solvent, which permits tuning of the switching process thoroughly. In this work we aimed to develop photoswitchable molecular glue, based on non-covalent interactions, to assemble a MWCNT-hybrid, containing a photoresponsive azo-system to allow conductivity switching.

4.2 Results and Discussion

Here we designed and synthesized photoresponsive molecular glue TPE-**1** having the azobenzene and the TPE units.

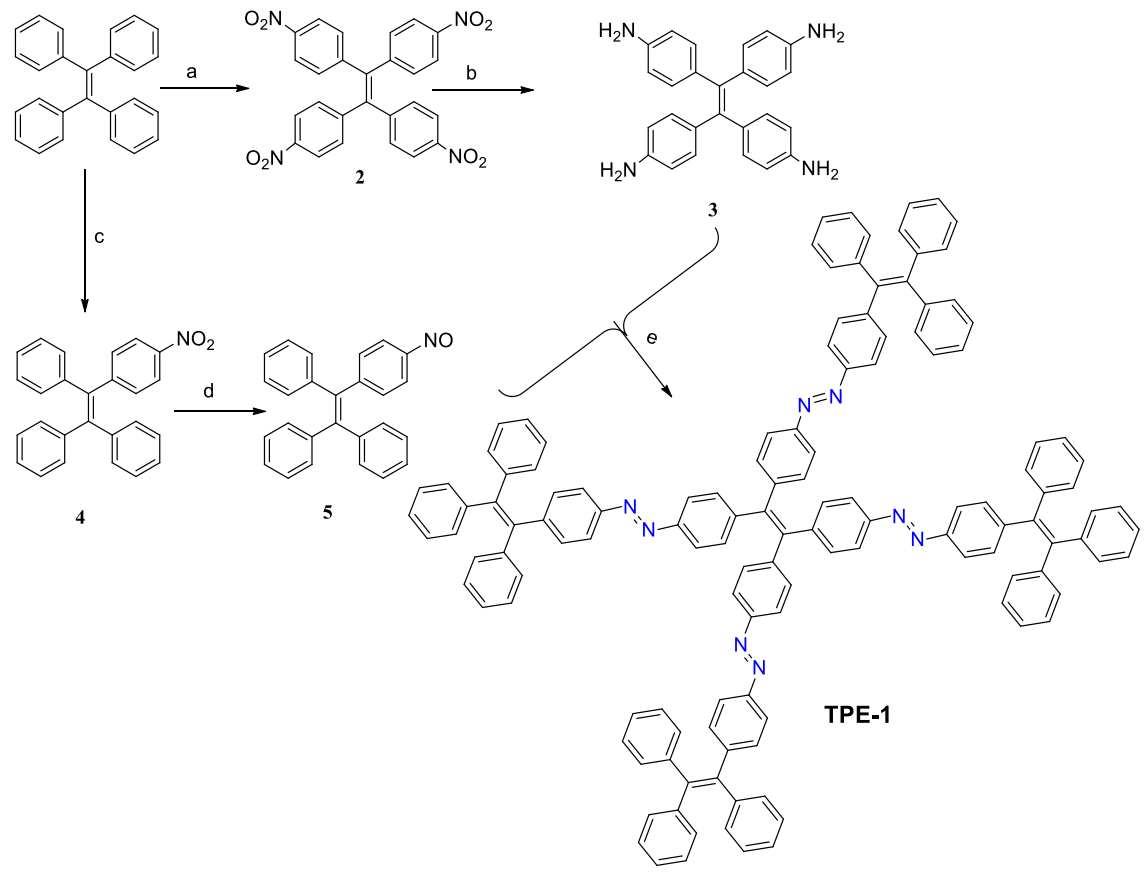

Scheme 4.1: Synthesis of **TPE-1** and the precursor of the **TPE-1.** (a)**.** HNO_3, H_2SO_4, Dry DCM, r.t.,

16h. (b). Pd/C, NH_2-NH_2, H_2O, 100 ^oC, 24 h. (c). HNO_3, AcOH, r.t., 20 min, (d) $FeCl_3$, NH_4Cl, Zn, EtOH, H_2O, 1 h, (e). AcOH, r.t., under N_2 atmosphere, 24 h.

Further the association of TPE-**1** with MWCT can occur via π–π stacking, electrostatic interactions or hydrophobic interaction, offering several benefits over covalent functionalization such as i) mild perturbation of the sp^2 structure of the carbon allotrope, ii) limited change in structure and iii) preservation of electronic properties.

The designed photochromic system TPE-**1** consists of five AIE-active tetraphenylethylene TPE chromophores bridged by azo-groups. Interestingly, the *trans-cis* isomerization leads to a significant change in the shape of the molecule, from an almost flat to a puckered structure that affects the interaction of the molecule with the MWCNTs, and affects the AIE behavior simultaneously. From above study it was found that the TPE-**1** indeed acts as photoswitchable molecular glue for the MWCNTs.

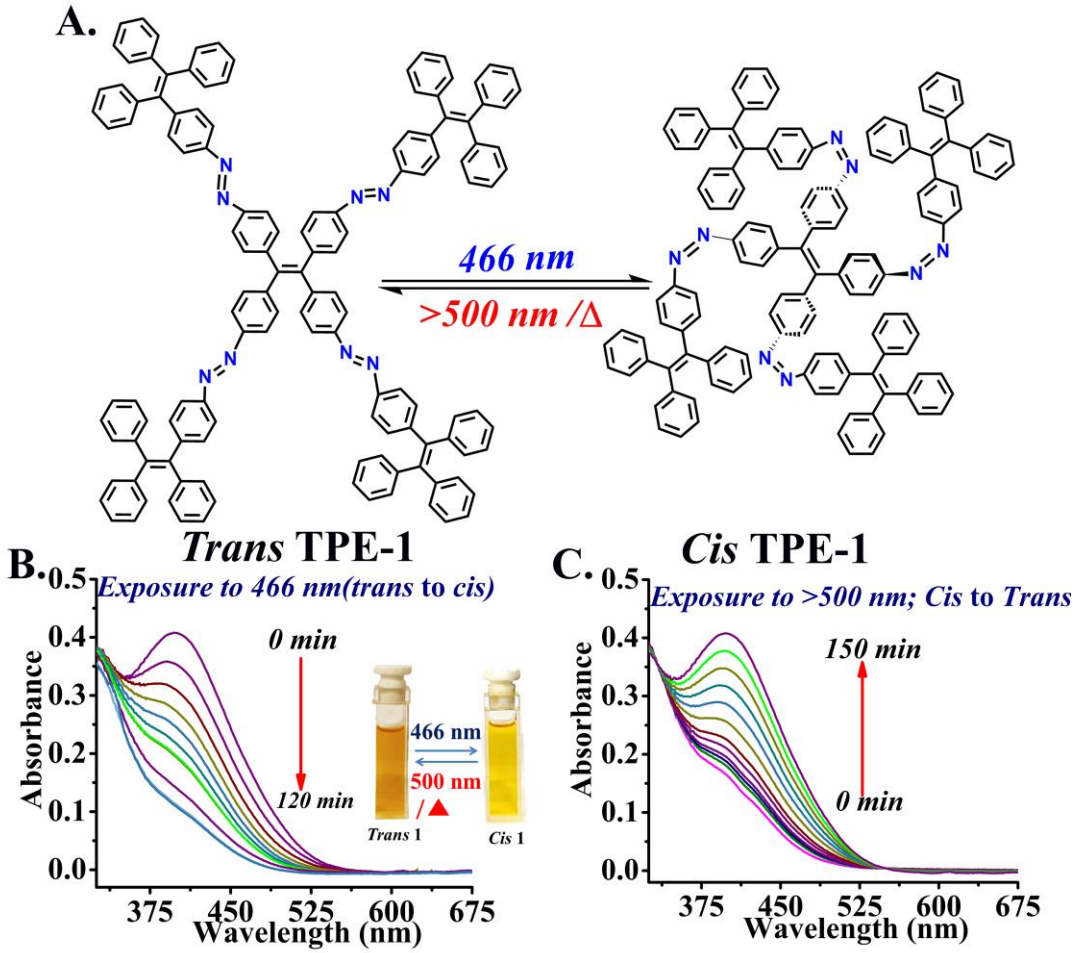

Figure 4.1 Photoisomerization of TPE-1 (6 μM) in THF solvent (A). Schematic representation of the photoisomerized TPE-1 in THF solvent at 273 K temperature (B). *trans*-1 to cis-1 conversion upon irradiation with 466 nm at 273 K temperature; in the inset visual colour changes (c). *cis*-1 to *trans*-1 conversion upon irradiation with >500 nm at 273 K temperature or heat >333 K.

In this work, the extreme change in the electronic mobility of the MWCNT-TPE-1 ensemble upon photoswitching of TPE-1 using light as an external stimulus has been successfully demonstrated. The synthesis of tetra-azo TPE-1 was done by coupling freshly prepared nitroso-TPE (5) with tetra-amino-TPE (3) in glacial acetic acid (Scheme 4.1).[56] After reaction completion, deep red colour precipitation of TPE-1 was obtained and it was purified and further characterized to confirm its structure via ^{1}H NMR, ^{13}C NMR, FTIR and mass spectrometry techniques.

Further the photoisomerization of TPE-1 was performed (in THF) with light and the reversal was also studied with heat as an external stimulus. The propeller-like structure of TPE-1 exhibited *trans*- *cis* photochromism under UV light (366 nm UV, 8 W, irradiation power 2.3 mW cm^{-2}, blue LED light (466 nm, 0.5 mW cm^{-2}) (Figure 4.1B). The reverse isomerization were carried out upon exposure to red right (> 500 nm, red or green LED light, 0.5 mW cm^{-2}) or heat (Figure 4.1C). Upon irradiation with UV or blue light in THF, the thermodynamically stable *trans*-1 was converted to the *cis*-1 isomer. This *cis*-1 isomer reverted to the *trans*-1 upon exposure to >500 nm or under heating form reverted to the *trans*-1 form. A striking red to yellow color change was also observed for the *trans*-1 to *cis*-1 photoisomerization for about 120 minutes. It was observed that spectral changes reached a photostationary state (PSS) where the absorbance value of the band at 405 nm ($\varepsilon \sim 7 \times 10^5$ M^{-1} cm^{-1}) reached a constant value (Figure 4.1A). Photoisomerization studies in other solvents such as CS_2, MeOH, $CHCl_3$, and CH_3CN were also conducted which showed similar results.

The reversible photoisomerization of TPE-1 was also studied to check the photostability. It was observed that the TPE-1 was stable, for five cycles without a fatigue loss (Figure 4.2).

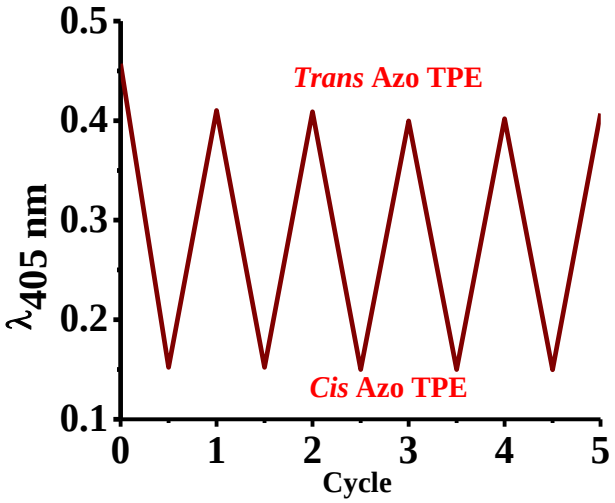

Figure 4.2: Reversibility studies of **TPE-1** in THF solvent under alternating photoirradiation with UV (366 nm) or 466 nm and visible light (> 500 nm) respectively.

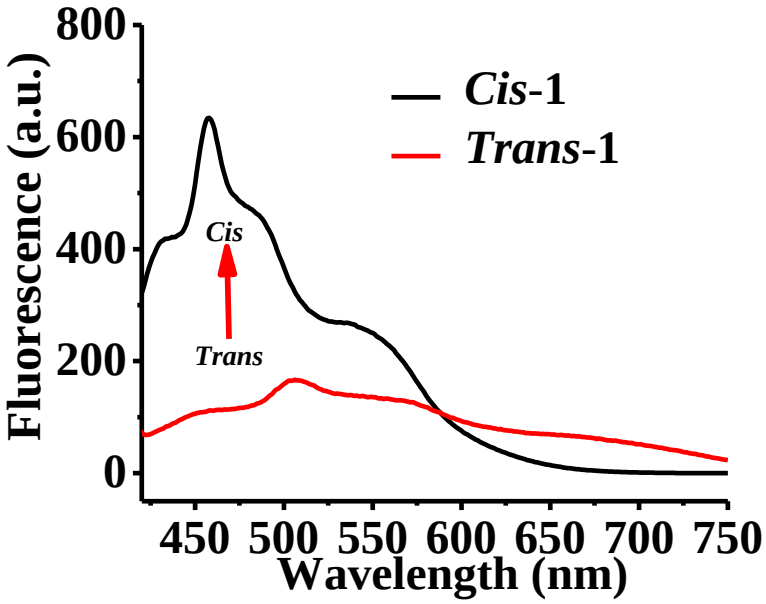

Figure 4.3: Fluorescence data of **TPE-1** red traces for the *trans* rich and black traces for the *cis* rich.

In fluorescence studies, both the *cis* and the *trans* forms of TPE-1 were undertaken at an excitation with 405 nm. A broad emission band was observed at 507 nm with an additional shoulder band at 575 nm. The photoisomerized *cis*-rich PSS exhibited a higher fluorescence than the *trans*-rich solution (Figure 4.3).

Moreover, the photoisomerization behavior of TPE-1 was also studied using the ^{1}H NMR spectroscopy. Upon exposure to UV or blue light the aromatic hydrogen peaks at δ□7.65, 7.61, and 7.04 in the *trans*-1 were shifted upfield to 7.59, 7.57, 6.96 ppm respectively, along with the formation of new peaks at □ 6.61 and 6.58 (Figure 4.4). These newly appeared signals diminished again upon the irradiation with > 500 nm light, which is consistent with the previously reported results.[57]

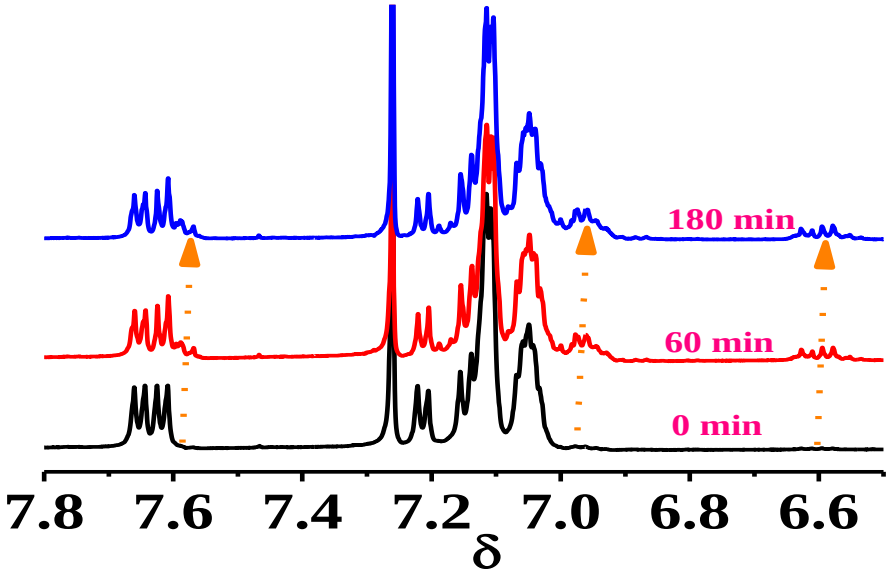

Figure 4.4: NMR traces of **TPE-1** in $CDCl_3$ (10^{-3} M) displaying the clear shift in the aromatic protons upon photo isomerization. (A) After radiation of the *trans* form with 466 nm for 180 min (Blue); (B) *trans* form (bottom trace black). New peaks are indicating by arrow sign**.**

Further HPLC analysis of the *cis*-**TPE-1** sample showed that about 60 % of the sample was in the all *cis* (Z4) form (Figure 4.5).

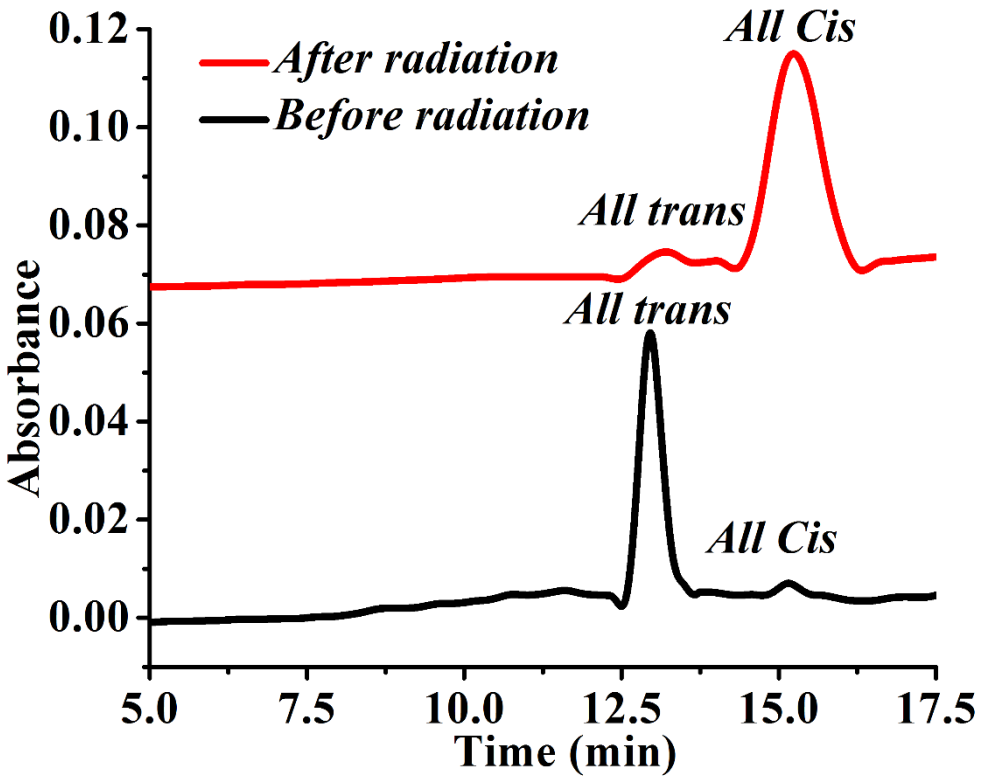

Figure 4.5: HPLC elution profile of the **TPE-1**. The *trans*-**1** sample was exposed to UV 366 nm or blue light as a result it reached the *cis* PSS. A red trace is the *trans*-**1** and black is the *cis* **1**. The isomeric ratios of the azobenzene tetramer in the PSS were estimated using HPLC

Firstly, before any irradiation, **TPE-1** displayed four distinct peaks with a retention time of 11.20, 12.53, 12.96, 15.15 minutes, most likely for the corresponding to the E_3Z, E_2Z_2, E_4, and *Z4* respectively. These assignment of the isomers are based on the expected polarities of the compounds and also by comparing with the literature report of a tetrameric azobenzene.[58] The maximum amount of isomer present was E_4 at 88%, followed by E_3Z at 6%, E_2Z_2 at 4%, and *Z4* at 2%. Upon irradiation with UV or blue light a corresponding *cis*-rich PSS was attained, which was apparent from the HPLC analysis as the isomer in the maximum amount was Z_4 at 60%. The ratios of the *trans* to *cis* were consistent with other reported results.[58]

For the determination of the stability of the *cis* TPE-1, kinetics studies were performed and different thermodynamic parameters, containing Activation energy (ΔE_{act}), Enthalpy of activation ($\Delta H^{\#}$), Entropy of activation ($\Delta S^{\#}$) and half life ($t_{1/2}$) were calculated from the variable temperature kinetics data (Figure 4.6 & Table 4.1). The $t_{1/2}$ values for *cis* TPE-1 to *trans* TPE-1 was 52 h at 273 K.

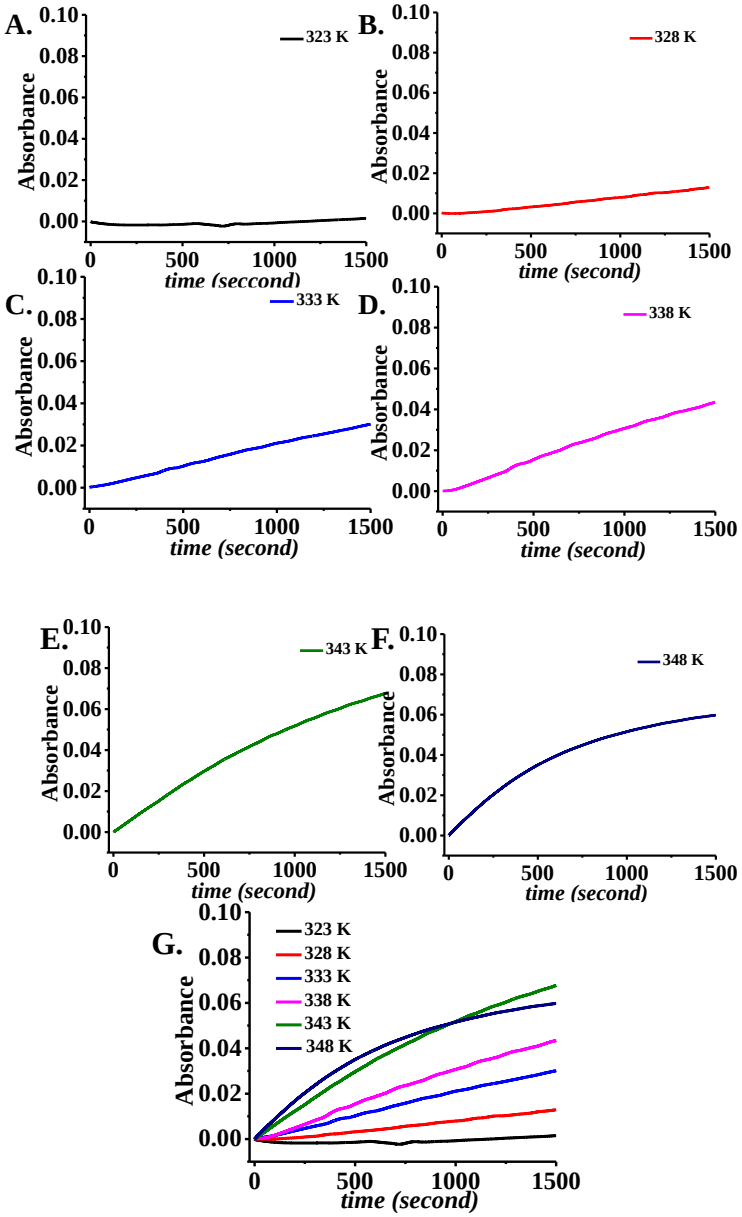

Figure 4.6: Thermal isomerisation studies of the *cis*-isomer of the TPE-**1** at various temperatures. (A)-(F) showed sis different temperature 323, 328, 333, 38,343, and 348 K respectively. (G) Showed the overlapping graph of all six temperatures.

Table 4.1: Thermodynamic parameters for the *cis*-**1** to *trans*-**1** isomerisation of the **TPE-1**.

Parameters	**ΔE_{act} (kcal mol^{-1})**[a]	**$\Delta H^{\ddagger}$ (kcal mol^{-1})**[b]	**$\Delta S^{\ddagger}$ (cal mol^{-1}K^{-1})**[c]
Values±(error)	24±(0.5)	23 ±(0.5)	36 ±(2)

a= Activation energy (Ea); b= Enthalpy of activation; c= Entropy of activation

Also we know that TPE-based molecules are well known for their AIE behavior.[59] The AIE behavior of the propeller-shaped azobenzene TPE-1 was studied in various THF: water ratios.

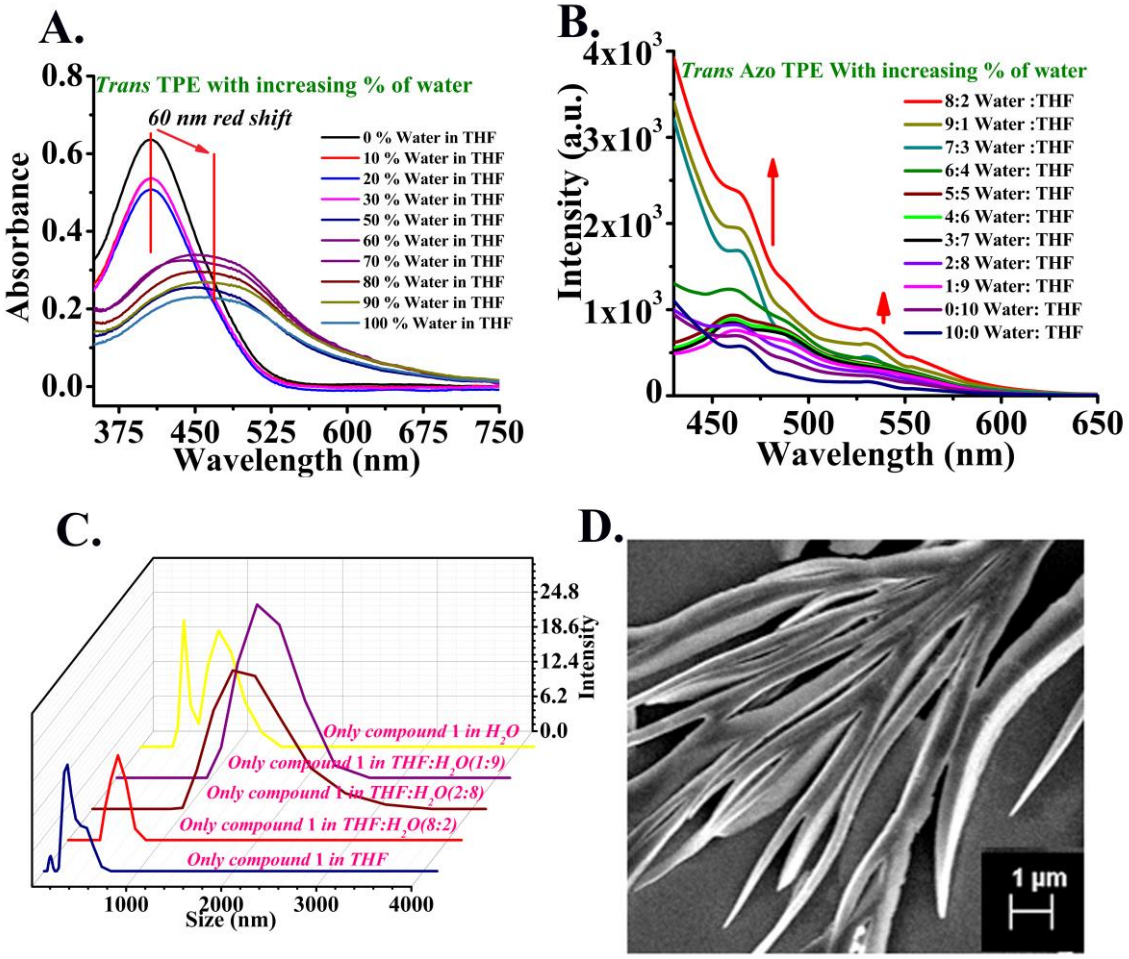

Figure 4.7: Aggregation behavior of TPE-1 in THF/water medium (A). Spectral changes in UV/Vis absorbance; (B). Spectral changes in emission spectra; (C). DLS studies of trans-1 in THF/water medium. (D). SEM images under aggregating conditions.

In pure THF, the TPE-1 was highly soluble; the monomeric form of TPE-1 was faintly emissive and was visually red in color. The AIE behavior, as expected, was observed with the *trans* form upon increasing the amount of water in the THF solution of TPE-1. It was noticed that the emission intensity increased and reached a maximum at 80% water-THF mixture (% *v/v*). Upon further increasing the water content it started to get precipited and stuck on the wall of cuvette. The band at 405 nm in the UV-Vis spectrum also underwent a drastic red-shift in the absorbance spectrum from 405 to 465 nm under these conditions (100% THF to 20% THF-water) (Figure 4.7A). In the emission spectra, red shift was observed in the weakly emissive bands at 465 and 520 nm, to 470 nm and 530 nm respectively (Figure 4.7B).

The appearance of a new absorption peak at 462 nm suggested that the *trans-TPE* 1 molecules stacked upon each other to form an aggregate. *J*-type aggregation was assumed for *trans* TPE-1, as its structure indicates propensity for π-stacking, with aggregation in the presence of aqueous solvent leading to characteristic photoluminescence (PL).

Prompted by this exciting observation, we turned our focus to the *cis*-TPE-1 and performed the same experiment. Surprisingly, the *cis*-TPE-1 did not show any such type of red shifts in the absorbance spectrum (Figure 4.8A), nor did it exhibit any significant increase in emission signal (Figure 4.8B). Therefore, the absorption peaks at 405 nm were found to decrease gradually with water addition.

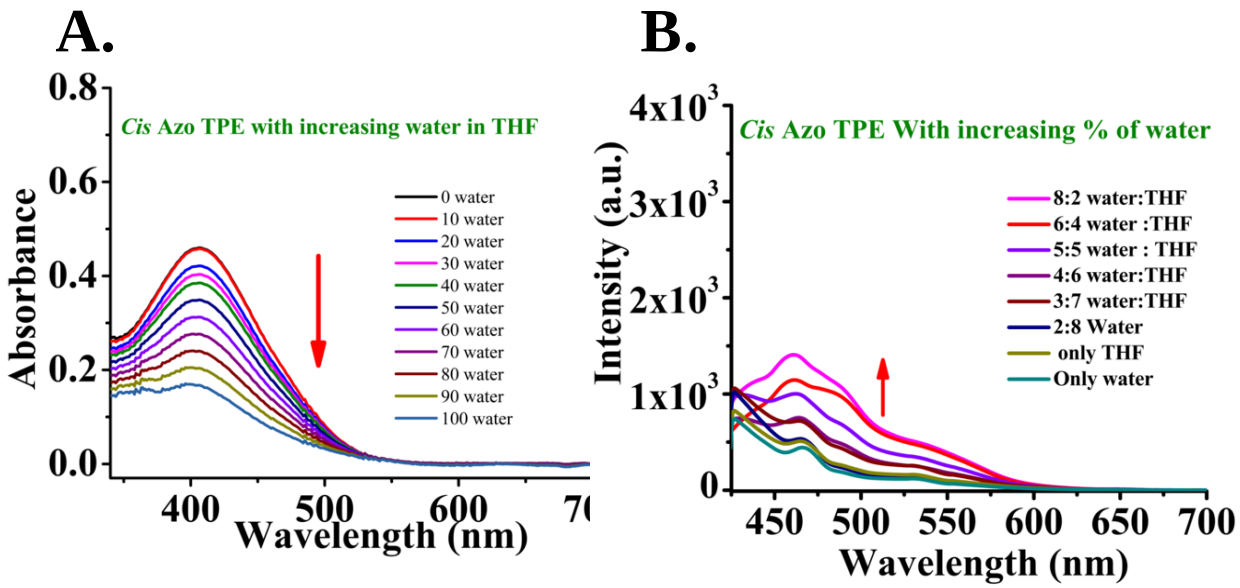

Figure 4.8: AIE studies of **TPE-1** in THF/Water medium; (A) UV-vis absorption spectrum of *cis* **TPE-1** under AIE conditions; (B). Emission spectrum of *cis* **TPE-1** under AIE conditions**.**

The aggregation behaviour was also studied and cross-verified through dynamic light scattering (DLS) experiments and scanning electron microscopy (SEM) (Figure 4.7D). DLS measurements monitored each step of the aggregation process for both the *cis*-TPE-1 and the *trans*-TPE-1. The DLS-data revealed the lack of any aggregated particles in the *cis*-isomer (Figure 4.7C). It did indicate the formation of an assembly of in the *trans* form in an aqueous-THF solvent mixture with an average hydrodynamic diameter of 1400 nm at 20% THF in water. The morphology of the *trans*-1 aggregated state were found to be flat-shaped plates, as observed through SEM after solvent evaporation onto a Si-wafer. Upon solvent evoporation the size of the aggregated state increased more compared to the DLS which was recorded in the solvent phase. The probable reason for aggregation of the *trans*-TPE-1 state but not the *cis*-TPE-1 was the difference in geometry of the molecules. In the *trans*-TPE-1 configuration, all the four TPE groups were almost coplanar, which is favourable for the π-π stacking.

These homomolecular aggregations of *trans*-TPE-1 in the aqueous-THF medium prompted us to wonder whether it would be possible to observe aggregation with larger π-systems like the MWCNT. Recently we have studied the selective capture of C_{60} using smaller TPE derivatives.[50] Thus, we studied the interaction of both the *trans*- and the *cis*-isomers of TPE-1 with carboxylic acid functionalized MWCNTs. For *trans*TPE-1 in THF, increasing the amount of MWCNT in the solution (MWCNT was dispersed in the THF solution) led to a decrease in peak intensity at 405 nm in the UV/vis spectrum, along with an 8 nm red shift and the formation of a new band at 580 nm (Figure 4.9A and Figure 4.10A).

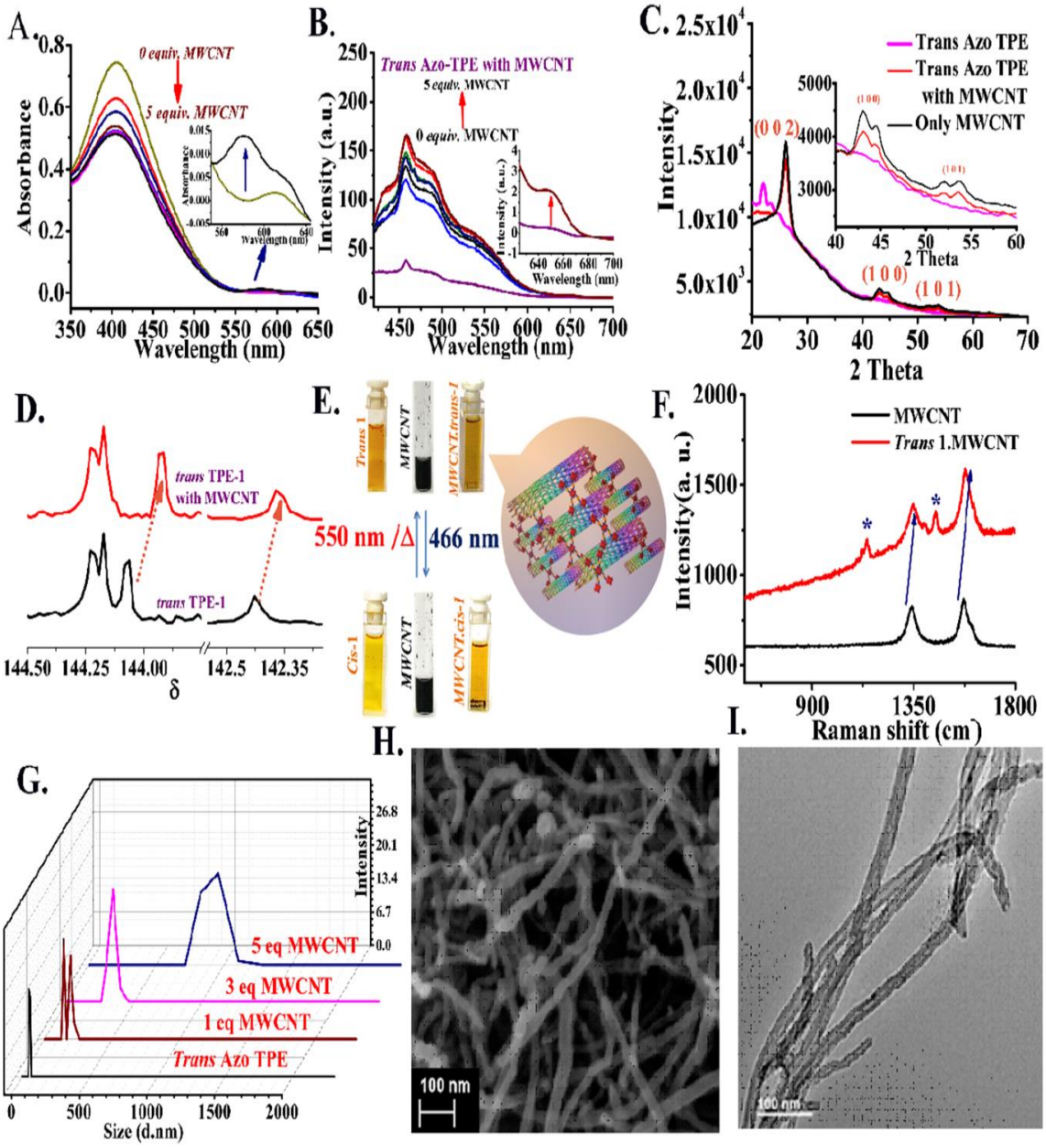

Figure 4.9 Spectral changes of TPE-1 with increasing the MWCNT: (A). Changes in the absorbance spectra of [***trans*-1.MWCNT**]; (B). Changes in the emission spectra of [***trans*-1.MWCNT**]; (C) PXRD of the [***trans*-1.MWCNT**]; (D) Changes in ^{13}C NMR spectra of **TPE-1** in presence and in absence of MWCNT; (E). Visual observation of colour change upon treatment of *trans* and *cis***TPE-1** with MWCNT, and the putative cartoon representation of the [***trans*-1.MWCNT**]; (F) Raman spectral shift of the [***trans*-1.MWCNT**]; (G). DLS studies of [***trans*-1.MWCNT**]; (H). SEM images of [***trans*-1.MWCNT**]; (I). TEM images of [***trans*-1.MWCNT**].

Fluorescence spectra collected with an increasing concentration of the MWCNTs to *trans*-TPE-1 showed a gradual increase in the emission bands at 485, 535 nm, and 650 nm (Figure 4.9B). The red shift in the absorption and emission bands indicated the interaction of *trans*-1 with MWCNTs to form an aggregate: [MWCNT.*trans*-TPE-1] through non-covalent interactions, which cannot occur for the *cis*-1 due to its twisted structure (Figure 4.10A-4.10B).

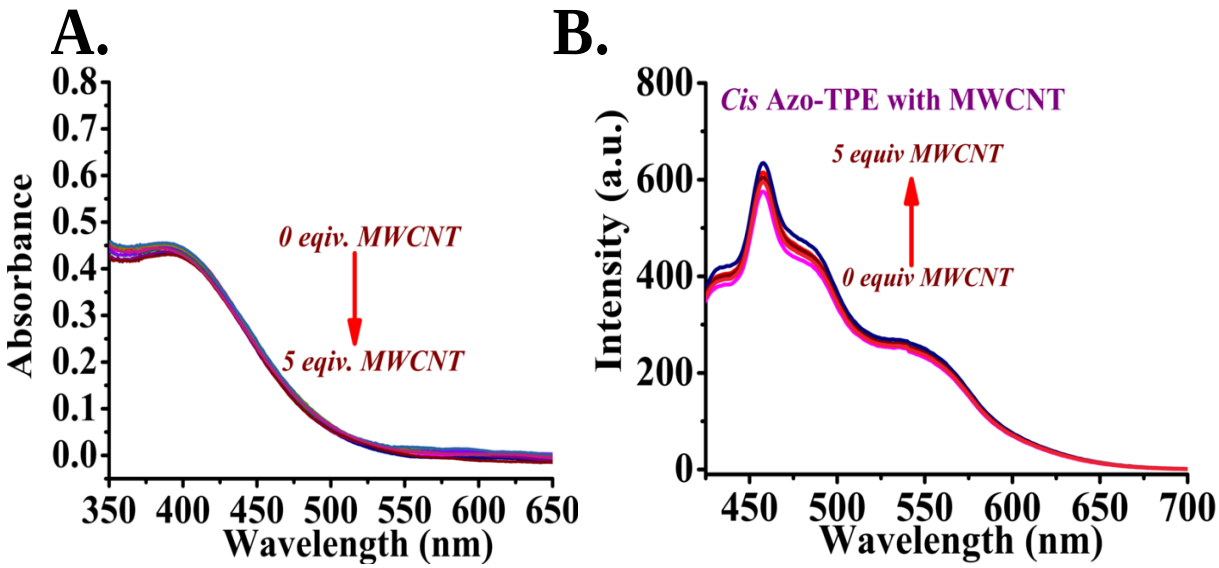

Figure 4.10: (A). UV/Vis absorbance changes spectra of **[*cis* TPE-1.MWCNT]**; (B) Emission spectral changes of **[*cis* TPE-1.MWCNT]** in THF solvent

The PXRD analysis was undertaken to investigate any change in the diffraction pattern of the MWCNTs after treatment with *trans* TPE-1 and also to study the effect of photoisomerization. The PXRD patterns for the free MWCNT (*sans* any TPE-1) and for the [*trans*-1.MWCNT] samples (Figure 4.9C & Figure 4.11) were similar.

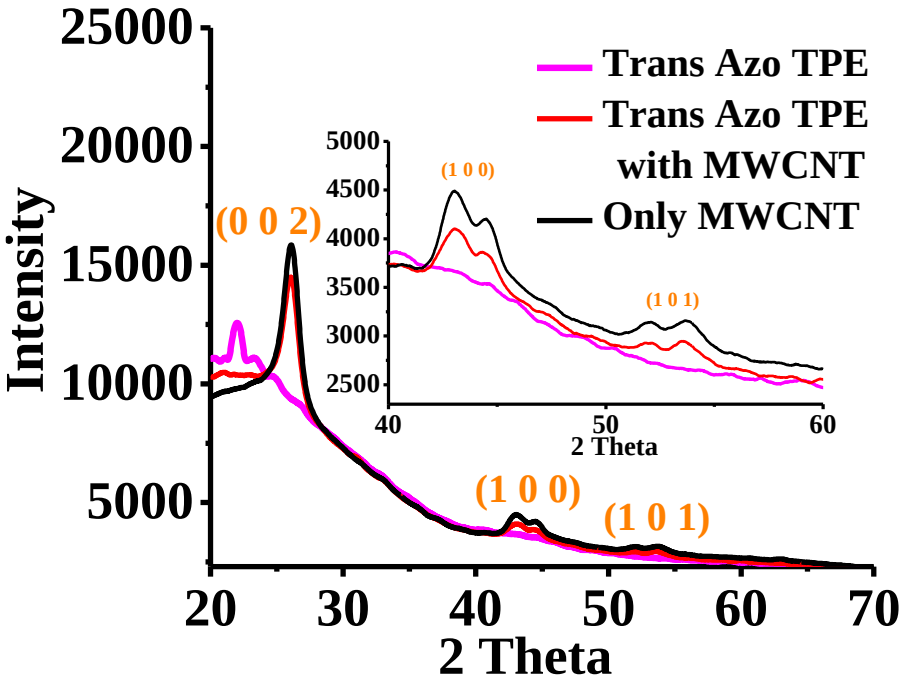

Figure 4.11: PXRD data of *trans*-**TPE-1** and the [***trans*-1.MWCNT**] recorded under 298K temperature.

The strongest and sharpest diffraction peaks for MWCNTs samples were at 2θ = 26.14°, (42.96°; 44.54°), and (52.04°; 53.80°) which labeled as *d* (002), *d* (100), *d* (001) respectively. The peaks for the [*trans*-1.MWCNT] were observed at 2θ = 26.00°, (42.55°; 44.20) and (51.70; 53.45), also indicated as *d* (002), *d* (100), *d* (001) respectively.[60] Compared to free MWCNT the [*trans*-1.MWCNT] aggregates shows a shift in the 2 θ values, which can be ascribed to a decrease in the sp^2 C-C layer spacing.[61] The *cis* form did not display any such changes. Raman spectroscopy was also performed with the *cis* and the *trans* samples in the presence of the MWCNT and studied against the controls. Two characteristics G and D-bands were observed for the MWCNTs at 1342 cm^{-1} (in-plane C-C vibration), and 1371 cm^{-1}.[62] The Raman spectra for the [*trans*-1.MWCNT] displayed new vibration band at1142 cm^{-1} and 1448 cm^{-1} and shifted bands at higher wave numbers 1350 cm^{-1} and 1378 cm^{-1} respectively. The bandat 1371 cm^{-1} indicated the lower inner tube interactions,and the new bands indicated the interactions of the MWCNT with the *trans*-1 (Figure 4.9F).[63]

In the IR-spectroscopy, the characteristic vibrations for the *trans*-1 and the MWCNT were observed at 1577 cm^{-1}, 2938 cm^{-1} , 2850 cm^{-1} , 1593 cm^{-1}, 1415 cm^{-1} and 1122 cm^{-1}respectively. With an increasing the amount of MWCNT with *trans*-1, these stretching bands were shifted to lower wavelengths at 2923 cm^{-1}, 2846 cm^{-1}, 1586 cm^{-1}, 1420 cm^{-1} and 1116 cm^{-1} respectively. These changes in the IR-stretching frequencies (Figure 4.12) indicate the changes in the dipole moment of the inner core of the MWCNT due to interaction with the *trans*-TPE-1. A Job's plot at 405 nm revealed an association with 1:1 stoichiometry between *trans*-1 and MWCNTs (Figure 4.13).

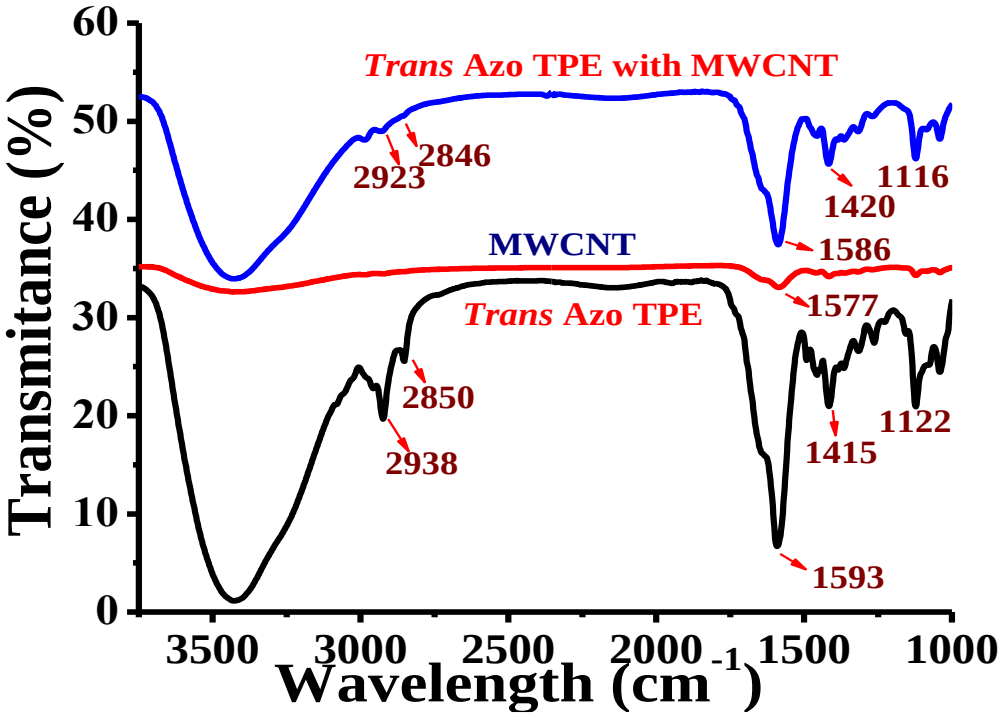

Figure 4.12: FTIR spectrum of **TPE-1** (Black traces), MWCNT (red traces) and [*trans* **TPE-1**.MWCNT] (blue traces).

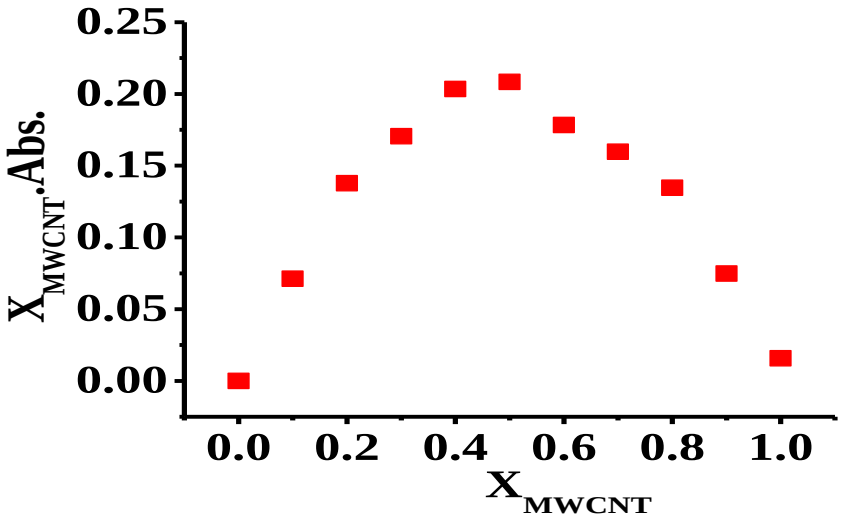

Figure 4.13: The Job's plot of the *trans* **TPE-1** with MWCNT showed 1:1 binding in THF solvent.

The absorbance data 405 nm leads to an estimated association constant of 2.2×10^4 M^{-1} (Figure 4.14).

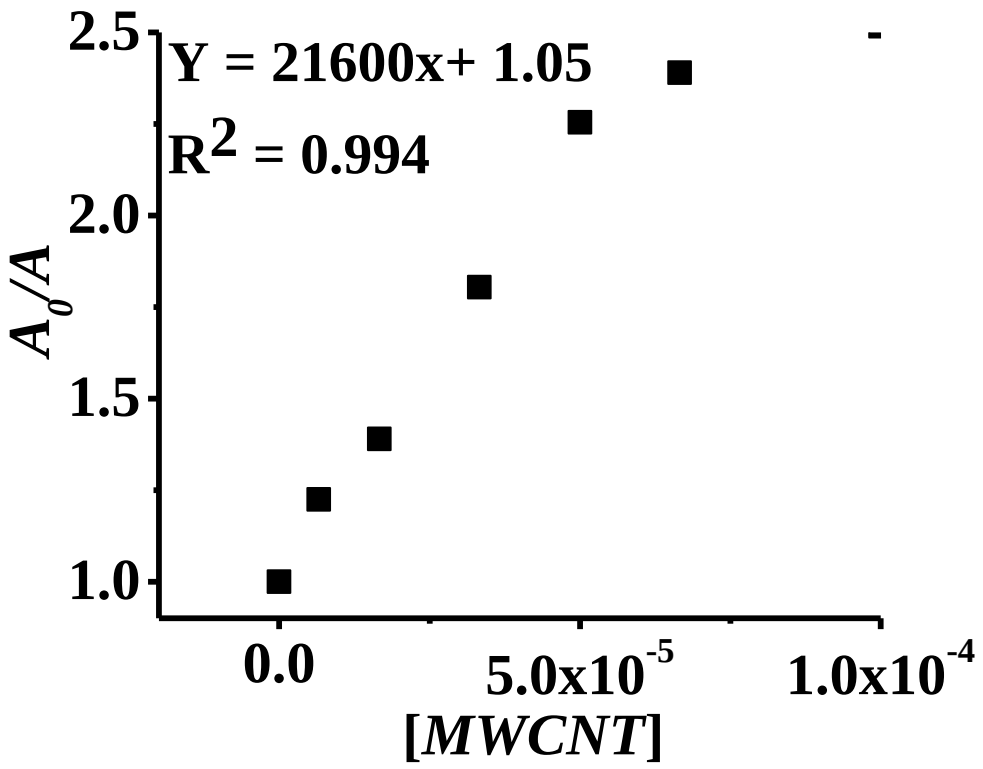

Figure 4.14: Binding constant calculation plot of the *trans* **TPE-1** in and **MWCNT**

association. No such changes of absorbance band were observed for the *cis*-1 and the calculated association constant value was $4.5\times10^{2}\ M^{-1}$ indicate limited association between *cis* TPE-1 and the MWCNT (Figure 4.15).

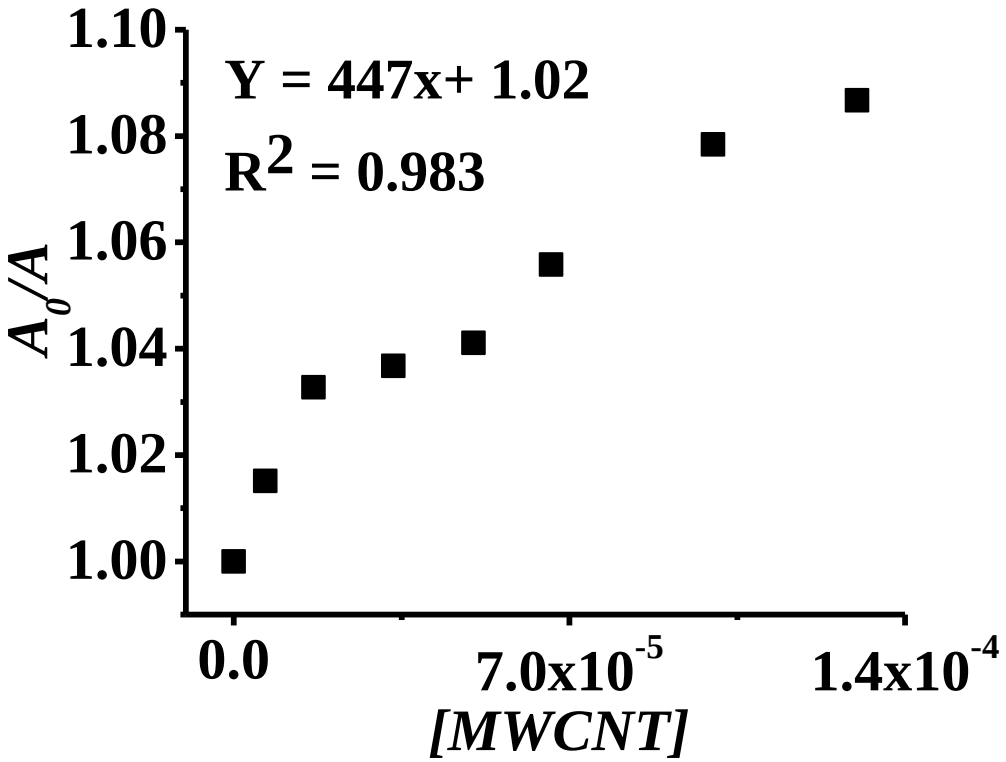

Figure 4.15: Binding constant calculation plot of the *cis* **TPE-1** in and **MWCNT** association.

Further to confirm the binding of MWCNT with the *trans*-1 the ^{13}C NMR spectra was recorded where it was observed that the characteristics TPE peaks were shifted to 143.92 and 142.37 ppm from 144.06 and 142.42 ppm with increasing the amount of MWCNTs (Figure 4.9D).

The assembly of the *trans*-1 with MWCNT was also studied through DLS (Figure 4.9G). The initial hydrodynamic diameter of the *trans*-1.MWCNT were around 100 nm, which increased to 1000 nm on increasing MWCNT in THF solvent. Morphology studies using SEM and TEM indicated a tube-like structure. The morphology studies of the *trans*-1

decorated over MWCNT was also observed from the SEM (Figure 4.9H) and TEM (Figure 4.9I), further supporting direct interaction of *trans* TPE-1 with the MWCNTs. The reason for binding strongly with *trans*-1 not with the cis-1 was the geometrical phenomenon.

We also wondered if the electrical conductance of the TPE decorated MWCNT can be modulated with stimuli. It is known that azobenzene systems by themselves cannot switch conductance upon photoisomerization.[64] However incorporation of azobenzene through covalent linkage displayed modulation of conductance in assemblies.[33] Therefore, the switching of the electronic mobility upon the *cis-trans* isomerization of our TPE-decorated MWCNT was investigated under spin coating. The reversible switching of the conductance was studied in the solid state in a thin-film on an indium tin oxide (ITO) surface. Fabrication of the device for the investigation of the conductance was done by wet-etching of the TPE-1 on the ITO glass substrate with a layer width of ~200 nm having an Ag-layer as the top contact (Figure 4.16A).

The current-voltage (*I-V*) characteristic studies shown in Figure 4.16B displayed a linear current−voltage (*I*−*V*) plot of the hybrid at a voltage ranging from -3 to +3 V. The [**TPE-1.MWCNT**] in the *trans* form displayed a strong I−*V* response compared to the *cis form*. The response ratio, defined by $I_{trans}(V)/I_{cis}(V)$ at 2V was found to be 7. We can thus conclude that the non-covalent interaction of *trans* TPE with the MWCNTs increased the current approximately 7 fold due to higher conductivity.

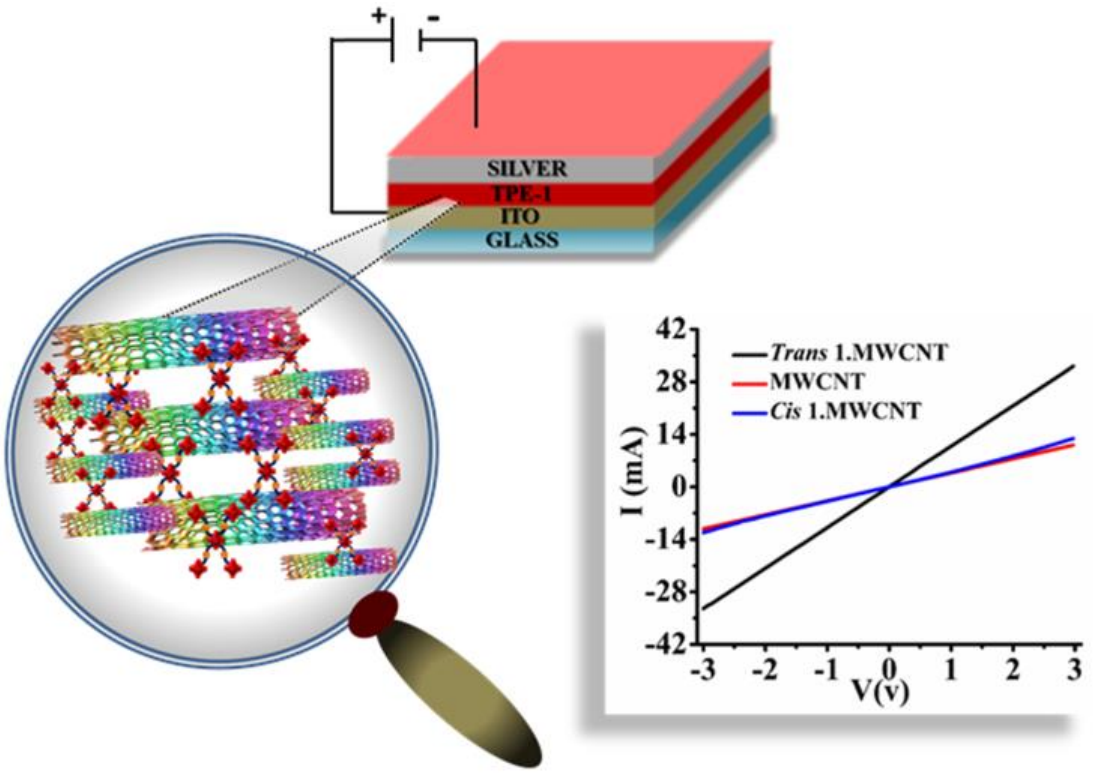

Figure 4.16(A) Schematic representation of the interaction between [***trans*-1.MWCNT**]; (B) I Vs V plot of the **TPE-1** dropped over MWCNT where black is for the [***trans*-1.MWCNT**], blue is [***cis*-1.MWCNT**] and red is only MWCNT.

4.3 Experimental Procedure

All reactants and reagent were commercially available and were used without furthure purification unless otherwise indicated TPE, chloroform (CHCL3), chcloroform-d (CDCL3), Methanol (MeOH), dichloromethane (DCM), Tetrahydrofuran (THF), CS2, MWCNT were purchased from Aldrich and used without purification, unless otherwise specified solvents used were purified and dried standard methods. The structure of the compound were determined by Nuclear magnetic Resonance (NMR) spectroscopy and other spectroscopic techniques. 1H NMR & 13C NMR spectral were recorded 400 MHz & 500 MHz instruments . chemical shifts are reported in delta values relative to solvent peak. The solvent used for the spectroscopy experiments were of the spectroscopic

grades and were free from any fluorescent impurities. Double distilled water was used for the spectroscopic experiments.

All reactants and reagents were commercially available and were used without further purification unless otherwise indicated. TPE, chloroform (CHCl3), chloroform-d (CDCl3), methanol (MeOH), dichloromethane (DCM), Tetrahydrofuran (THF), CS2, MWCNT were purchased from Aldrich and used without purification, unless otherwise specified. Solvents used were purified and dried by standard methods. The structures of the compounds were determined by nuclear magnetic resonance spectroscopy and other spectroscopic techniques. 1H and 13C NMR spectra were recorded with 400 MHz and 500 MHz instruments. Chemical shifts are reported in δ values relative to the solvent peak. The solvents used for the spectroscopy experiments were of the spectroscopic grades and were free from any fluorescent impurities. Double distilled water was used for the spectroscopy experiments. UV spectra were recorded with a Hitachi carry-60 UV-vis spectrophotometer. Fluorescence measurements were carried out using a JASCO flourmeter. Mass data were obtained from an Acquity TM ultra-performance LC. Mass spectra (MS) were obtained by using Bruker AutoFlex Matrix Assisted Laser Desorption/Ionisation (MALDI) Time of Flight (TOF)-Mass Spectrometer (MALDI-TOF-MS). FTIR-spectra were recorded in brukar-IR spectrometer. For Raman spectroscopy and X-ray diffraction experiments, high pressure is generated using a diamond anvil cell (Easylab Co., UK) with diamond culets of size 300μm. Sample was loaded in a 100 μm hole of pre indented stainless steel gasket of thickness of about 45μm together with 4:1 methanol–ethanol mixture as liquid pressure transmitting medium. For Raman measurements a thin pellet of CuO of approximate diameter 50–60 μm and thickness 10–20 μm is loaded in the pressure cell. Raman measurements at high pressures are carried out in a back scattering geometry with a resolution of 1.2 cm−1

using Horiba Jobin Yvon LabRam HR 800 Raman spectrometer and the sample was excited with the Ar+ ion (525 nm) laser at power 6mW. Pressure is measured using ruby fluorescence technique.i αThe XRD patterns were collected using the Rigaku Smart Lab diffracto meter attached with D/tex ultra detector and Cu K °source operating at 35 mA and 70 kV. Scan range was set from 10-60 and a count time of 2 seconds. The samples 2θ with a step size of 0.02 were well powdered and spread evenly on a quartz slide. TEM measurement was carried out using a high resolution FEG transmission electron microscope (JEOL, JEM 2100F) with a 200 keV electron source. Briefly, a drop of the sample dispersed in water was drop casted on a strong carbon coated 300 mesh Cu-grid and dried in air. Field emission scanning electron microscopy (FESEM) images were taken on the SUPRA 55-VP instrument with patented GEMINI column technology. Prior to loading of the samples into the chamber, they were coated with a thin film of goldpalladium in order to avoid charging effects.

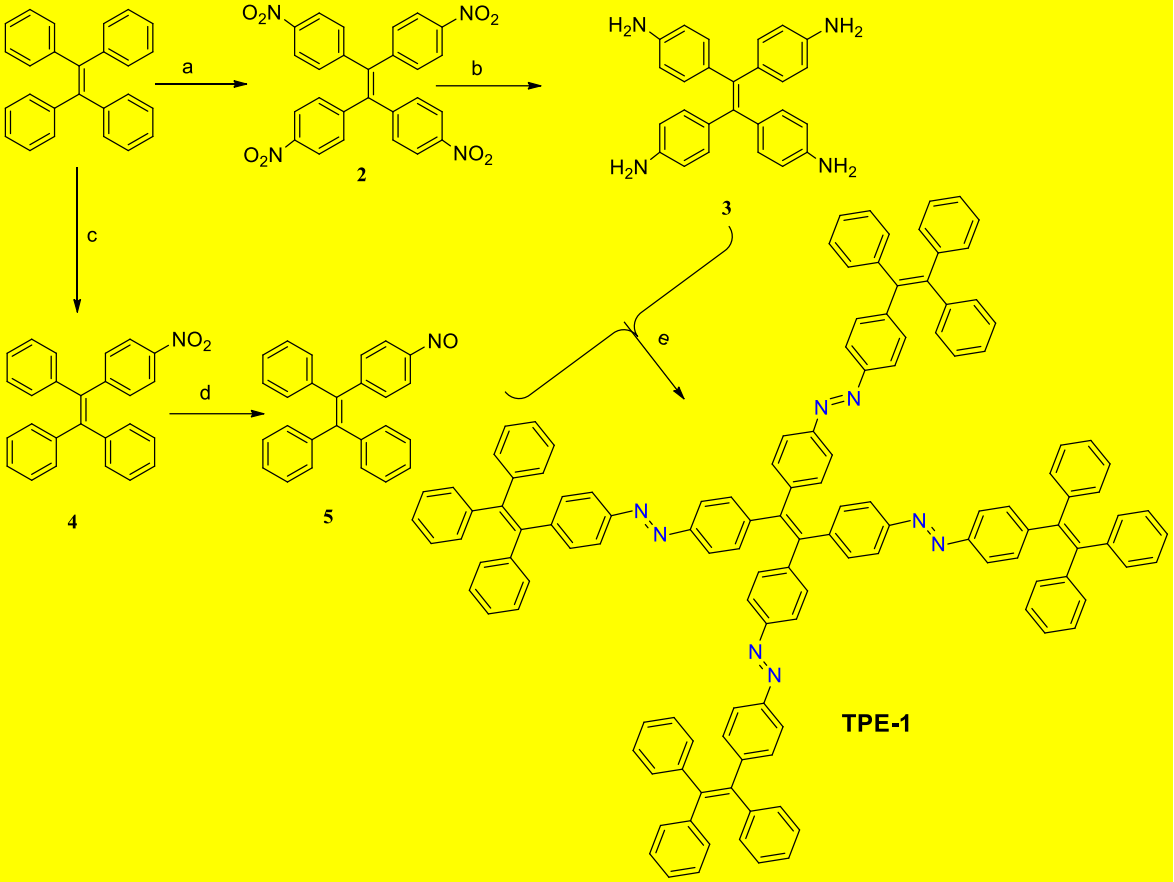

Synthesis of **TPE-1** and the precursor of the **TPE-1.** (a)**.** HNO_3, H_2SO_4, Dry DCM, r.t., 16h. (b). Pd/C, NH_2-NH_2, H_2O, 100 ^oC, 24 h. (c). HNO_3, AcOH, r.t., 20 min, (d) $FeCl_3$, NH_4Cl, Zn, EtOH, H_2O, 1 h, (e). AcOH, r.t., under N_2 atmosphere, 24 h.

Compound 3: Compound 3 was prepared by following known literature protocol,S1,S2 firstly nitration of tetraphenylethylene and followed by reduction of nitro-group in the presence of Pd/C, hydrazine hydrate.

Compound 4: mono-nitro-TPE was prepared by following literature protocol.S3

Synthesis of (2-(4-nitrosophyenyl) ethane-1,1,2-triyl) tribenzene (5):

To a mixture of nitro-TPE (4) (0.9 g, 2.3mmol) and ammonium chloride (0.4 g, 7.64 mmol), 30 mL ofethanol/water 5:1 was added. Zinc dust (0.31 g, 4.78 mmol) was added to the mixture in the portion. The resulting mixture was stirredat room temperature for 90 min, then filtered through ceilite bed, andcooled to 0 °C. A solution of iron(III)

chloride (1.9 g, 11.9 mmol) in 40 mL of ethanol/water 5:1 was kept at 0 °C before adding to the cooled filtrate. The mixture was stirred at 0 °C for 45 min; then, ethanol was removed under reduced pressure, the mixture diluted with 100 mL of water, and the product extracted with ethyl acetate (3× 80 mL). The combined organic layers were washed with 50 mL of brine solution. The organic layer was then dried over anhydrous MgSO4 and the solvent was removed using a rotary evaporator and the obtained greenish-yellow solid (0.65 g, 78%) was used in the next step without further purification; 1H NMR (300 MHz, CDCl3): δ 7.64 (d, J = 9 Hz, 2H), 7.02−7.26 (m, 17H), and used.

Synthesis of1,1,2,2-tetrakis(4-((4-(1,2,2-triphenylvinyl)phenyl)diazenyl)phenyl)ethane (TPE-1):

A solution of freshlyprepared nitroso-TPE (5) (0.55 g, 1.5 mmol) in 20 mL of glacialacetic acid was added to a solution of tetramino-TPE (3) (0.1 g, 0.25mmol) by diluting in 10 mL of glacial acetic acid. The mixture wasstirred at room temperature under N2 overnight. The reaction completion, evaporating the solvent,followed by dissolving the residue in 150 mL of ethyl acetate andwashing with 5% of aqueous potassium bicarbonate (3 × 40 mL) and then by 40 mL of brine solution. The organic layer was then driedover anhydrous MgSO4 and the solvent was removed using a rotaryevaporator. The residue was purified by column chromatography,eluting with (60:40) hexane/DCM to obtain an orange solid (0.09 g, 25%); 1H NMR (300 MHz, CDCl3) δ: 7.66 (d, J = 9.0 Hz, 8H), 7.63 (d, J = 9.0 Hz, 8H), 7.23 (d, J = 6.2 Hz, 8H), 7.07−7.18 (m, 68H), 13C NMR (75 MHz, CDCl3) δ: 151.43, 150.89, 147, 145.6, 143.45,143.4, 143.3, 142.1, 141.6, 140.22, 132.3, 132.1, 131.4, 131.3, 127.86, 127.8, 127.6, 126.8, 126.6, 122.5, 122.2, 30.9; MALDI-TOF, m/z: [M+] calcd for C130H92N8, 1765.75; found, 1766.09 [M + H]+.

4.4 Application Procedure of TPE1 to CNT

The chemical bonding of carbon nanotubes is composed of sp^2 bonds; thus, the bonding structure is stronger than the sp^3 bonds and aligns into ropes held organized by van der Waals forces and nanoscale cross-section electrons propagate only along the tube's axis. As a result, carbon nanotubes are frequently referred to as one-dimensional conductors. Importantly, when nanotubes are assembled non-covalently with donors such as porphyrin, pyrene or AIE-active TPE, these types of combined materials act as electron donor and nanotube alone act as electron acceptor. In this work we self-assembled electron donor i.e. Azo-AIE-active TPE with electron acceptor i.e. carbon nanotube via cis- or trans configuration to check balance of photoinduced electron transfer and in our finding electron-pooling, offering photoinduced charge-separation which can be potential operation of these materials shown to be light-energy harvesting with high electrical conductivity.

4.5 Conclusion

In summary, this paper reports the novel photoswitchable compound based on five TPE units that undergoes reversible *trans-cis* isomerization under UV and visible light respectively. The *trans* form of **TPE-1** is almost planar whereas the *cis* formed has more of a twisted shape. The *trans*-form displayed a clear AIE behaviour in aqueous THF mixtures whereas the *cis* form did not. The *trans* form efficiently binds to multiple MWCNTs and thus acts as a molecular glue for the CNT. These interactions were unequivocally established with various methods including UV-vis, fluorescence, Raman, FT-IR and ^{13}C NMR spectroscopy in addition to the PXRD studies. The aggregates of the nanotubes in the presence of the *trans*-form were also demonstrated by DLS studies and were observed under SEM and TEM imaging. The *cis* form, on the other hand, weakly interacts with the MWCNT samples. The conductance of the MWCNT samples in the presence of the *trans*-form was seven times higher than that of the ones with the *cis*-form. The conductance with the *cis*-form was

essentially close to the background conductance of the MWCNT samples. Thus the *cis* and the *trans* isomerization of the molecular glue demonstrates a fine example of controlling the conductance of CNTs with a photoswitchable molecular glue

4.6 REFERENCES

(1) Iijima, S. Helical Microtubules of Graphitic Carbon. *Nature* **1991**, *354* (6348), 56–58. https://doi.org/10.1038/354056a0.

(2) Cardano, F.; Frasconi, M.; Giordani, S. Photo-Responsive Graphene and Carbon Nanotubes to Control and Tackle Biological Systems. *Front. Chem.* **2018**, *6*.

(3) Bisoyi, H. K.; Li, Q. Light-Driven Liquid Crystalline Materials: From Photo-Induced Phase Transitions and Property Modulations to Applications. *Chem. Rev.* **2016**, *116* (24), 15089–15166. https://doi.org/10.1021/acs.chemrev.6b00415.

(4) Wang, L.; Li, Q. Photochromism into Nanosystems: Towards Lighting up the Future Nanoworld. *Chem. Soc. Rev.* **2018**, *47* (3), 1044–1097. https://doi.org/10.1039/C7CS00630F.

(5) Zheng, Z.; Li, Y.; Bisoyi, H. K.; Wang, L.; Bunning, T. J.; Li, Q. Three-Dimensional Control of the Helical Axis of a Chiral Nematic Liquid Crystal by Light. *Nature* **2016**, *531* (7594), 352–356. https://doi.org/10.1038/nature17141.

(6) Teradal, N. L.; Jelinek, R. Carbon Nanomaterials in Biological Studies and Biomedicine. *Adv. Healthc. Mater.* **2017**, *6* (17), 1700574. https://doi.org/10.1002/adhm.201700574.

(7) Pardo, J.; Peng, Z.; Leblanc, R. M. Cancer Targeting and Drug Delivery Using Carbon-Based Quantum Dots and Nanotubes. *Mol. Basel Switz.* **2018**, *23* (2), E378. https://doi.org/10.3390/molecules23020378.

(8) Mir, M.; Ishtiaq, S.; Rabia, S.; Khatoon, M.; Zeb, A.; Khan, G. M.; ur Rehman, A.; ud Din, F. Nanotechnology: From In Vivo Imaging System to Controlled Drug Delivery. *Nanoscale Res. Lett.* **2017**, *12* (1), 500. https://doi.org/10.1186/s11671-017-2249-8.

(9) Krishna, L.; Dhamodaran, K.; Jayadev, C.; Chatterjee, K.; Shetty, R.; Khora, S. S.; Das, D. Nanostructured Scaffold as a Determinant of Stem Cell Fate. *Stem Cell Res. Ther.* **2016**, *7* (1), 188. https://doi.org/10.1186/s13287-016-0440-y.

(10) Gao, C.; Feng, P.; Peng, S.; Shuai, C. Carbon Nanotube, Graphene and Boron Nitride Nanotube Reinforced Bioactive Ceramics for Bone Repair. *Acta Biomater.* **2017**, *61*, 1–20. https://doi.org/10.1016/j.actbio.2017.05.020.

(11) Hone, J.; Batlogg, B.; Benes, Z.; Johnson, A. T.; Fischer, J. E. Quantized Phonon Spectrum of Single-Wall Carbon Nanotubes. *Science* **2000**, *289* (5485), 1730–1733. https://doi.org/10.1126/science.289.5485.1730.

(12) Wong, E. W.; Sheehan, P. E.; Lieber, C. M. Nanobeam Mechanics: Elasticity, Strength, and Toughness of Nanorods and Nanotubes. *Science* **1997**, *277* (5334), 1971–1975. https://doi.org/10.1126/science.277.5334.1971.

(13) *Springer Handbook of Nanomaterials*, 1st ed. 2013.; Vajtai, R., Ed.; Springer Handbooks; Springer Berlin Heidelberg : Imprint: Springer: Berlin, Heidelberg, 2013. https://doi.org/10.1007/978-3-642-20595-8.

(14) Crescenzo, A. D.; Ettorre, V.; Fontana, A. Non-Covalent and Reversible Functionalization of Carbon Nanotubes. *Beilstein J. Nanotechnol.* **2014**, *5* (1), 1675–1690. https://doi.org/10.3762/bjnano.5.178.

(15) Dai, H. Carbon Nanotubes: Synthesis, Integration, and Properties. *Acc. Chem. Res.* **2002**, *35* (12), 1035–1044. https://doi.org/10.1021/ar0101640.

(16) Kucharski, T. J.; Ferralis, N.; Kolpak, A. M.; Zheng, J. O.; Nocera, D. G.; Grossman, J. C. Templated Assembly of Photoswitches Significantly Increases the Energy-Storage Capacity of Solar Thermal Fuels. *Nat. Chem.* **2014**, *6* (5), 441–447. https://doi.org/10.1038/nchem.1918.

(17) Wang, J. Special Issue for Wearable Electrochemical Sensors. *Electroanalysis* **2016**,

28 (6), 1148–1148. https://doi.org/10.1002/elan.201680631.

(18) Zhou, Y.; Azumi, R. Carbon Nanotube Based Transparent Conductive Films: Progress, Challenges, and Perspectives. *Sci. Technol. Adv. Mater.* **2016**, *17* (1), 493–516. https://doi.org/10.1080/14686996.2016.1214526.

(19) Baughman, R. H.; Zakhidov, A. A.; de Heer, W. A. Carbon Nanotubes--the Route toward Applications. *Science* **2002**, *297* (5582), 787–792. https://doi.org/10.1126/science.1060928.

(20) Wu, D.; Zhang, F.; Liang, H.; Feng, X. Nanocomposites and Macroscopic Materials: Assembly of Chemically Modified Graphene Sheets. *Chem. Soc. Rev.* **2012**, *41* (18), 6160–6177. https://doi.org/10.1039/C2CS35179J.

(21) Han, W.; Kawakami, R. K.; Gmitra, M.; Fabian, J. Graphene Spintronics. *Nat. Nanotechnol.* **2014**, *9* (10), 794–807. https://doi.org/10.1038/nnano.2014.214.

(22) Li, H.; Kang, Z.; Liu, Y.; Lee, S.-T. Carbon Nanodots: Synthesis, Properties and Applications. *J. Mater. Chem.* **2012**, *22* (46), 24230–24253. https://doi.org/10.1039/C2JM34690G.

(23) Caoduro, C.; Hervouet, E.; Girard-Thernier, C.; Gharbi, T.; Boulahdour, H.; Delage-Mourroux, R.; Pudlo, M. Carbon Nanotubes as Gene Carriers: Focus on Internalization Pathways Related to Functionalization and Properties. *Acta Biomater.* **2017**, *49*, 36–44. https://doi.org/10.1016/j.actbio.2016.11.013.

(24) Sanginario, A.; Miccoli, B.; Demarchi, D. Carbon Nanotubes as an Effective Opportunity for Cancer Diagnosis and Treatment. *Biosensors* **2017**, *7* (1), 9. https://doi.org/10.3390/bios7010009.

(25) Yuksel, R.; Sarioba, Z.; Cirpan, A.; Hiralal, P.; Unalan, H. E. Transparent and Flexible Supercapacitors with Single Walled Carbon Nanotube Thin Film Electrodes. *ACS Appl. Mater. Interfaces* **2014**, *6* (17), 15434–15439. https://doi.org/10.1021/am504021u.

(26) Palomar, Q.; Gondran, C.; Holzinger, M.; Marks, R.; Cosnier, S. Controlled Carbon Nanotube Layers for Impedimetric Immunosensors: High Performance Label Free Detection and Quantification of Anti-Cholera Toxin Antibody. *Biosens. Bioelectron.* **2017**, *97*, 177–183. https://doi.org/10.1016/j.bios.2017.05.052.

(27) Giroud, F.; Sawada, K.; Taya, M.; Cosnier, S. 5,5-Dithiobis(2-Nitrobenzoic Acid) Pyrene Derivative-Carbon Nanotube Electrodes for NADH Electrooxidation and Oriented Immobilization of Multicopper Oxidases for the Development of Glucose/O2 Biofuel Cells. *Biosens. Bioelectron.* **2017**, *87*, 957–963. https://doi.org/10.1016/j.bios.2016.09.054.

(28) Wu, Z.; Chen, Z.; Du, X.; Logan, J. M.; Sippel, J.; Nikolou, M.; Kamaras, K.; Reynolds, J. R.; Tanner, D. B.; Hebard, A. F.; Rinzler, A. G. Transparent, Conductive Carbon Nanotube Films. *Science* **2004**, *305* (5688), 1273–1276. https://doi.org/10.1126/science.1101243.

(29) Chen, Y.; Mitra, S. Fast Microwave-Assisted Purification, Functionalization and Dispersion of Multi-Walled Carbon Nanotubes. *J. Nanosci. Nanotechnol.* **2008**, *8* (11), 5770–5775. https://doi.org/10.1166/jnn.2008.215.

(30) Shannahan, J. H.; Brown, J. M.; Chen, R.; Ke, P. C.; Lai, X.; Mitra, S.; Witzmann, F. A. Comparison of Nanotube-Protein Corona Composition in Cell Culture Media. *Small Weinh. Bergstr. Ger.* **2013**, *9* (12), 2171–2181. https://doi.org/10.1002/smll.201202243.

(31) Salzmann, C. G.; Llewellyn, S. A.; Tobias, G.; Ward, M. a. H.; Huh, Y.; Green, M. L. H. The Role of Carboxylated Carbonaceous Fragments in the Functionalization and Spectroscopy of a Single-Walled Carbon-Nanotube Material. *Adv. Mater.* **2007**, *19* (6), 883–887. https://doi.org/10.1002/adma.200601310.

(32) Verdejo, R.; Lamoriniere, S.; Cottam, B.; Bismarck, A.; Shaffer, M. Removal of Oxidation Debris from Multi-Walled Carbon Nanotubes. *Chem. Commun.* **2007**, No. 5,

513–515. https://doi.org/10.1039/B611930A.

(33) Del Valle, M.; Gutiérrez, R.; Tejedor, C.; Cuniberti, G. Tuning the Conductance of a Molecular Switch. *Nat. Nanotechnol.* **2007**, *2* (3), 176–179. https://doi.org/10.1038/nnano.2007.38.

(34) He, Y.; Yamamoto, Y.; Jin, W.; Fukushima, T.; Saeki, A.; Seki, S.; Ishii, N.; Aida, T. Hexabenzocoronene Graphitic Nanotube Appended with Dithienylethene Pendants: Photochromism for the Modulation of Photoconductivity. *Adv. Mater.* **2010**, *22* (7), 829–832. https://doi.org/10.1002/adma.200902601.

(35) Wu, W.; Li, R.; Bian, X.; Zhu, Z.; Ding, D.; Li, X.; Jia, Z.; Jiang, X.; Hu, Y. Covalently Combining Carbon Nanotubes with Anticancer Agent: Preparation and Antitumor Activity. *ACS Nano* **2009**, *3* (9), 2740–2750. https://doi.org/10.1021/nn9005686.

(36) Gur, I.; Sawyer, K.; Prasher, R. Searching for a Better Thermal Battery. *Science* **2012**, *335* (6075), 1454–1455. https://doi.org/10.1126/science.1218761.

(37) Arico, A. S.; Bruce, P.; Scrosati, B.; Tarascon, J.-M.; van Schalkwijk, W. Nanostructured Materials for Advanced Energy Conversion and Storage Devices. *Nat. Mater.* **2005**, *4* (5), 366–377. https://doi.org/10.1038/nmat1368.

(38) Dunn, B.; Kamath, H.; Tarascon, J.-M. Electrical Energy Storage for the Grid: A Battery of Choices. *Science* **2011**, *334* (6058), 928–935. https://doi.org/10.1126/science.1212741.

(39) Kucharski, T. J.; Tian, Y.; Akbulatov, S.; Boulatov, R. Chemical Solutions for the Closed-Cycle Storage of Solar Energy. *Energy Environ. Sci.* **2011**, *4* (11), 4449–4472. https://doi.org/10.1039/C1EE01861B.

(40) North, M. A.; Del Grosso, C. A.; Wilker, J. J. High Strength Underwater Bonding with Polymer Mimics of Mussel Adhesive Proteins. *ACS Appl. Mater. Interfaces* **2017**, *9* (8), 7866–7872. https://doi.org/10.1021/acsami.7b00270.

(41) Zhang, X.; Hou, L.; Samorì, P. Coupling Carbon Nanomaterials with Photochromic Molecules for the Generation of Optically Responsive Materials. *Nat. Commun.* **2016**, *7* (1), 11118. https://doi.org/10.1038/ncomms11118.

(42) Srinivasan, S.; Babu, S. S.; Praveen, V. K.; Ajayaghosh, A. Carbon Nanotube Triggered Self-Assembly of Oligo(p-Phenylene Vinylene)s to Stable Hybrid π-Gels. *Angew. Chem. Int. Ed.* **2008**, *47* (31), 5746–5749. https://doi.org/10.1002/anie.200801000.

(43) Jia, C.; Wang, J.; Yao, C.; Cao, Y.; Zhong, Y.; Liu, Z.; Liu, Z.; Guo, X. Conductance Switching and Mechanisms in Single-Molecule Junctions. *Angew. Chem. Int. Ed Engl.* **2013**, *52* (33), 8666–8670. https://doi.org/10.1002/anie.201304301.

(44) Castellanos, S.; Vieira, A. A.; Illescas, B. M.; Sacchetti, V.; Schubert, C.; Moreno, J.; Guldi, D. M.; Hecht, S.; Martín, N. Gating Charge Recombination Rates through Dynamic Bridges in Tetrathiafulvalene–Fullerene Architectures. *Angew. Chem. Int. Ed.* **2013**, *52* (52), 13985–13990. https://doi.org/10.1002/anie.201306183.

(45) Guo, Z.; Panda, D. K.; Gordillo, M. A.; Khatun, A.; Wu, H.; Zhou, W.; Saha, S. Lowering Band Gap of an Electroactive Metal–Organic Framework via Complementary Guest Intercalation. *ACS Appl. Mater. Interfaces* **2017**, *9* (38), 32413–32417. https://doi.org/10.1021/acsami.7b07292.

(46) Li, T.; Jevric, M.; Hauptmann, J. R.; Hviid, R.; Wei, Z.; Wang, R.; Reeler, N. E. A.; Thyrhaug, E.; Petersen, S.; Meyer, J. A. S.; Bovet, N.; Vosch, T.; Nygård, J.; Qiu, X.; Hu, W.; Liu, Y.; Solomon, G. C.; Kjaergaard, H. G.; Bjørnholm, T.; Nielsen, M. B.; Laursen, B. W.; Nørgaard, K. Ultrathin Reduced Graphene Oxide Films as Transparent Top-Contacts for Light Switchable Solid-State Molecular Junctions. *Adv. Mater.* **2013**, *25* (30), 4164–4170. https://doi.org/10.1002/adma.201300607.

(47) Margapoti, E.; Strobel, P.; Asmar, M. M.; Seifert, M.; Li, J.; Sachsenhauser, M.;

Ceylan, Ö.; Palma, C.-A.; Barth, J. V.; Garrido, J. A.; Cattani-Scholz, A.; Ulloa, S. E.; Finley, J. J. Emergence of Photoswitchable States in a Graphene–Azobenzene–Au Platform. *Nano Lett.* **2014**, *14* (12), 6823–6827. https://doi.org/10.1021/nl503681z.

(48) Mei, J.; Leung, N. L. C.; Kwok, R. T. K.; Lam, J. W. Y.; Tang, B. Z. Aggregation-Induced Emission: Together We Shine, United We Soar! *Chem. Rev.* **2015**, *115* (21), 11718–11940. https://doi.org/10.1021/acs.chemrev.5b00263.

(49) Samanta, M.; Rananaware, A.; Nadimetla, D. N.; Rahaman, S. A.; Saha, M.; Jadhav, R. W.; Bhosale, S. V.; Bandyopadhyay, S. Light Triggered Encapsulation and Release of C60 with a Photoswitchable TPE-Based Supramolecular Tweezers. *Sci. Rep.* **2019**, *9* (1), 9670. https://doi.org/10.1038/s41598-019-46242-4.

(50) Tian, H.; Yang, S. Recent Progresses on Diarylethene Based Photochromic Switches. *Chem. Soc. Rev.* **2004**, *33* (2), 85–97. https://doi.org/10.1039/B302356G.

(51) Lukyanov, B. S.; Lukyanova, M. B. Spiropyrans: Synthesis, Properties, and Application. (Review). *Chem. Heterocycl. Compd.* **2005**, *41* (3), 281–311. https://doi.org/10.1007/s10593-005-0148-x.

(52) Klajn, R. Spiropyran-Based Dynamic Materials. *Chem. Soc. Rev.* **2013**, *43* (1), 148–184. https://doi.org/10.1039/C3CS60181A.

(53) Oudar, J. L. Optical Nonlinearities of Conjugated Molecules. Stilbene Derivatives and Highly Polar Aromatic Compounds. *J. Chem. Phys.* **1977**, *67* (2), 446–457. https://doi.org/10.1063/1.434888.

(54) Blanco, V.; Leigh, D. A.; Marcos, V. Artificial Switchable Catalysts. *Chem. Soc. Rev.* **2015**, *44* (15), 5341–5370. https://doi.org/10.1039/C5CS00096C.

(55) Saha, M.; Bandyopadhyay, S. Reversible Photoresponsive Activity of a Carbonic Anhydrase Mimic. *Chem. Commun.* **2019**, *55* (22), 3294–3297. https://doi.org/10.1039/C9CC00018F.

(56) Merino, E. Synthesis of Azobenzenes: The Coloured Pieces of Molecular Materials. *Chem. Soc. Rev.* **2011**, *40* (7), 3835–3853. https://doi.org/10.1039/C0CS00183J.

(57) Mogaki, R.; Okuro, K.; Aida, T. Adhesive Photoswitch: Selective Photochemical Modulation of Enzymes under Physiological Conditions. *J. Am. Chem. Soc.* **2017**, *139* (29), 10072–10078. https://doi.org/10.1021/jacs.7b05151.

(58) Baroncini, M.; d'Agostino, S.; Bergamini, G.; Ceroni, P.; Comotti, A.; Sozzani, P.; Bassanetti, I.; Grepioni, F.; Hernandez, T. M.; Silvi, S.; Venturi, M.; Credi, A. Photoinduced Reversible Switching of Porosity in Molecular Crystals Based on Star-Shaped Azobenzene Tetramers. *Nat. Chem.* **2015**, *7* (8), 634–640. https://doi.org/10.1038/nchem.2304.

(59) Zhao, J.; Yang, D.; Zhao, Y.; Yang, X.-J.; Wang, Y.-Y.; Wu, B. Anion-Coordination-Induced Turn-on Fluorescence of an Oligourea-Functionalized Tetraphenylethene in a Wide Concentration Range. *Angew. Chem. Int. Ed Engl.* **2014**, *53* (26), 6632–6636. https://doi.org/10.1002/anie.201402169.

(60) Das, R.; Hamid, S. B. A.; Ali, M. E.; Ramakrishna, S.; Yongzhi, W. Carbon Nanotubes Characterization by X-Ray Powder Diffraction – A Review. *Curr. Nanosci. 11* (1), 23–35.

(61) Zhang, H.-B.; Lin, G.-D.; Zhou, Z.-H.; Dong, X.; Chen, T. Raman Spectra of MWCNTs and MWCNT-Based H2-Adsorbing System. *Carbon* **2002**, *40* (13), 2429–2436. https://doi.org/10.1016/S0008-6223(02)00148-3.

(62) Bokobza, L.; Zhang, J. Raman Spectroscopic Characterization of Multiwall Carbon Nanotubes and of Composites. *Express Polym. Lett.* **2012**, *6* (7), 601. https://doi.org/10.3144/expresspolymlett.2012.63.

(63) Thomsen, C.; Reich, S. Double Resonant Raman Scattering in Graphite. *Phys. Rev. Lett.* **2000**, *85* (24), 5214–5217. https://doi.org/10.1103/PhysRevLett.85.5214.

(64) Feng, Y.; Zhang, X.; Ding, X.; Feng, W. A Light-Driven Reversible Conductance Switch Based on a Few-Walled Carbon Nanotube/Azobenzene Hybrid Linked by a Flexible Spacer. *Carbon* **2010**, *48* (11), 3091–3096. https://doi.org/10.1016/j.carbon.2010.04.045.

TPE-1 was characterized by ^{1}H NMR, ^{13}C NMR, FTIR and mass spectrometry techniques.

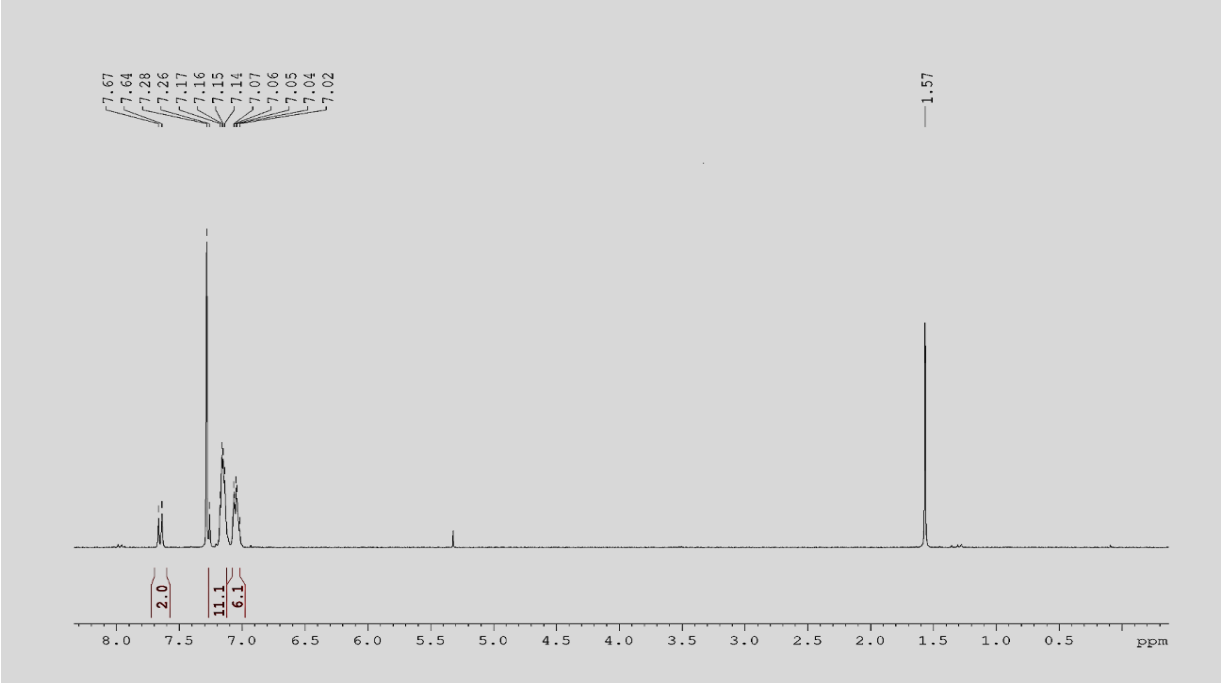

Figure 4.17: ^{1}HNMR of Synthesis of (2-(4-nitrosophyenyl)ethane-1,1,2-triyl) tribenzene (**5**), peak at 1.57 is water peak and 7.26 belongs to $CDCl_3$ residual solvent peak.

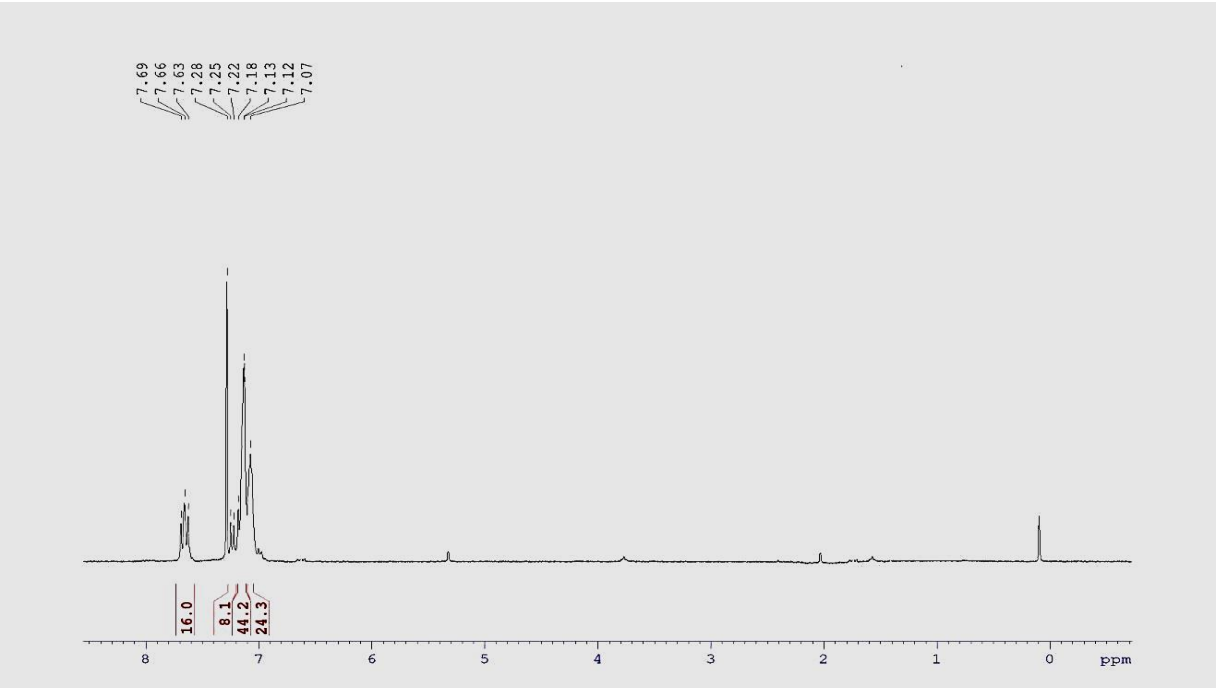

Figure 4.18: ^{1}HNMR of 1,1,2,2-tetrakis(4-((4-(1,2,2-triphenylvinyl)phenyl)diazenyl)phenyl)ethane (**TPE-1**).

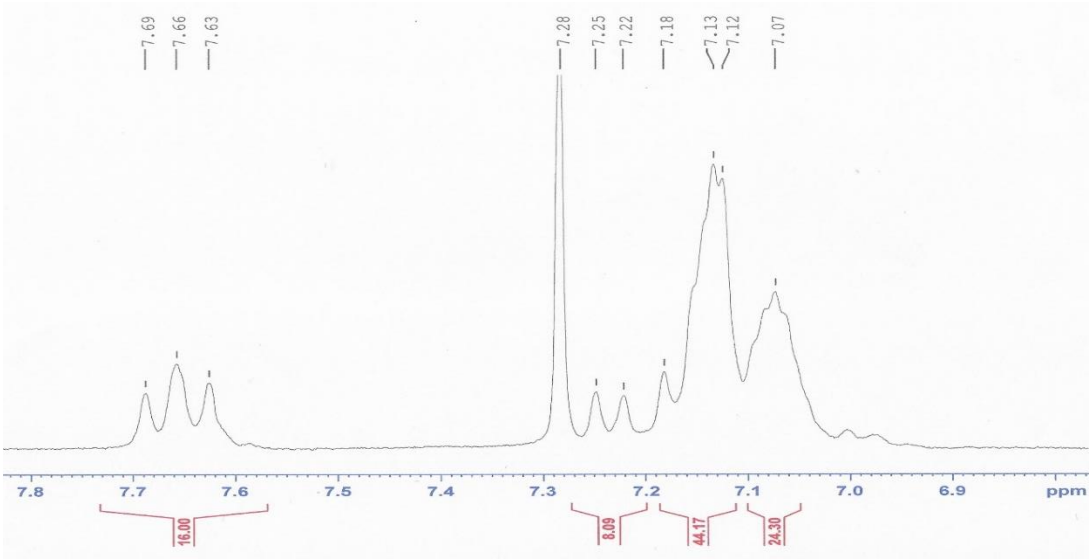

Figure 4.19: Expanded aromatic reason of ^{1}H NMR of 1,1,2,2-tetrakis(4-((4-(1,2,2-triphenylvinyl)phenyl)diazenyl)phenyl) ethane (**TPE-1**).

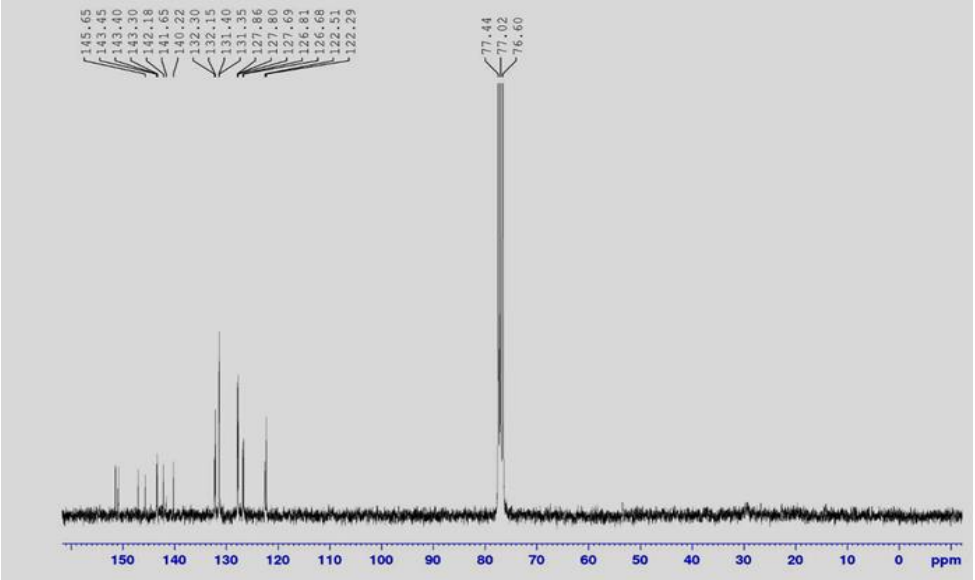

Figure 4.20: ^{13}CNMR of 1,1,2,2-tetrakis(4-((4-(1,2,2-triphenylvinyl)phenyl)diazenyl)phenyl)ethane (**TPE-1**).

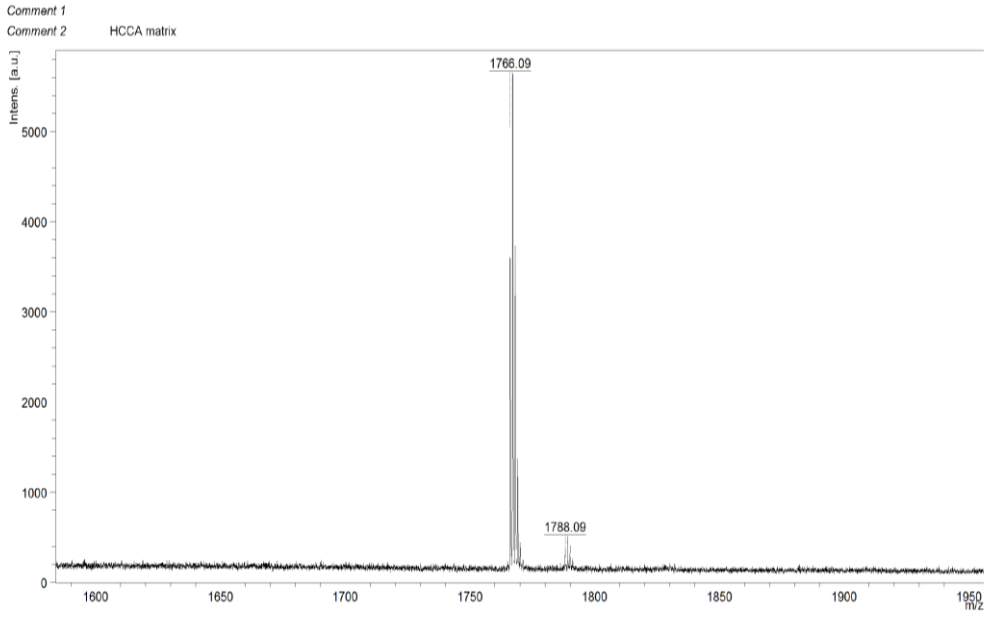

Figure 4.21: MALDI-TOF of1,1,2,2-tetrakis(4-((4-(1,2,2-triphenylvinyl)phenyl)diazenyl)phenyl) ethane (**TPE-1**).

Chapter 5: Iodine Catalysed New Method for Synthesis of Tetraester-Substituted Tetraaryl-1,4-Dihydropyrrolo [3, 2-b]pyrrole

5.1 Introduction

Recently we have seen that aggregation induced emission luminogens (AIEgens) have fascinated great attention of the researchers due to their applications in the materials and biotechnology fields such as sensors, organic light-emitting diodes, multistimuliresponsive materials etc.[1] Till now several AIEgens with excellent luminescence properties in the solid state have been reported and developed, which consist of 1,1- dimethyl-2,3,4,5-tetraphenylsilole (DMTPS), hexaphenylsilole (HPS), tetraphenylethene (TPE), tetraphenyl-1,4-butadiene (TPBD), tetraphenylpyrazine (TPP) etc.[1] However, out of these AIEgens some suffer from intrinsic drawbacks for example TPE and TPBD consist of double bonds which usually give rise to E/Z isomerisation, thus, it is very difficult for separation and also suffer from photo oxidation resulting in low quantum yields particularly in aggregation. From studying all these issues we came to know that, still there was a need to develop AIEgens with good stability and outstanding luminescence properties. While in literature study in 2013, Gryko reported for the first time the synthesis of tetraaryl-1, 4-dihydropyrrolo [3, 2-b] pyrroles (TAPP) and their derivatives in detail.[2] By observing TAPP structure it looks like a butterfly-shape structure and even the solvent polarity is increased, it shows intense emission. TAPP derivatives are one of the AIEgens molecules that have found utility in the design of highly fluorescent and stable materials and therefore TAPP derivatives have fascinated particular attention of the researchers. While explaining the properties of TAPP molecule, it is compact and extremely coloured and show violet blue or blue fluorescence with characteristic quantum yields of < 60%, very broad absorption bands between 300 and 450 nm and emission while in the solid state are observed specifically. By studying and considering rich spectroscopic and good properties of TAPP derivatives, they are ideally

suited for the design of light emitting diodes and sensors.

Due to all superior properties, TAPP molecules have been extensively used for different application containing solar cells, sensing, cellular imaging etc.[3] In 2013, Gryko *et al*. studied and reported for the first time three component one-pot straightforward synthesis of tetraaryl-1, 4-dihydropyrrolo [3, 2-b] pyrroles (TAPP) derivatives by reacting butane-2, 3-dione with aromatic aldehydes and aromatic amines in the presence of ammonium acetate in glacial acetic acid with reflux (3h) to give TAPP in ~15-30% yield.[2], [4]

Accordingly lot of efforts were carried out to improve the yield of TAPP by changing solvents, adding mild oxidants (dimethyl sulfoxide, DDQ, DMSO, $Ce(NH_4)_2$ $(NO_3)_6$, and nitrobenzene), changing the order of reagent addition and prolonging the reaction time failed. Moreover another research group studied and examined different reaction parameters including solvent, acid, temperature and also various reagents along with acetic acid (AcOH) as a solvent, such as TFA, H_2SO_4 , $AlCl_3$, TfOH and TsOH. Out of which, p-toluene sulfonic acid was known as the good catalyst, which produces 49% TAPP yield.[5, 6] Nevertheless, given the importance of the ring structure, further improvement is required to increase the yield protocol particularly.[7], [8]

5.2 Materials and Methods

In this paper, we report the synthesis of tetraestersubstituted tetraaryl-1, 4-dihydropyrrolo [3, 2-b] pyrroles (TAPP 1) by iodine-catalysed cyclocondensation of aromatic amine, aromatic aldehyde and 2,3-butanedione. This three components reaction is carried out in acetonitrile at 90^o C for 3h (Scheme 5.1).

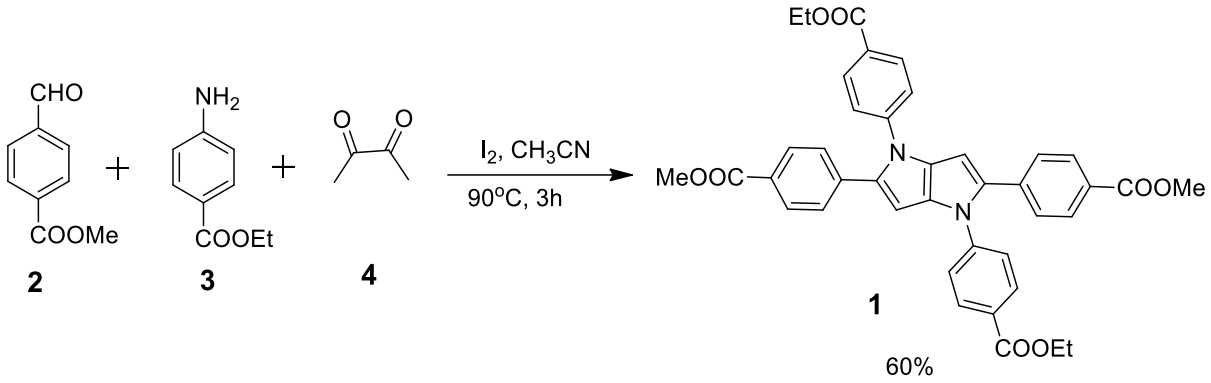

Scheme 5.1: Synthesis of tetraester-substituted tetraaryl-1, 4-dihydropyrrolo [3, 2-b] pyrroles.

Typically, ethyl 4-aminobenzoate (10 mmol) and methyl 4-formylbenzoate (10 mmol) were mixed in 10 mL acetonitrile followed by addition of 15 mol% iodine. After stirring for 30 min at 90^{o} C, 2,3-butanedione (5 mmol) was added and a fluorescent yellow crystalline product started to precipitate from the reaction mixture. Upon completion (3h) of the reaction, the yellow precipitated product was isolated by simple filtration and followed by washing twice with acetonitrile (10mL×2). This protocol offers four main advantageous: i) improved yield of tetra-ester TAPP i.e. 60%, ii) simple work-up, iii) acetonitrile can be distilled and reused and iv) tetra-ester TAPP can be prepared in gram quantities by simple filtration.

5.3 Results and Discussion

The Mechanism for synthesis of TAPP: In the first step, enol formation of butan-2, 3-dione takes place, followed by iminium ion formation from aromatic aldehyde and aromatic amine in the presence of Iodine (I_2) (Step 2) and enol form of butane-2-3-dione attacks on highly unstable iminium ion (Scheme 5.2). In the third step, intramolecular cyclization occurs to form unstable N-substituted five membered ring, which further reacts with same molecule

of iminium ion, followed by intramolecular cyclization and aerobic oxidation to give TAPP as a stable product. The intermediate tetrahydropyrrolo [3, 2-b] pyrrole is oxidized by the excess of Schiff base present in the reaction mixture. In the first step, iodine play a significant role for the formation of iminium ion. ^{1}H NMR of synthesised tetraester TAPP, it clearly shows protons of ethyl ester and methyl ester and doublets of aromatic protons.

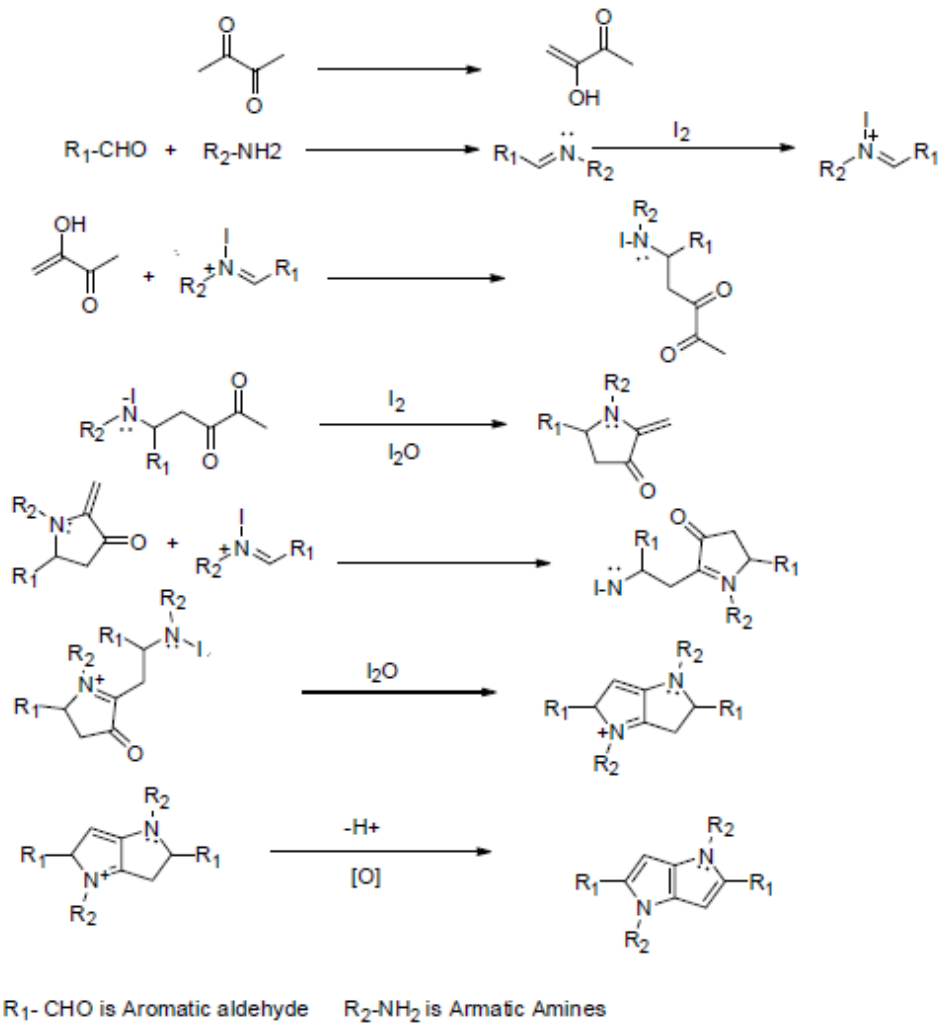

Scheme 5.2: Role of molecule iodine in the synthesis of TAPP molecule

The possibility and restrictions of this methodology was investigated by replacing methyl 4-formylbenzoate with a broad range of aromatic aldehydes with electron donor (OMe or Me) and electron acceptor (NO_2 or Br) moieties. Except methyl 4-formylbenzoate reaction with

ethyl 4-aminobenzoate, neither any substituted aldehyde reaction with aniline gives any products nor methyl 4-formylbenzoate reacts with any other substituted anilines. Thus, it is clear that when we use Iodine as a catalyst the most important factor is the use of ester as electron withdrawing species which needs to be present on aryl amines as well as aldehyde.

The UV-vis absorption of TAPP 1 in THF gives two clear bands at 330 nm and 395 nm, respectively. These two bands decrease with 15 nm red-shift with increasing water content, which clearly demonstrates aggregation of TAPP 1 in THF/water via J-type aggregation (Figure 5.1a). Interestingly, fluorescence emission of TAPP 1 in THF gives 465 nm peak (λex = 395 nm), while increasing water content in THF shows decrease in the emission (Figure 5.1b), which also demonstrates the self-assembly of TAPP 1 in THF/water. This phenomenon can be seen by naked eye, as such TAPP 1 in THF gives bright bluegreen color under 365 nm UV-light, while increasing percentage of water shows decreasing color intensity and in 99% water in THF clearly shows disappearance of blue-greenish color. In literature, other TAPP derivatives shows aggregation induced emission (AIE) phenomenon,3-5 however, this new tetraester TAPP 1 shows opposite phenomenon i.e. so called aggregation caused quenching. Further, research on synthesis of other derivatives using iodine catalyst as well as their AIE/ ACQ phenomenon is underway and will be reported due course.

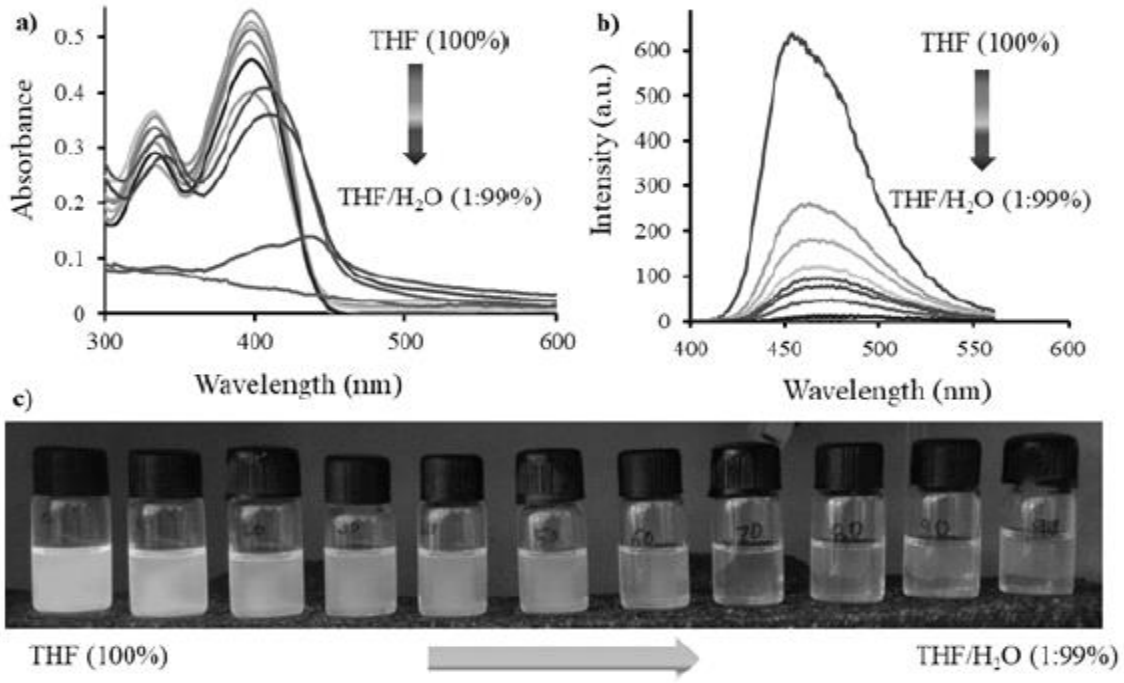

Figure 5.1: a) UV-vis absorption spectra of TAPP 1 in THF (100%) to THF/H_2O (1:99%) at room temperature, b) the fluorescence emission spectra of TAPP 1 (λex = 395 nm) in THF to 99% H_2O at room temperature, and c) naked eye luminescence images of 1 (λex = 365 nm) in THF/H_2O mixed solvents with the concentration kept at 1×10^{-5}M, respectively.

5.4 Conclusion

Low yields of TAPPs led to optimization of the conditions of this multicomponent reaction. This study concluded that the iodine catalysed reaction increases the reaction yield of tetra-ester TAPP. The most signiûcant yield for tetra-ester-TAPP analogue obtained was up to 60%. We are currently investigating change in solvents and percentages of catalysts required which will be reported in due course

5.5 References

(1) Mei, J.; Leung, N. L. C.; Kwok, R. T. K.; Lam, J. W. Y.; Tang, B. Z. Aggregation-Induced Emission: Together We Shine, United We Soar! *Chem. Rev.* **2015**, *115* (21), 11718–11940. https://doi.org/10.1021/acs.chemrev.5b00263.

(2) Janiga, A.; Glodkowska-Mrowka, E.; Stoklosa, T.; Gryko, D. T. Synthesis and Optical Properties of Tetraaryl-1,4-Dihydropyrrolo[3,2-b]Pyrroles. *Asian J. Org. Chem.* **2013**, *2* (5), 411–415. https://doi.org/10.1002/ajoc.201200201.

(3) Krzeszewski, M.; Gryko, D.; Gryko, D. T. The Tetraarylpyrrolo[3,2-b]Pyrroles—From Serendipitous Discovery to Promising Heterocyclic Optoelectronic Materials. *Acc. Chem. Res.* **2017**, *50* (9), 2334–2345. https://doi.org/10.1021/acs.accounts.7b00275.

(4) Janiga, A.; Bednarska, D.; Thorsted, B.; Brewer, J.; Gryko, D. T. Quadrupolar, Emission-Tunable π-Expanded 1,4-Dihydropyrrolo[3,2-b]Pyrroles – Synthesis and Optical Properties. *Org. Biomol. Chem.* **2014**, *12* (18), 2874–2881. https://doi.org/10.1039/C4OB00143E.

(5) Krzeszewski, M.; Thorsted, B.; Brewer, J.; Gryko, D. T. Tetraaryl-, Pentaaryl-, and Hexaaryl-1,4-Dihydropyrrolo[3,2-b]Pyrroles: Synthesis and Optical Properties. *J. Org. Chem.* **2014**, *79* (7), 3119–3128. https://doi.org/10.1021/jo5002643.

(6) Janiga, A.; Krzeszewski, M.; Gryko, D. T. Diindolo[2,3-b:2′,3′-f]Pyrrolo[3,2-b]Pyrroles as Electron-Rich, Ladder-Type Fluorophores: Synthesis and Optical Properties. *Chem. – Asian J.* **2015**, *10* (1), 212–218. https://doi.org/10.1002/asia.201402925.

(7) Mei, J.; Hong, Y.; Lam, J. W. Y.; Qin, A.; Tang, Y.; Tang, B. Z. Aggregation-Induced Emission: The Whole Is More Brilliant than the Parts. *Adv. Mater.* **2014**, *26* (31), 5429–5479. https://doi.org/10.1002/adma.201401356.

(8) Stężycki, R.; Reger, D.; Hoelzel, H.; Jux, N.; Gryko, D. T. Synthesis and Photophysical Properties of Hexaphenylbenzene–Pyrrolo[3,2-b]Pyrroles. *Synlett* **2018**, *29* (19), 2529–2534. https://doi.org/10.1055/s-0037-1610286.

^{1}H NMR of synthesised tetraester TAPP is shown in (Figure 5.2).

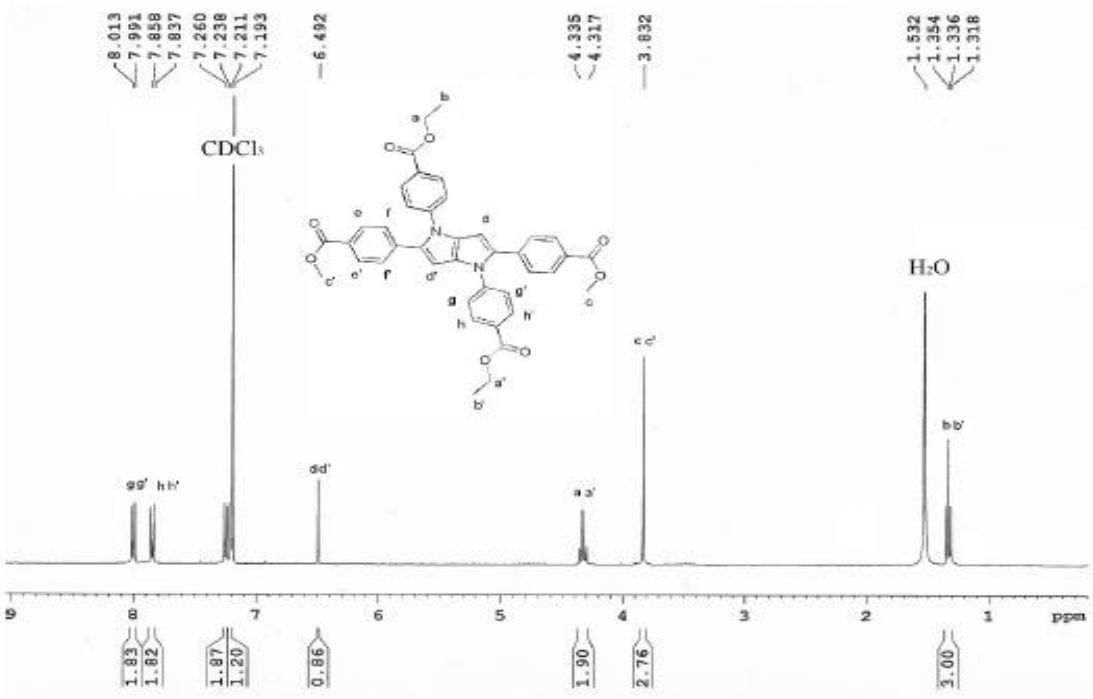

Figure 5.2: Typical ^{1}H NMR of tetra ester TAPP synthesized using molecular iodine as a catalyst

Chapter 6: Conclusion

In this chapter we conclude all thesis work, by studying scope of photoluminiscent materials we choose this topic and focus on novel organic photoluminiscent materials. For better understanding we carried out a detailed literature survey.

Initially in the chapter 1, we choose specific example TAPP and its derivatives and studied all the physical properties of TAPP derivatives that revealed TAPP to be a versatile core for materials with a wide range of significant applications. From structural features, it is clear that TAPP core having electron-rich nature makes it applicable in areas such as optoelectronics, imaging, and solar cells where the interaction of light is utmost. From reported work it was clear that organic molecules are quiet efficient in the areas OLEDS, organic solar cells and new generation solar cells which mainly require organic materials in different cell configurations, it is further expected that most of TAPP derivatives will progress and find further use in advanced technology. We have elaborated in this chapter how the synthetic usefulness of the TAPP core that can be leveraged to control the absorbance, emission, and physical properties of the analogues, permitting for fine-tuning of properties for each application in detail. To make advancement in this area, further use of AIE effect and more understanding of structure– function relationships are essential. It is also found that, TAPP a new and unique AIE core, has long been plagued by inefficient and complex synthesis problems. Till 2013, Gryko and his group first time reported TAPP synthesis, and they exposed a one-pot method for transforming simple and readily available building blocks into an unsurpassed variety of TAPP successfully. From this work, the synthesis and application of TAPP derivatives have been broadly studied. This chapter takes a detailed account of summary with the discovery of TAPP, the development of synthesis method, the reaction mechanism, the reactivity of TAPP, the π-expansion of TAPP, and their photo physical properties. The summary of TAPP research is timely and substantial in

content. It will certainly expand people's understanding and interest of this new AIE core. Afterwards, fundamental research efforts directed TAPP applications in the field of solar cells, self-assembly, sensor, host– guest chemistry, ion channels, and medicinal chemistry need to be established in future prospective given that easiness and scalable synthesis of TAPP and its derivate will also have great potential to functionalization at the periphery of four benzene rings and use them for various applications effectively. It is also expected that, if synthetic protocols can be developed to allow further derivatives with closely controlled physical properties, a greater range of application will come on top of those described here, and we expect TAPP derivatives to play a vital role in all these fields of applications in the near future with great extent. The AIE-active TAPP is found like a gleaming treasure; with all study here we report TAPP derivatives found excellent potential and also we believe there will be more exciting works on the synthesis and applications of TAPP derivatives in the future.

With reference to photoluminiscent materials in chapter 2, we have designed and synthesized the probe 4,9-bis(dimethylamine)-2,7-dioctylbenzo[lmn][3,8] phenanthroline-1,3,6,8 (2H,7H)-tetra one (DDPT **1**) with substituted dimethylamine at the core of NDI displayed reversible for 4 cycles with the frequent addition of acid and base to the synthesized NDI system in excellent yield. DDPT **1** was successfully synthesized and further characterized which showing the reversible response to trifluoroacetic acid which acts as proton source. It is observed that optical changes in the molecule showed the increase in fluorescence with the increase in proton source at the same time. We also studied and investigated the reversible nature of the probe by adding trimethylamine (TEA) as base acting as deprotonating base. From this work it clearly suggests that protonation of N atom of dimethyl restricts the PET transfer results into the increase in fluorescence. The probe was reversible for 4 cycles with the frequent addition of acid and base to the synthesized

NDI system. Additionally, the probe was employed for test strip sensing application which successfully indicates that the probe is very much selective to H^+ ion in the solution particularly. With simple route of synthesis of DDPT **1** it may useful to control of pH in various biological and physiological processes occurring in the system.

Chapter 3 take a detailed account of design and synthesis of naphthalene diimide-benzothiazole (NDI-1) conjugate and it is used for nucleophilic addition of cyanide ion. Synthesized **NDI-1** after nucleophilic addition of cyanide ion Showed color change which can be observed by naked eye. Sensing of CN^- ion is studied by UV-Vis spectroscopy measurements in chloroform solution. As **NDI-1** displayed high sensitivity and selectivity towards CN^- ions shows change in color from red to green, which was clearly visible to the naked eyes. Whereas, the addition of other anions i.e. F^-, Cl^-, I^-, Br^-, HSO_4^-, $H_2PO_4^-$, OAc^-, ClO_4^- and HCO_3^- resulted into no visible color change of the sensor **NDI-1**. The detecting mechanism of CN^- ion with **NDI-1** was demonstrated by ^1H NMR, DFT calculations, Job's plot analysis and cyclic voltammetry.

In chapter 4 we studied and developed novel photoswitchable compound based on five TPE units that undergoes reversible trans-cis isomerization under UV and visible light respectively. The trans form of TPE-1 is almost planar and displayed a clear AIE behaviour in aqueous THF mixtures whereas the cis form has more of a twisted shape and did not displayed a clear AIE behaviour. The trans form efficiently binds to multiple MWCNTs and thus acts as a molecular glue for the CNT whereas the cis form, weakly interacts with the MWCNT samples. These interactions were studied by various methods like UV-vis, fluorescence, Raman, FT-IR and ^{13}C NMR spectroscopy in addition to the PXRD studies. DLS study performed to study aggregates of the nanotubes in the presence of the trans-form and were observed under SEM and TEM imaging. Results obtained from this study indicates

that the cis and the trans isomerization of the molecular glue proves a fine example of controlling the conductance of CNTs with a photoswitchable molecular glue.

In another work included in chapter 5, we have studied for the first time to use moleculr iodine catalyst to enhances the reaction yield of tetra-ester TAPP. We synthesized TAPP 1 by iodine-catalysed cyclocondensation of aromatic amine, aromatic aldehyde and 2,3-butanedione at 90^{o} C for 3h in acetonitrile solvent. Notable yield for tetra-ester-TAPP analogue obtained was up to 60%.

Currently we are studying and investigating variation in solvents and percentages of catalysts that are required for better yield which will be reported in near future.

Finally, we conclude from this thesis work, the design and synthesis of novel organic photoluminiscent materials based on TAPP, DDPT **1**, naphthalene diimide-benzothiazole (NDI-1), photoswitchable azobenzene based tetraphenylethylene (TPE) system exhibits a promising potential for its applications in sensor, self-assembly, host–guest chemistry, ion channels, solar cells and OLEDs successfully.

List of publications:

Appended to thesis:

1. Saha, M.; **More, V. G**.; Aljabri, M. D.; Chatterjee, S.; Shahnawaz, M.; Bandyopadhyay, S.; Bhosale, S. V. Photoswitchable Molecular Glue for Carbon Nanotubes Reversibly Controls Electronic Mobility with Light. *ACS Appl. Electron. Mater.* **2021**, *3*, 309–315, https://doi.org/10.1021/acsaelm.0c00857

2. **More, V. G.**; Nadimetla, D. N.; Zalmi, G. A.; Gawade, V. K.; Jadhav, R. W.; Mane, Y. D.; Bhosale, S. V. A New'Off–On' System Based on Core-Substituted Naphthalene Diimide with Dimethylamine for Reversible Acid–Base Sensing. *ChemistryOpen* **2022**, 11, e2022000 https://doi.org/10.1002/open.202200060. The work also highlighted as a front cover art for the Journal ChemistryOpen

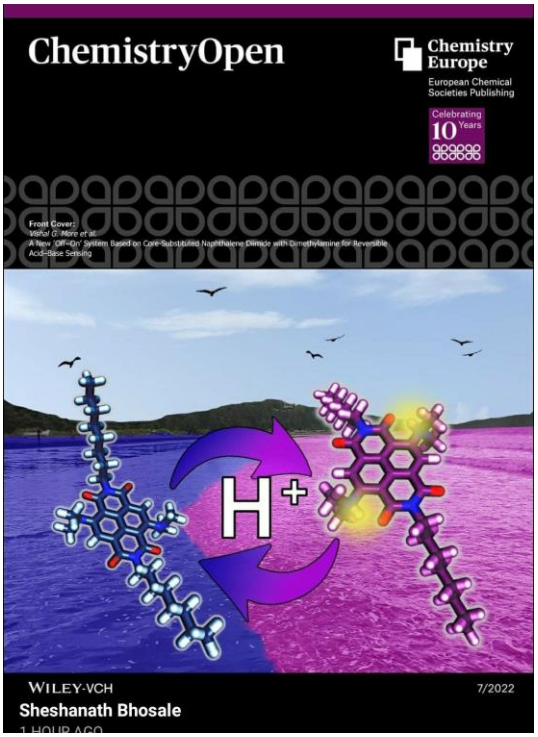

3. **More, V. G.**; Nadimetla, D. N.; Shaikh, D. B.; Puyad, A. L.; Bhosale, S. V.; Bhosale, S. V. Naphthalenediimide-Benzothiazole-Based Chemodosimeter for Selective and Sensitive Chromogenic for Cyanide Ion. *ChemistrySelect* **2022**, *7*, e202201537 https://doi.org/10.1002/slct.202201537

4. **More, V. G**.; Bhosale S.V. Iodine Catalysed New Method for Synthesis of Tetraestersubstitutedtetraaryl-1, 4-dihydropyrrolo [3, 2-b] pyrroles. G P Globalize Research Journal of Chemistry **2020**, *3*, 28-32.

Book Chapter:

1. **More, V. G.**; Jadhav, R. W.; Kobaisi, M. Al; Lathe, A. J.; Bhosale, S. V.; Development of a New Class of AIEgens: Tetraarylpyrrolo [3,2-b] Pyrroles (TAPPs). Published in *John Wiley & Sons*, 2022.

Other publications:

1. Goskulwad, S. P.; **More, V. G**.; Kobaisi, M. Al; Bhosale, R. S.; La, D. D.; Antolasic, F.; Bhosale, S. V.; Bhosale, S. V. Solvent-Induced Self-Assembly of Naphthalenediimide Conjugated to Tetraphenylethene through D- and L-Alanine. *ChemistrySelect* **2019**, *4*, 2626–2633.
2. Jadhav, R. W.; La, D. D.; **More, V. G**.; Tung Vo, H.; Nguyen, D. A.; Tran, D. L.; Bhosale, S. V. Self-Assembled Kanamycin Antibiotic-Inorganic Microflowers and Their Application as a Photocatalyst for the Removal of Organic Dyes. *Sci. Rep.* **2020**, *10*, 1–8.
3. Rao, P. S.; **More, V. G**.; Jangale, A. D.; Bhosale, S. V.; Bhosale, R. S.; Puyad, A. L.; Chen, J. Y.; Li, J. L.; Bhosale, S. V.; Gupta, A.; Sharma, G. D. A Series of V-Shaped Small Molecule Non-Fullerene Electron Acceptors for Efficient Bulk-Heterojunction Devices. *Dye. Pigment.* **2019**, *171*, 107677.
4. Goskulwad, S.; **More, V. G.**; La, D.; Bhosale, R.; Puyad, A.; Bhosale, S.; Bhosale, S. Solvent Directed Self-Assembly of Naphthalenediimide-Tryptophan-Glutamate Conjugates. *Indian J. Chem. -Section B* **2019**, *58*, 200–208.
5. Jangale, A. D.; Jadhav, R. W.; Nadimetla D. N.; Burud, M. D.; **More, V. G.** Meet the Board of *ChemistryOpen* : Sheshanath V. Bhosale. **2019**, *8*, 403-405.

Participation and presentation at National & International conferences:

- Participated as a Facilitator at "The Salters Chemistry camp" held at Department of Chemistry Goa University during 22nd -24th November 2018.

- Participated in two- day workshop on "Material Science" between University of Coimbra, University of Porto and Goa University on 18th and 19 th November 2019 at School of Chemical Sciences Goa University.

- Volunteered in Vigyan Sarvatra Pujyate, Festival of SCoPE (Science and Technology communication, Population and its Extension) for All, hosted and held at Goa University, Taleigao Goa.

RNI No. MAHENG/2017/74063
ISSN No. (Print) 2581-5911
ISI Impact Factor 1.022 (2019-2020)

Iodine Catalysed New Method for Synthesis of Tetraester-substituted tetraaryl-1, 4-dihydropyrrolo [3, 2-b] pyrroles

Vishal G. More, Dinesh N. Nadimetla and Sheshanath V. Bhosale*
School of Chemical Sciences, Goa University, Taleigao Plateau, Goa 403 206, India
*** Email: svbhosale@unigoa.ac.in**

Abstract
A new method to synthesise Tetraester-substituted tetraaryl-1, 4-dihydropyrrolo [3,2-b] pyrroles (TAPP) using molecular iodine as catalyst has been reported. The detailed mechanism of synthesis of TAPP has been elucidated.

Keywords: *TAPP, Iodine catalyst, synthesis, UV-Vis and HNMR Spectral analysis*

Introduction

Aggregation induced emission luminogens (AIEgens) have attracted great attention of the researchers due to their applications in materials and biotechnology such as organic light-emitting diodes, sensors, multistimuli-responsive materials etc.[1] Various AIEgens with excellent luminescence properties in the solid state have been developed, which include hexaphenylsilole (HPS). 1,1-dimethyl-2,3,4,5-tetraphenylsilole (DMTPS), tetraphenylethene (TPE), tetraphenylpyrazine (TPP), tetraphenyl-1,4-butadiene (TPBD) etc.[1] Nevertheless, some suffer from intrinsic drawbacks for example TPE and TPBD contain double bonds which usually give rise to E/Z isomerisation, thus, difficult for separation and also suffer from photo oxidation resulting in low quantum yields in aggregation. Thus, there was a need to develop AIEgens with good stability and excellent luminescence properties. In 2013, Gryko reported for the first time the synthesis of tetraaryl-1, 4-dihydro-pyrrolo [3, 2-b] pyrroles (TAPP) and their derivatives.[2] TAPP looks like a butterfly-shape structure and emission remains intense even as the solvent polarity is increased. Among AIEgens molecules that have found utility in the design of highly fluorescent and stable materials, TAPP derivatives have attracted particular attention. TAPP are compact and highly coloured and show violet-blue or blue ûuorescence with typical quantum yields of <“60%, emission while in the solid state, very broad absorption bands between 300 and 450 nm are observed. Considering their rich spectroscopic and good properties, they are ideally suited for sensors and design of light emitting diodes.

Therefore, TAPP molecules have been widely used for various application including sensing, solar cells, cellular imaging etc.[3] In 2013, Gryko reported for the first time three component one-pot straightforward synthesis of tetraaryl-1, 4-dihydropyrrolo [3, 2-b] pyrroles (TAPP) derivatives by reacting butane-2, 3-dione with aromatic aldehydes and aromatic amines in the presence of ammonium acetate in glacial acetic acid with reflux (3h) to give TAPP in ~15-30% yield.[2, 4]

ChemistryOpen

Research Article
doi.org/10.1002/open.202200060

Chemistry Europe
European Chemical Societies Publishing

www.chemistryopen.org

Special Collection

A New 'Off–On' System Based on Core-Substituted Naphthalene Diimide with Dimethylamine for Reversible Acid–Base Sensing

Vishal G. More,[a] Dinesh N. Nadimetla,[a] Geeta A. Zalmi,[a] Vilas K. Gawade,[a] Ratan W. Jadhav,[a] Yogesh D. Mane,*[b] and Sheshanath V. Bhosale*[a]

A new 'Off–On' system designed and synthesised by functionalisation of a naphthalene diimide (NDI) core with dimethylamine produces 4,9-bis(dimethylamino)-2,7-dioctylbenzo[*lmn*][3,8]-phenanthroline-1,3,6,8-(2*H*,7*H*)-tetraone, abbreviated as DDPT (**1**). DDPT **1** was synthesised using a simple strategy, namely aromatic nucleophilic substitution using Br_2-NDI with dimethylamine at 110 °C. DDPT was characterized by ^1H and ^{13}C NMR spectroscopy, ESI mass spectrometry and elemental analysis. DDPT **1** was then used for optical studies through protonation of its dimethylamine core with trifluoroacetic acid (TFA), blue-shifting the absorption band from 600 nm to 545 nm in solution. Interestingly, the fluorescence of DDPT **1** is weak in solution with a quantum yield $\Phi = 0.09$, which is significantly enhanced to $\Phi = 0.78$ upon addition of TFA. The limit of detection (LOD) was determined to 2.77 nM. Furthermore, DDPT **1** can be used for naked eyed detection not only under UV light (365 nm) but also using visible light, as clear changes can be clearly seen upon addition of TFA. The binding constant of DDPT was calculated to 2.1×10^{-3} M^{-1}. Importantly, DDPT **1** showed reversible switching by alternative addition of acid (TFA) and base (triethylamine) without loss of activity. Immobilised on paper, DDPT **1** can be used for strip-test sensing in which the colour changes from blue to reddish when expose to TFA vapours and reverse in the presence of triethylamine vapours.

Introduction

the pH value plays a critical role in many aspects such as chemical, environmental and biological processes. Hence, the accurate measurement of pH is of great significance in various fields of science and technology.[1] The cell homeostasis regulation and various metabolic pathways are governed by pH, showing the importance to not only being limited to chemistry but also applying to biochemistry, cellular biology and drug delivery systems.[2,3] To understand pH changes, different glass-pH-electrodes are widely used as pH sensors, measuring the pH in a wide range from acidic over neutral to basic media. The glass pH electrodes are free from interference, show low detection limit, and long-term stability with excellent reproducibility.[4] However, there are some drawbacks that limit the usage of these pH-glass electrodes such as their temperature-dependent nature, complex design and fragility. In addition, fabrication of the electrode is another difficult task, and their invasive nature makes it difficult to use them for more specialised sensing applications. Recently, optical pH sensing has thus attained great demand and became a widely accepted method as an alternative to glass-pH electrodes.[5]

There are several fluorescent molecules that have been developed to be used for pH sensing applications which are typically based on absorption and fluorescence changes of the indicator. As they exhibit high sensitivity, they can be employed in different areas.[6] There are different methods and devices available for measurement of pH, but fluorescence microscopy is among the most powerful tools for sensing applications. Fluorescent materials follow three important charge transfer mechanisms, namely photoinduced electron transfer (PET),[7] internal charge transfer (ICT),[8] and fluorescence resonance energy transfer (FRET).[9] A chemosensor useful for PET consists of a fluorophore-spacer-receptor arrangement, comprising a PET acceptor (denoted as fluorophore) and a PET donor (an amine).[10] Nevertheless, design, synthesis and application of the probe by applying the simplest synthetic strategies is very important. In addition, proper cell permeability is yet another necessary requirement for being able to detect pH in acidic cellular environments.[11]

Among planar aromatic molecules, naphthalene diimides (NDIs) have found wide application in various fields[10,12–15] due

[a] V. G. More, D. N. Nadimetla, G. A. Zalmi, V. K. Gawade, R. W. Jadhav, Prof. Dr. S. V. Bhosale
School of Chemical Sciences
Goa University
Taleigao Plateau
403 206 Goa (India)
E-mail: svbhosale@unigoa.ac.in
[b] Dr. Y. D. Mane
Department of Chemistry
BSS Art's, Science and Commerce College
Makni, Tq. Lohara,
413604 Maharashtra, Dist. Osmanabad (India)
E-mail: maneyd@gmail.com

Supporting information for this article is available on the WWW under https://doi.org/10.1002/open.202200060

An invited contribution to a Special Collection dedicated to the latest research of ChemistryOpen's Editorial Advisory Board Members.

ACS APPLIED ELECTRONIC MATERIALS

pubs.acs.org/acsaelm

Article

Photoswitchable Molecular Glue for Carbon Nanotubes Reversibly Controls Electronic Mobility with Light

Monochura Saha,[‖] Vishal G. More,[‖] Mahmood D. Aljabri,[‖] Sheelbhadra Chatterjee, Md Sahanawaz, Subhajit Bandyopadhyay,* and Sheshanath V. Bhosale*

Cite This: ACS Appl. Electron. Mater. 2021, 3, 309−315

Read Online

ACCESS | Metrics & More | Article Recommendations | Supporting Information

ABSTRACT: The use of light as an external stimulus to control organic supramolecular structures can play an important role in molecular devices. Photoswitchable azobenzenes are well suited for such applications due to their photoresponsive properties and a thermally induced reversal from the cis to the thermodynamically stable trans state. In this work, we have demonstrated for the first time that an azobenzene-based tetraphenylethylene (TPE) system capable of aggregation-induced emission (AIE) behavior can act as a molecular glue that can noncovalently functionalize multiwalled carbon nanotubes (MWCNTs). The resulting photoresponsive, noncovalent hybrid material shows reversible conductivity switching upon irradiation with light by making use of the reversible cis−trans isomerization.

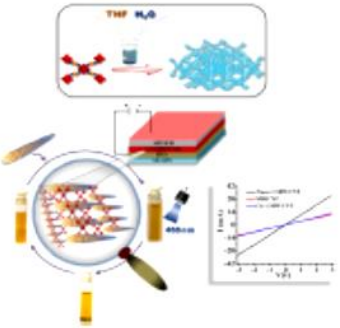

KEYWORDS: *photoswitching, reversible trans−cis isomerization, AIE-active molecules, photoswitchable conductance, carbon nanotube*

INTRODUCTION

Since the discovery of carbon nanotube (CNT) in 1991,[1] they have been recognized as promising scaffolds in nanotechnology.[2−13] CNTs can be either (1) single-walled (SWCNT),[14] generally having a diameter of 0.4−2 nm and lengths up to several cm or (2) multiwalled (MWCNTs), composed of multiple concentric cylinders of SWCNTs stacked on each other.[15] Both have their own unique advantages and have been applied in various fields.[16−29] MWCNTs have attracted particular focus as they can be produced in large quantities and are easier to purify. Therefore, the cost of production of MWCNTs is significantly lower than that of SWCNTs, which has been a prime reason for the former's adoption in many scientific research studies.[30−33] Both these nanotubes possess similar properties in terms of their high thermal and electrical conductivities.[34−36]

To improve usability, research has shown that the outer walls of CNTs can be altered with functional groups including hydroxides, carboxylic acids, and amides, which can act as sites for covalent functionalization.[37] This has been used to design MWCNT-based hybrid materials with tailor-made properties including improved stability, dispersibility, and processibility.[38,39] The functionalization can be carried out either on the main skeleton and/or at the periphery of the CNTs.[40] The functionalization of CNTs with photoswitchable molecules offers additional tunability of the material with light.[41−43] Advancement of MWCNTs integrated with molecular switching can thus offer new insights into optoelectronic materials.[44,45]

Controlled reversible photoswitching of conductivity is of particular interest in molecular electronics[46] and has been a subject of interest by several groups recently.[47,48] However, it remains a challenging task to control the conductivity reversibly using an external stimulus at the molecular level. The tetraphenylethylene (TPE) unit with four phenyl groups, a well-studied system for its aggregation-induced emission (AIE) properties, serves as an excellent candidate as a building block for the receptors of carbon-based frameworks.[49,50]

Among common photochromic molecules (diarylethenes,[51] spiropyrans,[52] oxazines,[53] stilbenes,[54] and azobenzenes), azobenzenes respond to two main external stimuli, light and heat, to reversibly switch between the isomers with different properties. Azobenzene switches from the thermodynamically favored trans-isomer to the cis-isomer upon exposure to ultraviolet (UV) light.[55,56] The reverse reaction occurs with visible light or heat, even at room temperature. This transformation is highly dependent on the structure of the azobenzene system and the local environment, such as the

Received: September 29, 2020
Accepted: December 27, 2020
Published: January 13, 2021

ChemistrySelect

Research Article
doi.org/10.1002/slct.202201537

Chemistry Europe
European Chemical Societies Publishing

www.chemistryselect.org

Organic & Supramolecular Chemistry

Naphthalenediimide-Benzothiazole-Based Chemodosimeter for Selective and Sensitive Chromogenic for Cyanide Ion

Vishal G. More[+],[a] Dinesh N. Nadimetla[+],[a] Dada B. Shaikh,[b, d] Avinash L. Puyad,[c] Sidhanath V. Bhosale,*[b, d] and Sheshanath V. Bhosale*[a]

A new receptor based on naphthalene diimide-benzothiazole (**NDI-1**) conjugate was designed and synthesized. The nucleophilic addition of cyanide ion to the **NDI-1** exhibited naked-eye, a colorimetric change is an optical response. The addition of CN^- ion to the **NDI-1** solution display change in red color to green. The UV-Vis spectroscopy measurements establish for the sensing of CN^- in chloroform solution. Moreover, **NDI-1** exhibited high sensitivity and selectivity towards CN^- ions in the presence of the interfering other anions such as F^-, Cl^-, I^-, Br^-, HSO_4^-, $H_2PO_4^-$, OAc^-, ClO_4^- and HCO_3^-. The detecting mechanism was established by ^{1}HNMR, DFT calculations and Job's plot analysis. Moreover, **NDI-1** exhibited very low limit of detection 85 nM.

Introduction

It is well reported that anion plays key role in many chemical, medicinal and biological processes.[1] Among them cyanide (CN^-) ion is more toxic in nature and harmful to environment and human health.[2] In human body when CN^- enters, it binds to ferric form of metalloenzymes such as cytochrome-c resulting in histonic anoxia.[3] Cyanide concentrations in blood reaches a level of 23–26 μM lead to human life causalities on large proportion.[4] According to World Health Organization (WHO) the determined permissible level of CN^- ions in drinking water required to be as low as 1.9 μM.[5] However, the utilization of CN^- ions in the form of salts are higher in gold mining, metallurgy, electroplating and synthesis of novel chemical entities as well as polymers such as nylon, nitriles and acrylic plastics.[6–7] In addition, human being accumulated higher level of CN^- ions *via* utilization of certain foods and plants.[8] Though monitoring of cyanide ion is under strict control, an accidental liberation of CN^- ion into the environment happens.

Therefore, it is extremely desirable to design, synthesize and employ new materials to monitor CN^- ion in environmental and biological systems. In this regard researcher developed large number of sensitive and selective chemosensors for CN^- ion detection.[9] Among them colorimetric and fluorescence sensors are selective and low cost materials.[10] Reported literature methods revealed that several chemosensors has been developed based on hydrogen-interactions, coordination with transition metal ions, deprotonation approach, boron-cyanide interactions, and furthermore few other approaches also developed to detect cyanide i.e. displacement and supramolecular self-assembly.[11] However, few of them suffer from drawbacks such as poor selectivity for CN^- ion detection in presence of interfering anions i.e. fluoride and acetate.[12] Moreover, nucleophilicity of the CN^- ion has been employed for its nucleophilic addition reactions with different chromophores such as oxazine, pyrylium, acyltriazine, acridinium, squaraine,[9a] carbazole, thiophene, tetraphenylethylene, trifluoroacetophenone, trifluoroacetamide and naphthalene etc.[13] However, some of these chemosensors display drawbacks i.e. poor selectivity, complicated synthetic protocol and a long reaction time for detection of cyanide ions.[14] To overcome these difficulties the development of simple and highly reactive chromophore towards CN^- ion still remains challenge.

It is well known that core-substituted NDI derivatives showed tuneable colorimetric, UV-Vis and emission response.[15] Chemical and biosensors have been established on the basis of core-substituted NDI and are one of the attractive chromophore. Several research groups investigated NDI based sensor towards cations, anions, pH and biosensor applications.[16] As a part of our research interest in this field we designed an efficient sensor for selective and sensitive detection of CN^- ion. In this paper, we have reported benzothiazole functionalized naphthalene diimide (**NDI-1**) based chemosensor, which could

[a] *V. G. More,[+] D. N. Nadimetla,[+] Prof. S. V. Bhosale*
School of Chemical Sciences
Goa University, Taleigao Plateau, Goa-403206, India
E-mail: svbhosale@unigoa.ac.in
[b] *Dr. D. B. Shaikh, Dr. S. V. Bhosale*
Polymers and Functional Material Division,
CSIR-Indian Institute of Chemical Technology,
Hyderabad-500007,
Telangana, India
E-mail: bhosale@iict.res.in
[c] *Dr. A. L. Puyad*
School of Chemical Sciences,
Swami Ramanand Teerth Marathwada University,
Nanded-431606,
Maharashtra, India
[d] *Dr. D. B. Shaikh, Dr. S. V. Bhosale*
Academy of Scientific and Innovative Research (AcSIR),
Gaziabad-201002,
Uttar Pradesh, India
[+] *These Authors contributed equally.*

Supporting information for this article is available on the WWW under https://doi.org/10.1002/slct.202201537